THE UNIVERSITY
of EDINBURGH

Understanding eruption dynamics: insights from volcanic seismicity in Ecuador

By

Sophie Butcher

A thesis submitted to
the University of Edinburgh
for the degree of
DOCTOR OF PHILOSOPHY

THE UNIVERSITY
of EDINBURGH

School of Geosciences
University of Edinburgh
August 2021

Acknowledgements

This work would not have been possible without the help and support of a number of people over the last four years. First of all I must thank my PhD supervisors, Andy Bell and Eliza Calder. It has been a privilege to be supervised by Eliza, who has been a constant reminder of why this field of research is so important, and who really is a phenomenal ambassador for women in STEM. Thank you especially to Andy for your endless support, open-door approach and constructive feedback, particularly in these last few months of writing. I have learned so much from you over the years - your advice and wisdom about everything from publishing to Python has been invaluable. This PhD has been so much more than a desk-based project in Edinburgh and I'm so grateful for all the opportunities you have provided to travel and work in the most amazing places. Thanks also to Meredith Corey, for getting me involved with the PTAS project, which is truly an experience I will never forget. Also, I would like to thank Ian Main, Mark Naylor, and my advisor Lara Kalnins for your advice and support.

Thanks should also go to my ever patient collaborators at IGEPN in Ecuador. Thanks to Patty, who's support and enthusiasm for new project ideas has always been unrivalled. Also to Daniel who was so unbelievably kind and helpful when I arrived in rural Tungurahua province in 2018, unable to speak a word of Spanish. Enormous thanks have to go to Mario and Stephen for their work in the seismology department at IGEPN. Without the groundwork they have done in volcanic and seismic hazards in Ecuador, much of the analysis in this thesis would simply not have been possible. Particular thanks to Stephen for answering my endless stupid questions on WhatsApp at all hours of the day.

Doing a PhD was always so much more than just writing this thesis. It was moving my whole life to a brand new city, aged 22, and setting up home in Edinburgh for a wee while. I couldn't have made it to this point without some very important people. My first thanks have to go to my fellow DTP students Aythya, Rosie and Fiona - you were the first friends I made in Edinburgh and convinced me in those early months that I had made the right decision to start this journey. Huge thanks have to go to the OG Grant Attic WI - Amy, Hannah, Isla, Kirsty, Paige, Roseanne and Berit - you all made coming into the office every day such a joy. Honorary member Gillian should also get a mention here, who was always on hand with a listening ear and a welcome hug in times of (relative-PhD) crisis. Especially thanks to Becca, Elizabeth and Zoi - I feel very lucky to have had you by my side all these years, but particularly in the depths of a pandemic. And thanks to KB Raptors past and present - James, Ben, Eleri, Alice and Davide - for dragging me away from my desk when I really needed it the most.

Huge thanks also need to go to some of the most important women in my life, who have offered so much support and encouragement over the last four years. Thanks have to go to my friend Gina for providing Python hacks, tutoring notes and tennis memes in equal measure. To Rachel, who was such a role model for me in this process - the living proof that you can drink the rosé, fangirl over the popstars *and* get the PhD done. Thanks go to Laura for providing invaluable emotional counselling during 7am cycles and maintaining my sanity during a global pandemic. Also to Sally, who always had faith that I could get this across the finish line, even when I was fairly sure I couldn't. I never anticipated meeting a like-minded, 5ft3, blonde volcanologist from 40 miles up the road, but I'm so glad that I did. To my good friend Eilidh - thanks for introducing me to munro bagging. Marching up a big hill and chatting total nonsense was always the perfect escape from the chaos of work. And finally I have to thank my queens, Emma and Katie. Even when strewn across three continents, I have always been able to count on your unshakeable love and support.

Last but by no means least, I need to thank my biggest cheerleaders, mum, dad and

Lacey. I know that most of the time you had no idea what I was working on or why I was having such a flap, but you've always been there on the end of the phone (and sometimes on the first available easyJet flight) to pick me up and help me get back on my feet. Whether it was words of encouragement, or another bank transfer to cover more physio, you were always there to help. I can never repay you for all you have done. Thank you.

Abstract

Persistently active volcanoes in close proximity to society can pose a huge danger to infrastructure, lives and the economy. Careful monitoring of volcanic seismicity is integral to successful hazard assessment and risk management. Geophysical monitoring at active volcanoes can provide rich datasets to examine internal systems. Specifically, seismic monitoring offers the potential to develop real time analysis and forecasts. The generation of volcanic seismicity has been linked to processes such as magma ascent, degassing and rock fracturing. However, studies are often limited to individual volcanoes or specific episodes of unrest, and so it is difficult to compare interpretations. This aim of this thesis is twofold: to develop methodologies to better quantify and characterise volcanic seismicity, and to use these to provide new understanding of volcanic systems, the hazards they might pose and how we can better forecast and monitor unrest.

First, I present an extensive literature review of our current understanding of volcanic seismicity. As there is no standardised procedure for the analysis of volcanic earthquakes, there are inconsistent uses of techniques and ambiguous terminology. Existing studies also tend to focus on a handful of well monitored volcanoes where dense arrays can be used to calculate source mechanisms and depths to interpret seismic swarms. In order to address this, I develop a thorough signal processing routine which generates a suite of metrics to characterise a single earthquake event. These metrics can be used across a sequence of earthquakes to track changes in the behaviour of seismicity, and distinguish different types of earthquakes. It is developed with poorly monitored volcanoes in mind, as metrics can be determined for signal from a single station, and even a single component instrument. I use parameters in the time domain including amplitude, duration and cross correlation,

and compare three different approaches to calculate the quality (Q) factor, in the frequency domain.

I then present two candidate volcanoes to apply the methodology and attempt to describe the internal processes at each. Tungurahua and Cayambe are two relatively understudied volcanoes and yet they are potentially the most dangerous natural hazards in Ecuador. Tungurahua's most recent eruptive phase (1999-2016) was explosive and persistent. In contrast, Cayambe volcano has not erupted in over 200 years and yet has been seismically restless in recent years. This presents an opportunity to compare the seismicity associated with ongoing, and reawakening volcanic processes.

In chapter 4, I characterise the seismicity at Tungurahua between 2012 and the final explosions in 2016. Seismicity at Tungurahua was dominated by long-period (LP) earthquakes, particularly episodes of highly periodic, repeating LP seismicity, known as drumbeats. In this chapter, I show that persistent drumbeats occur in phase with cyclical Vulcanian eruptions. These events are attributed to the initial failure and subsequent resealing of an upper conduit plug. In each explosive episode, the signal metrics are able to distinguish a shift in the signal properties of drumbeat LPs. In chapter 5, I focus specifically on accelerating rates of drumbeat LPs, often considered precursors to eruptions. I use temporal statistics and a Markov chain Monte Carlo (MCMC) approach to model three episodes of drumbeats. In one significant episode, the last ever recorded drumbeats at Tungurahua, I show these events are precursors to a 'failed' attempt at an explosion. In chapter 6 I then compare these findings at Tungurahua, with the 2016 seismic crisis at Cayambe. Here I demonstrate the repeating LP seismicity is likely a result of shallow hydrothermal systems, rather than surficial 'icequakes' or magmatic ascent. However, swarms of volcano-tectonic events (VTs) in 2016, are likely attributed to stresses on regional faults and ascent of a new pulse of magma. Finally, I begin to explore the complex volcano-tectonic interactions at both Tungurahua and Cayambe. Where there are high rates of tectonic events globally, and high rates of eruptions, it is important to distinguish causality and coincidence. VT swarms at Cayambe occur two months

after the M_w7.8 Pedernales earthquake, 200km west. Using models of static stress change I suggest the crust at Cayambe was subject to a dilational regime, prompting resumed activity in 2016. However, the Pedernales earthquake occurs just two months after the final eruption at Tungurahua and yet does not appear to promote or restrict further explosive activity.

This thesis presents case studies of two active volcanoes that are subject to limited seismic monitoring. These methods are not computationally intensive and could be readily adopted into routine volcano monitoring, to further inform hazard assessment. Although Cayambe and Tungurahua are neighbouring volcanoes, comparable in their rheology, they are very different in their current dynamic state, and this is evident in the seismicity. An enhanced understanding of these systems should inform further assessment of seismicity at intermediate-composition, arc volcanoes.

Lay Summary

Restless volcanoes in close proximity to society can be very dangerous. At an active volcano, we can use monitoring to understand how the eruption is unfolding and mitigate the risk of a disaster. We might do so, by carefully sampling the gases that are emitted, measuring the way the ground around the volcano deforms, or recording any earthquakes that are generated. It is often argued that the earthquakes might be the biggest indicator to help us understand and potentially forecast volcanic activity. We can use the earthquakes generated in a volcano, before, during and after an eruption to understand what internal processes are occurring. If a volcano is equipped with multiple seismometers, the same earthquake can be recorded in several places. We can then calculate the depth the earthquake occurred at and estimate what mechanism caused the earthquake. However, seismic monitoring is expensive and a good network requires well coordinated installation and maintenance. Some of the most dangerous volcanoes in lower and middle income countries are not densely monitored and perhaps only have one or two working seismic stations. This data can still be meaningful and used to inform hazard assessments. In this thesis I present a streamlined workflow to analyse earthquake data from volcanoes which only have limited earthquake monitoring. By unifying the analysis techniques, it will make it easier to compare the earthquakes from one volcano to the next. This will help us to further understand some of the fundamental internal processes that occur in an active volcano.

I focus specifically on two volcanoes in Ecuador: Tungurahua and Cayambe. Ecuador has a national geophysical monitoring agency (IGEPN) who maintain instruments on both volcanoes. However, at both Tungurahua and Cayambe there is only one station which

is reliable and operational, so both systems are set to benefit from a new approach to analyse earthquakes. Tungurahua volcano was continuously erupting between 1999 and 2016. Specifically I investigate episodes of unrest where the earthquakes occur at regular repeating intervals. These are often referred to as 'drumbeats' because of their regular rhythm. Drumbeats have been recorded and described before, although often as isolated events and associated with a specific process unique to one volcano. Here, I identify seven instances of drumbeats between 2012 and 2016 at Tungurahua, in the first study of its kind. Using the new methodology, I am able to quantitatively describe the behaviour and the style of these earthquakes. By using a long term study, I then relate the appearance of drumbeats to a more generalised model, where a sealing plug of cooled rock at the top of the volcano controls the internal pressure. This is important to understand as drumbeat earthquakes may then, in turn, be indicative of an imminent eruption.

In contrast, Cayambe volcano has not erupted for over 200 years. In 2016, however, there was a significant episode of unrest where over 50 times the number of daily earthquakes were recorded for a prolonged period of several months. There was concern that an eruption may be imminent. Unlike Tungurahua, there is not an extensive recent record of activity at Cayambe so it is not clear what a 'typical eruption' might look like. Furthermore, there is an added hazard at Cayambe, as the volcano is capped by a glacier, which in the event of an eruption could melt and contribute to significant mud flows called lahars. Therefore it is important to understand what the earthquakes mean and whether they might be indicative of a probable eruption. In this thesis I establish that the earthquakes here are generated by a different process to those at Tungurahua. Specifically, they indicate brittle failure and rocks breaking. This is associated with the possible arrival of new magma in the system at Cayambe. This is important to establish and it suggests that a rapid eruption could be possible.

The volcanic earthquakes in 2016 at Cayambe also occurred just six weeks after a large tectonic earthquake struck 200 km to the north west, near the town of Pedernales. This was

one of the largest earthquakes experienced in living memory in Ecuador. Here I use a model to show that the Pedernales earthquake created a significant change to the state of stress in the subsurface at Cayambe and suggest that this promoted the up-welling of new magma. At the same time there appears to be no triggered activity at Tungurahua in response to the Pedernales earthquake. This relationship between earthquakes and volcanoes is complicated and sensitive but could be crucial to inform future modelling efforts.

By taking a detailed analysis of the earthquakes at these two systems we are in a better position to understand the internal processes that cause eruptions. The findings in this research will assist monitoring teams in Ecuador and inform hazard assessment in the case of future unrest. They also help us to understand the eruption processes at similar comparable volcanoes around the world, which also may be subject to limited monitoring and research.

Table of Contents

List of Figures

List of Tables

1 Introduction

1.1 Motivation and significance

It is estimated that 500 million people are living in areas affected by volcanic activity (Baxter & Horwell, 2015). It is therefore important that we understand the nature of unrest at active volcanoes, in order to provide timely, useful and accurate information about eruptions for these communities. Whilst deformation studies can resolve movement to a scale of millimetres (Biggs & Pritchard, 2017), and gas monitoring can give greater geochemical insights (Edmonds, 2008) - it is seismicity that offers us the greatest potential to develop real time analysis and forecasts (Poland & Anderson, 2020). There are 565 volcanoes on Earth that scientists have recorded eruptions at and more than half of these were accompanied by heightened precursory seismicity in or surrounding the volcano (McNutt & Roman, 2015). Despite this, only around 200 volcanoes worldwide are equipped for seismic monitoring (Loughlin et al., 2015). Those that are best monitored tend to be a co-ordinated effort, in countries with well funded and established monitoring agencies. A 2012 study identified nearly 90% of 441 volcanoes across 16 developing countries, were poorly monitored or completely unmonitored and 15% of these posed significant risk to large populations (Sparks et al., 2012). The study also cites that unlike global passive seismic data which is well organised and freely available, volcano seismic data is rarely shared between different, independent agencies. This means that despite these monitored volcanoes covering a wide range of geographical and tectonic settings, magmatic compositions and eruption styles, we are still without a comprehensive

database of global volcano-seismic records.

Beyond inconsistencies in monitoring, there is often ambiguity in the terminology associated with volcanic seismicity. The formal study of volcanic earthquakes began with Omori in Japan, over 100 years ago (Omori, 1911), and since, the variety of observations worldwide has lead to inconsistent and conflicting vocabulary and models (Chouet & Matoza, 2013). Qualitative descriptions of earthquake signal properties have broadly classed earthquakes into distinct categories, however, the more detailed phenomenology and associated source process of volcanic earthquakes is typically poorly understood (Zobin, 2012). This is particularly problematic at poorly monitored volcanoes where there is limited access to data. Where some quantitative methods do exist, again, there is again ambiguity and conflict in the methods used. For example, the metric 'Q factor' is often used to describe the spectral properties of a signal, but in the literature, there are at least three different methods described in the application to volcanic earthquakes (Cusano et al., 2008; Del Pezzo et al., 2013; Kumazawa et al., 1990). In turn, this also causes disparities in the literature and means that comparing seismicity from one volcano to the next can be particularly challenging. In order to combat any uncertainty in both the terminology and the approach to analysis, there is a clear need for a single unified approach to quantify the characteristics and behaviour of volcanic seismicity.

There is also a limited understanding as to how seismicity varies with different eruption processes. Often the most well-monitored volcanoes are also the ones which have had recent or ongoing eruptions and subsequently, many specific volcanic-seismicity studies relate to only the shallowest eruption processes. Specific source mechanisms such as the extrusion of dacitic magma spines (Iverson, 2008) or repeated growth and collapse of lava domes (Gottschämmer et al., 2021) have been associated with particular patterns of seismicity. However, there are very few long term studies, or generalised models that are be applicable to many volcanoes. Again, this makes it difficult to compare one volcanic seismicity study to another. There is of course, a danger of over-simplifying the way we study and interpret

volcanic seismicity. Nonetheless, to further our understanding of the driving source processes, and to inform future hazard assessment, there is a need for a more unified approach to quantitatively examine volcanic-seismicity.

1.2 Study area

Ecuador is home to over 50 active volcanoes in the Northern Andean Volcanic Zone (NAVZ) which extends over 600 km down the central spine of the country (fig 1.1). This presents an opportunity to study continental arc volcanoes which although are in close proximity to one another and typically of intermediate composition, have very different eruption styles and histories. Some volcanoes have been recently active and have presented themselves as significant hazards to local communities. For instance, in this most recent eruptive phase at Tungurahua volcano, the seismicity was remarkably uniform and over 97% of catalogued earthquakes between 1999 and 2016 were identified as long-period (LP) earthquakes. Specifically, there have been a number of episodes of the poorly understood phenomenon, known as drumbeat seismicity (Bell et al., 2017; Molina et al., 2004), where earthquakes occur with a consistent repeating inter-event time. Drumbeat seismicity has been observed at similar, persistently active, intermediate-composition volcanoes (Green et al., 2006; Petersen, 2007; Varley et al., 2010a), however, there is little agreement on how these should be be characterised or the source mechanism that generates them.

In contrast, there are other volcanoes in Ecuador that are known to be a potential hazard, and whilst they have not erupted in tens or hundreds of years, they are now showing signs of unrest. For instance, in 2016 there was an uncharacteristic seismic swarm at Cayambe volcano, after more than 200 years of quiescence. Daily earthquake rates increase by 10–100 times those seen previously and prompted discussions locally about a possible imminent eruption. Unlike the seismicity seen at Tungurahua, however, the earthquakes in this swarm were mostly described as volcano-tectonic (VT) and therefore thought to be from a different

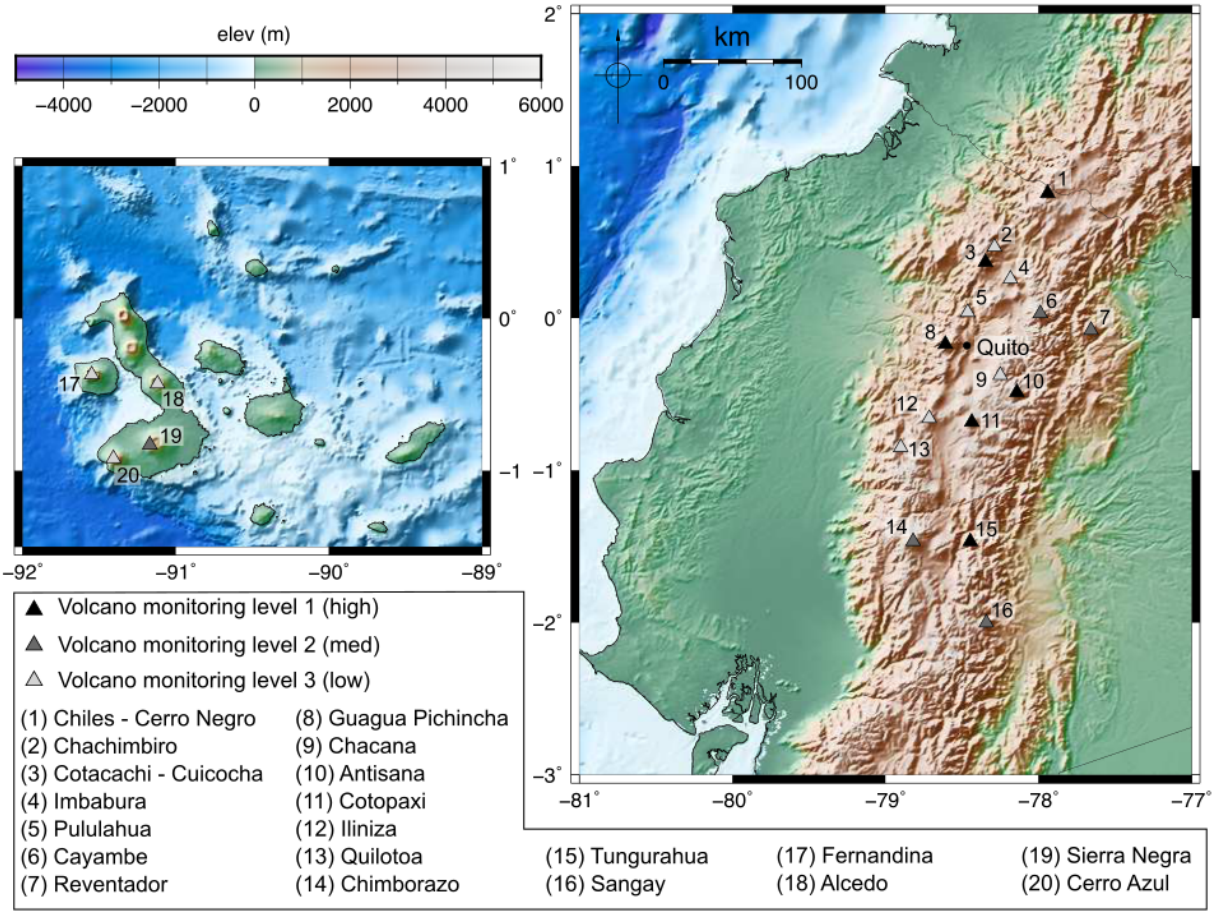

Figure 1.1 Volcanoes in Ecuador that are monitored by Instituto Geofísico de la Escuela Politécnica Nacional (IGEPN). Monitoring archives and current activity status of volcanoes can be found https://www.igepn.edu.ec/red-de-observatorios-vulcanologicos-rovig.

type of source process.

There is a national agency coordinating geophysical monitoring in Ecuador, *Instituto Geofísico Escuela Politécnica Nacional (IGEPN)*, however, their capacity for research is limited by funding. In turn, there are a handful of volcanoes, including Tungurahua and Cayambe, which would benefit from a thorough investigation into seismic unrest, with the limited data available. Particularly as both of these volcanoes are now quiet, a detailed retrospective analysis of the seismicity would inform decisions in hazard assessment in a future unrest.

Furthermore, Ecuador is also subject to frequent tectonic seismicity from the subduction of the Nazca plate to the west. This adds another layer of complexity to the dynamics of the volcanic systems throughout the country. It is also an exciting opportunity to examine the delicate relationship between volcanic and tectonic processes and the susceptibility for one dynamic system to influence or trigger another (Hill et al., 2002b).

1.3 Proposal

In this thesis, I propose a new streamlined methodology for the analysis of volcanic seismicity. The method is designed specifically for use in poorly monitored volcanic settings, with limited data. I use synthetic waveforms and a sample of real earthquake events from Ecuador to develop the methodology. It is readily adaptable and could be used to examine any earthquake catalogue, where single station and single component waveform data are available. I then test the effectiveness of the methodology and examine seismicity at Tungurahua and Cayambe. By comparing these two volcanoes, this presents an opportunity to examine seismicity at neighbouring volcanoes, which although have similar geology and composition, also have very different eruption histories. Tungurahua was persistently active between 1999 and 2016, demonstrating Strombolian to sub-Plinian eruption styles, whereas Cayambe has been dormant for over 200 years. The seismic swarm recorded in 2016 caused alarm for the monitoring agency in Ecuador and prompted discussions of an imminent eruption (El Comercio, 2016). By quantitatively rather than qualitatively comparing the earthquake signals from both Tungurahua and Cayambe, I am able to compare the seismicity and further understand how it relates to fundamental internal processes at each volcano. I then also use any additional geophysical monitoring data including deformation and gas flux to infer source models at both Tungurahua and Cayambe. By studying two such contrasting systems, I demonstrate the flexibility of the methodology and begin to decipher the differences in the source mechanisms associated with persistent and emergent seismicity.

At Tungurahua, where the seismicity is dominated by LP earthquakes, I specifically investigate episodes of periodic drumbeat LPs. I use my new methodology to conduct a long term examination of drumbeats. To my knowledge, this is the first long term study of it's kind. Rather than considering the seismicity as an isolated phenomena, I attempt to relate the periodic seismicity to a more generalised model that could be adapted for prolonged unrest at intermediate-composition volcanoes globally. At Cayambe, I demonstrate the value of the methodology and distinguish different seismic source processes, where accurate depths and focal mechanisms cannot be determined. I then consider both systems in relation to large tectonic earthquakes, specifically examining the impact of the M_w7.8 Pedernales earthquake which occurred just 200 km to the north west of the NAVZ.

1.4 Thesis outline

The thesis is constructed as follows:

- In chapter 2, I present a literature review structured in two parts. First, on the current state of knowledge of volcanic seismicity and shallow conduit dynamics, and then on two case study volcanoes examined in this thesis, Tungurahua and Cayambe volcanoes in Ecuador. At the end of chapter 2 I explicitly state my research questions to be addressed in the succeeding chapters.

- Chapter 3 is a methodology for volcano-seismic event analysis. This is also split broadly into two sections: a signal processing routine for individual earthquake waveforms, and broad catalogue statistics for interpreting long episodes of unrest.

- In chapter 4, I present the first long term analysis of persistent seismicity at Tungurahua from 2012 - 2016. I identify seven key episodes of periodic LP seismicity and apply the methodology from chapter 3 to interpret each sequence. I then use additional geophysical monitoring data to speculate on the source mechanism and suggest the

state of the shallow conduit in each instance.

- In chapter 5, I introduce Bayesian statistics to understand the significance of temporal rates and patterns in LP seismicity at Tungurahua. This is with particular focus on one episode of accelerating rates of LP seismicity up to what I propose is a 'failed' explosion at Tungurahua.

- To contrast the LP and drumbeat seismicity that dominates at Tungurahua, chapter 6 then explores the 2016 seismic swarm that marked the reawakening of Cayambe volcano. I distinguish subsets of seismicity from the 12 month catalogue including LPs relating to a shallow hydrothermal system, and distal VTs. I also propose a mechanism for triggering the reactivation at Cayambe as a result of the M_w7.8 Pedernales earthquake.

- Chapter 7 is the discussion chapter for the thesis. Here I evaluate the results from chapters 3-6 in relation to the research aims and questions laid out in chapter 2. I also consider the broader implications of the findings from this thesis and how these might contribute to our understanding of volcanic processes at analogous intermediate-composition arc volcanoes around the world.

- In chapter 8 I summarise and conclude the thesis.

Two chapters in this thesis have been published. They are included here with a preface and post-script to contextualise the research within the thesis. The details of the publications are as follows:

- Butcher, S., Bell, A.F., Hernandez, S., Calder, E., Ruiz, M. and Mothes, P., 2020. Drumbeat LP "aftershocks" to a failed explosive eruption at Tungurahua Volcano, Ecuador. *Geophysical Research Letters*, 47(16), p.e2020GL088301.

- Butcher, S., Bell, A.F., Hernandez, S. and Ruiz, M., 2021. Evolution of seismicity during a stalled episode of reawakening at Cayambe Volcano, Ecuador. *Frontiers in Earth Science*, 9, p.464.

2 | Literature Review

This chapter examines the current state of volcanic seismicity research and how it relates to internal processes. I have outlined the current understanding of volcano-seismic event types and classification efforts. I also present some of the models suggested as source processes of seismicity, and some examples from volcanoes around the world where these have been proposed. Further to these general models, I have examined the current understanding of the phenomenon known as drumbeat seismicity and published episodes from the literature. The research presented in chapters 4 – A has largely been in collaboration with the national geohazards monitoring agency in Ecuador, *Instituto Geofísico de la Escuela Politécnica Nacional (IGEPN)*. In particular, the focus of my reasearch is at Tungurahua and Cayambe volcanoes, Ecuador, which I have introduced here in detail. From the review, I have identified the key gaps in our current understanding, why they are important, and how I plan to address them.

2.1 Volcanic monitoring and forecasting

Routine geophysical, geochemical and surface monitoring is key to forecasting eruptions and issuing early warnings. Volcano observatories operate on a range of scales, from small groups dedicated to a single volcano to national agencies. As well as more permanent, long term instrumentation, temporary networks may be deployed by visiting researchers during periods of interest to capture high resolution data. Seismic recording is core to the monitoring

efforts of any volcano observatory (Loughlin et al., 2015; McNutt & Roman, 2015). In the best resourced monitoring efforts, seismic data can be telemetered and therefore interpreted in real time. Often recording between 50 and 100 samples per second, they also provide very rich datasets even in short periods of monitoring. Unlike remote methods, the quality of data obtained is dictated by seismometer coverage. Extreme terrain and altitude can make installation almost impossible in certain locations. Climatic factors including rainy seasons, and even ash fall can inhibit solar power and battery function, and so data outages are routine in many networks. However, as it stands, seismic monitoring at volcanoes still likely offers the best possible opportunity for short term forecasting eruptions (Poland & Anderson, 2020). In order to try and distinguish and interpret possible source mechanisms, earthquake signals can be divided into subsets according to their properties. This is detailed further in section 2.2. Earthquakes occurring in the very shallowest part of the volcano may be indicative of fluid movement, such as magma or gas. They may also suggest a small perturbation in the local stress field, or slip on a plane of weakness. Even surface processes such as rockfalls and lahars have distinct signatures in seismic records (Zobin, 2012). A full summary of volcano seismicity source models is included in section 2.2.2. By recording earthquakes on multiple stations, the source location of the earthquake can be determined (Chouet et al., 2010; Fremont & Malone, 1987; Lehr et al., 2019). By using series of these earthquakes, the locations can be traced sequentially to assess whether there is a singular moving source or if there are multiple mechanisms at play (Woods et al., 2018). A sound and robust method to analyse and interpret sequences of seismicity is key to understanding the internal processes and inform hazard assessments.

Infrasound data, captured during explosions at volcanoes, is processed in a similar way to seismic waveform data. Acoustic records, however, are indicative of very shallow crater and conduit processes, unlike seismic sources which may originate several kilometres below the surface (Johnson & Ripepe, 2011). Infrasound signals can be used to quantify the energy associated with explosions, reported in joules. These signals can also be used in conjunction

with numerical models of conduits and craters, as a remote monitoring tool (Johnson et al., 2018). For example, fluctuating heights of the lava-lake in Villarica, Chile, have been modelled using infrasonic signals (Richardson et al., 2014). Remote techniques are not only cost-effective but keep monitoring teams safe and can limit the need for dangerous fieldwork. Volcanic deformation can be monitored with tiltmeters installed on the flanks of the volcano, by calculating small shifts from a network of GPS stations or over a much wider field using interferometric synthetic-aperture radar (InSAR). Tiltmeter and GPS networks in the field offer opportunities to study very localised flank instabilities or map the stress and strain associated with magmatic processes. Whilst InSAR allows monitoring for the most remote and inaccessible volcanoes. Biggs and Pritchard (2017) cite a five fold increase in reported volcano deformation between 1997 and 2017, with thanks to the rise of InSAR studies. Whilst such extensive deformation studies have flourished in the literature, their variety have illustrated that simple volcano deformation cycles of co-eruptive deflation and inter-eruptive inflation are simply not adequate to describe many systems (Biggs & Pritchard, 2017). InSAR can also be used to quantify external volcanic changes, such as lava flow volumes (Wadge, 2004). This has been done at Reventador, Ecuador and Tolbachik, Kamchatka, and just as with other remote techniques, this avoids the need for potentially dangerous in-person fieldwork, and allows monitoring in the most remote and inaccessible locations. Volcanoes also emit gases both during and between eruptions. Monitoring the flux, chemistry and temporal variations in volcanic gases can tell us about magmatic processes in the very shallow subsurface. Gas flux measurements have been used to calculate magmatic masses in the conduit (McGonigle & Oppenheimer, 2003) whilst the addition of spectroscopic methods can help to constrain the depths from which volcanic gases originate (Edmonds, 2008). Although gas monitoring can be done on the ground and semi-remotely, methods can be easily hampered by wind conditions, and as such the plume direction, and atmospheric factors such as the presence of ash (Kern et al., 2012; Varnam et al., 2020). In addition to geophysical surveying of the subsurface, photo and thermal imagery can be used to compliment the

monitoring efforts and constrain any interpretations. Many monitoring agencies during an eruptive period will freely publish these online, and more recently, on social media. Following an eruptive event, fieldwork to map pyroclastic deposits and lahars, petrological studies of ballistics and analysis of ash fall can retrospectively add to eruption records.

The amount of instrumentation and monitoring efforts used on any one volcano depends on accessibility, the perceived danger of the volcano, the level of risk associated with surrounding communities and ultimately, financial cost. Each year, volcano monitoring can cost anywhere from several thousands to several million USD (Loughlin et al., 2015). Comprehensive monitoring with multiple instruments and techniques allows us to describe detailed conceptual models for eruption processes, which should educate and inform future decisions in forecasting. A review of volcanic forecasting approaches is detailed in Poland and Anderson (2020). This review draws on the benefits and challenges of different approaches to forecasting including probabilistic forecasting, using historical and geological records, pattern recognition techniques and magma system modelling. A statistical model should relate to a physically or chemically plausible model, although we may not yet understand the causality of that process. One early study states, *"No single predictive index appears to be the master key to volcanic forecasting"* (Decker, 1973). Ultimately an integrated approach is the only way in which it is likely that forecasting could be possible. And even then this may not be in a timely fashion or with enough confidence to influence decisions about warnings and evacuation of people. However, technology is improving - both in terms of instrumentation and computational approaches. Through community science and more affordable equipment, there are more data being generated than ever before. And with developments in machine learning and artificial intelligence there is more potential to harvest information from archived data. As stated in a 2003 review, *"Forecasting is a central goal of volcanology"* (Sparks, 2003) and that remains the case at the time of writing this thesis.

2.2 Seismic monitoring

The first organised volcano seismic monitoring was conducted in Japan in the 1910s (Zobin, 2012). Fusakichi Omori recorded seismic unrest at Usu, Asama and Sakurajima volcanoes between 1910 and 1914 with a single three-component pendulum seismometer (Omori, 1911). They noted 'microtremors' occurring alongside explosions, and even reported increasing numbers of earthquakes prior to explosions. This is the first documented investigation into seismicity as a precursor for unrest at a volcano. In the following 100 years significant research has been undertaken to better understand the causes and nature of earthquakes at active volcanoes. This is in part thanks to advances in technology; both in computational methodology and wider accessibility to seismometers (McNutt & Roman, 2015). One study assessed the Global Volcanism Programme (GVP) database and found that between 2000 and 2010, from 228 active volcanoes, 121 had reported seismicity either prior or during an eruption (53%) (Phillipson et al., 2013).

As with many other characteristics of volcanic unrest, seismicity at one volcano can look significantly different to seismicity at another. Even from one eruption to the next at the same volcano, the seismicity can be wholly different. In order to decipher the signals, research has focussed on classifying earthquakes by 'types' (section 2.2.1). Then, in conjunction with other geophysical monitoring, historical records and laboratory analogue experiments, associate these earthquake types with 'typical' source mechanisms (section 2.2.2). This section goes on to introduce some well known studies of volcanic unrest and their contribution to our understanding of volcanic seismicity. Finally, I detail a particular phenomenon of repeating seismicity known as 'drumbeats'.

2.2.1 Volcano seismic earthquake classification

It was Omori (1911) who first cited that volcanic eruptions in Japan were frequently preceded by an increase in earthquakes. This initiated the discussion around volcanic seismicity, its origins and how best to describe the style of the seismicity. It was Minakami et al. (1951) who developed this idea further and proposed the first classification system for earthquakes recorded during volcanic unrest. An A-type volcanic earthquake was considered to be indistinguishable from a shallow tectonic earthquake. The waveforms should have both clear P and S phases and it is was suggested these earthquakes occurred $\geq$ 1 km below the volcano. B-type earthquakes were strictly associated with shallow processes $\leq$ 1 km below the surface. These waveforms typically had much lower frequencies, smaller magnitudes and lacked a clear S phase. The characteristics of these B-type earthquakes were thought to be a result of path effects as these waves propagate through the very shallowest part of the volcanic edifice (Sherburn et al., 1998). Explosion earthquakes had less rigorous definitions about their waveform characteristics. They occurred during explosive eruptions, and crucially the magnitude of the earthquake scaled with the magnitude of the eruption (Nishimura & Hamaguchi, 1993). As these earthquakes are associated with explosions, waveforms can be identified by compressive upward first motions (Zobin, 2012). Volcanic tremor was also defined as the final category of earthquake types, although as is still the case today, there was uncertainty around their origin.Tremor was identified as constant amplitude signal occurring from several seconds, to hours and days at a time. This early Minakami work also suggested that tremor occurred when successive B-type earthquakes repeated with small inter-event times and merged to form a continuous signal.

There is an important point to make at this stage regarding earthquake classification and interpretation. Minakami's definitions of A- and B- earthquake types rely on pure signal properties (including frequency magnitude and amplitude) but also some interpretation (source depth and seismic phases). Whilst signal properties may be universal, the interpre-

tations associated with these classifications may not be applicable to every volcanic setting. For example, depending on the rheology of the magma and the structure of the edifice, a depth restriction of 1 km may be relatively shallow or deep and relate to different components of a volcanic system from one volcano to the next. As such, great care should be taken when describing volcanic earthquakes with pre-defined labels, and comparing seismicity across different publications.

A- and B- type earthquakes structured the discussion around volcanic seismology for many years, and were used to interpret eruptive sequences (Latter, 1981; McNutt, 1986). Minakami's original definitions relied mostly on depth restrictions, however through time, more specific terminology for classifying volcanic earthquakes was introduced (McNutt, 2002). The significance of the first part, or the onset, and the second part, the coda tail, of a signal are considered under the updated terminology. A review of volcano seismic processes by Chouet and Matoza (2013) details notable case studies from volcanoes exhibiting these characteristic earthquake types. Many of these classifications still carry a significant amount of interpretation and assumption about the specific source mechanism. Here, I carefully explain the different classifications defined in the literature. These are summarised in table 2.1 and figure 2.1.

Typically, high frequency (HF) seismicity is considered any volcanic seismicity with a majority frequency content >5 Hz. A-type earthquakes might be considered a subset of HF seismicity, as these earthquakes are typically defined with a higher frequency content, but have the imprint of interpretation in that they must occur $\geq$ 1 km below the surface. Today, the description for A-type earthquakes most closely matches that of volcano tectonic (VT) earthquakes. Much like A-types, VT signals look very similar to tectonic earthquake waveforms, with distinct P and S wave arrivals (fig 2.1b). In comparison to some other volcanic-earthquake types, they will likely have a very sudden onset with a clear first arrival, and a fundamental peak frequency between 5 and 20 Hz. In a movement away from A-type definitions, it is thought that VTs are generated by short, sharp failure events like fault slip

or brittle fracturing (McNutt & Roman, 2015). From the visual appearance of the signal waveform itself, these are indistinct from tectonic earthquakes.

Much like high frequency seismicity, we may consider all seismicity with a majority frequency component ≤ 1 Hz as low frequency (LF). The signal itself can be an individual earthquake, sustained tremor or even an explosion. Minakami's B- type earthquakes maybe be considered a subset of LF seismicity. Similarly, the more recently defined long-period (LP) earthquakes, may also be considered a subset of LF seismicity. LPs have more rigorously defined features that are a result of the proposed source mechanism. Much like B-type earthquakes, LPs do not show clear S wave phases and often the P phase is indistinct as the onset of the earthquake is more emergent. LPs typically have fundamental peak frequencies ≤ 5 Hz (Zobin, 2012), with a long, extended, monochromatic coda tail (fig 2.1a). LP earthquakes are thought to be associated with fluid processes, including magma, gas and hydrothermal interactions. An early study modelled crack waves as a two part process, an excitation followed by resonance of a fluid-filled crack (Chouet, 1988). This is reflected in the waveform as LPs tend to have a more broadband onset (excitation) but long, low frequency, coda tail (resonance) (McNutt, 2002). Typically LPs have a longer event duration than VTs, as a result of this long coda (Lees et al., 2008). Subsequently laboratory analogue studies and numerical models have attempted to create synthetic LP earthquake signals and demonstrate how subtly changing media can change the LP signal properties (Kumagai & Chouet, 1999, 2000). Some contrasting studies have demonstrated that the resonant coda tail in an LP earthquake is actually a product of the path and media rather than the source process (Bean et al., 2014). The vocabulary in volcano-seismology literature can be ambiguous and LP and LF are often used interchangeably when they actually refer to different categories of seismicity. It is therefore important to be clear about whether an earthquake meets all the criteria, including the signal properties and the source interpretation, to be defined an LP rather than a more general LF earthquake. Many earthquake catalogues will also separate earthquakes into LPs and VTs rather than LFs and HFs. These labels are often attributed by

trained monitoring agency professionals who have an intricate knowledge of the volcano and have some confidence in the source properties of these earthquakes. LPs and VTs generally are not bound by depth restrictions and we have evidence of both deep and shallow LPs and VTs. Therefore, although comparisons may be made between A-types and VTs, and B-types and LPs, these sets of earthquake categories are not completely identical.

If LP and VT are considered as two end member extremes of seismicity, then the earthquakes which sit between these two extremes have been labelled hybrid earthquakes (HYB). They exhibit both quite a high frequency and sudden onset, but also a low frequency long coda tail. Unlike the Minakami definitions, these HYB earthquakes are not depth restricted and we have records of both deep and shallow HYBs. Some argue that HYB earthquakes are generated by a similar excitation-resonance process as LPs, but with a more pronounced separation (fig 2.1c). Moran et al. (2008) demonstrate HYBs appearing in a transition from LPs to VTs during dome growth at Mount St. Helens in 2004. Just as attenuation and path effects were discussed in Minakami's definition of shallow B-type earthquakes, there is debate as to whether the fraction of high frequency signal retained is due to the source depth and as such distinguishes whether an event is LP or HYB (Neuberg, 2000).

LPs, VTs and HYBs have been described in a large variety of volcanic systems. Again, the detection and classification of these is dependent on the monitoring capabilities and subsequent interpretation. However, it is significant that seismicity that (at least broadly) matches these definitions, has been identified in a range of settings, from silicic (Waite et al., 2008) to basaltic magmas (Chouet & Dawson, 2011), and continental arcs (Anzieta et al., 2019) to intraplate volcanoes (Kumagai et al., 2005).

These three earthquake types dominate catalogues of volcanic seismicity and much of the literature. However, more detailed subsets and categories of seismicity have further been described. Again, these are defined by physical signal properties and interpretations of the source mechanism.

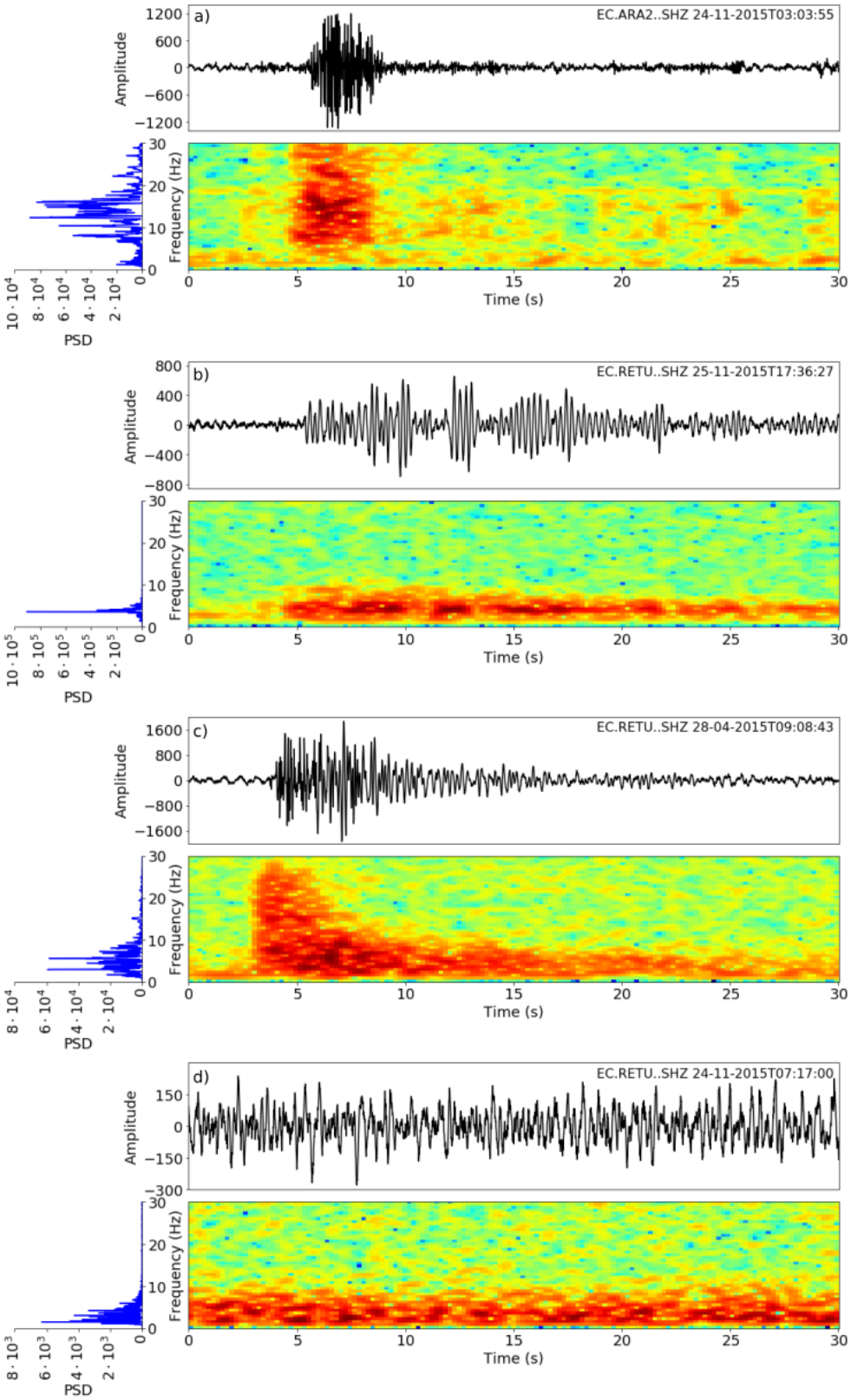
a)
EC.ARA2..SHZ 24-11-2015T03:03:55
Amplitude
Frequency (Hz)
PSD
Time (s)
b)
EC.RETU..SHZ 25-11-2015T17:36:27
Amplitude
Frequency (Hz)
PSD
Time (s)
c)
EC.RETU..SHZ 28-04-2015T09:08:43
Amplitude
Frequency (Hz)
PSD
Time (s)
d)
EC.RETU..SHZ 24-11-2015T07:17:00
Amplitude
Frequency (Hz)
PSD
Time (s)

Figure 2.1

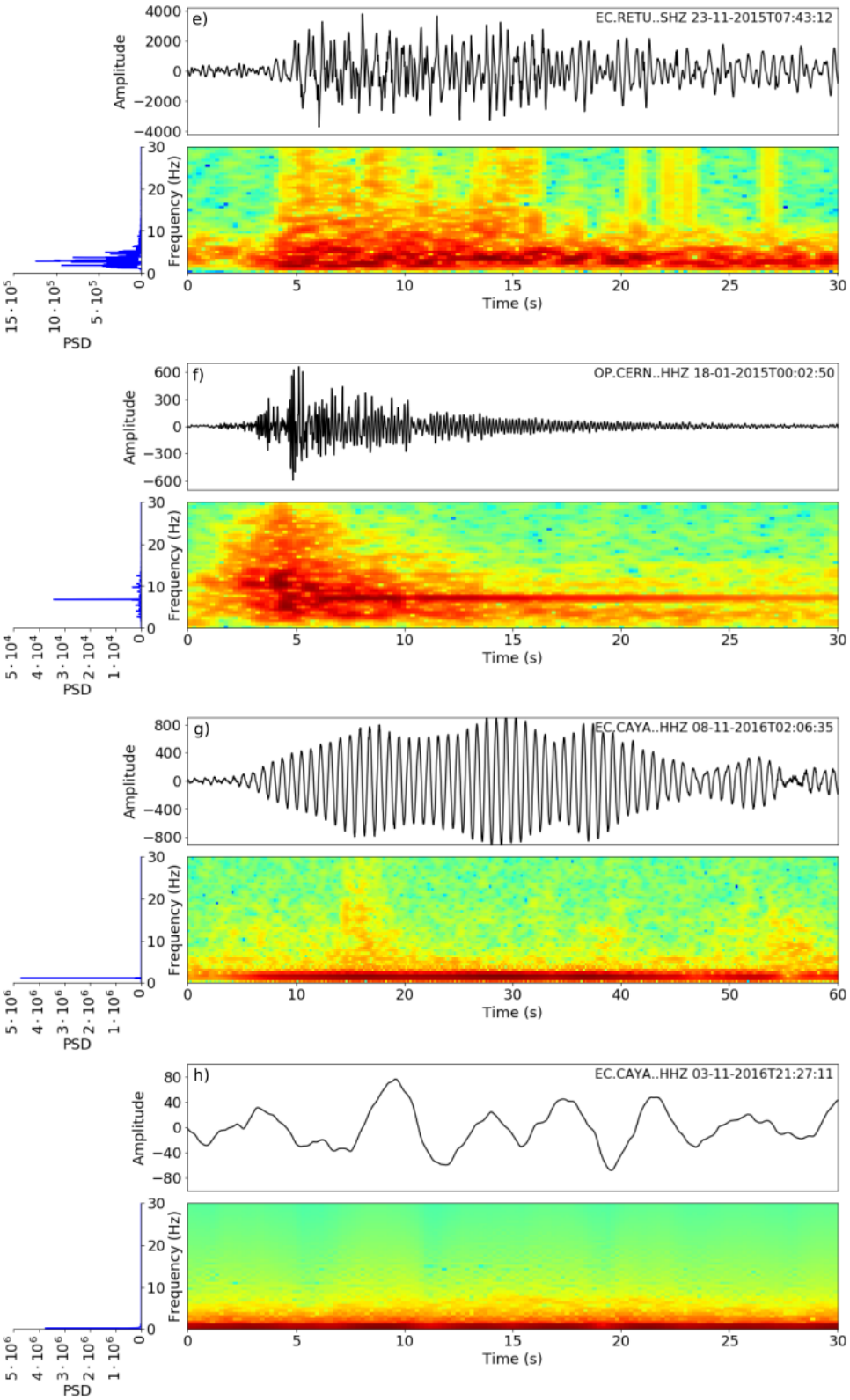
e)
EC.RETU..SHZ 23-11-2015T07:43:12
Amplitude
Frequency (Hz)
PSD
Time (s)
f)
OP.CERN..HHZ 18-01-2015T00:02:50
Amplitude
Frequency (Hz)
PSD
Time (s)
g)
EC.CAYA..HHZ 08-11-2016T02:06:35
Amplitude
Frequency (Hz)
PSD
Time (s)
h)
EC.CAYA..HHZ 03-11-2016T21:27:11
Amplitude
Frequency (Hz)
PSD
Time (s)

Figure 2.1 (Previous page.) *a)* Volcano-tectonic (VT) earthquake recorded at station ARA2 on Tungurahua, *b)* Long period (LP) earthquake at RETU station on Tungurahua, *c)* Hybrid (HYB) earthquake, RETU, Tungurahua, *d)* Continuous emission tremor, RETU, Tungurahua, *e)* Explosion (EXP) earthquake, RETU, Tungurahua, *f)* Tornillo earthquake recorded at station CERN in the Chiles-Cerro Negro volcanic complex, Ecuador, *g)* Very harmonic earthquake recorded at Cayambe volcano, station CAYA, *h)* Very long period (VLP) signal recorded at station CAYA, Cayambe.

For instance, with improved instrumentation over the last 20 years, earthquake signals with even longer periods have been observed. Very long period (VLP) earthquakes have frequencies 0.01–0.5 Hz and so broadband and long period seismometers are required to capture these earthquakes (Chouet & Matoza, 2013) (fig 2.1h). Much like their LP counterparts, VLPs are thought to originate from a resonating process. However, as these earthquakes are characterised by such a low frequency, it is thought they are associated with inertial changes in magma or gas flow. Unlike the A- and B-type definitions, VLP earthquakes are not constrained by depth and may be associated with shallow bubble dynamics, gas bursts in a conduit or pressure changes in a deep magma chamber (Dawson et al., 2010; Park et al., 2020). The signals with the lowest frequencies are known as Ultra long period (ULP) earthquakes. Much like VLPs, these rely on a dense seismic array of broadband stations as their frequencies are typically ≤ 0.03 Hz. ULP seismicity has been recorded during eruptions and attributed to pressure and volume changes in magma storage (Sanderson et al., 2010).

Volcanic tremor has also been recorded with a broad variety of characteristics across systems of all compositions. It was long thought that tremor is simply series of LPs repeating at very short intervals, such that the signal merges into one continuous event (Neuberg et al., 2000). Whilst this is certainly the case in some instances (Bell et al., 2018), more isolated episodes of tremor without LPs have also been documented (Sgattoni et al., 2017). Tremor with a dominant spectral peak frequency is known as harmonic tremor. This single frequency may be accompanied by weaker harmonic overtones at an integer separation from the peak (Roman, 2017). Identifying a dominant peak frequency in tremor may be indicative of a

particular geometry or process generating the tremor. For instance, Arámbula-Mendoza et al. (2016) identified harmonic tremor during unrest in 2000 and 2012 was associated with magma ascent and lava dome growth. Systematically increasing or decreasing fundamental peak frequencies occur in a phenomenon known as gliding harmonic tremor (Hotovec et al., 2013). As tremor can exhibit so many varying characteristics, there is a little poetic license around labelling further observations of tremor. For example, a review study of the seismic and infrasonic recordings at Reventador Volcano by Lees et al. (2008), also separates out pulsed and spasmodic tremor as two further sub-categories of tremor, where the amplitude is not always constant. Arámbula-Mendoza et al. (2016) cites the occurrence of spasmodic tremor with lava dome destruction, whilst Bell et al. (2017) notes that pulsed tremor between episodes of LP seismicity at Tungurahua could be due to changes in gas flux. Where there is a degree of confidence that tremor is a result of choked gas flow, tremor can also be called chugging (Johnson & Lees, 2000; Lees et al., 2008; Ruiz et al., 2006).

Further specific volcano-seismic earthquake types may be described and named as they are identified. Highly monochromatic, low frequency earthquakes recorded at Galeras, Colombia, set the benchmark for 'tornillos' (*tornillo* as the Spanish for screw, describing the characteristic waveform envelope, Narváez et al. (1997)) (fig 2.1f). Additional external complexities such as glaciers may also contribute to the seismic record. Basal slip from glaciers or hydrothermal networks may generate so called 'icequakes' (Jónsdóttir et al., 2009; Lamb et al., 2020; Métaxian, 2003). If lahars, landslides, pyroclastic density currents (PDCs) and rockfalls are commonplace at a particular location, then signals associated with these events may be catalogued accordingly. A summary of some examples of different volcano-seismic earthquake types can be seen in figure 2.1 and table 2.1.

Name	**Description**
High frequency (HF)	Any seismicity with a majority frequency content $\geq$ 5 Hz. The seismicity may be continuous signal (such as tremor lasting several minutes, hours or $\geq$days) or discrete earthquakes (lasting only a few seconds).
Volcano tectonic (VT)	A discrete high frequency earthquake, which is visually indistinct from a tectonic earthquake. The waveform is characterised by a rapid onset with clearly visible P- and S- phases. These events are often associated with brittle failure (fig 2.1a).
A-type	Defined by Minakami (1951). Visually indistinguishable from a tectonic earthquake, with clear P- and S- phases. Generated by a process $\geq$ 1 km beneath the volcano, but no restrictions on the process itself.
Low frequency (LF)	Any seismicity with a majority frequency content $\leq$ 5 Hz. The seismicity may be continuous signal (such as tremor lasting several minutes, hours or $\geq$days) or discrete earthquakes (lasting only a few seconds).
Long period (LP)	A specific type of discrete LF earthquake, defined by an emergent signal onset and indistinct S- phase. LPs are associated with fluid resonance processes. The signal reflects this process and is defined by an initial excitation, and a long single frequency coda tail (fig 2.1b).
B-type	Defined by Minakami (1951). Strictly associated with shallow processes $\leq$ 1 km beneath the volcano. They have no clear S- phase and lower magnitudes than A-type earthquakes. There is no definition on their source process.
Very long period (VLP)	Discrete LF earthquake with a majority frequency content 0.01 – 0.5 Hz, associated with fluid resonance. They may be considered a subset of LPs (fig 2.1h)

Ultra long period (ULP)	Discrete LF earthquake with a majority frequency content $\leq$ 0.03 Hz, associated with fluid resonance. They may be also considered a subset of LPs.
Hybrid (HYB)	Discrete earthquake with distinct high frequency onset and low frequency coda tail. The two components should be more pronounced than an LP, with an initial signal onset $\geq$ 5 Hz. There is no strict definition for the source process (fig 2.1c).
Tornillo	A particular type of LF earthquake with a distinct single frequency coda tail (fig 2.1f).
Tremor (TRE)	Signal of continuous amplitude lasting for minutes to days. Tremor can be high or low frequency. If the source of the tremor is known it may be labelled, for example, *Emission Tremor* (fig 2.1d).
Harmonic tremor	When a tremor signal is dominated by a single frequency (monotonic) or a single peak frequency with integer harmonics (fig 2.1g).
Spasmodic tremor	When tremor continues with an oscillating amplitude variations. This is also known as pulsed or pulsing tremor.

Table 2.1 Summary of volcano earthquake classifications.

2.2.2 Source processes

Alongside classifying and describing the volcanic earthquake signals, it is important to understand the driving source mechanisms for seismicity. Some of the broader earthquake classes are associated with characteristic source processes. Although seismicity should be interpreted carefully in the context of the rheology and recent eruptive history of the volcano. Figure 2.2 illustrates a summary of the possible source processes for volcanic seismicity.

The two broad extremes of volcanic earthquakes, LPs and VTs, are thought to be

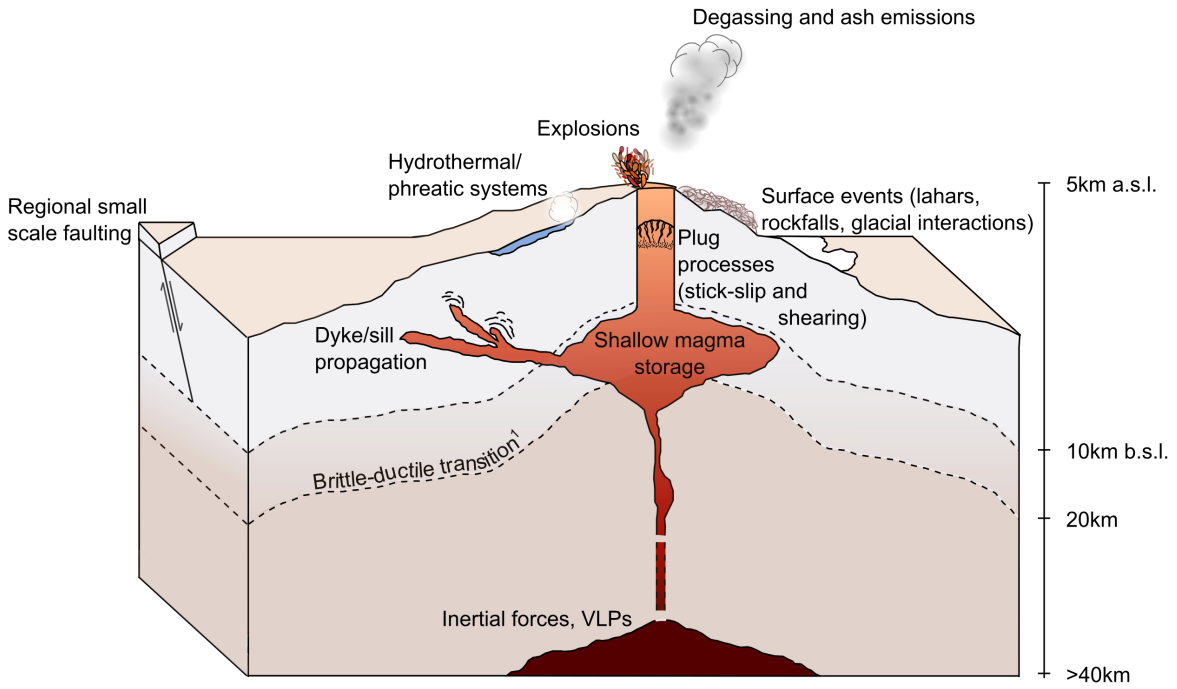

Figure 2.2 Schematic diagram illustrating volcano seismic source mechanisms.
[1] The brittle ductile transition zone beneath an active volcano depends on rheology, temperature and pressure conditions. Sample depths indicated here are a suggested range (Parisio et al., 2019)

generated by very different processes. LP seismicity is thought to be the product of a resonance process and so source mechanisms are often hinged on fluid movement including magma ascent, degassing and hydrothermal activity (Cusano et al., 2008; Petersen, 2007; Varley et al., 2010a). Early dynamic models proposed that a fluid filled crack could be excited into a state of resonance when a small pressure gradient is applied (Chouet, 1988). This is in contrast to VT events which are thought to be the result of brittle failure (Power et al., 1994). Magma may be involved in the overall process, but the source mechanism is specifically from rock failure. This may either be the propagation of existing fractures or slip on an existing plain of weakness. For example, an ascending pulse of magma may cause shear failure in the surrounding brittle rock, or a cooling and contracting magma body may lead to tensile failure of the host rock (Chouet et al., 1994). As such, the type of seismicity

may depend on the depth of the source process, particularly relative to the brittle-ductile transition zone. The depth at which this transition occurs is dependent on factors such as rheology and temperature-pressure conditions (Parisio et al., 2019). That said, this is not a fixed boundary condition for the existence of VTs or LPs and they often occur in conjunction with one another. For example during dyke propagation, VTs associated with rock fracturing may be seen before or in conjunction with LPs associated with fluid movement (Woods et al., 2018).

These dynamic models have been subsequently supported by laboratory analogue experiments. Microseismic signals, or acoustic emissions (AEs) are generated by high pressure deformation experiments. When scaled up appropriately to seismic frequencies both extremes of seismicity, LPs and VTs, occur as well as hybrid-style events (Benson et al., 2008). Furthermore, in a triaxial compression laboratory set-up, subtle changes in the coda and frequency of some events can even be controlled by varying gas pressures (Fazio et al., 2019). James et al. (2006) use a laboratory analogue experiment to demonstrate how gas slugs ascending a magma column can generate seismicity. If there is a sudden change in conduit geometry, perhaps from a constriction, then a resultant change in the flow regime can cause a sudden pressure gradient. This can cause velocity changes, even slug break up and LP and VLP seismicity. These experimental approaches minimise some of the speculation associated with interpreting volcano seismic events.

If there is sufficient network coverage, then located seismic events can often very clearly map out the responsible source mechanism and there can be more confidence in the interpretation. One of the most striking examples, comes from a study in Iceland where over 30,000 events were recorded across a 72-station network in 2014 - 2015. VT seismicity was used to clearly map the progression of dyke at Bárðarbunga, over the course of a week in August 2014 (Woods et al., 2018). Even without such a dense network, analysis of from first motions from a handful of stations, in conjunction with a numerical modelling from synthetic waveforms, can reveal the most likely source mechanism of the seismicity (Chouet

et al., 2010; Chouet et al., 2003). Figure 2.3 is adapted from Chouet and Matoza (2013). First motions from VLP events at Stromboli, pinpoint the source location as a change in the flow regime, and these can be mapped to flank vent locations to suggest the likely path of dyke propagation (Chouet et al., 2008). However, detailed studies like these can only be undertaken where earthquakes are clearly recorded on multiple stations in a network, with a good distribution around the volcano.

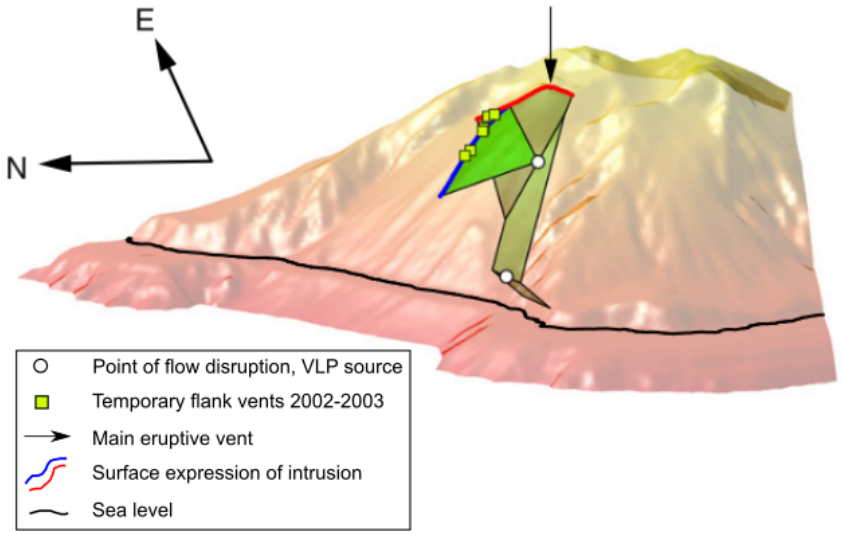

Figure 2.3 Adapted from Chouet and Matoza (2013) and Chouet et al. (2008). First motions of VLP events and surface expressions can be used to map most likely dyke propagation pathways at Stromboli, Italy in 1997. White circles show the locations of the VLP mechanism, green squares show positions on the flank where venting occurred between 2002 and 2003, and the arrow indicates the main explosive vent.

It is the very shallowest sources of seismicity that present perhaps the most conflict in the literature. Earthquakes located in the upper 5 km of the volcano may be indicative of imminent activity; as this source is now shallower than the brittle-ductile transition and may be a process associated with magma ascent in the conduit (White & McCausland, 2019). In the case of a sealing plug at the top of the conduit, it is thought that a stick-slip mechanism between the magma plug and conduit margins can cause LP seismicity (Iverson, 2008).

Whilst others present a model whereby ascending magma exerts a shear stress on the conduit walls, causing the magma itself to undergo brittle failure (Neuberg et al., 2006). Further models for this shallowest seismicity and plug processes are often something of a hybrid of these ideas, and specific to individual observations (Bain et al., 2019; Bell et al., 2017; Gaunt et al., 2020). Shallow hydrothermal systems, glacier cover and weak, unconsolidated edifices can also complicate the seismic record and generate very shallow earthquakes (Cusano et al., 2008; Hickey et al., 2020; Jónsdóttir et al., 2009). These need to be carefully distinguished from magmatic processes.

Complex, long sequences of volcanic seismicity are best interpreted with input from field data, numerical models, historical eruption evidence and, where suitable, laboratory analogues. Sequences of hundreds or thousands of events, in what is known as swarm seismicity, may be indicative of a more sustained long term source mechanism. Seismic swarms may be precursory to an explosive event (Chouet et al., 1994), associated with an eruption process such as dome collapse (Hammer & Neuberg, 2009), or occur following an explosion (Kim et al., 2014). Seismic swarms which are exlusively LPs, VTs or a mixture of both might be indicative of the source process (White & McCausland, 2019). High seismic event counts can be concerning when actively monitoring a volcano and so it is important to understand the source processes and the significance of these episodes, and where they sit within the narrative of the eruption.

2.2.3 Drumbeat seismicity

The most curious and arguably, most poorly understood strand of volcanic swarm seismicity, is a phenomenon known as drumbeat seismicity. There is no clear established definition of drumbeats in the literature as they are uncommon and observations vary. It is not clear whether the rarity of drumbeat seismicity in the published literature is because they have not been occurring, or they have not been successfully recorded and analysed. Just as with

LF and LP seismicity, there is a distinction to be made in the terminology. There is no strict definition for what qualifies as drumbeat seismicity, and this may also contribute to the hesitancy to publish studies of drumbeat seismicity. Generally, any swarm of earthquakes which exhibit a constant repeating inter-event time, are best described as quasi-periodic seismicity. If the recurrence time between earthquakes is particularly periodic and however, these are what are generally referred to as drumbeats. If the earthquakes in a swarm also have very similar waveforms, it is suggested they are from a similar repeating source (Pallister et al., 2013). Drumbeat sequences may be LP or VT sequences, although LPs are more commonly reported in the literature. These have been observed in volcano seismic records from the field (Bell et al., 2017; Lees et al., 2008; Power & Lalla, 2010) and generated under controlled situations in the laboratory (Kendrick et al., 2014). As is the case with many volcanic earthquakes, drumbeat seismicity episodes have been observed with a variety of characteristics in terms of spatial and temporal rate and magnitude, however, the broader phenomenology of drumbeats is still poorly understood. When these drumbeats occur in such quick succession (separated by 10^0-10^1 seconds), it has been suggested that they are generated by a single non-destructive source that is able to quickly recharge (Petersen, 2007). Due to the variety of drumbeat behaviours, a number of different physical models have been used to describe their source mechanism.

2.2.4 Observations of drumbeats during volcanic unrest

LP event swarms and drumbeat seismicity have been observed at different volcanic systems around the world. Figure 2.4 illustrates some examples of swarm seismicity in terms of earthquake rate and amplitudes. In these studies, some explicitly define the swarm as a drumbeat sequence, whereas others use the broader description of 'LP swarm' or 'VT swarm' and go on to describe temporal patterns in the earthquake rates, which exhibit quasi-periodic behaviour. Due to the limited number of reported 'drumbeats' in the literature, these are

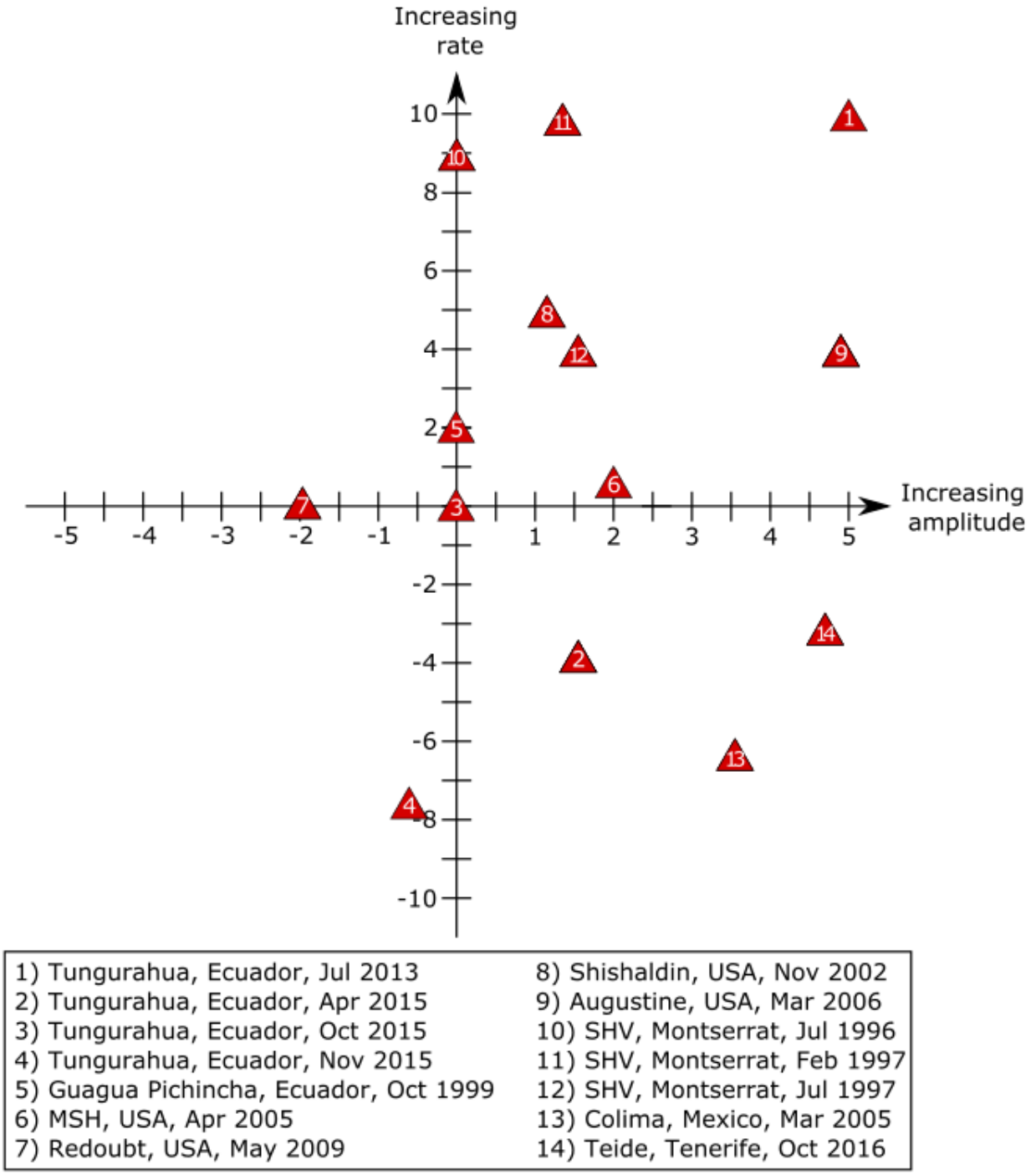

Figure 2.4 Global volcanic drumbeat seismicity studies presented in terms of rate of occurrence and amplitude changes. Due to the small number of drumbeat episodes presented in the literature, these are not all precursory or following an explosion. These episodes span from hours to days in duration, and are discussed in the text. These are relative changes in rate and amplitude, within each episode of unrest. The values on the axis represent the relative change from the start to the end of the period of interest.

not exclusively precursory, or associated with explosions. Some episodes last just hours, whereas others last several days and they're detailed in the rest of this section. There is no standard for reporting the amplitude of earthquakes as this is dependent on network capabilities. Amplitudes can be reporting as a maximum, a root-mean squared maximum (RMS) or if possible, a local magnitude. As such, in figure 2.4, changes in event occurrence and amplitude are plotted as a relative change from the start to the end of the period of interest.

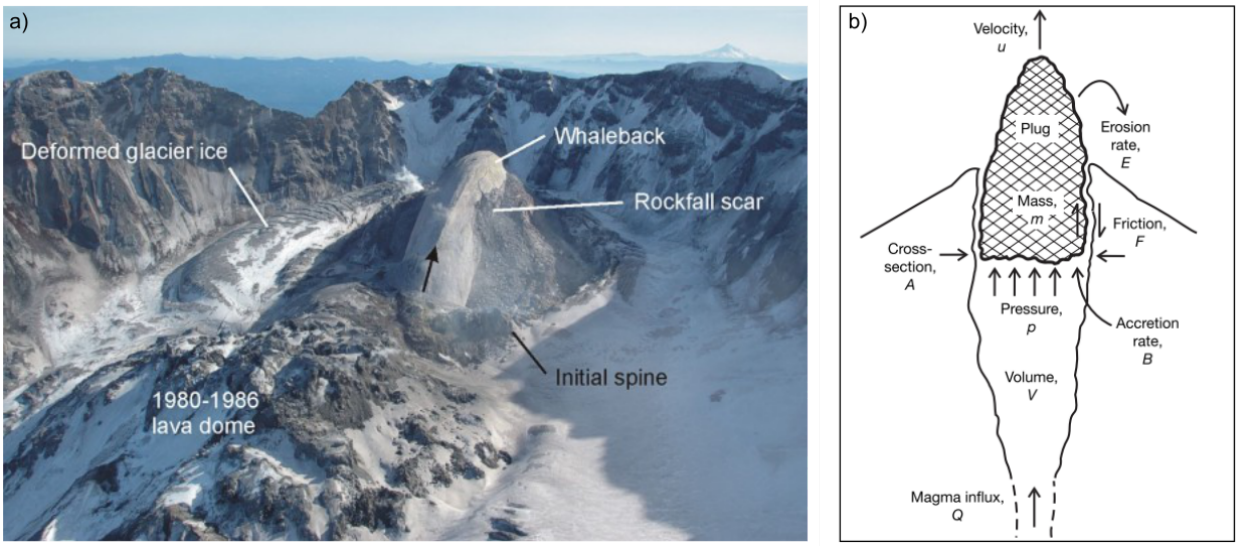

Figure 2.5 Drumbeat seismicity associated with spine extrusion events at Mt St Helens: *a)* Adapted from Major et al. (2005), a *USGS Fact Sheet* on the reawakening of MSH in 2004. Extruded whale back spine marked, and *b)* The plug stick slip model proposed by Iverson (2008).

The clearest, and perhaps the most famous, case study of drumbeat seismicity comes from Mount St. Helens (MSH). During 2004 and 2005 a series of drumbeats occurred during 'whaleback' spine extrusions (fig 2.5). This process generated several months of persistent drumbeat seismicity. The seismicity was modelled as a stick-slip process, where periodic earthquakes were repeatedly generated by friction between the spine material and conduit margin (Iverson, 2008). A study by Moran et al. (2008) examined individual episodes of the drumbeat activity in closer detail. The change in amplitudes and rate of seismicity in each

episode was strongly correlated, such that if the rate increased, so did the amplitude and the same was true where a decrease was seen (fig 2.4). The rate and amplitude variations in the drumbeats correlated with the extrusion style but not necessarily the magma flux, suggesting the drumbeats are controlled by the mechanics of the extrusion (Moran et al., 2008).

These increases in rate and amplitude are smaller than in swarms seen at some of the Alaskan volcanic systems. During a period of relative quiescence at Augustine volcano in March 2006, an episode of drumbeat seismicity was recorded. The rate of these earthquakes accelerated until individual events merged into tremor (Power & Lalla, 2010). This period of unrest was also associated with an instance of blocky lava effusion. Swarms of LP seismicity were also identified in four distinct episodes at Shishaldin volcano between 2001 and 2002 (Petersen, 2007). Given the volcano is known to have been persistently degassing during this period, it is believed LP swarms were a product of choked flow in the conduit and interaction with a shallow, complex hydrothermal system. In November 2002, the amplitudes of LP swarm events gradually increased over a period of 7-10 days, before a sudden pressure drop and reduction in event amplitudes. These changes in the waveforms correspond to changes in the hydrothermal systems being activated. This is in contrast to seismicity recorded at the reawakening of Redoubt volcano in 2009. A series of different LP swarms are documented between February and May. Much like at Augustine volcano, Hotovec et al. (2013) cite the use of frequency analysis tracking LP seismicity that merges into tremor to understand changes in source processes. Buurman et al. (2013) discusses six different episodes of drumbeat seismicity in 2009. Most do not show systematic variations of rate or amplitude with time, with the exception of one swarm on 29 March. This episode was attributed to dome growth. Initially events were increasing in amplitude as a stick-slip process in the conduit generated seismicity. As the extrusion continued, the conduit widened causing a weakening of the shear failure source and as such a decreased amplitude for the resultant earthquake events. Dome growth eventually became aseismic.

In contrast to the Alaskan volcanoes, Soufrière Hills Volcano (SHV) in Montserrat has demonstrated a number of consistently similar drumbeat style seismic episodes during it's reactivation in 1995 - 1997. This is a more andesitic system than Mount St Helens, and so contrary to previous models of stick-slip processes, drumbeat seismicity here was attributed to repeated brittle failure of and healing of magma at conduit margins (Neuberg et al., 2006). As a body of magma ascends, there is increased strain on melt at the conduit margins, and brittle failure occurs (Tuffen et al., 2003). Magma with brittle behaviour nears the glass transition; shear failure at the conduit walls acts as a trigger and resonance of that wave in the conduit completes the LP coda. Drumbeats at SHV occurred in very uniform and periodic cycles. Whilst their amplitudes have rarely been noted to change, that rate of seismicity in drumbeat episodes has been seen to accelerate up to dome collapse events (fig 2.4) (Green & Neuberg, 2006; Hammer & Neuberg, 2009).

Two case studies that sit apart in figure 2.4 are drumbeats observed at Volcán de Colima in Mexico and Teide in Tenerife. Varley et al. (2010a) identified a number of episodes of drumbeat seismicity associated with Vulcanian explosions in 2005 at Colima. In some instances the seismicity was very reactionary to explosive behaviour and changed remarkably, whereas some episodes the seismicity persisted despite ongoing explosions. Both March and June saw instances where amplitudes increased and rates decreased surrounding explosions. Whereas later in the year, in September, the seismicity was much less affected by explosions. In this case it was thought that the Vulcanian explosion acted to reduce the loading on magma in the conduit, and so ascent accelerated, increasing amplitude. As the conduit relaxed, the rate at which seismicity is generated slows. At Teide volcano a much more slow and progressive increase in amplitude and decrease in event rate persisted over several hours. The seismicity was thought to be generated by a pressurised hydrothermal system which was likely triggered by a much deeper magmatic injection process (D'Auria et al., 2019).

Drumbeat seismicity has also been reported at Tungurahua, Ecuador. Studies in the literature include a sequence of accelerating rates of events in July 2013 (Bell et al., 2018)

and the step-wise breakdown of a sequence of distinct drumbeat phases in April 2015 (Bell et al., 2017). These episodes both show increasing rates of events and plot in the top right quadrant of figure 2.4. Both studies suggest the source of the LP seismicity is associated with shallow conduit processes and a sealing upper conduit plug. Between 2013 and 2015, Tungurahua exhibited very periodic 3-4 month cycles of Vulcanian eruptions (Hall et al., 2015). However, there have been no long term studies of the seismicity during this process.

2.2.5 Summary

In 110 years of volcano-seismic studies there has been an enormous variety of observations and models presented in the literature. There is a fine balance to be struck between quantifying seismicity in great detail, and over-interpreting such that one model cannot be applied at any other volcano. Currently, simple classifications such as LP and VT seismicity act to conceal important variations in volcanic earthquakes caused by very different source mechanisms. However, over-complicating a classification system could lead to confusion and ambiguity in the terminology used. It is clear that there needs to be a better way to characterise seismicity in a quantitative as opposed to a qualitative manner. These quantitative metrics should be presented in a standardised unit to ease the comparison of analyses globally.

Understanding the seismicity associated with shallow conduit processes is particularly complex. In the upper few kilometers of the edifice, shallow magma storage, exsolved volatiles, hydrothermal systems, surface events such as lahars ad debris flows, and flank instability can all act to generate and complicate seismic signals. Much like the classification of volcanic earthquakes there is a need to refine the models for sources of shallow volcanic seismicity without over-simplifying, as understanding shallow conduit processes is crucial to informing future hazard assessment. In particular, it is concerning how little is understood of the phenomenology of drumbeat seismicity. Figure 2.4 demonstrates how the rates and amplitudes of drumbeat earthquakes, can occur on very different scales, even within the

same volcano. Drumbeats have also been linked with the shallowest magmatic processes and often cited as a precursor to explosive activity and yet there is no agreement on the source processes for these earthquakes.

In this review, examples where seismicity is well modelled, are from heavily monitored volcanoes where depths and focal mechanisms can be readily constrained. However, these processes exist in volcanoes regardless of how well monitored they are. There is an urgent need to study and develop reproducible analysis for seismicity observed at poorly-monitored volcanoes. Such volcanoes are more likely to be in middle to lower income countries where failure to suitably assess and model volcanic hazards, would have disastrous implications.

2.3 Case study locations

Ecuador is home to the striking landscape of the NAVZ. The volcanic arc spans over 600 km along the length of the country, but is only 180 km at its widest point. Either side of the arc, there are the plains towards the coast in the west, and to the east, the Amazon basin (Coltorti & Ollier, 2000) (fig 1.1). The arc is separated into the Eastern and Western Cordillera, by a central Andean high plateau. Volcanoes reach over 6000 m elevation, whilst the high plateau sits at approximately 3000 m. Ecuador is home to 55 active volcanoes, including the Galapagos archipelago, 1400 km from the west coast (Global Volcanism Program, 2013b). A number of these intermediate composition stratovolcanoes, including Tungurahua and Cotopaxi volcano, are particularly high risk (Kumagai et al., 2007). More than 20,000 people live on the flanks of Tungurahua, whilst summit glaciers on Cotopaxi pose significant risk for long-running lahars towards the capital city, Quito. Subduction of the Nazca plate to the west of Ecuador, also means the country is exposed to the risk of large mega-thrust earthquakes (Yepes et al., 2016). Most recently, this includes an offshore M_w7.8 thrust earthquake in April 2016 (He et al., 2017), although Ecuador is also often impacted by large thrust earthquakes in continental crust below Peru and Chile. These

conditions make Ecuador a particularly interesting and diverse setting to study geophysical hazards. A community that faces multiple geophysical hazards, such as volcanic eruptions and major tectonic earthquakes may be vulnerable to cascading hazards and increased risk. Coordinating the national effort to monitor these geophysical hazards is Instituto Geofísico de la Escuela Politécnica Nacional (IGEPN) based in Quito. IGEPN established in 1983 and to date, maintain permanent geophysical instrumentation networks across 20 volcanoes as well as monitoring tectonic earthquake hazards.

The data analysed in this thesis are kindly provided by collaborators from IGEPN. This includes raw seismic waveform data, radial tilt data and catalogues of earthquake pick times. Archives of daily reports, special issue bulletins and detailed studies following significant eruptions are all available from the IGEPN website (https://www.igepn.edu.ec/red-de-observatorios-vulcanologicos-rovig). Key visual observations during eruptions and quantitative data such as gas flux are extracted from these reports. In this thesis, I will be concentrating efforts on two volcanoes in particular, Tungurahua and Cayambe. In many aspects these volcanoes are comparable - andesitic-dacitic arc stratovolcanoes in the Eastern Cordillera, with significant populations of tens of thousands of people within 15 km. Both are monitored with permanent networks of seismometers, gas flux stations and tiltmeters. Understanding the eruption styles and typical characteristic seismicity at these volcanoes is crucial to inform hazard assessment and forecasting activity. However, Tungurahua began erupting in 1999 and continued until 2016, whilst Cayambe volcano last erupted in 1785. And so there are very different amounts of literature and information available about eruptions at each of these volcanoes. A number of seismic studies at Tungurahua are cited in section 2.2.4, and recent explosive activity has encouraged field campaigns to study ejecta and tephra fallout. Whereas, at the time of writing, there has been just one published study, on the seismicity at Cayambe volcano, and is focussed specifically on hybrid earthquakes. Both Tungurahua and Cayambe have the potential to be very dangerous in the instance of another eruption, and yet are relatively understudied.

2.3.1 Tungurahua Volcano

Eruptive history

Tungurahua volcano is a 5,023m high andesitic stratovolcano in the Eastern Cordillera of the Ecuadorian Andes. It has has extreme relief over 3200m, steep flanks and an asymmetric, north-westerly facing open crater (Ruiz et al., 2006). The present cone is the third major edifice on this site. Each previous andesitic cone was destroyed by one or more sector collapse events, and Tungurahua III has grown to around half the size of Tungurahua II, following collapse ∼3,000 years ago (Hall et al., 1999) (fig 2.6). In this most recent phase, major eruptive events have occurred approximately every 100 years, with known events in 1640-1641, 1773-1777, 1886-1888 and 1916-1918. Erupted product compositions have ranged from basaltic andesites to dacites (Le Pennec et al., 2008). Activity resumed at Tungurahua in 1999 and for the first 7 years of this eruption, activity was dominated by episodes of Strombolian and Vulcanian type explosions, interspersed with quieter periods of passive emissions of gas and ash (Arellano et al., 2008). Significant sub-Plinian activity began in July 2006 with pyroclastic density currents (PDCs) and an ash plume extending 14 km above the crater (Steffke et al., 2010). These were the first PDCs observed in this recent phase of activity and marked a distinct shift to a new style of eruption. 2013 and 2014 were characterised by episodes of Vulcanian explosions corresponding to plug formation and destruction cycles. These cycles occurred with a period of approximately 3-4 months and typically generated modest eruptions. This episodic behaviour commenced with an intense Vulcanian eruption in July 2013, which infrasonically, was one of the most powerful eruptions recorded globally (Anderson et al., 2018; Gaunt et al., 2020). Tungurahua was well monitored through this time frame and PDCs are well documented with field studies, video footage and seismic records in Hall et al. (2015). Throughout 2015 moderate explosions continued, but less periodically, whilst substantial cycles of inflation and deflation were recorded (Hickey et al., 2020; Neuberg et al., 2018). Drumbeat seismicity has been documented at Tungurahua

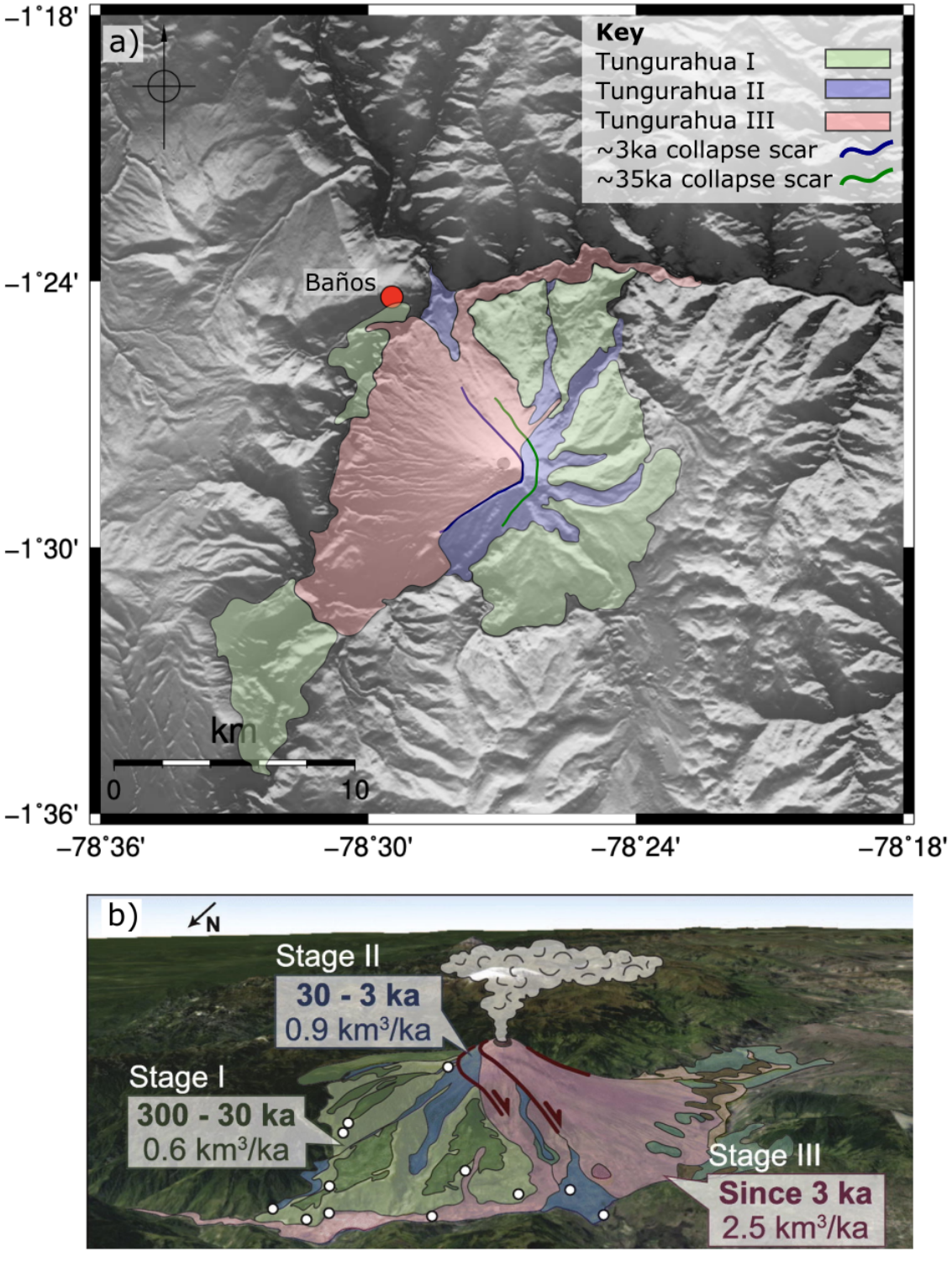

Figure 2.6 Adapted from Bablon et al., 2018. a) Simplified map illustrating the locations of the main units remaining from Tungurahua I, II and III. The scar faces from the last two major collapse events are indicated. b) The graphical abstract from Bablon et al., 2018 which shows the units mapped onto a 3D topographic image.

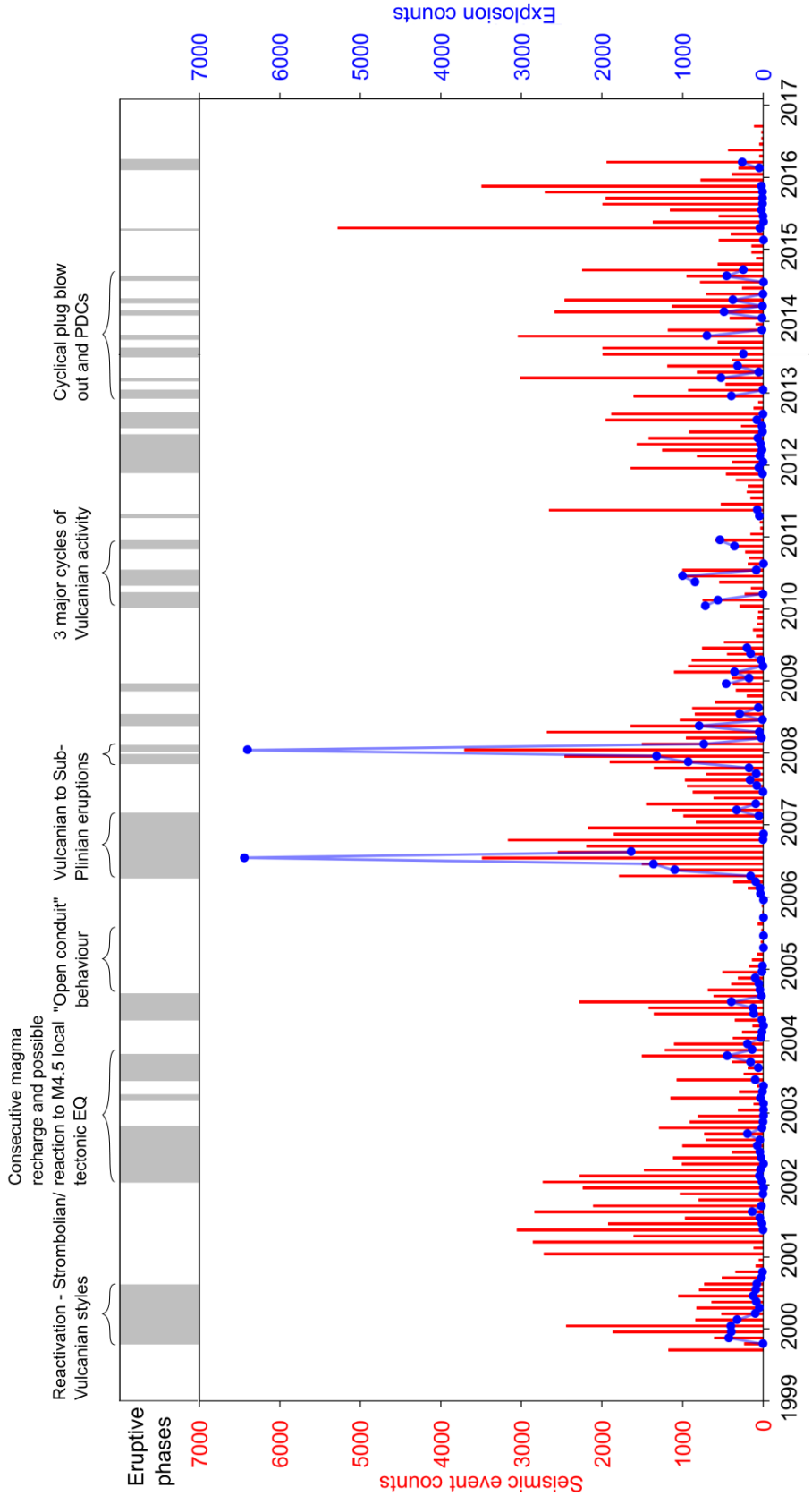

Figure 2.7 Seismicity history at Tungurahua. Red bars show monthly seismic event counts and blue circles mark monthly explosion counts. The top panel indicates periods of eruptive phases and annotations detail specific eruption styles.

both in 2013 and 2015. There was a brief repose period before the final explosions in February and March 2016. Since 2016, activity has been minimal at Tungurahua, with only 1-2 VT events occurring each day. Isolated periods of heightened LP seismicity in September 2016 were accompanied by fumerolic activity at the crater (Global Volcanism Program, 2018). Seismic event counts and explosions are marked in figure 2.7 and the different styles and eruption phases are marked. At the time of writing, Tungurahua has been quiet for five years and it is thought the system has, for now, 'switched off'.

Monitoring network

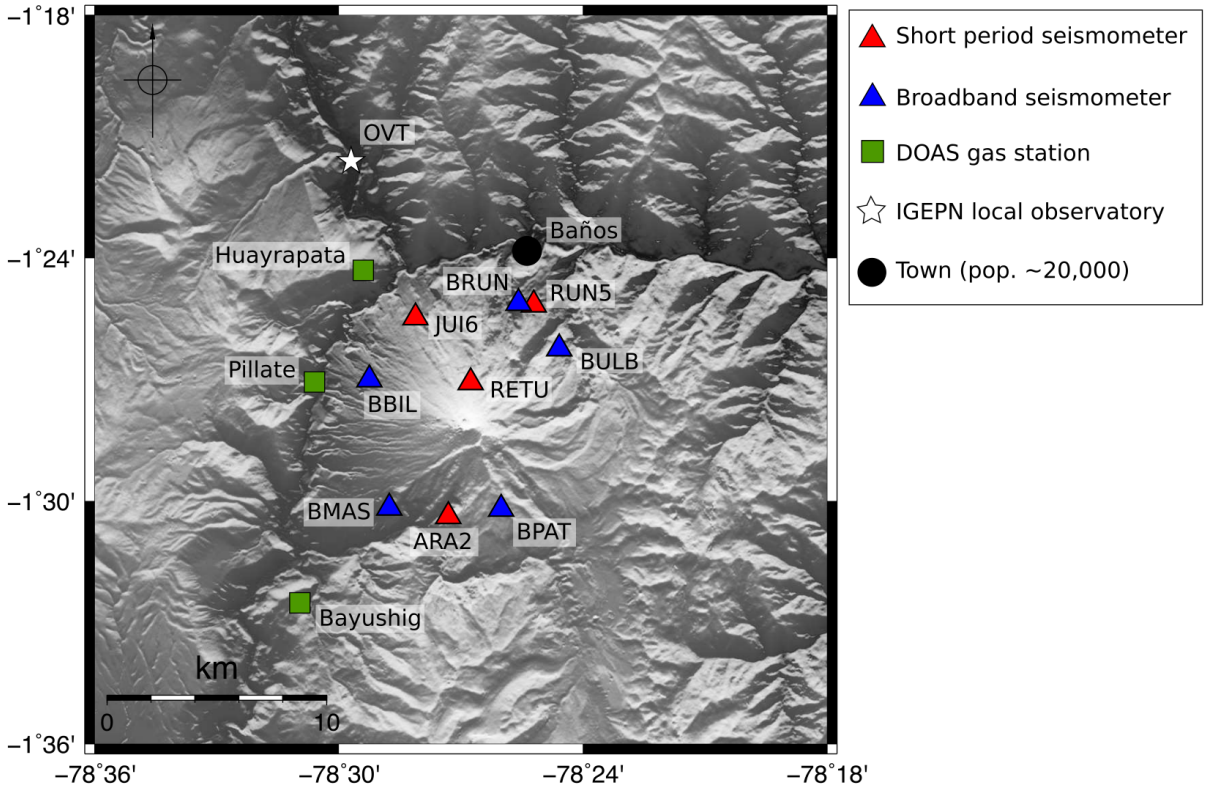

Figure 2.8 Map of geophysical monitoring efforts on Tungurahua. OVT is the local observatory operated by IGEPN. Local popular tourist town, Baños, is also marked.

Tungurahua is monitored locally by IGEPN. There is a permanent network of broadband and short period seismometers and Differential Optical Absorption Spectroscopy (DOAS)

gas flux stations. Broadband seismometer stations are also fitted with GPS and tiltmeters (fig 2.8). IGEPN also maintain a catalogue of recorded seismic events. Where possible these are labelled by earthquake type (LP, VT, HYB, TECT) and if possible, depth and magnitude estimates are provided. Despite best efforts from IGEPN to maintain the monitoring network, the seismic network has limited capacity. Altitude and weather conditions on Tungurahua mean that solar powered batteries are unreliable and station outages are common. Due to the steep relief, only one short period station, RETU, is positioned on the very upper flanks of Tungurahua and is sensitive to the shallowest seismicity. As well as being centrally monitored by IGEPN in Quito, a local observatory, *Observatorio del Volcán Tungurahua* (OVT) was established after the onset of activity in 1999. Located just 13 km NW of the volcano, it has a good line of sight to the crater. The observatory was manned 24/7 by a team of scientists on rotation. Once activity had significantly subsided in 2017, the decision was made to reduce the operational working hours at OVT to just a few days a week. Staff at OVT were supported by a network of volunteer watchkeepers, known as *vigías*, who would document daily observations of surface activity. They are situated all around the flanks Tungurahua and have a direct radio to IGEPN monitoring staff (Mothes et al., 2015). The IGEPN have archives of daily, weekly, monthly and special bulletins, documenting specific eruptions, available online (https://www.igepn.edu.ec/tungurahua-informes). These detail, where possible, seismic event counts, gas flux measurements, ash plume heights, lahars and descriptions of ash fall in different locations.

Seismicity

Although different eruption styles have dominated different phases between 1999 and 2016, generally seismic unrest at Tungurahua has been characterised by unsually high rates of LP seismicity. In the IGEPN catalogues of recorded seismic events, which span September 1999 to September 2016, over 97% of labelled events are LPs. Due to the instrument locations on Tungurahua, LPs related to shallow source processes are often only seen clearly on short

period station RETU (fig 2.8). The instrument response for the L4C short period station, RETU, is shown in figure 2.9. Data from RETU are only robust ≥ 1 Hz. When initially processing waveform data, the signal should be filtered ≥ 1 Hz to eliminate any erroneous data points or interference that could be misinterpreted as true signal. At the other extreme, the Nyquist frequency is 50 Hz for these stations. Although VTs have been recorded with frequencies up to 30-40 Hz (Chouet & Matoza, 2013), waveforms should also be bandpass butterworth filtered ≤ 40 Hz to eliminate any signal associated with external events such as rockfalls (Feng et al., 2019). By examining the signal in the window 1 – 40 Hz, it is still possible to clearly distinguish LF and HF seismicity.

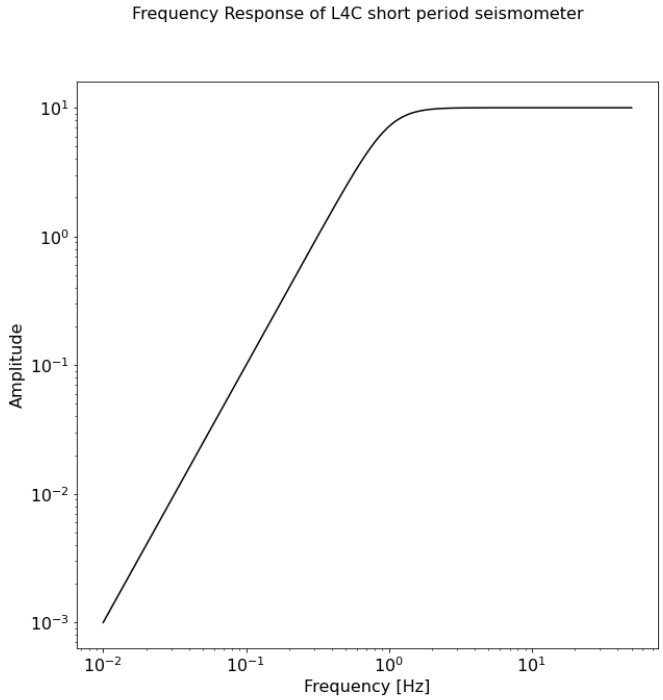

Figure 2.9 Short period instrument response for L4C seismometer used at RETU, Tungurahua.

If careful filters are used then occasionally the largest LP events may be recorded at the more distant broadband network, however the broadband stations generally are most useful to examine distal VT events and tectonic earthquakes. Observations from a single

station unfortunately means that depth location and moment tensor solutions cannot be determined. Studies of the LP seismicity need to be carefully planned and rely on only single station and single component data. This has perhaps limited the number of published studies on Tungurahua, despite the complex and detailed seismic record available.

There are a few published studies of LP seismicity at Tungurahua. For example, an early article examined a swarm of LP seismicity in December 2001 (Molina et al., 2004). Careful analysis of individual event waveforms indicated an evolving process which was attributed to repeated injection of increasingly ash laden gas. This systematic change was quantified with the Q factor (further discussed in section 3.4 of this thesis). Two episodes of drumbeat seismicity recorded at Tungurahua have been presented in the literature, in July 2013 (Bell et al., 2018) and April 2015 (Bell et al., 2017). The first demonstrated increasing rates of earthquake counts and increasing amplitudes in LP events before merging into tremor and explosion. The April 2015 drumbeats show a distinct step-wise breakdown with unique families of events dominating consecutive phases of seismicity prior to small explosions (fig 2.4).

Seismo-acoustic studies have focussed on describing source processes around major explosive events at Tungurahua. Kim et al. (2014) were able to constrain the source process during explosions in May 2010. Moment tensor inversions from stacked VLP signals at broadband stations, localised a source to 1.5 km below the crater. By cross correlating with the infrasound recordings they were able to identify two distinct phases in the episode - a deep seismic event, and a subsequent surface explosion. An analogous but much deeper process is documented early in February 2010 (Kumagai et al., 2011). Both low and high frequency components of the event were analysed separately to identify an initial source mechanism 6 km below the crater. It was then inferred, from the delay time in the infrasonic pulse and waves speed models, that this deep seismic event triggered a pressure wave to ascend the conduit. Distinct pulses of gas emissions and jetting behaviour have been characterised by shallow seismic source signals (< 200m) and infrasonic data during 2004 (Ruiz et al., 2006).

Research has concentrated primarily on large explosive events in the 1999-2016 eruptive phase - not only because there were plenty to analyse, but also as they pose the largest risk to local communities. However, there have also been significant episodes of unrest that do not culminate in explosions. This is particularly the case in 2015, where there were high rates of seismicity, co-incident with significant inflation and deformation cycles. A rare swarm of several hundred VTs in November 2015, prompted a cross disciplinary study to examine internal processes. Using InSAR deformation data and seismic event counts, Hickey et al. (2020) identified an injection of magma and shallow storage along a plane of weakness at the fault scarp from the edifice collapse event 3000 years ago (Hall et al., 1999). Numerical models have also been used to constrain the complex relationship between magma flow and strain at the conduit margins (Marsden et al., 2019). This study suggested that LPs can be the product of shearing at the conduit margins, similar to processes described at Soufrìere Hills Volcano (Neuberg et al., 2000) and are therefore not always indicative of magma ascent or imminent eruption. These seismicity studies cover a small portion of the 17 years of activity at Tungurahua and many episodes of unrest have not yet been investigated and published.

Community

To contextualise the discussion around Tungurahua, the view from a roadside viewpoint, overlooking the north-west flanks of the volcano is shown in figure 2.10. The nearby town of Baños, population 20,000, is nestled in a river valley just at the base of the northern slopes of the volcano. Baños is also known as *'the gateway to the Amazon'* and is a popular spot for tourists. Alongside this, there are a further 10,000 people considered to be living in high risk areas in rural and agricultural communities. Also marked in figure 2.10 are pyroclastic deposits, whilst old lava flows can be identified in dark grey lobes where the land cannot be farmed. Marked in red is a major road connecting rural farming communities on this north west side of Tungurahua. This road has been rebuilt across the pyroclastic deposit. There is

Figure 2.10 North west flanks of Tungurahua. Inset, elevation map of area. Viewpoint location for photo marked in red. Nearby town of Baños is marked. White dashed lines show recent pyroclastic deposits. Red dashed line marks roads, including a major connecting road which has been rebuilt over recent volcanic deposits.

a complex history between the local community, scientists and civil defence. A review paper by Mothes et al. (2015) presents the successes and challenges surrounding the monitoring of Tungurahua since 1999. The unique relationship between the scientists, the volunteer *vigía* network and the community has taken time to balance. Identifying geophysical precursor signals, effectively communicating hazard and risk, and maintaining good relationships are cited at the biggest challenges faced in monitoring efforts. Lessons learned in retrospect and including hind-casting and understanding past eruptions at this volcano, may be useful for similar community groups and volcano monitoring teams at other intermediate composition volcanoes.

2.3.2 Cayambe Volcano

Eruptive history

Cayambe Volcano, lies at the northern end of the Eastern Cordillera, just 60 km north of the capital, Quito (fig 1.1). The complex is a notably large volcanic centre, with a peak elevation of 5790 m (Guillier & Chatelain, 2006). Cayambe is defined by three volcanic cones, and bound by regional fault to the north east, 'La Sofía-Río Chingual'. Old Cayambe forms the majority of the western flanks of the present day complex but has been significantly eroded. Lava flows are mostly andesitic although punctuated with rhyolitic pumice deposits, suggesting episodes of explosive activity. A caldera forming event around 1 million years ago marked the end of Old Cayambe (Samaniego et al., 2005). The more recent Nevado Cayambe, a composite cone, has been built over the eastern flanks of Old Cayambe. Nevado Cayambe is thought to have had three main volcanic edifices aged from 600 ka to the youngest Holocene stratocone (Samaniego et al., 2005) (fig 2.11). Detailed tephrochronology studies identify 21 eruptions in the last 4000 years including cycles of lava dome extrusion and collapse events (Samaniego et al., 1998). One of the largest collapse events, thought to be 200,000 ka, generated a 3 km wide horseshoe shaped scar on the western flank. This sits at the upper end of the Río Blanco Valley - one of a number of rivers that flow towards and into the towns of Cayambe and Ayora, below the western flanks (Detienne et al., 2017). Finally, there is a third volcanic centre, known as the Cono La Virgen - a small Holocene age vent, that is 1 km across and lies 8 km east of the central summit (Samaniego et al., 2005). Lava flow deposits from Cono La Virgen extend up to 10 km east of the cone (Samaniego et al., 1998). There has only been one historically documented eruption at Cayambe volcano, in 1785, it has been persistently restless in the last 20 years and mountaineers regularly report sulphur smells from the upper flanks.

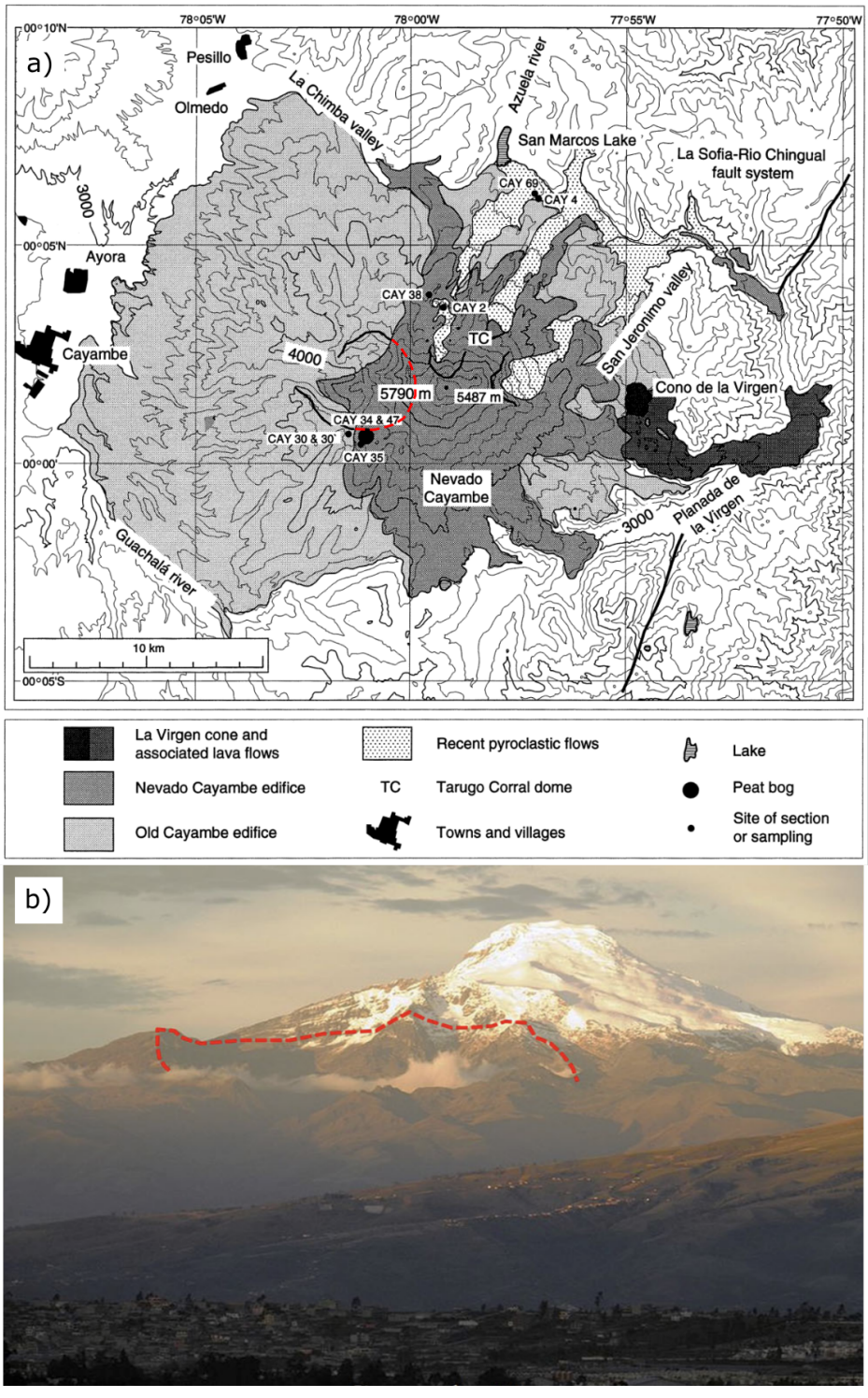

Figure 2.11 Structure of the Cayambe Volcanic Complex (CVC). a) Adapted from Samaniego et al., 1998 illustrates the three main components of the CVC, and b) Photograph of Cayambe volcano over the town of Cayambe, from Detienne et al. (2017). The red dashed line marks the horseshoe shaped scar from the last collapse event, which is also marked in a)

Permanent glacial cover

Above 4800 m, the volcano is covered in a 22 km^2 ice cap, which in places is as thick as 100 m (Detienne et al., 2017; Guillier & Chatelain, 2006) (fig 2.12). The glacier extends down to 4600 m on the drier western flanks, but down to 4200 m on the more humid eastern descent to the Amazon basin (Samaniego et al., 2005). The presence of a glacier adds complexity to an already fragile volcanic system. The glacier contributes to a loading stress on the volcano, particularly for any shallow magma storage (Sigmundsson et al., 2010). Glacial retreat has been ongoing for 150 years but accelerated by anthropogenic climate change in the last 30 years (Thompson et al., 2011). Rapid retreat acts as an unloading process and so a shallow magma chamber may be susceptible to these changes in pressure. Should these exceed failure pressures, this could act to trigger activity such as dyke injection or an eruption (Sigmundsson et al., 2010). Hydrothermal alteration of flank deposits and thawing soils from glacial retreat act to destabilise the western slopes of Cayambe. Small perturbations in the system, for example, from a magmatic intrusion or seismic event, could lead to catastrophic failure and significant landslides (Detienne et al., 2017). In the instance of an eruption, there are immediate hazards present from ice retreat and rapid glacier melt (Tuffen, 2010). It is estimated around 4.2 km^2 of ice was lost during the 1985 eruption of Nevado del Ruiz, contributing to devastating secondary lahars (Ceballos et al., 2006). In the short term, increased meltwater also has the potential to interact further with hydrothermal systems, increasing pore pressure. Basal slip from the glacier can also be seen in the seismic record, in so called 'icequakes'. Studies further south in the Chilean Andes have shown icequakes to be much more common than previously thought (Lamb et al., 2020). Icequakes observed at Katla volcano, Iceland, show waveforms that look very similar to long period (LP) events (Jónsdóttir et al., 2009). As previously cited, LP events in volcanic settings are often associated with fluid movement, including magma emplacement and hydrothermal systems (Varley et al., 2010a; Woods et al., 2018). Therefore being able to clearly distinguish

between the two phenomena is key to reducing uncertainty in hazard assessment.

Glaciers in the Eastern Cordillera are in a unique position due to their location on the equator and exposure to humid winds from the Amazon to the east (Manciati et al., 2014). The glacier on Cayambe has not been extensively studied, but it is believed Glacier 15α on Antisana volcano is a good analogue for other Eastern Cordillera glaciers (Basantes-Serrano et al., 2016). Unlike volcanic glaciers closer to the tropics, that are subject to extremes in climate such as El Niño and La Niña (Ceballos et al., 2006), the equatorial glaciers do not experience extremes of seasonality in precipitation, winds or temperature (Basantes-Serrano et al., 2016; Manciati et al., 2014). Therefore strong seasonal episodes of glacial melt and drainage are unlikely to be seen at Cayambe (Jónsdóttir et al., 2007).

When evaluating geophysical monitoring data on Cayambe for hazard assessment, influence from the glacier and associated processes such as hydrothermal systems, should be considered.

Monitoring network

There is a permanent geophysical monitoring network on Cayambe, maintained by IGEPN (fig 2.12). Real time status and archived reports on Cayambe activity can be found online (https://www.igepn.edu.ec/cayambe). This includes one three-component broadband seismometer (CAYA) and two short period seismometers (CAYR, ANGU). The short period instrument at ANGU was replaced by a broadband instrument in December 2016. There are two GPS stations and a permanent DOAS gas flux station was installed in December 2016. IGEPN also manage a catalogue of recorded seismic events, and labelled by event type. Where possible events are located and magnitude and depth estimates are provided. The majority (>80%) of events in the catalogue are identified from short period station CAYR, as this lies closest to the Nevado Cayambe cone.

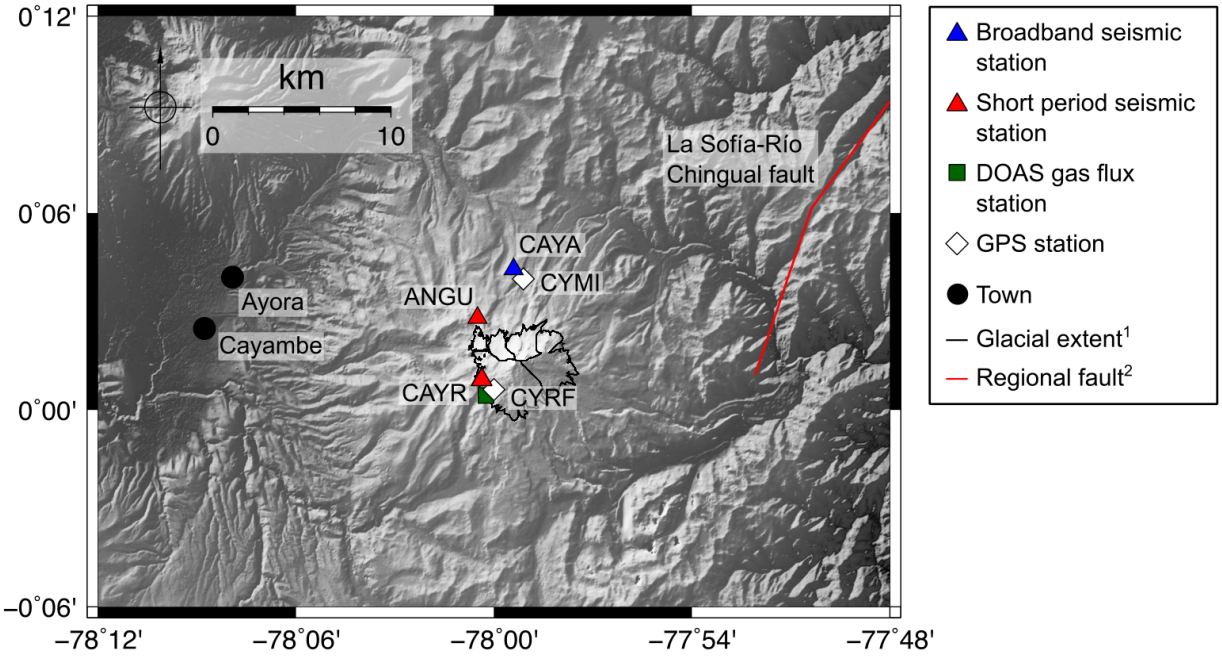

Figure 2.12 Permanent geophysical monitoring network on Cayambe, maintained by IGEPN. Two large towns, including Cayambe (population ∼20,000) are marked in black circles. [1]Black lines on the summit show the glacial extent, sourced from the Global Land Ice Measurements from Space (GLIMS) database (Cogley et al., 2015). [2]Red lines indicate regional fault lines from the Active Tectonics of the Andes (ATA) GIS database (Veloza et al., 2012).

Seismicity

Between 2000 and 2015, there was a constant but low rate of LP seismicity, <5-10 events per day, punctuated by isolated days of VT swarms, >300 events in a single day (fig 2.13). VT swarm events in 2003 - 2005 included a handful of events >M 3.5, which is uncommon at Cayambe volcano. These were located under the SW flanks and attributed to magma movement (IGEPN, 2016a; Sennert, 2016). Station CAYR was inactive between 2007 and 2015 and so the most complete record of seismicity in the catalogue is from 2015 to present day. The characteristic low level LP seismicity continues, but the VT swarms in 2016 and onwards are much more prolonged than the isolated incidents in 2003 - 2005.

There has only been one specific study on the seismicity at Cayambe (Guillier & Chate-

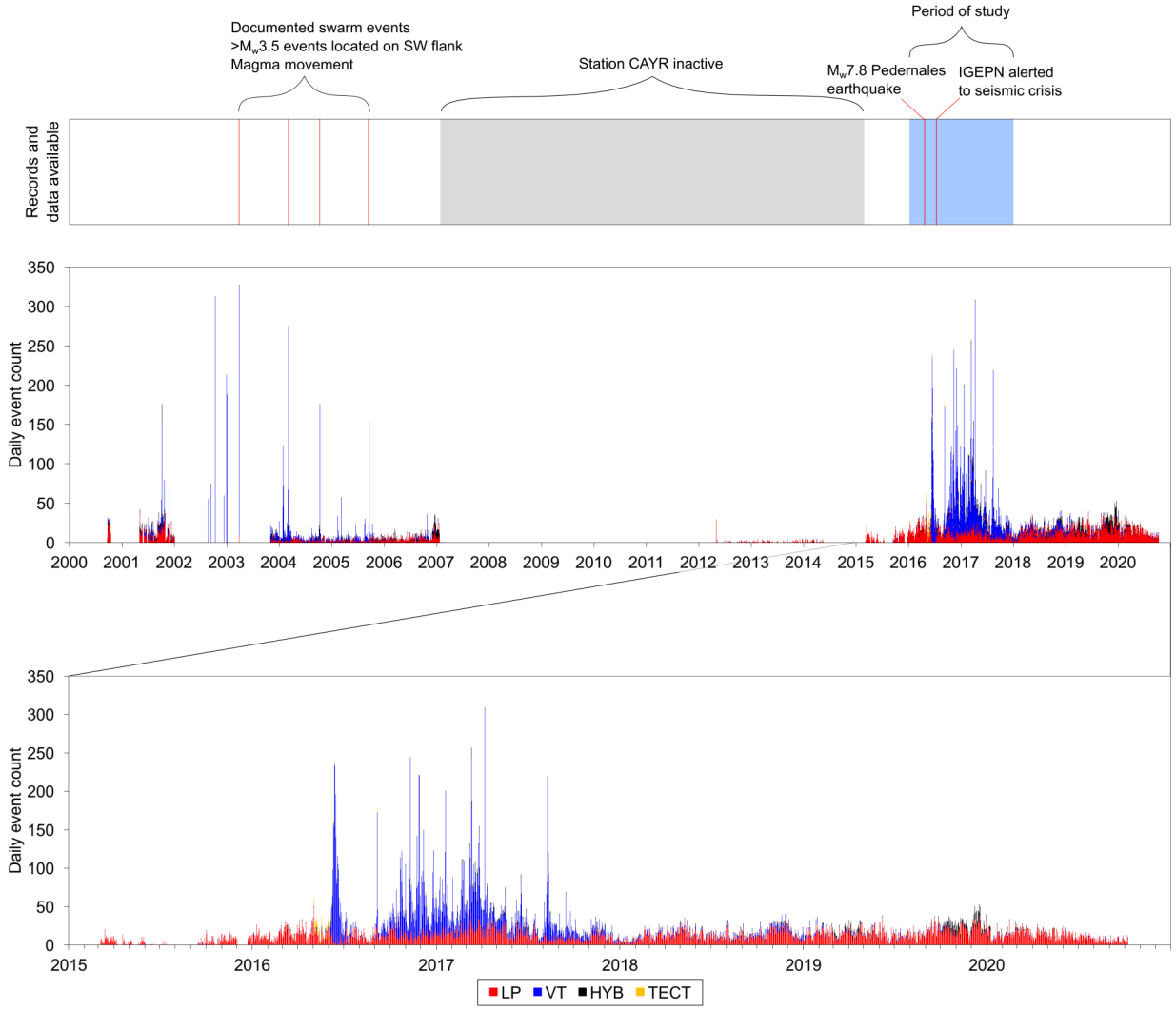

Figure 2.13 Seismicity at Cayambe Volcano from catalogue records. The top panel shows episodes of documented seismicity, whilst the two charts show daily seismic event counts from the catalogue. Red shows LP events, blue show VT events, black shows hybrid events and yellow shows tectonic events.

lain, 2006). A short temporary deployment of one component short period seismometers recorded over 5000 events between November 1997 and March 1998. The study re-classified the persistent long period seismicity as hybrid events, with mixed frequency content, caused by hydrothermal interactions. This study cites only one recorded earthquake on the 'La Sofía-Río Chingual' fault, approximately 15 km north east of Cayambe volcano in 1987 (Sipkin & Needham, 1989). The only other slip event on the fault with a verified location and

depth was in January 2018, approximately 10 km further north east than the 1987 event (USGS, 2021). However, the local tectonics in the Cayambe region are complex and there are likely many more smaller faults beyond the 'La Sofía-Río Chingual', which are not included in continental-scale databases. IGEPN tectonic earthquake catalogues contains many more events in this region, although with significant errors and may be attributed to local, small scale faults. The seismic record is complicated further as Reventador volcano lies just 40 km to the east of Cayambe. Reventador is also persistently restless and can generate tens of VT earthquakes per day (Global Volcanism Program, 2013e) It is important to remove any contamination in the Cayambe seismic record which may be from Reventador volcano.

A period of interest and the focus of chapter 6 in this thesis, is the seismicity crisis in 2016 - 2017. Two large pulses of VT swarms persisted first in April 2016 and then again in November 2016 (fig 2.13). These swarms generated seismicity significantly greater than the average daily rate and at the time caused concern at IGEPN that an eruption may be imminent. At the time IGEPN issued special reports updating the public on the unrest, and it was also covered in national newspapers (El Comercio, 2016; IGEPN, 2016b). However, there have been no published studies of this anomalous seismic swarm. This episode is also of note as the increased seismicity began just 8 weeks after the Pedernales M_w7.8 mega-thrust earthquake, just 200 km west of Cayambe volcano. The interaction between regional tectonics and volcanic activity has long been debated. It is possible for passing teleseismic wave to cause large but temporary, dynamic changes in the stress field (Hill & Prejean, 2015). Smaller more permanent deformation can cause a static change to the stress field around a volcanic system (Manga & Brodsky, 2006). It is not explicitly clear, however, whether either of these processes are enough to trigger a new phase of eruption (Prejean & Hill, 2018). This complex relationship and evidence for possible triggering is discussed further in chapters 6, A and 7.

Community

Cayambe volcano lies just 15 km from the town of Cayambe, with a population of ∼20,000 people (fig 2.12). Unlike Tungurahua, there have been no eruptions at Cayambe within living memory and there is not a formal established relationship between the community, volunteers and scientists. Therefore, in the event of increased activity, hazard assessment needs to be timely and handled carefully. In addition to the local community, the Trans-Ecuadorian oil pipeline and major highways to the oilfields in northeastern Ecuador pass to the south east of Cayambe. In the instance of an eruption, mass debris flows and lahars descending the eastern flanks of Cayambe could also easily put these at risk, with knock on effects for the whole country (Schuster et al., 1996).

2.3.3 Summary

Tungurahua and Cayambe present an opportunity to study seismicity at two volcanoes which are in some respects, very similar but in many aspects are quite contrasting. Whilst they are both monitored by a centralised agency, the capacity for seismic monitoring on each is typically limited to just one well-operating station. As a result, the seismic unrest at each volcano has also been relatively understudied and presents a challenge for seismic analysis. Seismicity at Tungurahua corresponds to a 17-year eruptive phase that includes varied eruption styles and notable LP and drumbeat seismicity during unrest. Whereas Cayambe has not erupted for over 200 years and the most recent seismic swarm was dominated by VT earthquakes. This allows us to contrast two intermediate-composition volcanoes by investigating the source mechanisms of seismicity and asking questions about the shallow dynamics at each system. This is also an opportunity to explore the differences and similarities between persistent and ongoing seismicity, and sudden swarm seismicity at a volcano that has long been dormant.

As well as considering the two systems independently, there is a unifying dynamic

that affects both volcanoes - the M_w7.8 Pedernales earthquake in northern Ecuador. Seismic swarms at Cayambe commenced within weeks of the earthquake, as did the end of the eruptive phase at Tungurahua. This overlapping timeline of events in 2016 present an opportunity to also examine the more complex relationship between volcanic unrest and tectonic earthquakes.

Both Tungurahua and Cayambe volcanoes are still potentially very dangerous to the local communities, and so careful monitoring of the seismicity and understanding of the shallow edifice is crucial to successful hazard assessment.

2.4 Research questions

In this chapter, I have reviewed the literature in two sections; first by establishing the current understanding of volcano seismicity and then two case studies of volcanoes in Ecuador. Currently, the literature is dominated by studies of volcanic seismicity where there are dense monitoring networks in place and depths and focal mechanisms of earthquakes can be accurately pinpointed. However, as highlighted in the second half of the review, poorly monitored volcanoes, particularly in middle to lower income countries, still have the potential to be very dangerous. There is also a lot of conflict and ambiguity in the methods used to approach the analysis of volcanic seismicity. As such, there is a need for a unified approach to study seismicity with limited data. This frames the first research questions for this thesis:

1. How can we better quantify volcano-seismic events with limited data?

2. Can this be streamlined into a unified signal processing routine, for adaptation around the world?

Once a methodology has been defined and rigorously tested, I will use it to analyse seismic unrest at two potentially dangerous volcanoes in Ecuador. Quantifying the seismicity in a meaningful and unified way, is progress from the current state of the art. But in order to

understand the significance of the seismicity, it needs to be contextualised within a timeline of activity. To do this, I will utilise all other available data including eruption reports, tilt meter data, and gas flux to establish:

3. What can we learn about the shallow dynamics at Tungurahua and Cayambe volcanoes, from analysis of the seismicity?

Both Tungurahua and Cayambe have recent histories of seismic unrest, which have yet to be analysed and published in the literature. Therefore, my next research question is:

4. With better characterisation techniques, can volcano-seismic events be used to interpret episodes of unrest at poorly monitored volcanoes?

One of the reasons for studying Tungurahua in particular, is the frequent observations of the poorly understood drumbeat seismicity. When developing models for the internal processes and how these relate to eruption dynamics, it is important to understand:

5. What is the significance of periodic, drumbeat LPs?

Tungurahua and Cayambe have very contrasting recent eruption histories. As such, the source model for seismicity in each case will likely be very different - this should be explored. This in turn, also means that the neighbouring communities at each volcano, have contrasting experiences of living in close proximity to a volcano. If I can successfully quantify and characterise the seismic unrest and relate this to a dynamic model of the ongoing internal processes, I then ask:

6. Can this detailed volcano-seismic analysis better inform hazard assessment?

And finally, despite there being some initial apparent differences between the two volcanic systems chosen for analysis, there is common ground. Both Tungurahua and Cayambe were active during the significant M_w7.8 Pedernales mega-thrust earthquake in 2016. Ecuador is frequently subject to large magnitude subduction earthquakes and so it is important

to further understand the complex relationship between tectonic earthquakes and volcanic unrest. As such, my final research question is:

7. Is there any evidence for volcano-tectonic interactions at Tungurahua and Cayambe?

These research questions have focussed my investigation and the findings take significant steps to fill some of the gaps in our understanding. In the following chapters I note where each of these questions is addressed. Then in chapter 7, I discuss the success of each research question and scope for further research beyond this thesis.

3 | Methodology

3.1 Introduction

In order to address the research questions 1 and 2 and to better quantify and characterise volcanic seismicity, I have developed a thorough signal processing routine to analyse earthquakes. The workflow comprises individual event waveform analysis and catalogue statistics. To address the gap in the literature and focus efforts on poorly monitored volcanoes, the analysis is designed for single station and even single component data. This signal processing routine is the basis of initial seismic analysis at the two case studies in this thesis, Tungurahua and Cayambe (chapters 4 - 6), and can be readily adopted at analogous, under-monitored volcanoes globally. This approach can also be very easily expanded to gather results from multiple components and stations.

In this thesis, all seismic data are handled with the ObsPy toolkit (Krischer et al., 2015). This streamlines the process of reading and analysing seismic data files. Data can be handled as a `Stream` object, a `Trace` object or a NumPy array. Waveform data are kindly provided by monitoring teams at IGEPN. Data are stored in individual day files. A `Stream` object includes a dictionary of file metadata including start and end times of the file and the sample rate. When specific station data are used, the sampling frequency is included in the text. The vast majority of analyses in this thesis come from stations RETU and CAYR at Tungurahua and Cayambe volcanoes respectively, which sample at 100.0 Hz. Any synthetic seismograms demonstrated in this chapter are generated to reflect this.

First I introduce some approaches to identify earthquakes in waveform data. I then detail the signal processing methods in the time and frequency domain, and introduce the Q factor. Finally, I discuss some of the longer catalogue approaches that are used to contextualise the individual waveform analysis.

3.2 Generating catalogues of earthquakes

As an active geohazard monitoring agency, IGEPN routinely maintain and update catalogues of manually picked seismic events from volcanic monitoring networks. Catalogues will list the time of the picked event, the station the event was identified at and a label corresponding to the type of volcanic earthquake. If it is possible to locate the event, then a magnitude estimate may be provided along with the latitude, longitude and depth along with their respective errors. The picks in the catalogue may be recalculated if it was possible to relocate the event on the basis of data from another station.

For comprehensive analysis of a sequence of seismicity, it is important that all possible earthquakes are included in a catalogue. It is also important for these events to have an accurate pick time for the first P-phase arrival. The best picks are those located manually by trained analysts, such as those in the IGEPN catalogue. However, when handling many years of data across several stations, manual scanning is not feasible and there are sometimes incomplete sections in the IGEPN catalogue. Particularly in some of the lesser studied drumbeat episodes, there were often visible periods where existing IGEPN catalogues do not include every event. As such, for analysis in this thesis, I opted to complement existing catalogues with my own picks. If the period of interest is short (<10 days) I used an interactive Python script to manually pick the first P-wave arrivals and generate a catalogue (appendix C.5). However, for much longer episodes over several weeks or months, manual picking was too time consuming and I opted to use an automated picking algorithm to identify all possible events. For over 40 years, methods have been proposed to detect seismic

phases in teleseismic events. These studies have broadly fallen into three fields: methods considering time series in the time domain, the frequency domain, and adaptive methods which update once a particular phase has been identified (Withers et al., 1998). For volcano seismic event analysis we are primarily interested in the first P phase and S phases are often not clear, and so the adaptive methods are less applicable (McNutt & Roman, 2015).

It was important to determine which automatic picking method was the most accurate before proceeding. In order to test each method, I manually picked a short episode of unrest at Tungurahua volcano as a ground truth data set. I used a Python script in which the user can dynamically interact with a `matplotlib` figure and use the cursor to pick the first arrival time. I was able to confidently pick 2097 events from first arrivals for 30 days of waveform data at short period station, RETU in November 2015. It was particularly important to test these automated methods on LP events. Not only do they dominate the seismicity recorded at Tungurahua which forms a significant part in this work, but the characteristic emergent onset of LP events, can make picking the first arrival quite difficult. All methods, regardless of their approach, are looking to quantify a sudden change in amplitude, and hence a first arrival. This is very sudden in VT events, however, there is more room for uncertainty in the emergent LP onsets. The events are plotted in 30 second windows and so it is estimated that manual picks are accurate within ± 1 second at most. These 2097 manual pick times were then compared with the catalogue pick times and results from seven different automatic pickers, which are detailed as follows.

3.2.1 Short Term Average/Long Term Average (STA/LTA)

For a given time series, at each time step the STA/LTA algorithm calculates the average waveform amplitude in a short window and a longer window, and calculates the ratio between the two (Vanderkulk et al., 1965). If there is an abrupt change in the short window as opposed to the longer window, the ratio will be much higher for that time step. The output at each

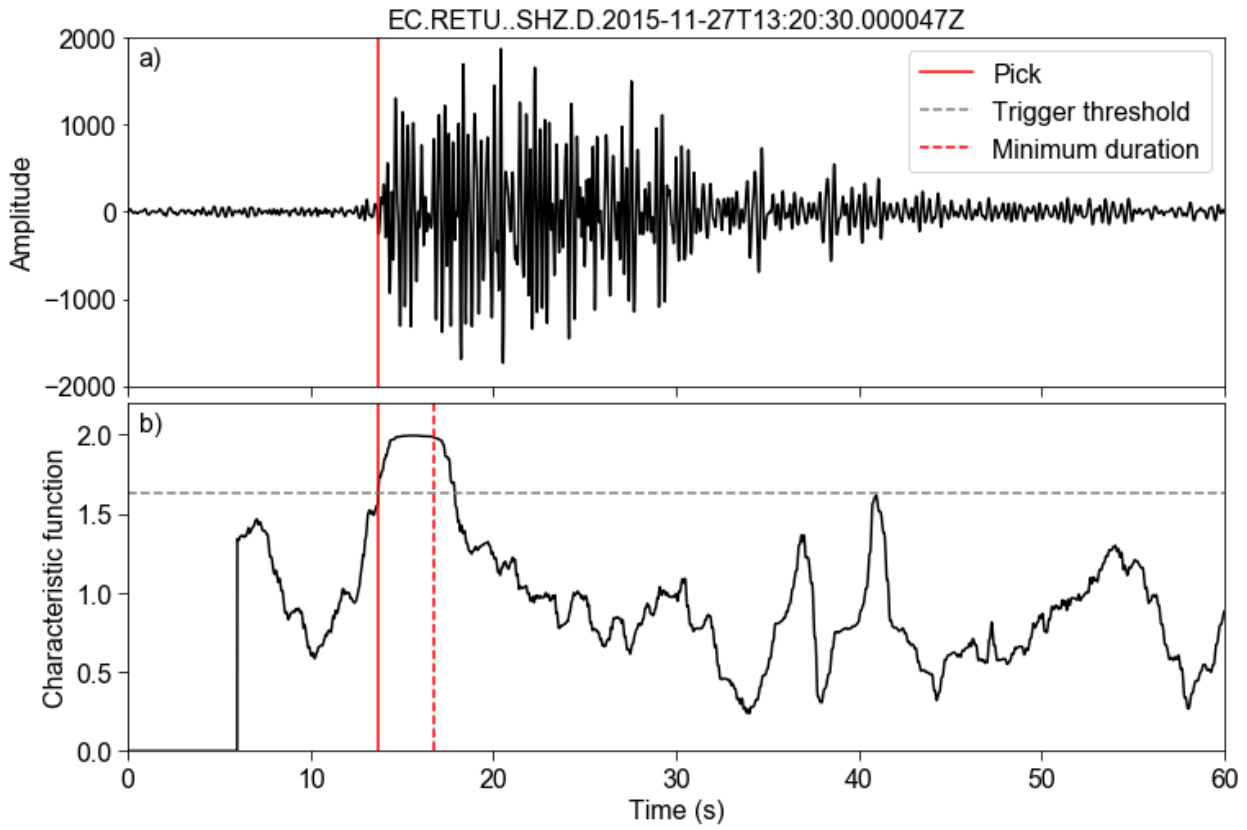

Figure 3.1 STA/LTA triggering *a)* LP event recorded at RETU, Tungurahua, *b)* The characteristic function generated by the classic STA/LTA algorithm. The grey dashed line shows the threshold that must be passed to trigger a pick. The red dashed line marks the minimum event duration imposed by the difference between the short and long term window lengths. In both panels, the red vertical line marks the pick time.

time step then defines a characteristic function. A threshold must then be set and when the characteristic function exceeds the threshold, a trigger will mark a pick as the first P-phase arrival. A number of variants of this STA/LTA method are available as functions in the ObsPy packages. This characteristic function approach is referred to as the 'Classic STA/LTA' method (fig 3.1). ObsPy hosts a second method considered in this verifying process, the 'Recursive STA/LTA' method. Rather than considering rectangular response windows, the recursive methods relies on the characteristic decay time, T, the time required for an impulse to decay to $1/e$ of its maximum amplitude (Evans & Allen, 1983). In this

case the short term average is defined as:

$$STA_i = Cx_i + (1 - C)STA_{i-1} \tag{3.1}$$

where

$$C = 1 - e^{\frac{-S}{T}} \tag{3.2}$$

and S is the sampling interval. Given the STA/LTA method is a simple algorithm comparing the averages of two sliding windows, further adapted variations of event picking have been proposed whereby the input parameters are adjusted. Rather than using the raw time series, (Allen, 1978) proposed using STA/LTA on a characteristic function, $E(t)$, where:

$$E(t) = f(t)^2 + f'(t)^2 + C \tag{3.3}$$

C is a weighting constant associated with the instrument response, and can therefore be neglected when we are considering only one station. This characteristic function defines the energy density. Classic STA/LTA can then be run over the resulting envelope. This approach using equation 3.3 is referred to as the *Allen (1978)* method hereafter.

The input parameters for the STA/LTA algorithms can be very sensitive. The characteristic function will abruptly increase and trigger a pick at the end of the first long window (fig 3.1, at 6s). If the algorithm is run over individually sliced event traces, as opposed to continuous waveform data, this should be considered. The absolute value at which the trigger should be activated is be dependent on the absolute signal amplitude and the length of the windows chosen. The trigger value can be determined from an average success value from a sample before running on a larger time frame, or it can be set as a relative percentage of the maximum of the characteristic function. For both classic and recursive STA/LTA testing here, the short term window used was 3 seconds, the long term window 6 seconds and the threshold at 80% of the maximum of the characteristic function. I also imposed a minimum duration for period over which the characteristic function is greater than the threshold. An example of an STA/LTA pick is in fig 3.1, where the characteristic function

peaks and is sustained for more than them minimum duration. The minimum duration imposed is 3 seconds.

3.2.2 Z-detect

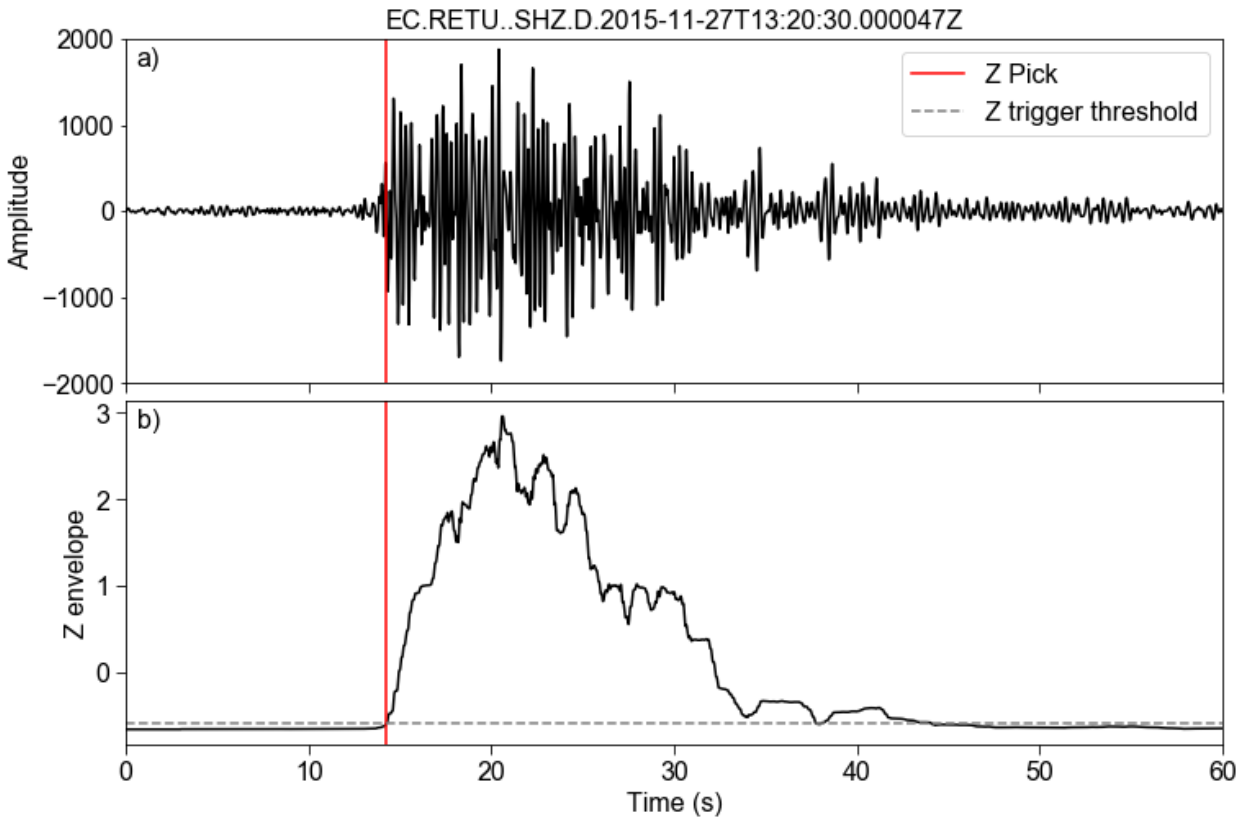

Figure 3.2 Z-detect method *a)* LP event recorded at RETU, Tungurahua, *b)* The signal envelope generated by the Z-detect method. In both panels, the red vertical line marks the pick time and the grey dashed line shows the threshold that must be passed to trigger a pick.

The Z-detect method generates a signal envelope, defined as:

$$Z(x_i) = \frac{x_i - \mu}{\sigma} \tag{3.4}$$

In this case, x_i is a window of the signal, where the window length is defined by the user, and μ and σ are the average and standard deviation of the signal, respectively (Swindell

& Snell, 1977). The raw Z-detect signal envelope itself can be used to locate a pick time, by setting a trigger threshold. The trigger is set at 10% above the baseline of the envelope (fig 3.2). The signal envelope can also be passed to an STA/LTA algorithm and a trigger is calculated using the same parameters as the classic and recursive STA/LTA methods in this thesis.

3.2.3 Kurtosis and skewness

In statistics, kurtosis describes the 'tailed-ness' of a distribution. It is important to stress that kurtosis is not a measure of 'peakedness' as is often interpreted. Whilst a 'heavy' or 'light' tail on a distribution may appear to affect the overall shape of a distribution, the quantity associated with kurtosis is derived from values beyond one standard deviation from the mean (Westfall, 2014). When considering probability distributions, the kurtosis is calculated as the standardised fourth moment. That is, for a random variable X, if μ is the central moment, σ is the standard deviation and E is an expectation operator, our kurtosis value, K can be expressed as

$$K[X] = E\left[\left(\frac{X-\mu}{\sigma}\right)^4\right] = \frac{\mu^4}{\sigma^4} \tag{3.5}$$

This kurtosis equation can be discretised to be applied to a time series (Baillard et al., 2014). The kurtosis function is a readily available function in the Python SciPy package. For Gaussian distributions kurtosis is zero, and its value increases for non-Gaussian distributions. In this approach for earthquake picking, the kurtosis is applied in sliding windows of a fixed length, determined by the user. For all testing, I used two second windows. Prior to an earthquake when the input signal is random noise, the kurtosis for a two second window timeseries will be near zero. At the onset of an earthquake, the timeseries becomes more extreme, with large amplitude arrivals and so the kurtosis value will rapidly increase and can therefore be used as a triggering algorithm (Baillard et al., 2014; Saragiotis et al., 2004).

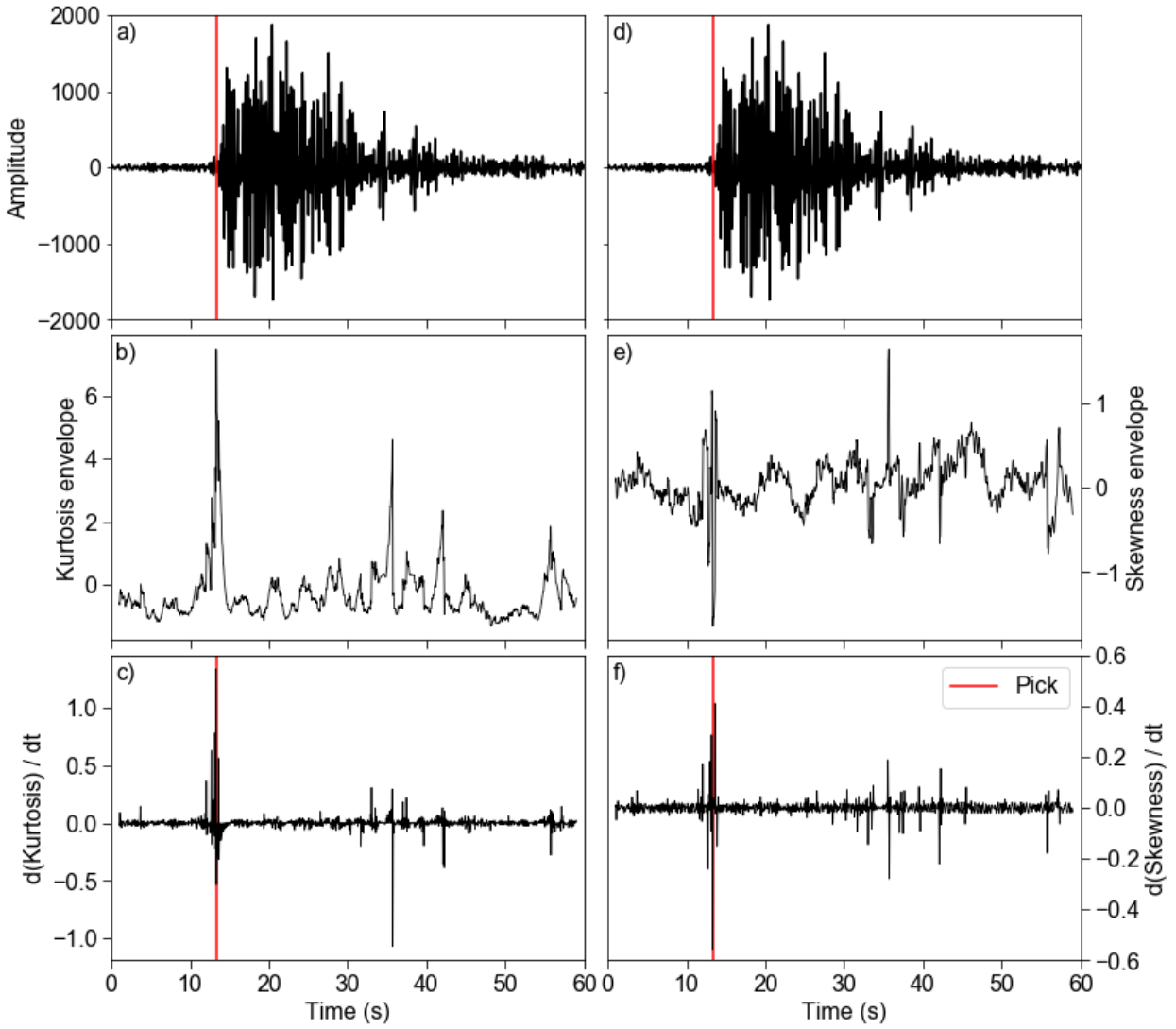

Figure 3.3 Kurtosis and skewness methods *a), d)* LP event recorded at RETU, Tungurahua, *b)* kurtosis envelope, *c)* first derivative of the kurtosis envelope, *e)* skewness envelope, *f)* first derivative of the skewness envelope. In all panels, the red vertical line marks the pick time. In this case, the largest absolute value in the derivative is used to mark the pick time.

As with the Z-detector, the kurtosis function generates an envelope, from which a triggering threshold will determine a pick time. The kurtosis is susceptible to spiking in long noisy coda tails, which inhibits the success of the first arrival pick. To overcome this, the first derivative with respect to time of the kurtosis envelope is computed, and the trigger threshold can be applied. The onset of an event typically causes a more rapidly changing kurtosis, and so the gradient captures this arrival more precisely (Baillard et al., 2014) (Figure 3.3).

The skewness is a related method, also often associated with statistics and quantifying probability distributions. The skewness typically describes the asymmetry of a probability distribution. The skewness is calculated as the standardised third moment, as opposed to the fourth (in eq 3.5). This can also be discretised and applied to a time series in sliding windows to generate an envelope, just as the kurtosis method (Saragiotis et al., 2004). Again, the first derivative is then calculated to apply the trigger threshold. The pick time is chosen at at the largest amplitude peak in the derivative signal (fig 3.3).

3.2.4 Power detectors

A number of automatic picking methods in the frequency-domain were developed by Shensa (1977). The average power detector works similarly to the Z-detector, only in the frequency domain. Again, the method is applied in sliding windows, generating an envelope from which the pick can be identified by a sharp contrast in the output parameter.

$$Y_i = \frac{\frac{1}{N}\sum_{N_2}^{k=N_1} P_i(k) - \mu}{\sigma} \tag{3.6}$$

The power spectral density (PSD, P) is calculated over a given frequency band ($N_2 - N_1$) at each time step, i. The Z-detector method is then utilised by subtracting the mean (μ) and dividing by the standard deviation (σ). The average power detector returns a signal envelope, Y_i, from which a pick can be triggered by surpassing a threshold. Much like the kurtosis and skew methods, the first derivative in time can be used to refine the pick time

(Berger & Sax, 1981) (fig 3.4).

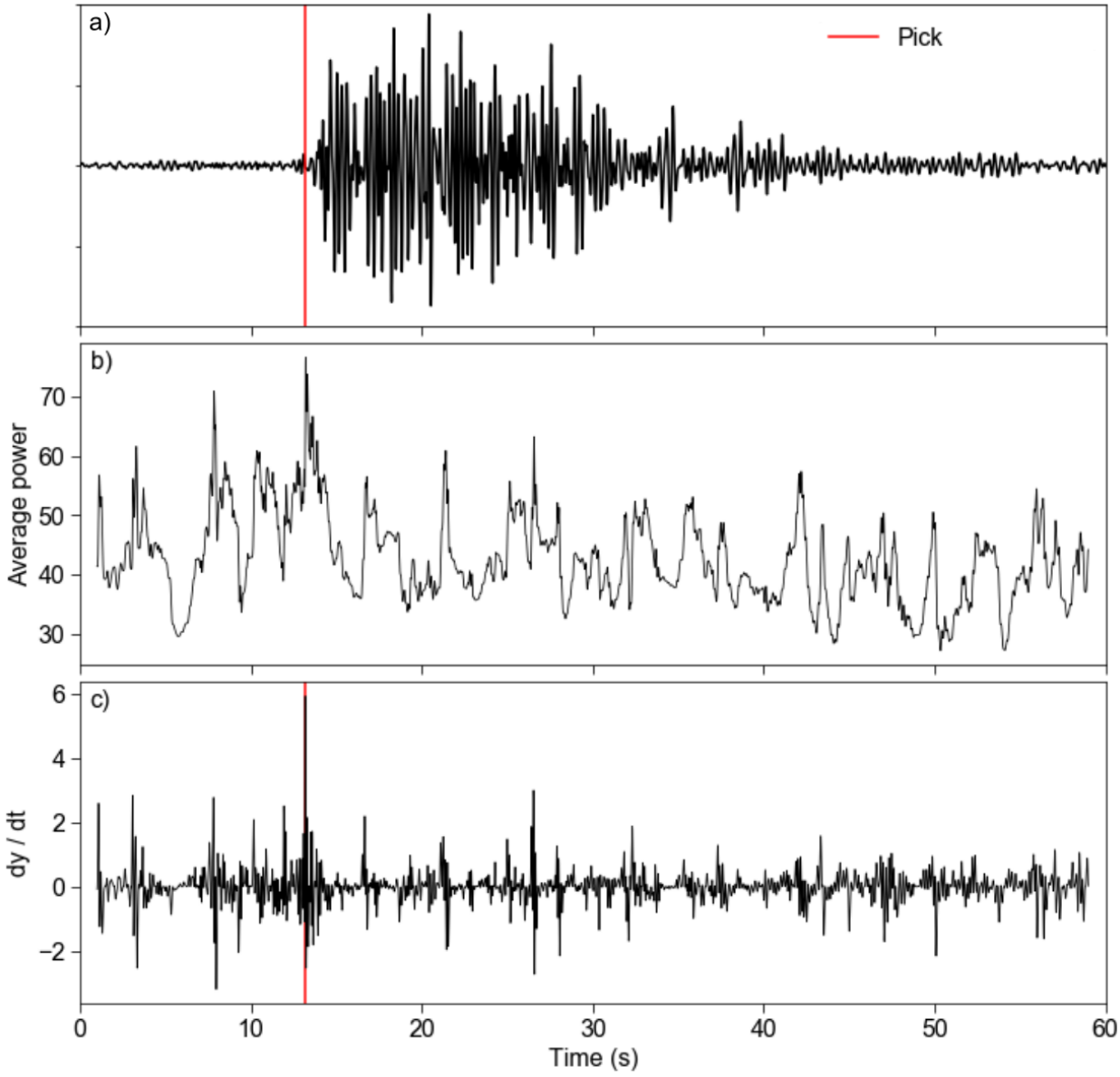

Figure 3.4 Average power picking method *a)* LP event recorded at RETU, Tungurahua, *b)* average power envelope, *c)* first derivative of the average power envelope. In all panels, the red vertical line marks the pick time.

3.2.5 Method testing

All automatic picking methods were tested on a handful of sample events before expanding to a wider catalogue of events. Figure 3.5 illustrates two very different LP events in the catalogue, separated by around 15 minutes. A lower amplitude and more emergent LP is shown in figure 3.5a, whilst the event in panels 3.5b and 3.5c is the same event demonstrated in figures 3.1-3.4. The pick times plotted in figure 3.5 are detailed in table 3.1. The more emergent event causes some automatic methods to miss the first arrival quite significantly and they are a mixture of early and late. Whereas for the second event, the picks were all within 1s of the catalogue pick and consistently late rather than early.

Method	**Relative shift (s)**	
	Event *a*	**Event *b***
Manual	± 0	± 0
Catalogue	-4.49	-0.58
Classic STA/LTA	-6.79	0.09
Recursive STA/LTA	-8.8	0.08
Allen (1978)	-1.19	-0.02
Z-detector	-8.8	0.08
Kurtosis	-0.6	-0.43
Skewness	23.35	-0.62
Average Power	28.6	-0.45

Table 3.1 The relative shift between automatic pick with the manual pick for events *a)* and *b)* in figure 3.5. A positive value suggests the pick is late, and negative is when the pick is early.

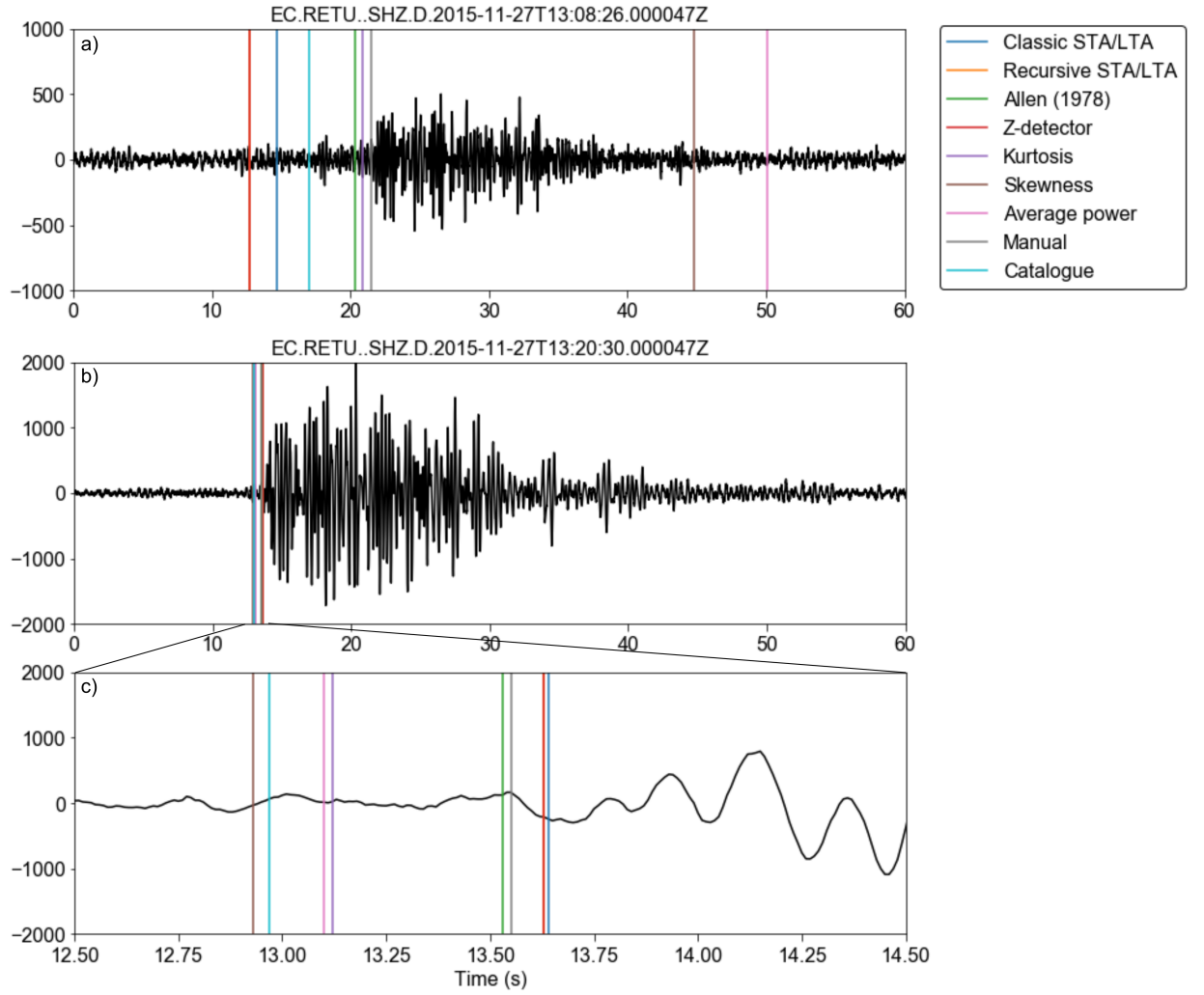

Figure 3.5 Comparing all automatic picking methods *a)* an emergent, lower amplitude, LP event recorded at RETU, Tungurahua, *b)* a contrasting higher amplitude LP event at RETU, and *c)* a cropped window view around the P-phase arrival. The coloured pick marks correspond across all plots. Exact pick times are detailed in table 3.1

The automatic picking methods were then applied to all 2097 events that were manually picked during November 2015 at RETU station. They contained a mixture of emergent and more rapidly onsetting signals as shown in figure 3.5. The mean and the standard deviation of the shifts relative to the manual pick are listed in table 3.2. For this study, I chose to use my manual picks as the ground truth data, as opposed to pre-prepared catalogue picks. Although the monitoring staff at IGEPN are expertly trained to identify and catalogue

these earthquakes, for the purposes of this research I had time to carefully inspect these. Occasionally I found that these were a few seconds away from what appeared to be the first P- phase arrival. These few seconds could be crucial in determining which was the most appropriate automated method to use. As such, I manually picked the events, to account for the highest possible accuracy.

The Recursive STA/LTA method proved to be the most reliable on this particular data set, with a low mean and small standard deviation. The Kurtosis/Skewness methods and the Average Power approach demonstrated too many inconsistencies and a high standard deviation. All mean values calculated were positive, indicating that picks are consistently later than manual picks. This is important with regard to further methods of signal analyses which rely on accurate measures between event onset and peak amplitude, for example. In particular, certain Q factor methods (section 3.4) will fail or be incredibly inaccurate if pre-pick noise is included in the signal. As such, where automatic picking is required in this thesis, the Recursive STA/LTA algorithm is used. Unless otherwise stated, the search parameters are a 3s short term window, a 6s long term window and a threshold at 80% of the maximum characteristic function value.

Method	**Mean, μ (s)**	**Standard deviation, σ (s)**
Classic STA/LTA	1.517	1.148
Recursive STA/LTA	0.752	1.176
Allen (1978)	1.049	1.166
Z-detector	0.873	1.828
Kurtosis	0.458	3.994
Skewness	2.047	5.708
Average power	0.351	7.213

Table 3.2 Mean and standard deviation of the required shifts to match automatic method picks to manual picks, the ground truth dataset. Tested over 2097 picks at RETU station.

3.2.6 Template matching

Another approach used to identify events in the waveform data is template matching. A low signal to noise ratio at a particular station may cause many events to be missed both by manual picking and automatic methods. The automatic methods rely on a significant amplitude change to trigger a pick time, and even a trained eye may be inconsistent in picking low amplitude events. Template matching has been used to identify small events and expand catalogues in tectonic (Ross et al., 2019) and volcanic settings (Lengliné et al., 2016; Shelly et al., 2013). The method works on the premise that earthquakes with similar source mechanisms, in close proximity, will generate very similar signals at the surface (Gibbons & Ringdal, 2006). As such this method is used in studies of repeating seismicity, such as VT swarms or drumbeats, where it is speculated the source mechanism is a single repeating source (Shelly et al., 2007). In this approach, an earthquake signal is scanned over raw continuous waveform data in the time domain, as a sliding window, cross correlating the two signals. If the cross correlation coefficient spikes above a certain threshold, it is considered there is a significant similarity between the earthquake event and the continuous signal, and a pick time is made in the continuous signal. As such this approach works best if the template is representative of a repeating event, such as one identified in a family (see section 3.5.1). Of course, a scatter gun approach, using many hundreds or thousands of templates to cross correlate with continuous signal may detect small events that are undocumented in the catalogue. However, this may, be computationally expensive and yield low results. Another approach is to continually update the template as cross correlation progresses. When an event is found, a new template is generated which is a stacked event, representing the average of the original template and the newly identified event (Chamberlain et al., 2020). Unsupervised machine learning techniques using neural networks are beginning to overcome the issue of having *a priori* templates (Mousavi et al., 2019).

In this thesis, I have generally worked to complement existing catalogues of data, rather

than starting from scratch, and so template matching is used to identify very specific traces, or those belonging to families (see section 3.5.1). As such, known events are used as templates and methods of dynamically updating the template are not used. The specific parameters used in each instance are detailed where used (section 6.2.2), although at this stage, I would like to draw attention to one point of discussion - the cross correlation coefficient threshold. When conducting cross correlation, the coefficient threshold for further action, be that family extraction (section 3.5.1) or template matching is somewhat arbitrary and subject to the user. Examples in the literature, however, tend to set the threshold for template matching to be lower than that for identifying families. This is particularly true when the template is not dynamically updated, but chosen to be representative of a certain type of seismicity. For example, template matching small VT swarm events at Piton de la Fournaise, used a threshold at 0.4 (Lengliné et al., 2016), whilst VLP template matching at Whakaari/White Island volcano use a threshold of 0.6 (Park et al., 2020). In tectonic template matching efforts, where there are clear P- and S- phase separations to constrain events, a higher threshold, closer to 0.8 can be used (Shelly et al., 2013). Template matching in this thesis, used a cross correlation coefficient threshold at 0.5 to trigger an earthquake pick. The majority of events considered are LP events with no visible S- phase and so I opted to use a lower threshold in accordance with the published literature.

3.3 Signal processing

Once all possible earthquakes have been picked, a complete catalogue can be passed for processing. Analysis falls broadly under two categories: individual waveform analyses, and long term catalogue analyses. Rather than qualitatively describing an earthquake, the individual event analysis generates a suite of metrics to quantify a given earthquake. These can be used in long sequences of seismicity, particularly drumbeats, to track small shifts in the seismicity properties. They are also used to identify sub-classes of earthquakes beyond the

simple definitions that exist in the literature such as LP, VT, HYB.

3.3.1 Time domain

If an earthquake is recorded on multiple stations, or has clear P- and S- phase arrivals, then it is possible to estimate the magnitude of the event. The vast majority of LP type earthquakes examined in this thesis, however, are recorded at only one station and demonstrate no clear S- phase. In this instance, the absolute magnitude of the signal is considered a proxy for magnitude. Given the recorded signal is a superposition of the source process, path effects and instrument response - it is assumed that over a short period of study the path effects and instrument response are stable, such that a change in amplitude is a direct result of a change to the source process. This metric should be used carefully, as very shallow, large events, close to the seismometer may saturate the signal and put an unnatural constraint on the upper limit of any subsequent modelling. For particular episodes of unrest, I have used Real Time Seismic Amplitude (RSAM) (Endo & Murray, 1991) to illustrate event amplitudes. This emphasises episodes of high amplitude tremor and explosions. Over a long timescale, artefacts in the RSAM can appear where there are station outages and should be carefully considered. RSAM is calculated in sliding windows, and depending on the episode of interest this window can be on the scale of minutes, hours or days.

Earthquake event types are often easily spotted by eye on the basis of the waveform shape. Quantifying the signal envelope can be difficult as a smoothing parameter adds an element of human subjectivity. A smoothed signal envelope can be generated by calculating a spline function between maximum peaks in sliding windows of a fixed length (fig 3.6c). However this is still only really helpful as a visual tool. Given one of the defining features of LP earthquakes is their emergent onset, I have quantified the rise and decay time of the signal amplitude using a metric K (Lees et al., 2008). I refer to K_1 as the exponent for the rise time, and K_2 for the decay time. Three key points are located in the signal: the

average amplitude at the very beginning of the event (calculated in a 2s window either side of the pick time) y_1 at t_1, the maximum amplitude, y_2 at t_2, and the amplitude at the end of the event, y_3 at t_3 (fig 3.6). The initial amplitude is calculated in a 4s window surrounding the pick, to best capture the average amplitude for the very onset of the event. The second parameter, y_2 is calculated as the maximum amplitude of the signal. The exact time and amplitude of the end of the event (t_3, y_3) is determined by a threshold parameter, which needs to be defined by the user. This threshold is a proportion of the pre-event amplitude, and does not need to be the same as the pre-event amplitude. For example, in Lees et al. (2008), this threshold is set to 10% of the pre-event amplitude. However, in method testing, very rarely did the signal ever decrease to 10% of the pre-event amplitude, and so no K_2 value was returned. This can be due to a noisy background signal in the data, and so the parameter is adaptable. As with the picking methods, a sample of events from the study period in question is used to test a suitable threshold parameter and then remains consistent within one study to ensure results are comparable. I used a simple exponential curve fit between (t_1, y_1) and (t_1, y_1) to define a positive K_2 rise value, and then the same again between (t_2, y_2) and (t_3, y_3) to define a necative K_2 decay value 3.7.

$$y = Ae^{Kt} \tag{3.7}$$

The exponents, K_1 for the onset and K_2 for the decay of the signal, quantitatively describe the emergence of the event. The decay time of a signal is physically linked to the source process and the attenuation of a signal (Rossing & Fletcher, 2004). This is explored further in section 3.4. The emergence of the signal, however, is a characteristic used to track subtle changes in seismicity behaviour and can help to identify similar events.

3.3.2 Frequency domain

A number of methods used to characterise earthquakes, stem from the spectral content of the signal. In particular, I have used the peak or dominant frequency of a signal as a key initial

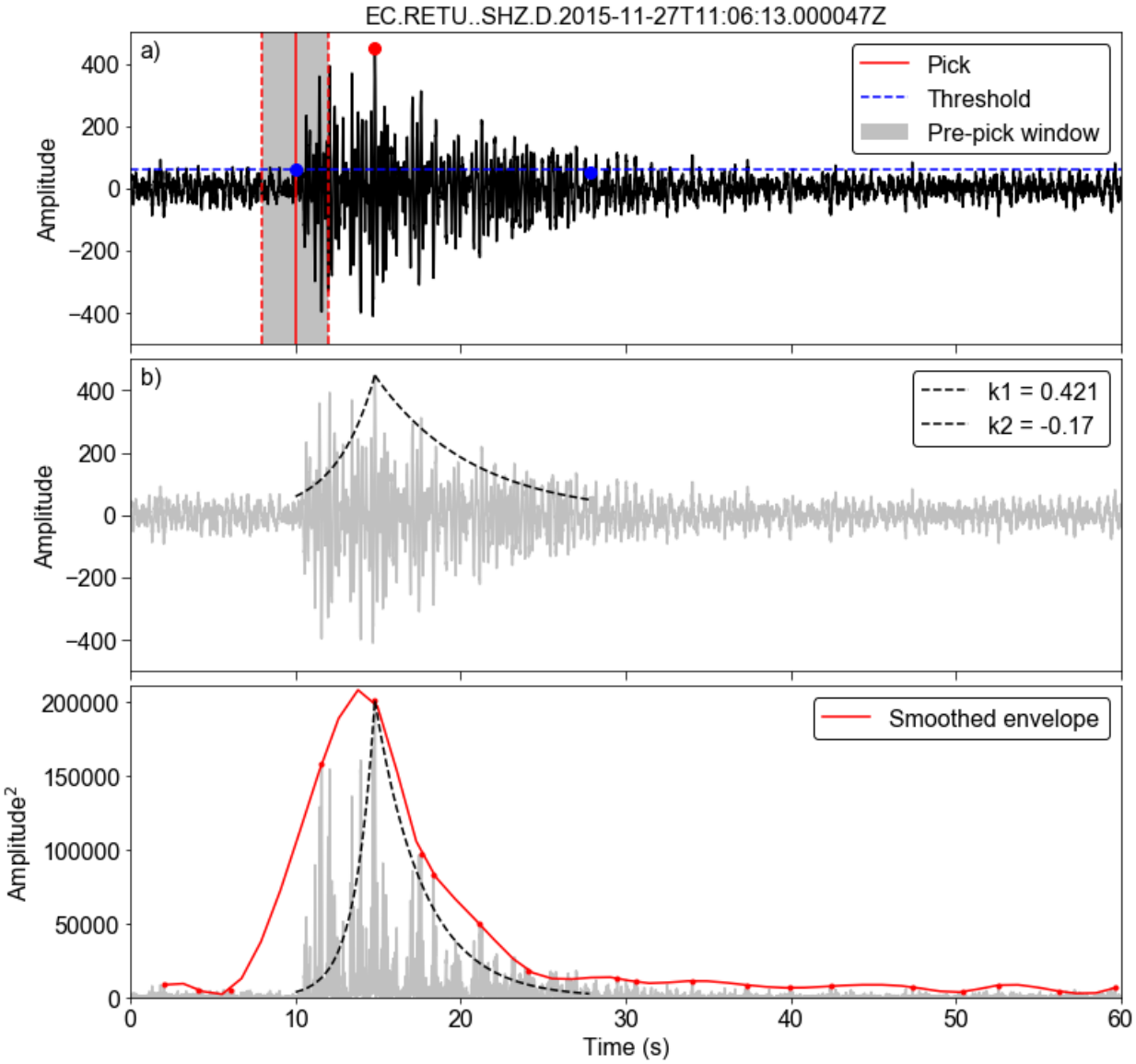

Figure 3.6 Determining signal emergence, using K (Lees et al., 2008) *a)* Key defining points of a signal to calculate K. Grey panel marks the region from which the pre-event average amplitude is calculated, solid red line shows pick time, red circle shows the peak signal amplitude, blue circles show the positions at which the threshold, blue dashed line, is met, *b)* Black dashed lines show the calculated exponential functions defining the onset and decay of the signal, *c)* The same exponential curves are shown on the squared amplitude of the signal, along with a spline interpolated smoothed signal envelope in red.

indicator. The peak frequency is most clearly seen by plotting the power spectral density (PSD). This illustrates how the power of the signal is distributed across the frequencies

present in the signal (Stoica & Moses, 2005). The PSD can be estimated using several methods, including Welch's Method and the Lomb-Scargle (Attivissimo et al., 2000). In this thesis I have calculated PSD using a periodogram, from an inbuilt SciPy function. The periodogram is the squared magnitude of the discrete Fourier Transform of the signal (Bisina & Azeez, 2017), and so has units of x^2/Hz where x represents the input signal unit. A number of studies rely on plotting the PSD to better understand and visualised earthquake events (Alparone et al., 2003; Moran et al., 2008; Unglert & Jellinek, 2017) and it is a method used for analagous studies in medical sciences (Akin & Kiymik, 2000). However, the resolution of the PSD, and subsequently the peak frequency chosen, is controlled by the length of the Fourier Transform window. Figure 3.7 illustrates how the identified peak frequency varies as a result of the sampling frequency in the periodogram. In this thesis all periodograms are calculated with 10000 fast Fourier Transforms, such that the periodogram has a power value for every 0.01Hz.

The power spectral density can then be used to better understand earthquake events. For the most harmonic events, periodograms can look very striking with a single monotonic peak in the spectra. An automated method for detecting harmonic events is presented in Roman (2017). The Harmonic Product Spectrum (HPS) scans continuous seismic data in a given window length, searching for peaks in the spectra with corresponding harmonic overtones at integer increments. The algorithm compares the power in a spectral peak to it's neighbouring 'inter-harmonic' - the next highest value between the peak and it's next integer overtone. If this ratio surpasses a threshold, then a trigger will mark the start of harmonic tremor. In testing the HPS method on data at both Tungurahua and Cayambe, it was challenging to tune the parameters. Whilst HPS was very successful at finding very strongly harmonic episodes, it very easily missed events which were clearly very harmonic, but did not have overtones in exactly integer increments. This was the case for discrete earthquakes and more sustained, long duration tremor. For this reason, I also used a more approximate scanning method to identify harmonic events in conjunction with the HPS. A

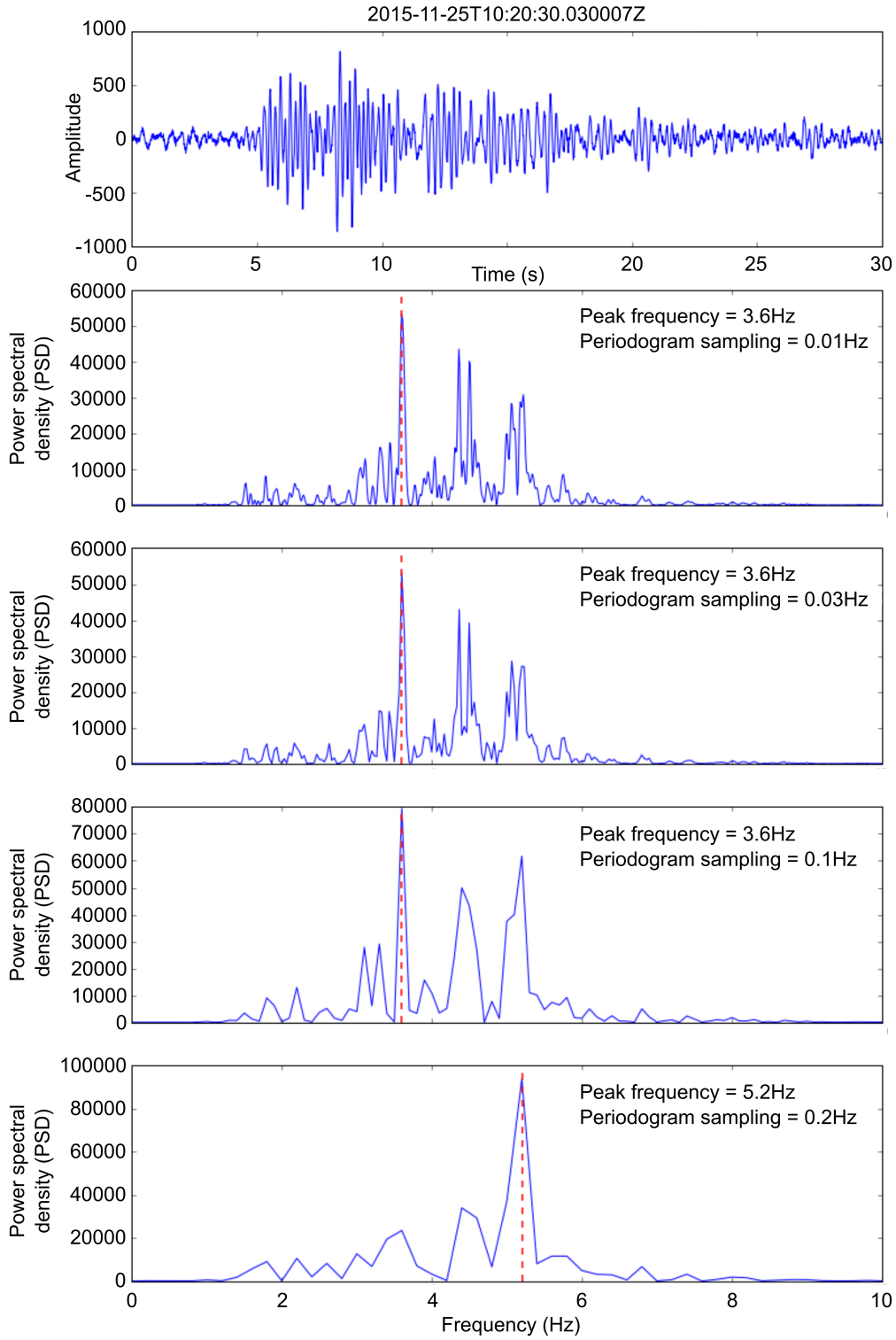

Figure 3.7 Testing Fourier Transform window lengths in periodograms. The top panel shows a sample event from RETU, Tungurahua. The periodogram is calculated at different sampling frequencies and the peak frequency in each instance is marked with a red dashed line.

sliding window, of fixed length 10 seconds, is passed through continuous seismic data and a periodogram is calculated for each window. The NumPy function `find_peaks` is used to identify the 5 largest peak values, separated by more than 0.2Hz. The power of these 5 peaks are then compared and if the largest peak exceeds the next peak by a factor of more than 10^2, a time-stamp was logged as a potential harmonic episode. This runs rapidly and so several months of data can be scanned very quickly. I then used a manual verification process, to determine whether a pick is true harmonic data or a false pick. In addition to looking at the spectrogram and periodogram and visually verifying whether a signal is harmonic or not, I used an ObsPy function to compress the signal and write is as an audio file. When listening to compressed earthquake signals, the human ear is more perceptive to harmonic tones. Broadband signals sound like pops, and harmonic events sound more squeaky. If there is a gliding frequency, this upward tick in the frequency can be heard. By simultaneously listening and looking at the potential harmonic events, several months worth of potential harmonic picks can be sorted through very quickly.

This is the first technique described in this methodology which specifically targets tremor. Both peak searching and HPS can be effective on discrete events, however, they also offer a unique opportunity to quantify and start to understand tremor. On visual observation alone, in several days or weeks of continuous seismic data, it can be difficult to identify tremor, particularly if it is low amplitude and there is a noisy background signal present. Employing an automatic search like this is an effective method to highlight areas for further subsequent investigation.

3.4 Q factor

In an attempt to generate as many usable and quantifiable metrics to describe an earthquake signal as possible, the quality (Q) factor can shed light on the source and path process (Kumagai & Chouet, 1999; Lokmer et al., 2008; Molina et al., 2004). Q describes how

quickly energy in a signal is attenuated (Rossing & Fletcher, 2004). It is difficult to separate attenuation related to the source and path, particularly given heterogeneity in volcanic edifice and uncertainties around source mechanisms. However, in volcano-seismology, Q is often employed to quantify LP events specifically. If the source of an LP event is assumed to be a fluid filled crack then Q is a measure of the damping of that resonance (Chouet, 1992; Lipovsky & Dunham, 2015). For a series of earthquakes in short succession, recorded at the same station, we might assume the path effects are unchanging and therefore a direct measure of the resonating process. Changes in Q may therefore suggest either the media or crack geometry are also changing (Cusano et al., 2008).

Reported values for Q in the literature vary between $10^0 - 10^3$ (Molina et al., 2004). This range is, validated by a series of numerical synthetic tests for resonating fluid-filled cracks where the fluid compositions, temperatures and pressure conditions are varied (Kumagai & Chouet, 2000). However, where a variety of methods are commonly used, comparing Q values across multiple studies can lead to very different interpretations. In this thesis, I have used three popular approaches and discuss the merits and flaws of each.

All methods ultimately hinge on the amplitude decay of oscillations associated with a single frequency (Elmore & Heald, 1985). As such, they are useful to understand LP seismicity, in particular tornillos and infrasound data (Del Pezzo et al., 2013; Johnson et al., 2018; Kumagai et al., 2005). Whilst Q values hold no such physical meaning for broadband VT events, they describe something about the amplitude decay of the oscillations of the largest peak frequency. In this thesis I have used these Q values as a verification method to distinguish LP and VT style events, and as a metric for event classification. Where appropriate, I have compared calculated Q values for LPs with empirical acoustic impedance calculations to speculate the composition of the resonating fluid-filled crack (Aki et al., 1977; Métaxian, 2003). It is important to recall though, that Q does not hold the same physical meaning for broadband VTs caused by brittle failure or rock fracture.

3.4.1 Methods

Amplitude decay

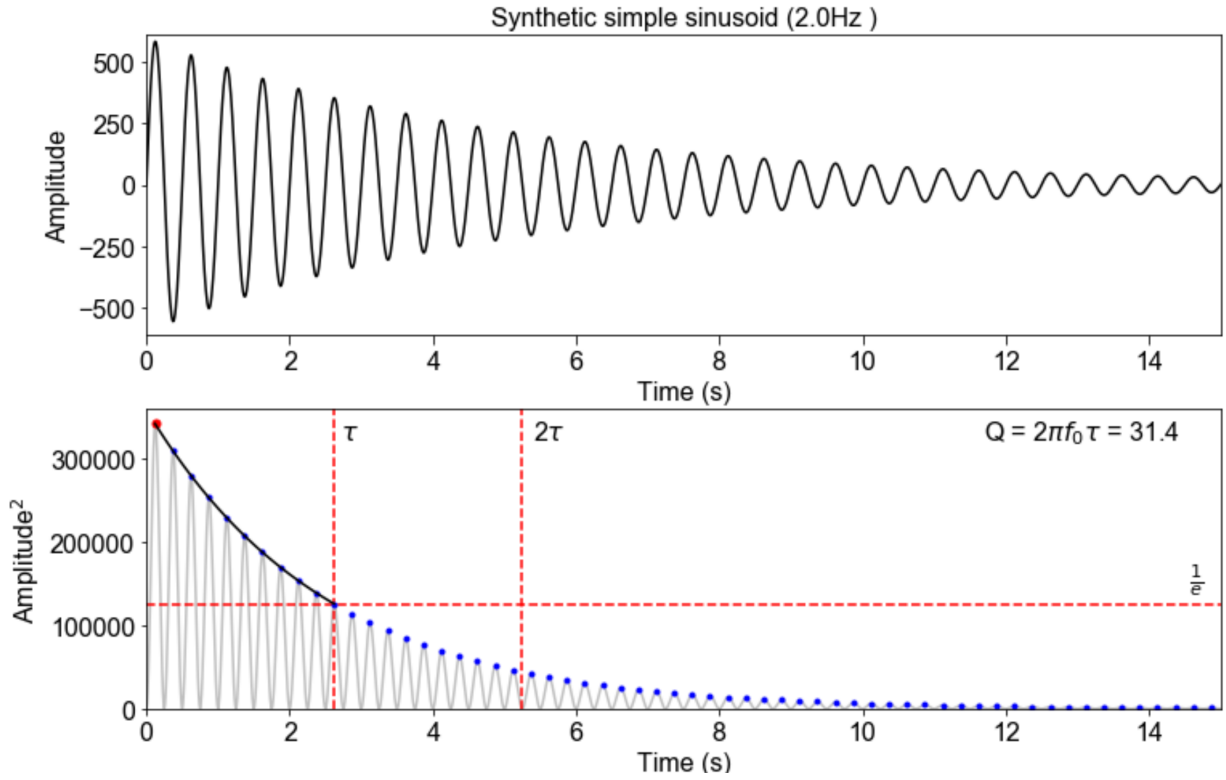

Figure 3.8 Q determined by amplitude decay for a synthetic signal with a fundamental frequency of 2.0Hz. Blue circles mark the peaks of the squared sinusoid through time. Horizontal red dashed line shows $\frac{1}{e}$ of the maximum amplitude of the signal. Vertical red dashed lines show the time required to reach the $\frac{1}{e}$ threshold (labelled τ), and 2τ.

This approach considers the damping of a single oscillation in its purest form (Elmore & Heald, 1985). Q of the resonating media is defined by equation 3.8, where f_0 is the single peak frequency and τ is the time taken for the squared amplitude of the signal to decay to $\frac{1}{e}$ of the maximum value. For an idealised or synthetic waveform, the amplitude of a single frequency oscillator will decay according to how damping the resonator is.

$$Q_{decay} = 2\pi f_0 \tau \tag{3.8}$$

Del Pezzo et al. (2013) approximate that the 'duration' of a signal can be quantified as 2τ, where the signal amplitude is >5% of the maximum (Lipovsky & Dunham, 2015). Figures 3.8 and 3.9 illustrate how Q_{decay} is determined from a synthetic waveform and an LP event at Tungurahua.

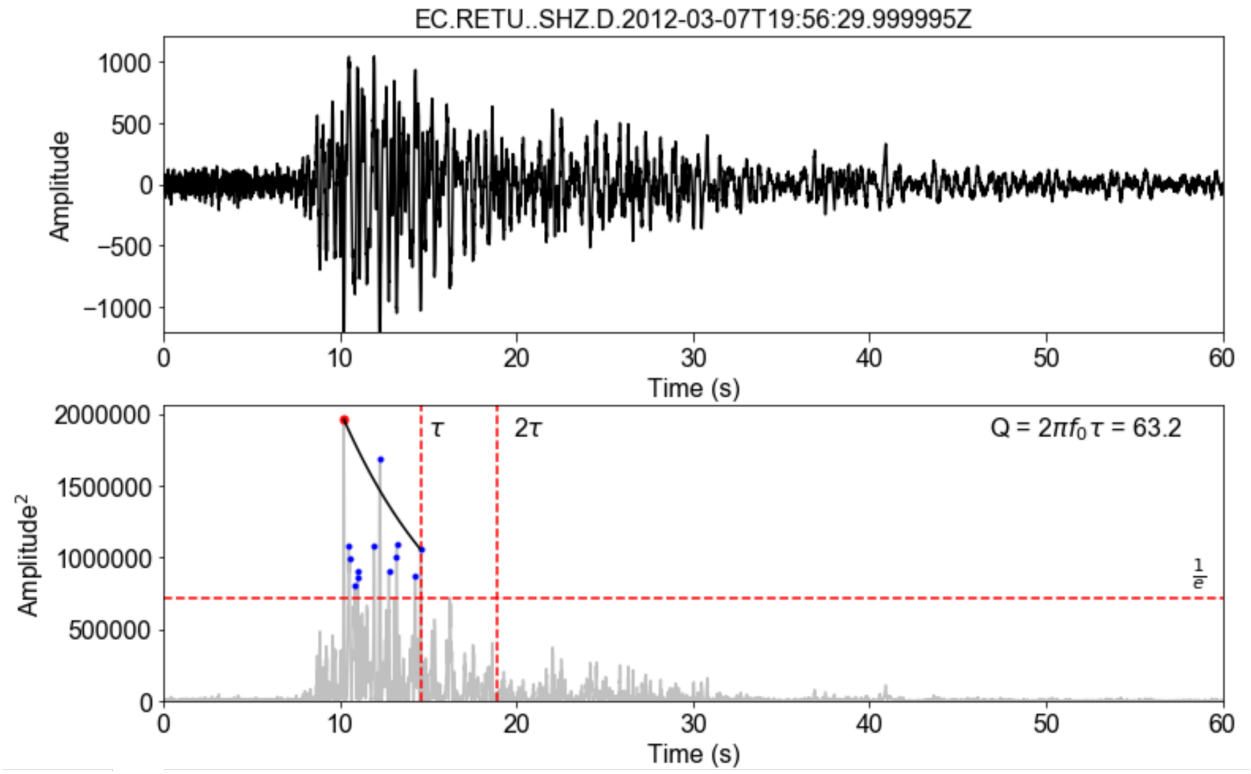

Figure 3.9 Q determined by amplitude decay for an LP event recorded at Tungurahua.

Spectral bandwidth

Inherently related to the damping and exponential decay of a signal amplitude, this approach calculates Q from the bandwidth of the spectral peak of a signal (Rossing & Fletcher, 2004). Q is defined as the ratio between the single peak frequency (f_0) and the spectral bandwidth (δf), where the PSD drops to half the value of the maximum (eq 3.9).

$$Q = \frac{f_0}{\delta f} \tag{3.9}$$

This approach is used in a study of infrasound tornillos at Cotopaxi, Ecuador (Johnson et al., 2018). Again, as with the amplitude decay, this relies on modelling a single fundamental frequency. Johnson et al. (2018) suggest using a smoothed spectra, however, in this thesis, particularly with more broadband events being considered, I have not applied any smoothing to avoid imprinting interpretation on the spectra. Figures 3.10 and 3.11 illustrates calculating the bandwidth on both a synthetic signal and a harmonic signal from Chiles-Cerro Negro volcano.

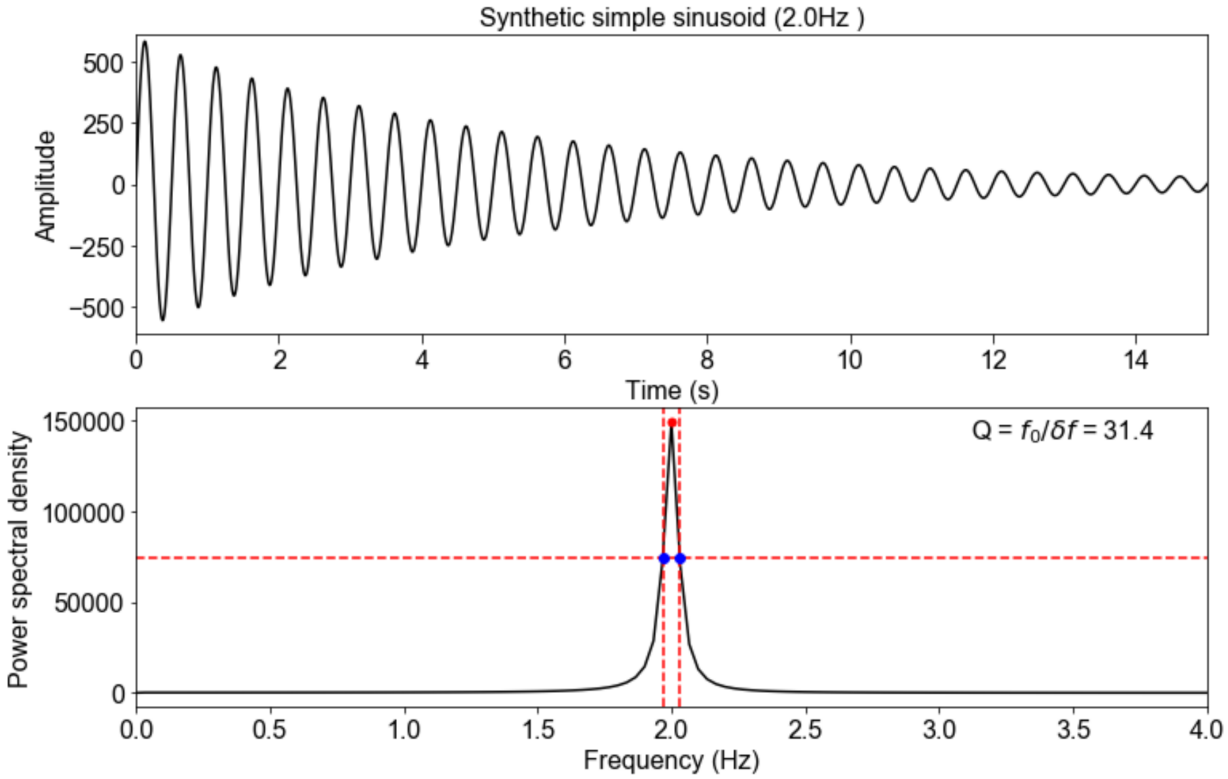

Figure 3.10 Q determined by spectral bandwidth for a synthetic signal with a fundamental frequency of 2.0Hz.

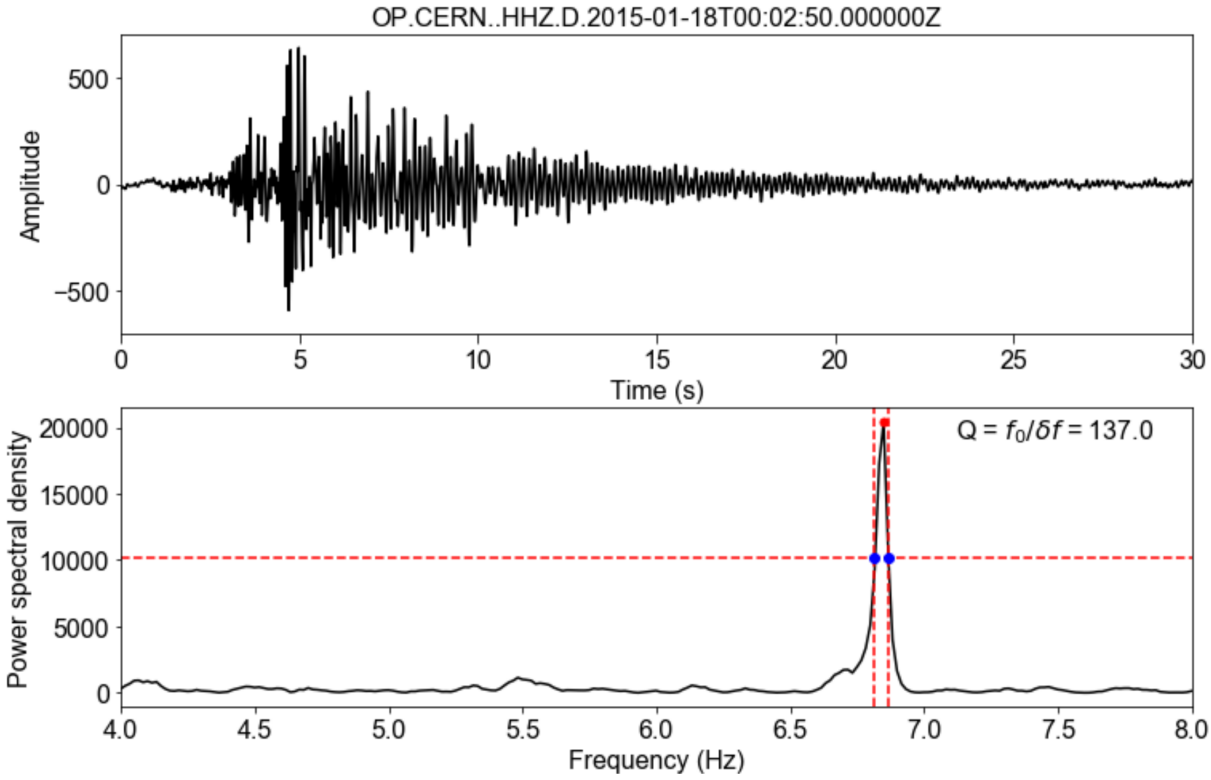

Figure 3.11 Q determined by spectral bandwidth for a real tornillo event recorded at Chiles-Cerro Negro volcano

Auto-regressive methods

The third approach used in this thesis is auto-regressive (AR) methods. AR methods seek to decompose a complicated signal with multiple spectral peaks into individual components of harmonic decaying oscillations. Each of these components can be represented in the complex frequency space and quantified by their fundamental frequency, f (Hz), and a decay rate g (s^{-1}) (Kumazawa et al., 1990). As such, AR methods work well to describe systems with resonance, for example LPs in the fluid-filled crack model (Chouet, 1996). A discrete time series can be considered as several complex functions, each with solutions that are linear differential equations (Lesage, 2008). This discrete time series, x_n, may be expressed as:

$$x_n = \sum_{k=1}^{p} a_k x_{n-k} \tag{3.10}$$

where p is the number of poles and the order of the AR filter, and a_k are the AR coefficients (Hori et al., 1989). There are different ways to calculate the AR coefficients - the most popular is the Sompi method, which uses eigen decomposition (Kumazawa et al., 1990). The Sompi method has been used to determine the Q factors of LP events at Tungurahua, Campi Flegrei and Teide (Cusano et al., 2008; D'Auria et al., 2019; Molina et al., 2004). In this study, however, I have used an adaptation of the auto-regressive moving average (ARMA) method to calculate the Q factor. This is largely supported by MATLAB package, *Seismovolc Analysis* (Lesage, 2007, 2009). The ARMA filter combines the AR filter (eq 3.10) and the moving average (MA) filter (eq 3.11).

$$x_n = \sum_{k=1}^{p} a_k x_{n-k} + \sum_{k=1}^{q} b_k y_{n-k} \tag{3.11}$$

In the ARMA filter, p still represents the order of the AR filter and the number of poles, whilst q indicates the order of the MA filter and the number of zeros. The method relies on calculating the autocorrelation of the signal. The AR and MA coefficients, a_k and b_k respectively, are determined with the Yule-Walker equation and Durbin method (Friedlander

et al., 1984; Lesage, 2008; Marple et al., 1989). Following previous examples in the literature, I calculate cumulative $f - g$ plots for all AR orders from 2 to 30. Points that cluster around a pole at the maximum spectral peak are used to calculate Q (eq 3.12).

$$Q = \frac{-f}{2g} \tag{3.12}$$

The *Seismovolc Analysis* software has a user friendly interface that allows a user to manually select the points associated with a pole to calculate Q, one event at a time (Lesage, 2009). This is how the method is graphically presented in the literature when using Sompi and ARMA (Lokmer et al., 2008; Métaxian, 2003). However, this is not practical for the analysis of tens of thousands of events in a catalogue. As such, I have adapted the method to automatically identify points associated with a pole, using a hierarchical clustering algorithm (Eads, 2008). A minimum number of 10 points is required, within a distance threshold of 0.1 (fig 3.12). If this threshold cannot be satisfied, then no Q value is calculated. When running on a catalogue of mixed LP and VT events, this prevents Q values being falsely calculated for very broadband VTs with no dominant spectral peak.

3.4.2 Synthetic waveform testing

To ensure the output from the Q analyses were robust, I used synthetic earthquakes as a controlled input. This is particularly important given that even very narrow-band LP signals will have a certain amount of noise. It was important to ensure that, for example, systematic increases and decreased in a peak frequency correspond correctly with Q.

Initially I generated single peak frequency sinusoids and applied a taper with time, such that the amplitudes decay exponentially. I systematically increased this single peak and experimented with adding harmonics at integer intervals. I kept the damping factor consistent as a control variable, and so any changes in Q are directly associated with the changing frequency. I ran all three methods to calculate Q and benchmark the different

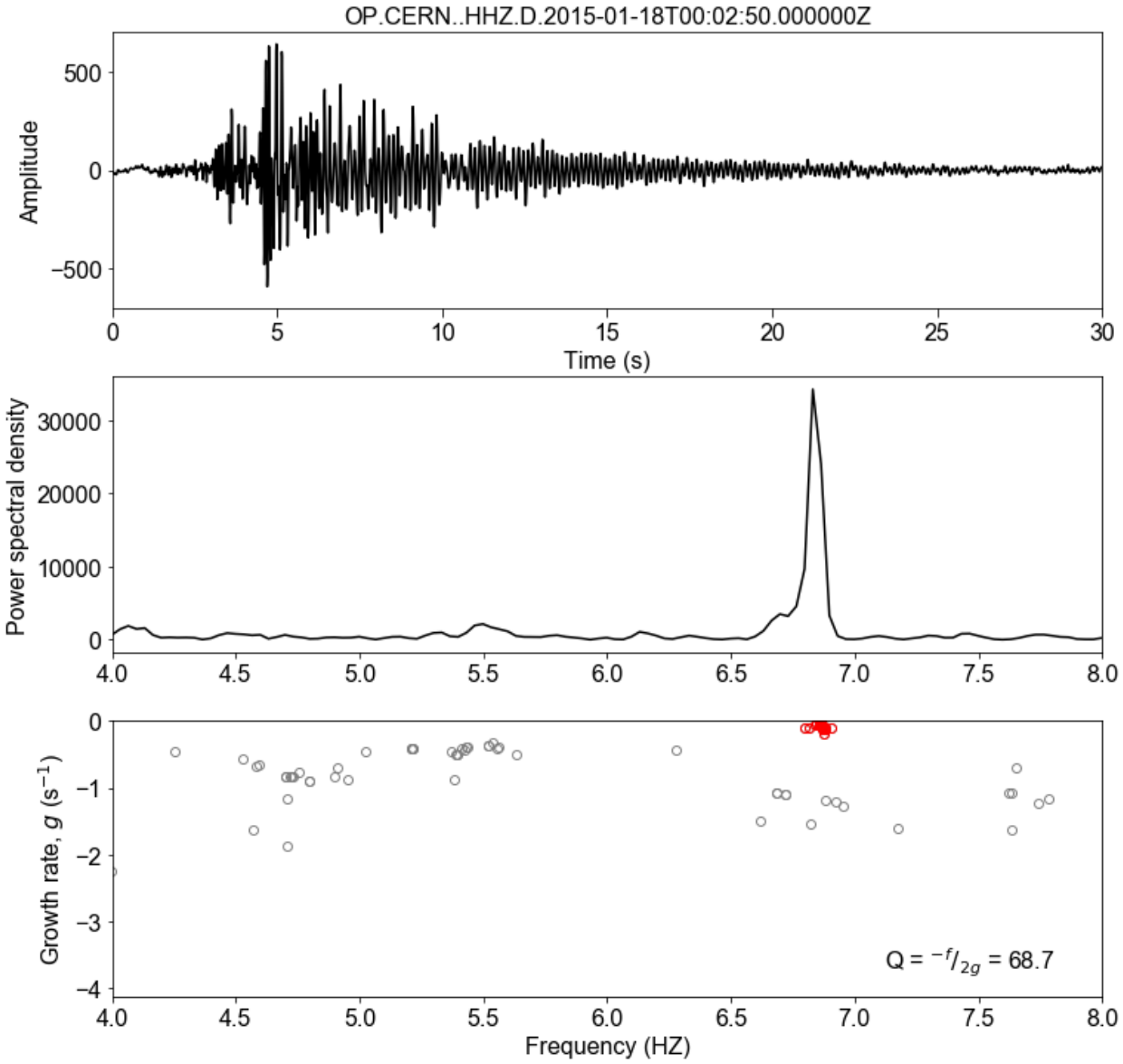

Figure 3.12 Q determined by ARMA for an tornillo event recorded at Chiles-Cerro Negro volcano. Red indicates points that are detected by the clustering algorithm to be within a suitable threshrold around the a pole at the spectral peak.

outputs. I then made synthetic seismographs to imitate certain types of real events, such as LPs and VTs. In reality, an LP event is typically described as a broadband emergent onset signal, followed by a low frequency, long coda tail. Synthetically generating signals with this two-part behaviour is quite complicated, and so this is a simplified approach to generate LP-like events. As an extension of the monochromatic sinusoid testing, initially I generated synthetic seismographs to mimic LPs with a dominant peak frequency. Starting with a single peak sinusoid, I then added gaussian white noise and bandpass filtered between the desired range (1-5Hz). I then applied a taper the continuous signal, to generate an LP-type event. This method is illustrated in the flow chart in figure 3.13. This works particularly well for recreating narrow band LPs that have one dominant peak frequency (fig 3.14).

To test the sensitivity of the Q methods with synthetic data on a larger scale, I created a catalogue of 1000 events where the fundamental frequency systematically increased between events. The increasing peak frequency and resultant Q_{ARMA} values are shown in figure 3.15 and are in a comparable range (5-15) to LPs in the 30 day manually picked dataset at Tungurahua.

3.5 Catalogue analyses

To then contextualise the individual earthquake analysis, I also consider some larger statistics to quantify the whole catalogue of events. These may help to underpin some of the trends, or lack of trends, seen in the signal metrics.

3.5.1 Cross correlation methods

Every event in a catalogue is cross correlated with every other event in the catalogue. Whilst one event is fixed, the other is translated through a sliding window of a fixed length, and at specified increments, returns a cross correlation value. The series of these coefficients generates the characteristic function (fig 3.16). The maximum of this characteristic function

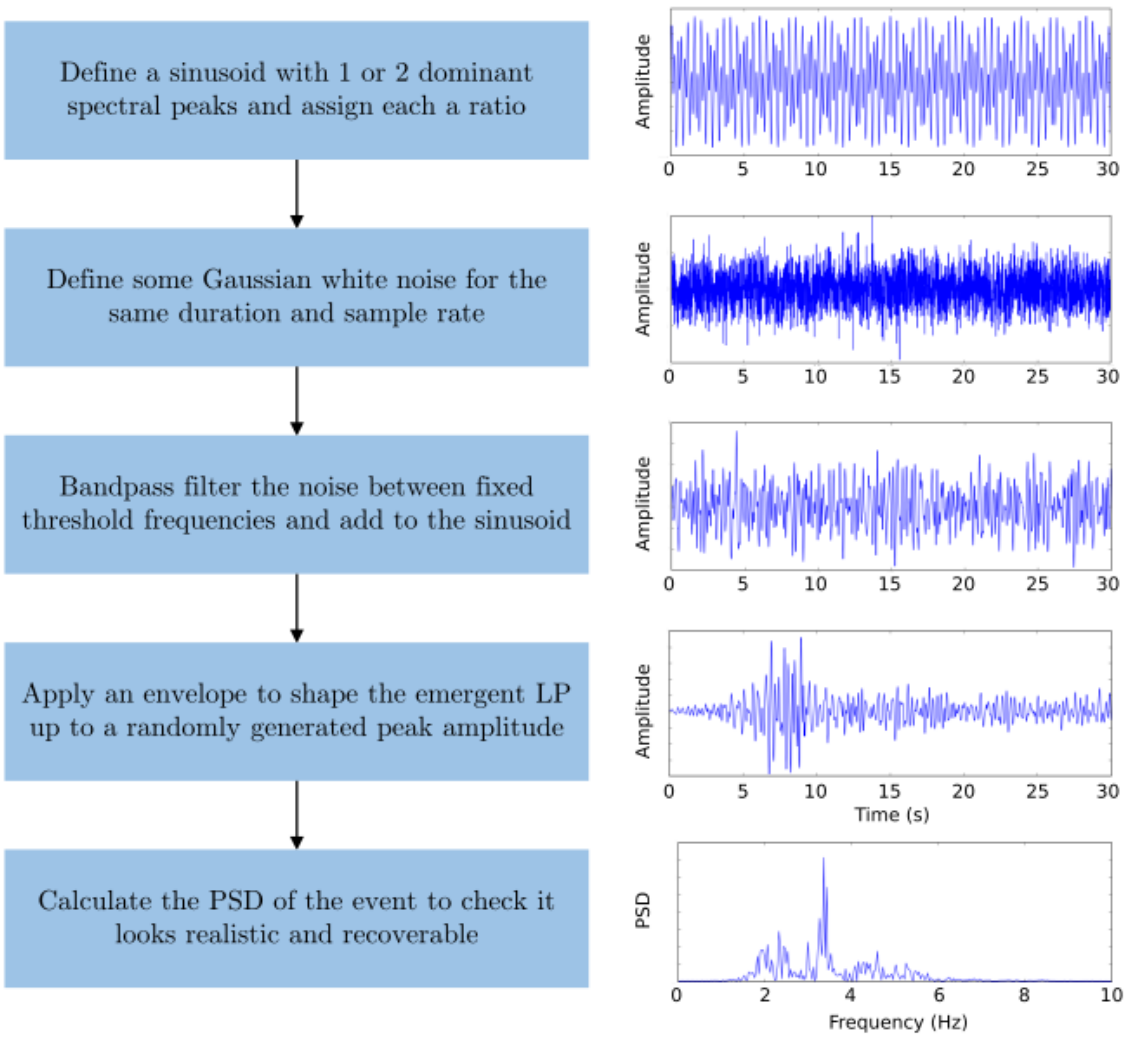

Figure 3.13 Process to generate synthetic seismograph for Q method testing

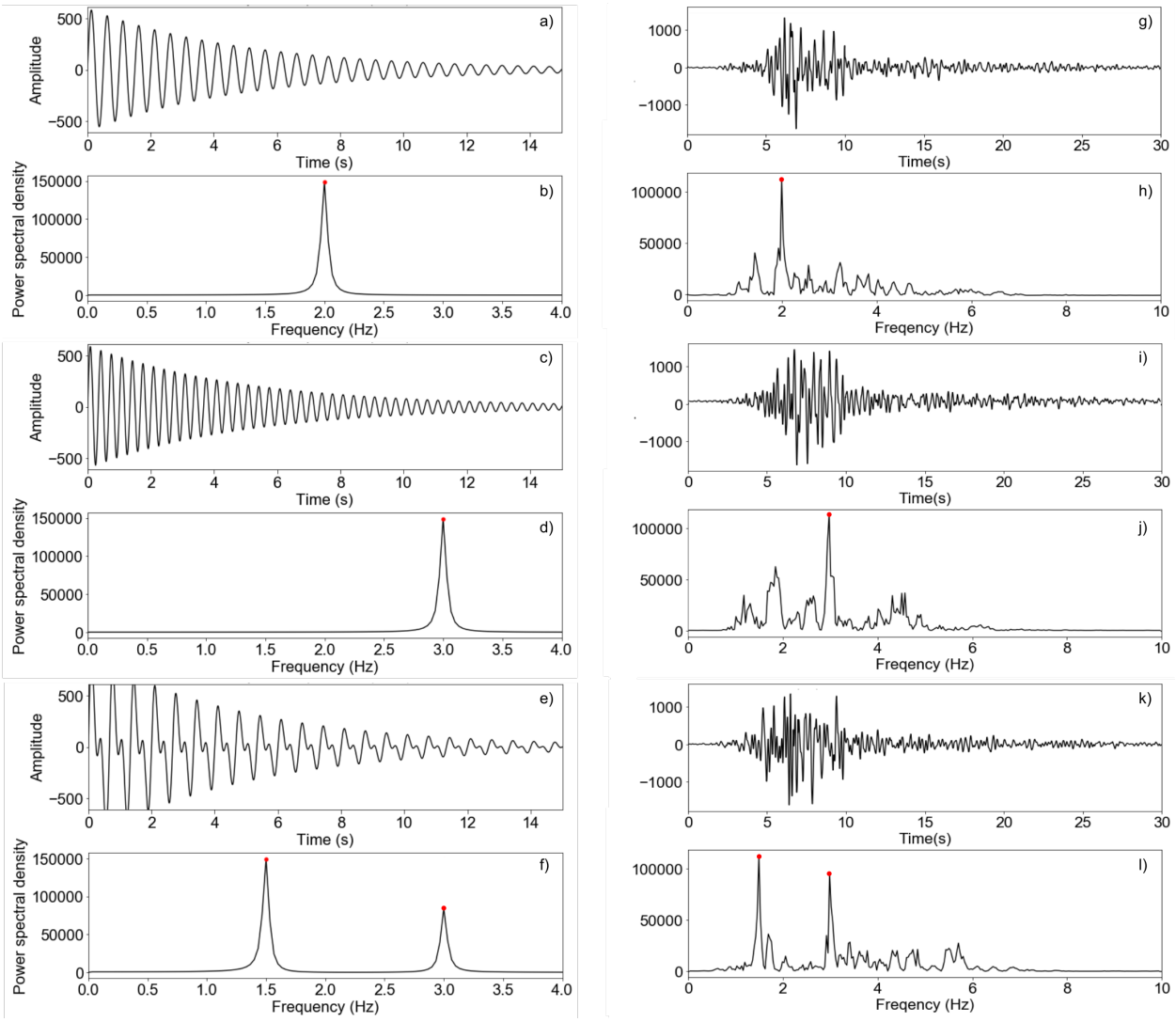

Figure 3.14 Synthetic waveforms for Q factor testing. Left hand side (*a* - *f*) shows sinusoids and periodograms. Right hand side (*g* - *l*) shows synthetic 'LP' events. Panels *a), b), g), h)* have fundamental frequency 2.0Hz, panels *c), d), i), j)* have fundamental frequency 3.0 Hz and panels *e), f), k), l)* have fundamental frequency 1.5 Hz with a smaller harmonic at 3.0Hz.

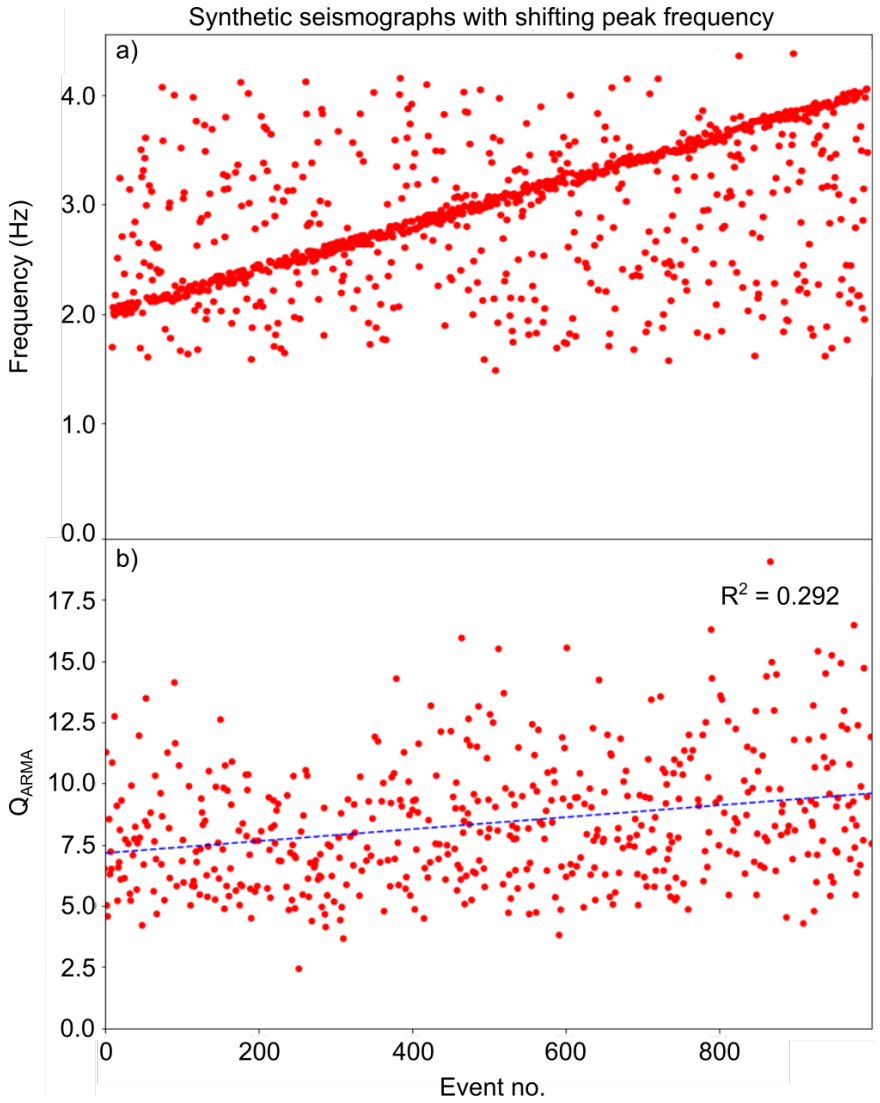

Figure 3.15 1000 synthetic events are generated with a systematically increasing fundamental peak frequency, *a)* spectral peak frequency of the event, and *b)* corresponding Q_{ARMA} value.

is referred to as the cross correlation coefficient (XCC) for the pair. The time needed to translate one signal relative to the other, to generate the maximum XCC, is also returned. The XCC can be considered a measure of similarity (Petersen, 2007). I calculate the absolute maximum XCC and so values are reported between 0 (completely dissimilar) and 1 (completely identical). As with the individual event analysis, this is run initially with a single component from a single station and only requires a single P-wave pick time. However, with further station data available, this can be modified to incorporate more stations and components (Matoza et al., 2013).

Cross correlation analysis has been used in volcano-seismology studies to identify patterns of repeating events, called multiplets or families (Salvage & Neuberg, 2016; Varley et al., 2010b; Waite et al., 2008). Multiple events with high XCCs are considered to be so similar they are indicative of a single source mechanism repeatedly generating the same earthquake signal (Hotovec-Ellis et al., 2018). In order for an event to be considered in a family, I have followed previous studies and impose a threshold XCC value of 0.7. I also set a minimum requirement of 10 events in a family, to avoid over interpreting localised pairs of similar events. From the matrix of XCC values, the event with the most XCC values > 0.7 is extracted as the 'master' event of Family 0. Every event that has an XCC > 0.7 with respect to the master is included in the family. Once an event is in a family, it cannot be included in any subsequent families. This process is then repeated for Family 1 and continues until the no more families can be defined. Within each family I stack all the events to generate an average event that represents the family. I have also calculated the cross correlation between all the master events and between all the stacked events in order to determine how similar the families are to one another. By grouping the events into families, I can then look at the individual signal processing metrics to establish if there are any distinct patterns or differences between the families of earthquakes and perhaps infer a distinct or changing source mechanism.

I ran the cross correlation analysis using the ObsPy function `xcorr_pick_correction`

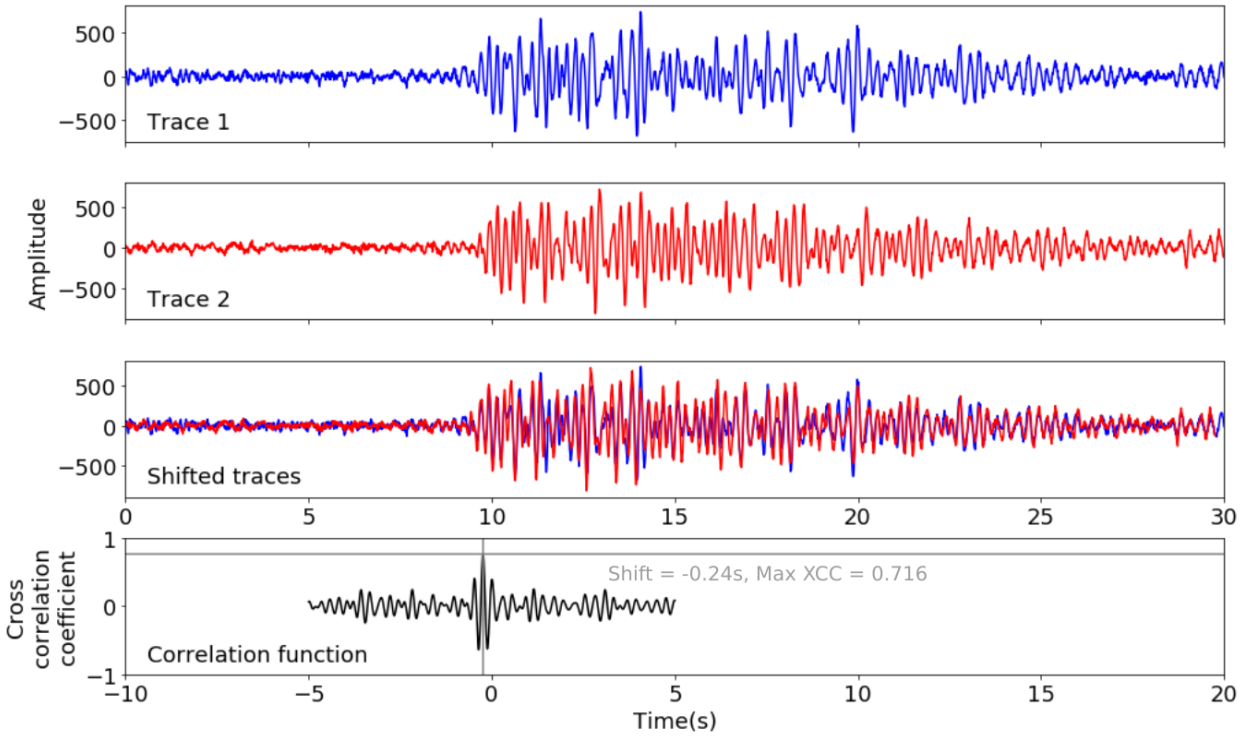

Figure 3.16 Cross correlation analysis for two sample events from station RETU. The absolute maximum cross correlation coefficient (XCC) and the relative shift required is determined from the characteristic function.

(Krischer et al., 2015). There are a number of similar functions which all ultimately cross correlate two signals, however, this function specifically allows the user to control the search window. It is important to consider which part of the earthquake signal has been correlated and what a high XCC value physically means. For example, if there is a high XCC between two LP events, then a high XCC in the coda might imply the same resonance fluid or geometry, whereas a high XCC in the onset might relate to the excitation mechanism. The length of the search window used, should also be informed by the picking method. Manually picked catalogues have small errors in the P-wave pick time ($\pm$1s) whereas automatically picked event may have larger associated errors (>3s), and so the search windows should be more generous for automatically picked catalogues. This is to ensure that the pick time and event onset are firmly within the chosen window to be cross correlated. The `xcorr_pick_correction` function allows the user to define the time before and after the pick to be correlated, rather than being centred on the pick time. By default I cross correlate 3s before the pick time and up to 6s after the pick time, although where used in chapter 4, 5 and 6, specific parameters are stated.

3.5.2 Temporal methods

In order to understand how the seismicity varies through time within a specific catalogue, I also generate metrics relating to seismicity rates. For the whole catalogue, I calculate the inter-event times (IETs) and from these values I calculate the periodicity (Bell et al., 2017). The periodicity is defined in Bell et al. (2017) as the ratio between the mean (μ) and the standard deviation (σ) of the IETs. This approach assumes that for events that are randomly distributed, the IETs will follow an exponential distribution and periodicity, $\mu/\sigma = 1$. As illustrated in figure 3.17, events which are clustered in time have a periodicity value much less than 1, and periodic events have a periodicity much greater than 1. The periodicity is calculated in fixed bins of 10 - 25 events, depending on the length of the catalogue.

This metric is particularly useful in drumbeat studies to determine whether the events are becoming increasingly or decreasingly periodic. In chapter 5, I have explored further Bayesian statistical approaches to modelling temporal rates of seismicity at Tungurahua.

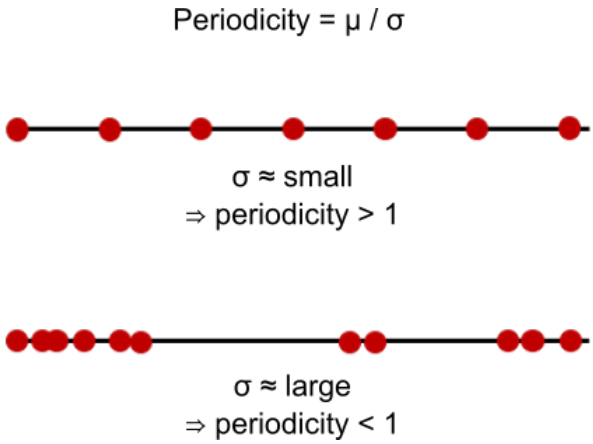

Figure 3.17 Periodicity values for repeating, periodic and clustered, swarm earthquakes. In the equations, μ is the mean, and σ is the standard deviation.

3.6 Summary

I have addressed research questions 1 and 2 by generating a reproducible, simple workflow that can be adopted for single station, single component data and tested the methods on synthetic and real seismographs. The signal processing routine and catalogue statistics laid out in this chapter form the basis of initial inquiries into seismic unrest at Tungurahua and Cayambe volcanoes in chapters 4 - 6. The suite of metrics generated by this methodology are then be used in conjunction with additional available geophysical monitoring data to inform interpretations of source processes and conduit dynamics. I have also justified the use of automatic and template matched picks alongside manually picked earthquakes and catalogues provided by IGEPN. For a volcano with some historic seismic data, but no formalised catalogue of located earthquakes, this small investigation into automatic picking methods could inform the approach to curating the first catalogue.

4 | Periodic seismicity at Tungurahua Volcano

Preface

In the literature review in chapter 2, I introduced Tungurahua volcano and some of the existing studies from the most recent eruptive phase. Tungurahua was persistently active for over 17 years in which time a significant volume of data was recorded - much of which has not been documented in the literature. Whilst IGEPN work hard to maintain a permanent geophysical monitoring network, there are also limitations in its capacity. This in turn means that research into the seismicity here, has often been limited to only a few individual episodes of unrest. In this chapter, I have examined a longer timeline of activity at Tungurahua. Predominantly using a single station and a single component, I applied the signal processing routine described in chapter 3 to attempt to quantify the behaviour of the seismicity from 2012 - 2016. I chose to look at these five years for two reasons: existing studies of pyroclastic deposits and SO_2 flux suggest there is a transition from more continuous to more episodic activity in this time. This includes the end of the eruptive phase at Tungurahua. It is well known that the end of eruptions can be hard to accurately pinpoint (Manley et al., 2020). However, in this chapter, I aim to investigate whether the last-seen activity at Tungurahua was truly the end of the eruption, using evidence from the seismic record. The signal processing workflow has been thoroughly tested on synthetic waveforms and idealised samples

of real earthquakes, however, this chapter provides an opportunity to test the methods on complete catalogue of events.

I have specifically focussed on episodes of periodic drumbeat seismicity. Figure 2.4 illustrates examples of swarm seismicity and drumbeats recorded around the world, however, these are often modelled according to a specific source mechanism relevant to a unique volcano. By examining a longer timeline of activity across different eruption styles, I investigate whether drumbeats can be explained by a more generalised model for intermediate-composition arc volcanoes.

In this chapter I address research questions 3, 4 and 5. This chapter has been written in a manuscript format, with intention for adaptation and publication following submission of the thesis.

4.1 Introduction

4.1.1 Tungurahua Volcano

The most recent eruptive phase at Tungurahua began in 1999 and remained persistently active until the last recorded explosions in March 2016. At the time of writing, there have been no significant episodes of unrest for over five years and it is thought that the system has 'switched off' (IGEPN, 2016a). Activity between 1999 and 2006 was continuous but rarely explosive, with ongoing Stromboblian style eruptions and no recorded pyroclastic density currents (PDC) (Bustillos et al., 2018). However, following a subplinian explosion in August 2006, the first PDCs were generated and there was a marked shift in eruption style (Hidalgo et al., 2015). Eruptions transitioned from being continuous to episodic, particularly during 2013 - 2015 when VEI 2 events became particularly periodic and occurred repeatedly every 3 - 4 months (Hall et al., 2015). This shift in style has been captured in the geophysical monitoring

data. Patterns in SO_2 flux distinguish four main periods of activity from 2007-2014 (Hidalgo et al., 2015), whilst geodetic studies have also been used to identify separate phases of magma ascent (Muller et al., 2018). Studies of the seismicity, however, have typically focussed on individual explosions. For example, the largest and only sub-Plinian eruption from this eruptive phase occurred in August 2006 (Fee et al., 2010b; Matoza et al., 2014). The intense Vulcanian eruption in July 2013 was accompanied by one of the largest infrasonic signals ever recorded and has also been well documented (Anderson et al., 2018; Bell et al., 2018). Here, I take the opportunity to examine a much longer eruption timeline in detail, encompassing several eruption styles. Careful understanding of the eruption dynamics, and particularly what can be determined from the seismicity, may be beneficial in informing the monitoring and decision making at nearby and analogous volcanoes.

A summary of eruptive activity between 2012 and 2016 is shown in figure 4.1, including a panel detailing specific publications that cover episodes of unrest. I have chosen to examine this window as it encompasses several shifts in eruption style and the transition to quiescence in 2016. In 2012, after 6 months of repose, activity resumed and was almost continuous throughout the year (Hidalgo et al., 2015). However, in 2013 and 2014, cycles of repeating Vulcanian explosions began, including the powerful Vulcanian eruption on 14th July 2013 (Battaglia et al., 2017). Petrological studies of the ejecta, suggest that a conduit plug was entirely blown out during this eruption (Bustillos et al., 2018; Gaunt et al., 2020). Complete removal of a plug caused a change in the dynamics of the system, and thereafter the seismicity and activity was distinctly different. Studies of tephra deposits from sequential events in 2013 and 2014, also infer repeated sealing and partial rupture of a conduit plug (Hall et al., 2015). Seismicity and explosions persisted into 2015 although much more erratically and without a clear repose period between each episode of unrest. It is suggested that these irregular episodes of seismicity were the result of more complex interactions in the conduit and plug (Bell et al., 2018; Butcher et al., 2020). The final explosions and apparent 'switching off' of the system at Tungurahua is currently undocumented in the published literature. Although

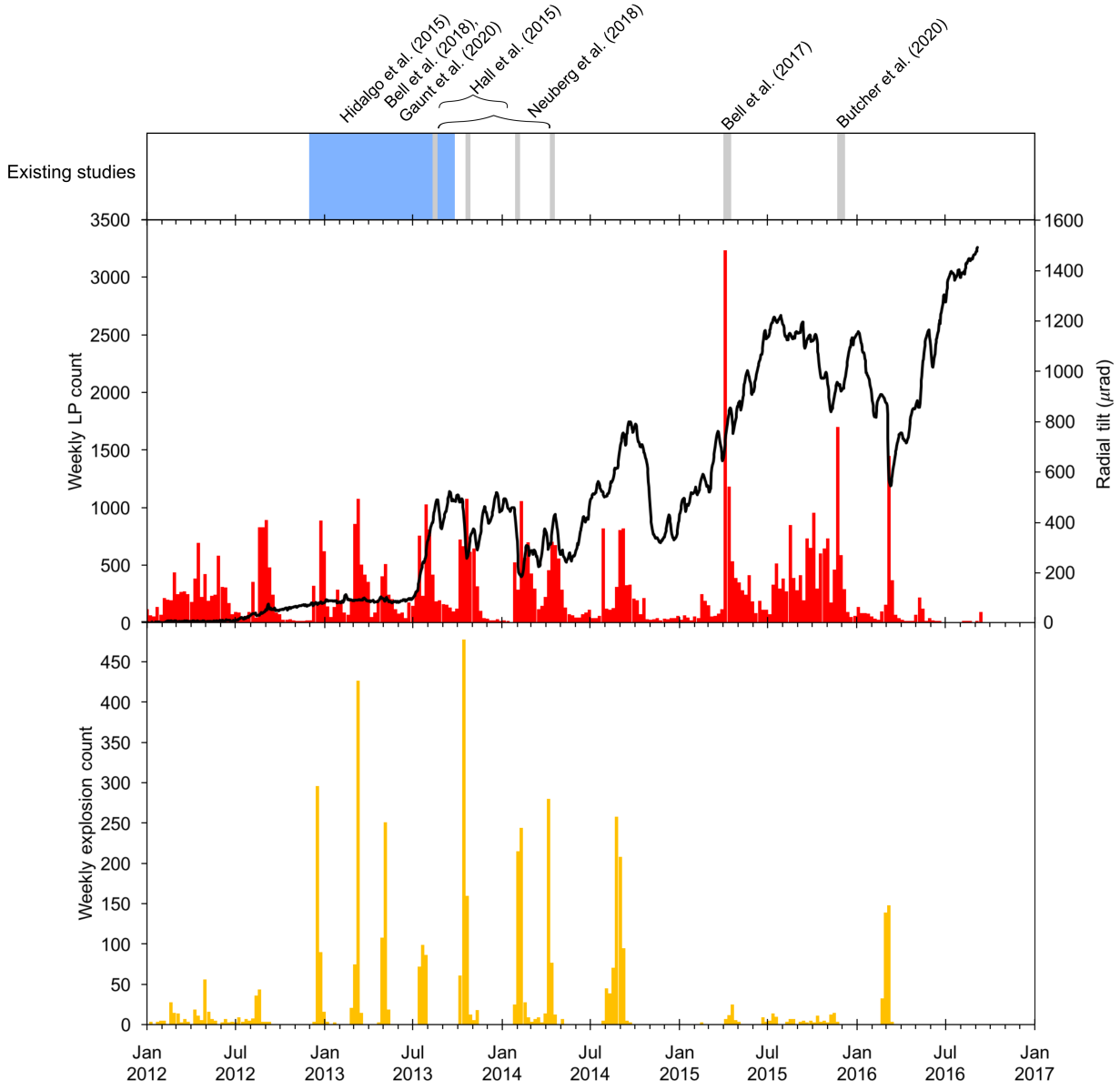

Figure 4.1 Summary of activity at Tungurahua 2012 - 2017. Weekly LP event counts are shown in red bars, and weekly explosion counts are show in yellow bars. Radial tilt data at station RETU is overlain in black, relative to the reading on 1st January 2012. The top panel indicates publications relating to seismicity and significant explosive episodes at Tungurahua.

the seismicity and explosions appear to stall after March 2016, the radial tilt measurements show a continued inflation signal (fig 4.1). Here I look to quantify the seismicity across four years; including two years which are very well studied (2013-2014), and two years which are

relatively poorly understood (2015-2016).

4.1.2 Long period seismicity

I have focussed on the significant episodes of long-period (LP) seismicity, as these dominate the records at Tungurahua volcano (fig 4.1 and section 2.3.1). An LP earthquake is defined as an emergent signal, with a long (<30 s) low frequency (≤5 Hz) coda (Chouet, 1996). LP signals have been modelled as a two part process, caused by the excitation and subsequent resonance of a fluid-filled crack (Chouet, 1992). As such, LP seismicity in the very shallow edifice is often associated with fluid processes such as magma emplacement, degassing, and hydraulic fracturing of rock (Almendros et al., 2014; Fournier, 2007; Frank et al., 2018; Kumagai et al., 2005) (section 2.2.2). Specifically, periodic and repeating LP swarms, sometimes known as drumbeats, have been modelled as processes associated with stick-slip ascent of a shallow conduit plug (Iverson, 2008), and shearing of the conduit margins (Neuberg et al., 2006). Repeating LP seismicity may also be generated by hydrothermal interactions (Cusano et al., 2008) or material failure (Bean et al., 2014). Therefore, understanding the characteristics of LP seismicity and distinguishing sources, may be crucial to identifying precursors to an eruption (Poland & Anderson, 2020). Not only do LPs dominate much of the seismicity at Tungurahua, but previous studies have shown swarms of LP events and radial tilt cycles occurred out of phase with one another (Bell et al., 2017; Neuberg et al., 2018). As figure 4.1 illustrates, the explosions at Tungurahua also occurred during key cycles of LP swarms. This raises questions about the driving processes and inherent links between deformation, drumbeat LPs and explosive activity. It is important to carefully explore the behaviour of the seismicity in these episodes, relative to one another and any other geophysical time series available.

Here I investigate in detail, episodes of repeating LP seismicity by quantifying and characterising the signals in each instance. In particular I focus on any changes in behaviour

through known cyclical eruptions, to the breakdown and termination of eruptions in 2016. By tracking subtle changes in the signal properties I suggest the likely source mechanisms. I then use surface observations, gas flux and deformation data to complement the findings from the seismicity and describe the timeline of activity from 2012 - 2016, and propose a model for the dynamics of the shallow conduit at each stage.

4.2 Data & Methods

4.2.1 Geophysical monitoring

Since the resumption of eruptive activity in 1999, Tungurahua volcano has been continuously monitored by the Insituto Geofísico Escuela Politécnica Nacional (IGEPN) (section 2.3.1, fig 2.8). As a result, there is a vast amount of qualitative and quantitative data capturing the 17 years of activity at Tungurahua. For this study, I began with a catalogue of picked seismic events, collated by IGEPN. Where possible, these are labelled according to event type, as either long-period (LP), volcano-tectonic (VT), hybrid (HYB) or tectonic (TECT) (section 2.3.1). For the period 2012 - 2016, 97.5% of events are labelled LP, and 97.2% of total events are recorded at RETU (fig 4.1). This is likely a result of the network geometry, as RETU lies just 2 km from the crater edge and so many more small LP events in the shallow edifice are well captured here. VT seismicity accounts for only 1.9% of the total number of events, but often occur in short swarms when they dominate the catalogue, deeming them worthy of investigation. Initially, however, I focussed only on LP events at RETU. Using a fixed bin width of 25 events, I calculated the periodicity. The periodicity is defined as the ratio between the mean, μ, and standard deviation, σ, of the inter-event times (IETs). It is assumed that randomly distributed events in time will have a periodicity of 1, clustered events will have a periodicity much less than 1, and periodic events will have a periodicity much greater than 1 (Bell et al., 2017). I then manually inspected the waveform data where periodicity values

were greater than 1.5. In some instances, where seismicity rate was very low, for example, one event per day, a high periodicity value was generated. These periodicity highs are an artefact of the method, rather than truly an instance of a repeating LP drumbeat process and so these were eliminated from further investigation. In this study, I refer to to drumbeats as any episode of LPs where the periodicity is > 1.5. Later in the signal processing I run cross correlation analysis to determine similarity and suggest whether events are repeating. However, at this stage there is no requirement for any event similarity.

From the remaining periodic episodes, I have defined seven episodes of unrest to examine. For each episode, I had to ensure a robust catalogue of earthquakes was used. Whilst the catalogues provided by IGEPN are an excellent resource, there are periods where clearly earthquakes have not been picked. Where periodic seismicity is confined to just a few hours or days, I manually picked events to ensure all events are identified and the pick time is as accurate as possible. The human error associated with manually picked events is constrained to ± 1 s. For longer episodes of unrest over several months, I utilised automated picking methods. I ran a short-term-average/long-term-average (STA/LTA) algorithm over the waveform data (section 3.2.1). This method compares the ratio of signal amplitudes over a short and a long term range and when the ratio exceeds a certain threshold a pick time is automatically triggered. I used 3 and 6 seconds for the short and long term windows respectively. I then cross referenced the STA/LTA picked events with catalogued events. Those that lie within 2 seconds of a catalogue pick were retained and the remaining events were considered newly identified. The automated STA/LTA method is prone to identifying erroneous events such as noise spikes. In order to quality control the newly identified picks, a manual inspection of all the new picks was used to reject invalid events that are evidently noise spikes. The verified new STA/LTA picks were then added to the existing catalogue picks, to proceed with waveform analysis. The study periods identified are illustrated in figure 4.2.

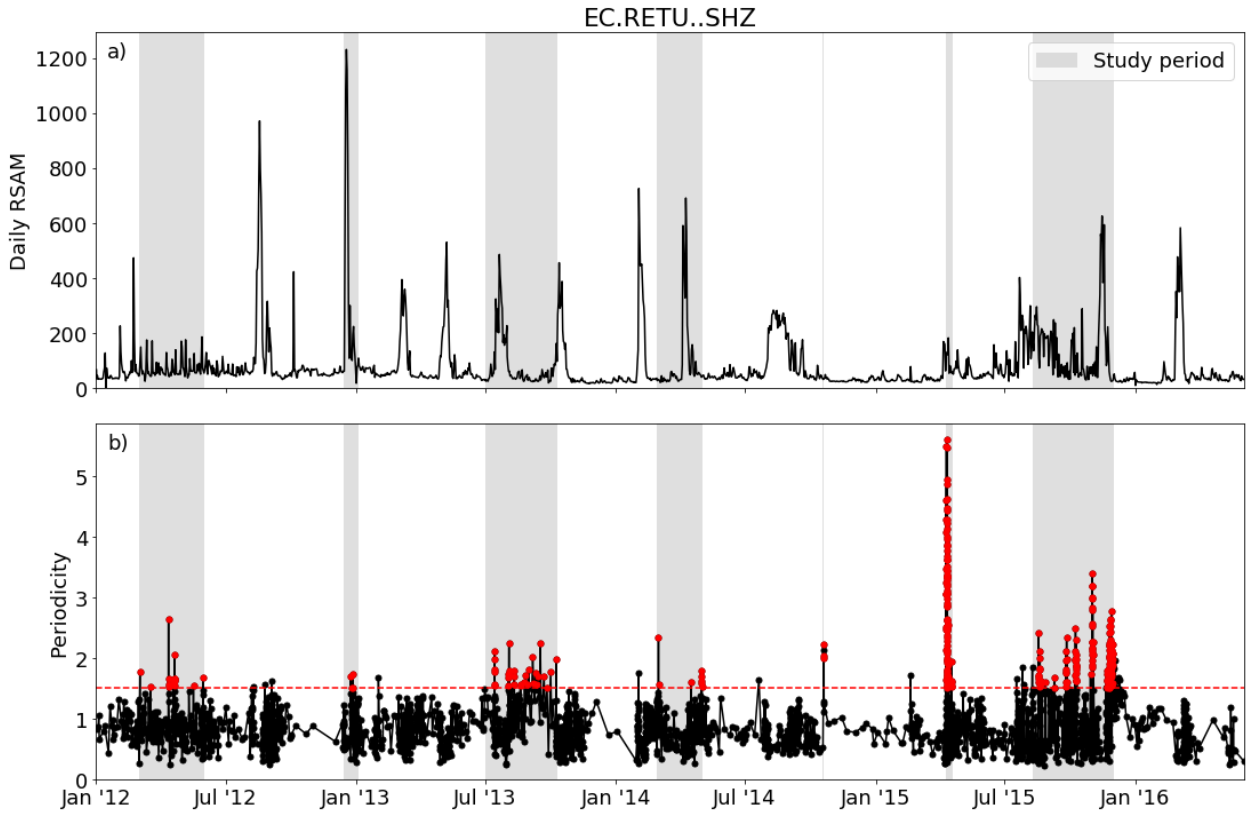

Figure 4.2 Catalogue periodicity at Tungurahua. Periodicity is calculated in a fixed bin width of 25 events. *a)* Daily relative seismic amplitude (RSAM) at station RETU, *b)* periodicity. Red dots show sustained or significant periodicity values >1.5 examined in this study, and grey panels show study periods.

4.2.2 Signal processing

In order to quantify the LP seismicity in each periodic episode, each event is individually analysed through a comprehensive workflow to determine the signal metrics. Raw seismic data is handled and initially processed with the ObsPy toolkit (Krischer et al., 2015). The L4C short period instrument at RETU is only robust $\geq$ 1 Hz (fig 2.9). RETU samples at 100 Hz, and so the Nyquist frequency is at 50 Hz. In order to eliminate any erroneous low frequency signal, or high frequency external events, such as rockfalls (Feng et al., 2019), the waveform data from RETU is bandpass filtered between 1 and 40 Hz. For each picked event time, the waveform is sliced 5 seconds before the pick time, and 25 seconds after, to create

a 30 second trace. I followed the signal processing routine as described in detail in chapter 3, although some of the individual parameters used are summarised here.

To initially understand how similar the events in an episode are, I ran a cross correlation analysis. Each event is cross correlated with every other event, returning a cross correlation coefficient (XCC) between 0 and 1 and a lag time. I followed previous studies and enforced a threshold XCC value of 0.7 and a minimum family size of 10 events (Butcher et al., 2021; Petersen, 2007; Thelen et al., 2011). One event cannot belong to more than one family, even if the XCC value is >0.7 for multiple master events.

For every waveform, I then calculated the maximum amplitude, peak frequency and Q factor of the signal. Given the majority of the LP seismicity is only well captured station RETU, I was not able to accurately determine locations, depths or magnitude estimates for these events. The absolute maximum of a waveform is considered a proxy for magnitude, as discussed in section 3.3.1. I calculated the peak frequency from the periodogram of the event. This can be a misleading metric for very broadband events, however, a single consistent peak frequency in a series of many hundreds or thousands of events may be indicative of a more sustained and significant repeating process. I calculated the Q factor using an auto-regressive moving average method (Q_{ARMA}) (Kumazawa et al., 1990). This is a similar approach to the commonly used Sompi method (Hori et al., 1989) and assumes that an earthquake signal is the superposition of multiple individual decaying harmonic oscillations. Each oscillation can be defined by a complex frequency, f (Hz), and growth rate, g (s^{-1}). I generated cumulative $f - g$ diagrams for all AR filters from 2 to 30, and points that cluster around a pole are used to determine the Q_{ARMA} factor (Lesage, 2009). Following Q factor methods in Del Pezzo et al. (2013) (and section 3.4 in this thesis) which assumes that the squared amplitude of the signal decays to e^{-1} of its maximum in time, τ (s). I used the metric τ as a proxy for event duration.

If there was reason to investigate a specific episode, for example a clear distinction in families or a significant step up in absolute amplitudes, then I also quantified the signal

envelope by calculating the $K_{1,2}$ values (Lees et al., 2008). I assume the emergence of a signal, from the picked first arrival to the maximum amplitude, can be defined by an exponential curve, $y = Ae^{K_1 t}$. Similarly the decay of the signal can also be quantified with an exponential decay fit between the point of maximum amplitude and a 'background' threshold. This decay parameter, K_2, should mirror the findings of the τ metrics. However, one of the defining features of LP events their emergent onset, and the K_1 metric aims to quantify this feature.

Finally if visual inspection of the waveform data suggested extended periods of tremor, I ran an automated scan for harmonic signals. I used a 60 second running window across waveform data and calculate the periodogram. If the power spectral density (PSD) at the peak frequency, f_0 was more than 10^2 times greater than the next peak in the periodogram, the window was flagged as being potentially harmonic tremor. These are then manually verified. I ran a second pass using the Harmonic Product Spectrum (HPS) method (Roman, 2017) to quantify any integer harmonics associated with the peak frequency, f_0 and the intensity of the harmonicity.

4.3 Results

The catalogue periodicity search highlighted seven episodes of drumbeats to focus my efforts. Notably, there was no periodic seismicity beyond 2015, including within the final series of explosions. The cyclical Vulcanian bursts are clearly visible in the RSAM (fig 4.2) although not all of these are associated with periodic seismicity. The study periods range in duration from a single day up to several months. Here I present the results of the waveform analysis for each of the episodes, to describe the characteristics of the seismicity in each instance.

4.3.1 Episode 1: April - May 2012

This was a moderately active period for Tungurahua. There were explosions documented most days although often described as small and typically <10 per day. SO_2 flux measure-

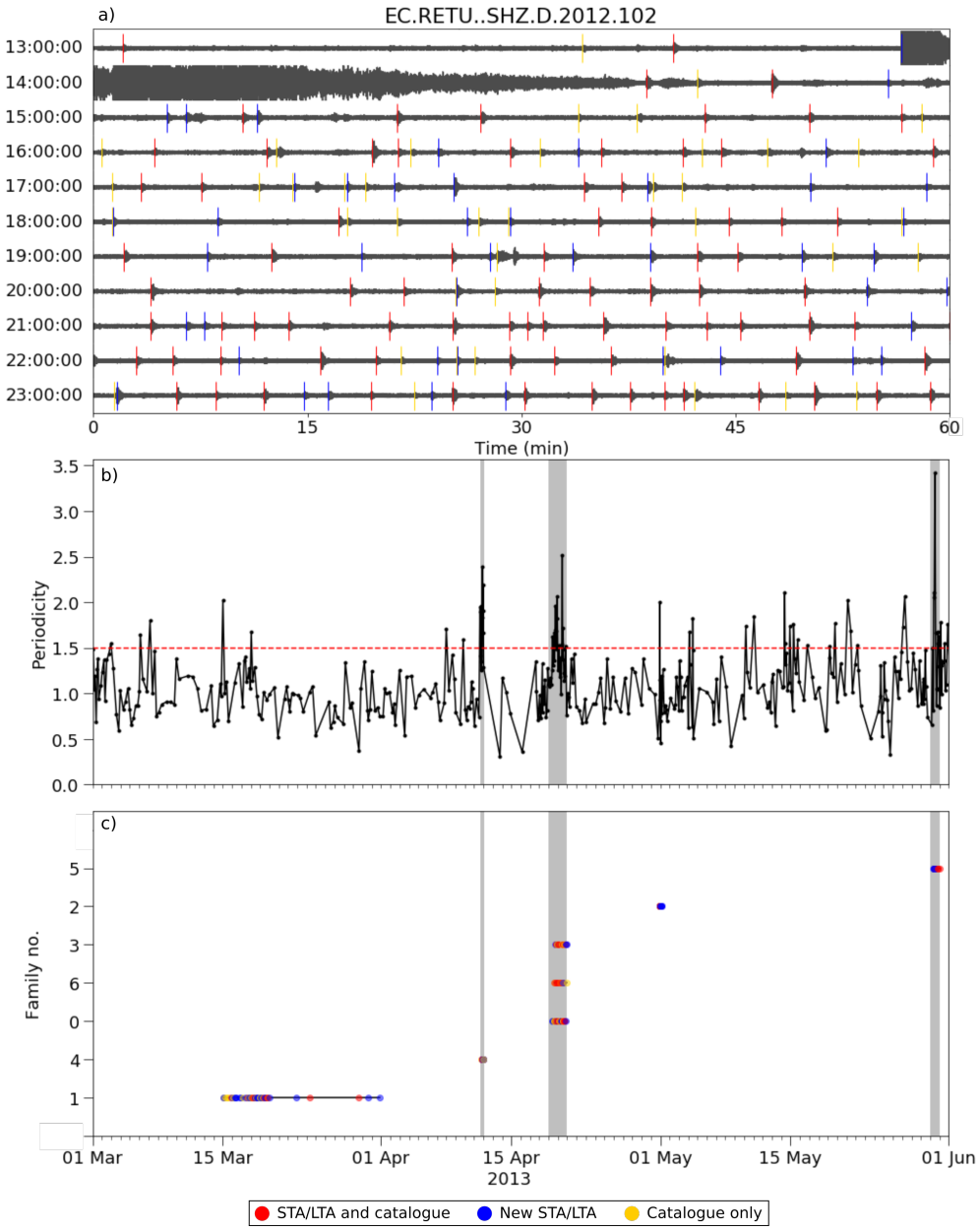

Figure 4.3 Episode 1: periodic seismicity in April 2012, *a)* Waveform data at station RETU, 11th April 2012, *b)* Periodicity calculated from all picks, including catalogue and STA/LTA picks, *c)* Families identified by cross correlation analysis. There is a connecting vertical line connecting the first and last event in a family (although due to the spread of events, this is only visible in family 1). In all panels, red events are those that were in the catalogue but were also identified by STA/LTA, blue shows new events found by STA/LTA that were not previously in the catalogue and yellow marks events from the catalogue that are used but were missed by STA/LTA methods. Grey panels indicate the 3 major bursts of periodic seismicity identified from the initial catalogue scan of 2012-2016.

ments range from 500 - 1500 tonnes per day and emissions with moderate ash loads were recorded between 1 and 5 km above the crater (fig B.1). Small episodes of magma extrusion were documented although there is no record of lava fountaining during this time.

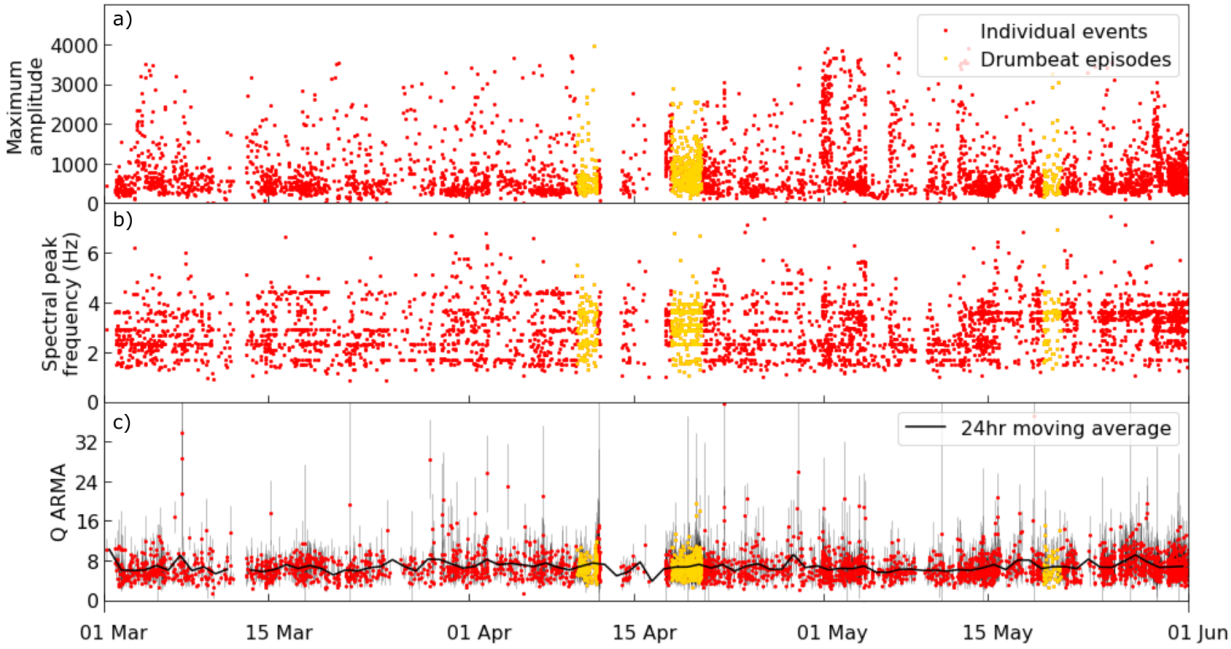

Figure 4.4 Episode 1: Individual event metrics for Spring 2012 seismicity, *a)* Maximum event amplitude, *b)* Peak spectral frequency, *c)* Q_{ARMA}. In all panels, red circles mark all events, but yellow events are within the automatically identified drumbeat windows.

The initial search for periodic events, identified three separate instances where periodicity exceeded 1.5, on 11th April, 18th April and 31st May 2012. Individually these three days appeared to be clear instances of drumbeats, however manual inspection of the signal at RETU, suggested there may be ongoing quasi-periodic seismicity throughout May. As such, I used STA/LTA methods to automatically pick events at RETU between 1st April and 1st June 2012. The STA/LTA identified 2773 new events in this 2 month period, in addition to the 3290 catalogue events, which were passed for analysis. Figure 4.3a shows the short, intense burst of drumbeats identified on 11th April and how the picks were identified. Here, red picks show events that were in the IGEPN catalogue and were also identified

by the STA/LTA search. Blue picks show events which were found by STA/LTA but were not in the IGEPN catalogues. Yellow picks are catalogue picks which were not identified by STA/LTA. The number of blue picks in figure 4.3a indicate that although the IGEPN catalogue was very thorough, additional STA/LTA fills in some gaps. The high number of yellow picks, however, highlights that STA/LTA parameters are very sensitive to small or closely consecutive events and missed a considerable number of events from the catalogue. This drumbeat sequence occurred immediately after a burst of high amplitude clipped signal, associated with explosions. Surface records also describe an ash column extending 5 km above the crater during the afternoon of 11th April.

I re-calculated the periodicity for this episode, using the extended STA/LTA picks and several more instances of periodic seismicity (>1.5) are identified. The cross correlation analysis, however, reveals the events in this sequence are all very dissimilar to one another. From the 6063 input events, only 191 events have XCC >0.7 and meet the conditions to be placed into a family. This represents just 3% of all the seismicity in this episode. The families that emerge, represent the previously identified drumbeats on 11th April, 18th April and 31st May. Further metrics from the episode including the Q factor and amplitude are all very consistent through the two month period (fig 4.4). Spectral peak frequencies are typically limited to 2 - 5 Hz, however, there is no increasing or decreasing trend, or single dominant frequency. The events that belong to families are not distinguished from the remaining 97% of events, according to these metrics. This episode is defined by quasi-periodic seismicity where the events are consistent and moderately similar, but not clearly identical and repeating.

4.3.2 Episode 2: December 2012

This episode is much shorter than episode 1 and is defined by explosive activity and harmonic tremor. The periodicity search initially identified a short sequence of LPs where the inter-event times accelerate up to an explosion on 14th December. Given there are around

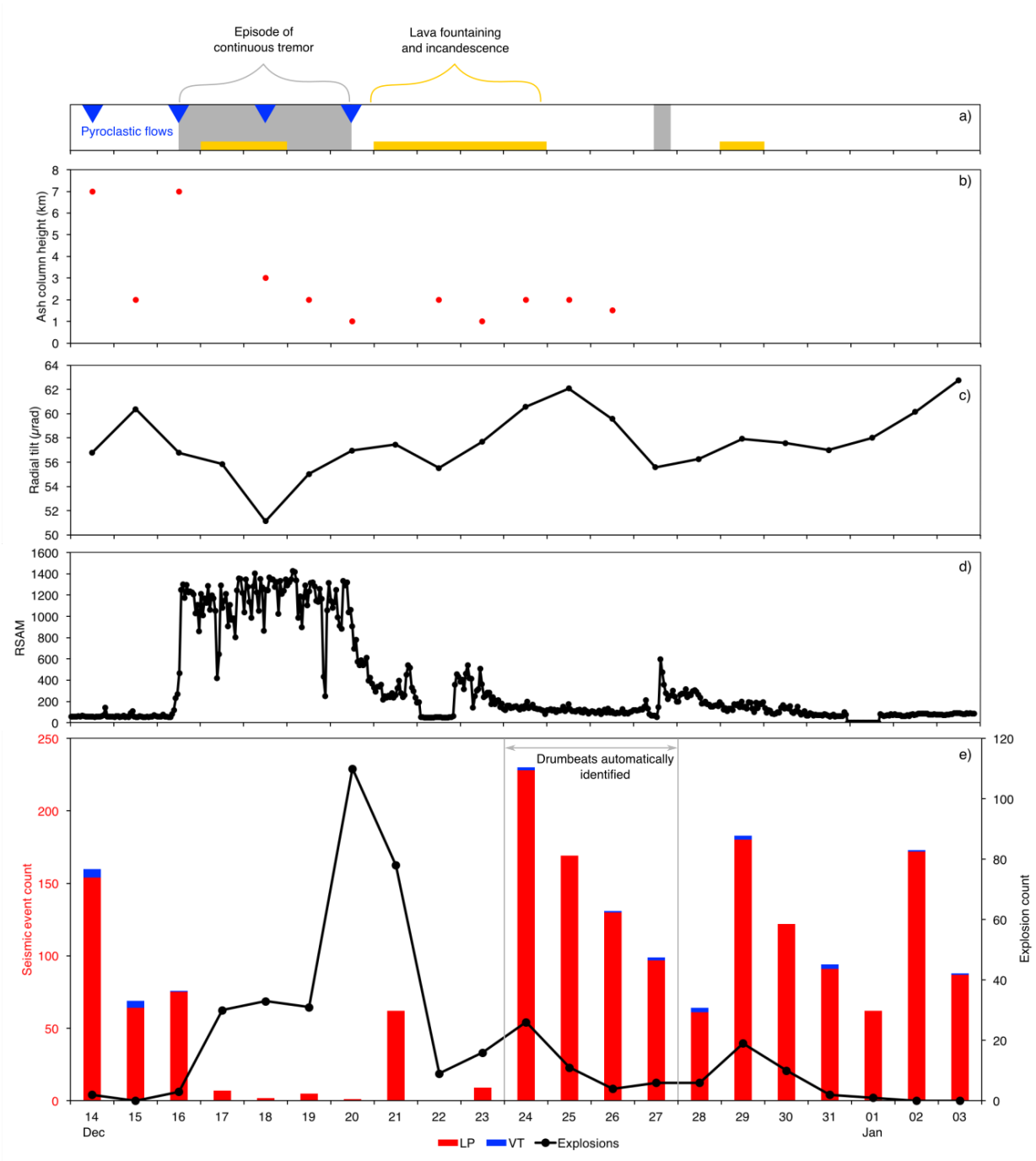

Figure 4.5 Episode 2: Timeline of activity 14/12/2012 - 03/01/2013. *a)* Summary of eruptive processes, *b)* Ash column height, *c)* Radial tilt measured at station RETU, *d)* Hourly real time seismic amplitude (RSAM) at station RETU, *e)* Seismic event and explosion counts from catalogue record. Marked is the period of drumbeat seismicity identified by scanning for peak periodicity values.

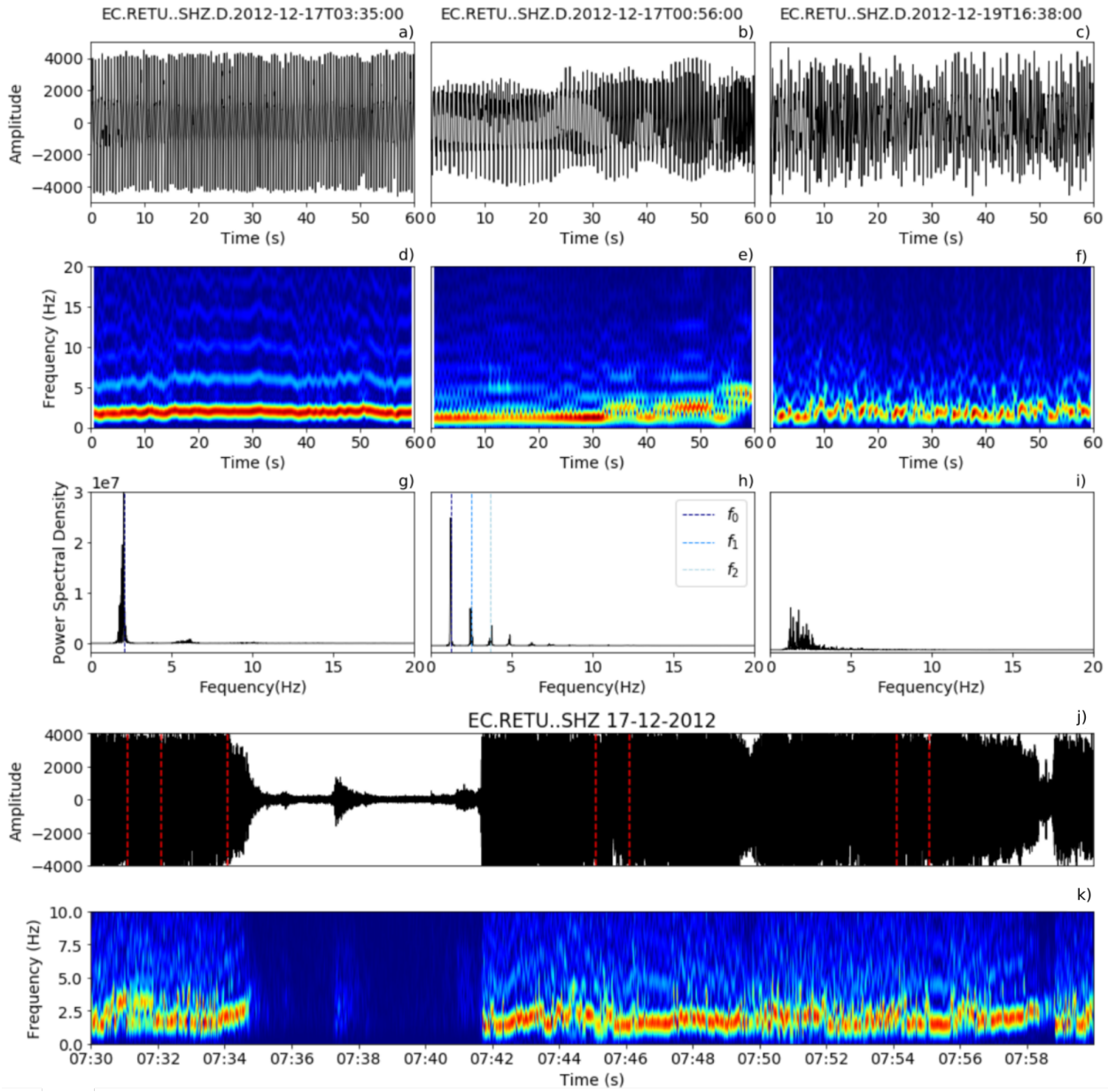

Figure 4.6 Episode 2: examples of tremor, December 2012. Panels *a)*, *d)* and *g)* show monochromatic tremor, with a single fundamental peak frequency. Panels *b)*, *e)* and *h)* show harmonic tremor with harmonics at integer increments from the fundamental frequency. Both panels *g)* and *h)* indicate the peaks identified by the harmonic product spectrum method. Panels *c)*, *f)* and *i)* show non-harmonic tremor. All traces shown are 60 seconds long. Panels *i)* to *k)* show the breakdown and resumption of harmonic tremor over a 30 minute window.

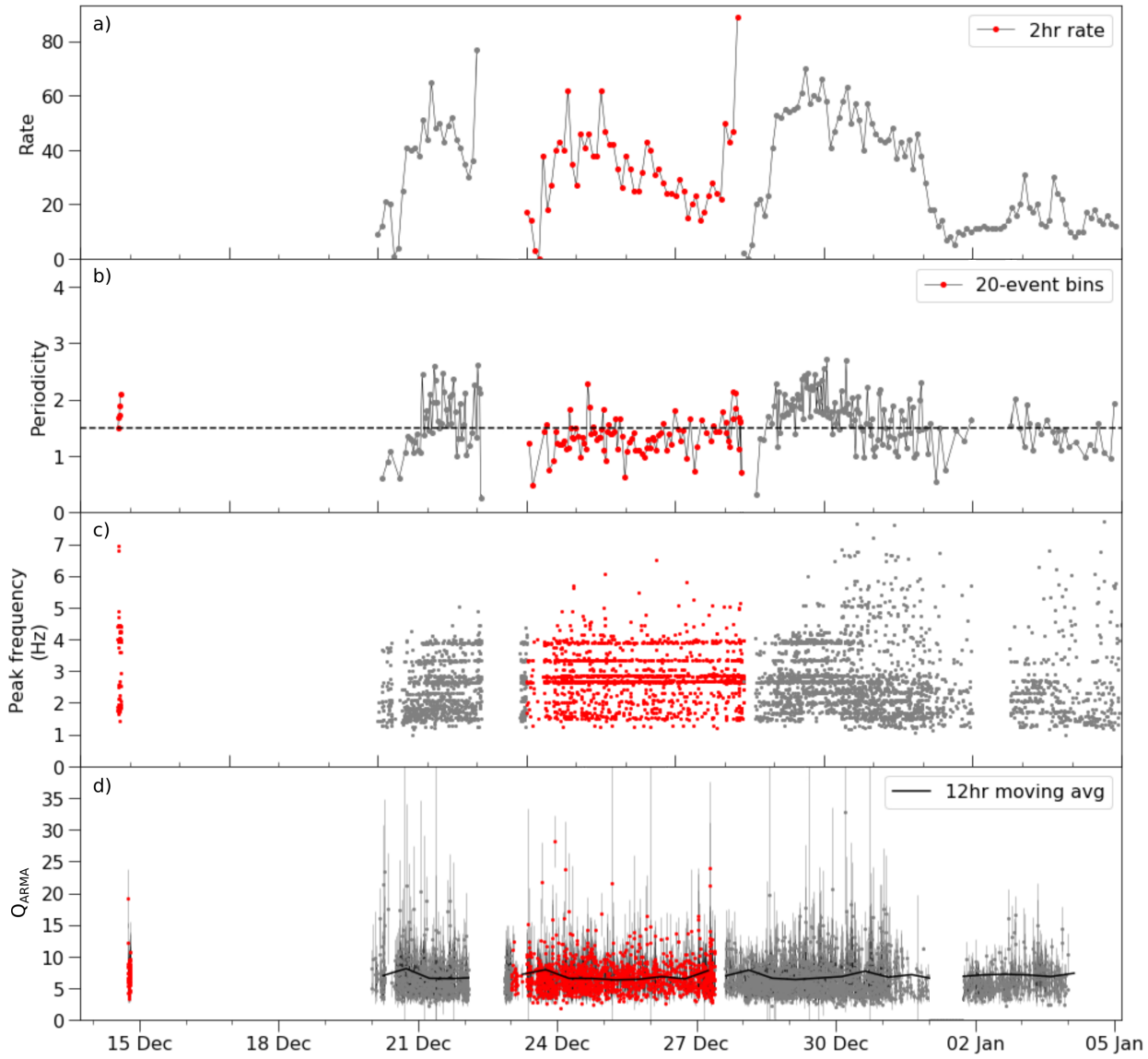

Figure 4.7 Episode 2: waveform analysis from all events in December 2012. Red marks manually picked sequences, initially highlighted by catalogue periodicity scan, grey shows STA/LTA picked events. *a)* Seismic event rate in 2 hour windows, *b)* Periodicity calculated in fixed bin widths of 20 events, *c)* Peak spectral frequency (Hz) and *d)* Q_{ARMA} with a 12hr moving average value.

100 events over 90 minutes I manually picked these to ensure any temporal analysis is as accurate as possible. This was a notably large explosion that generated a pyroclastic flow that descended to the south west and an ash column up to 7 km above the crater. The cross correlation shows these events to be very similar to one another, grouping into the same family and so likely from the same repeating source mechanism. Following this explosion, between 16th and 20th December, the signal at RETU is high amplitude and often, unfortunately, clipped. This is likely due to significant numbers of continued daily explosions - as many as 112 were recorded on 20th December. There were three further pyroclastic flows reported as well as lava fountaining from the crater. Within this window, however, there are a several episodes of harmonic tremor. Some episodes are very monotonic, whilst others show clear integer harmonics, which are also well mapped by the Harmonic Product Spectrum (HPS) method (fig 4.6). The duration of the tremor bursts vary from just a few minutes to several hours. Figure 4.6 illustrates a 30 minute sequence in which the tremor stops and resumes and exhibits gliding frequencies. Eventually the tremor becomes less continuous and breaks down into discrete LP events. The catalogue was very limited during 20th and 21st December. High amplitude and clipped signals meant that manual picking was not reasonable without significant human bias, and so I used STA/LTA picks initially and then manually removed obvious noise events. The events here are consistently periodic, more so than the initial catalogue indicated. This window sees the emergence of four dominant spectral bands at 2.7, 2.9, 3.3 and 3.9 Hz (fig 4.7). These persisted in the manually picked sequence between 23rd and 27th December, where drumbeats were first identified, and to the end of 2012. Following 31st December, event rate, periodicity and peak frequency all decrease and the errors associated with Q factor are smaller. There were no further reports of lava extrusion or explosive activity.

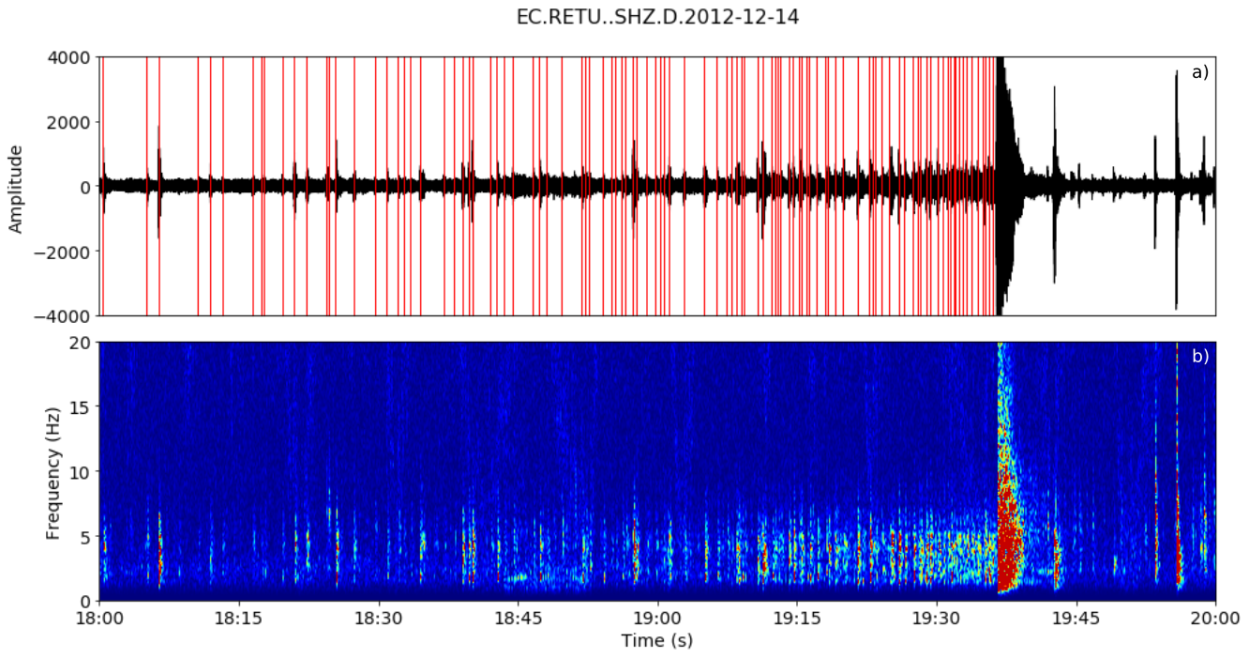

Figure 4.8 Episode 2: December 2012. *a)* Raw seismograph from RETU and manually picked events indicated with red markers, and *b)* spectrogram showing the frequency content.

4.3.3 Episode 3: July - September 2013

The catalogue scan for periodic seismicity highlighted three instances of drumbeats: 14th July, 3rd - 13th August and 24th - 30th August (fig 4.2). Although each sequence occurred around 2 weeks apart, this was an important period in the longer eruptive timeline at Tungurahua and so I generated STA/LTA picks to use alongside the catalogue, to include all of July - September (fig 4.9). The sequence of accelerating rates of LPs up to the intense Vulcanian eruption on 14th July have been well documented (Bell et al., 2018; Gaunt et al., 2020). Following 14 July, there were 251 further smaller explosions, during which time the signal at RETU is frequently clipped and the number of picked events here is limited. The drumbeat seismicity began immediately after the explosive phase. There is no apparent overlap in the explosive phase and the drumbeat seismicity, although this may be a result of saturated signal. Even when the signal is filtered between 1 and 4 Hz, LP earthquakes cannot

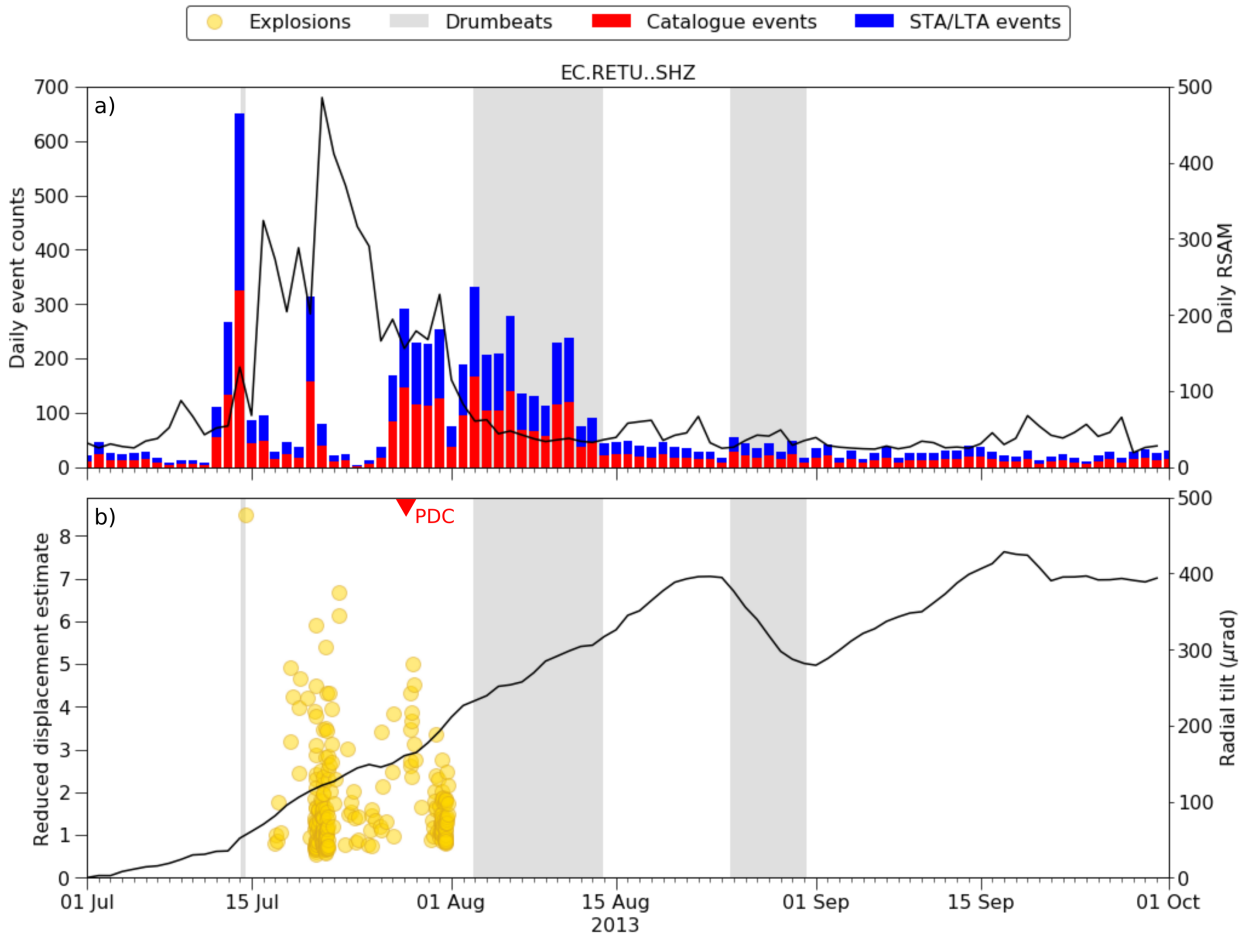

Figure 4.9 Episode 3: summary of surface activity, July - September 2013. *a)* Daily seismic event counts, red bars mark events already in the catalogue and blue bars show additional events identified by STA/LTA automated picking. Black solid line shows daily RSAM. *b)* Explosions are shown in yellow according to their magnitude (reduced displacement estimate), red triangle indicates the one PDC to occur during the episode, and the solid black line shows radial tilt recorded at RETU (μrad). In both panels, grey shading indicates periods where periodicity > 1.5 and drumbeats were identified.

be distinctly identified. The radial tilt at RETU, however, continued to show an inflation signal across the explosive phase and the early-August drumbeats, until a final drumbeat phase at the end of August. From the cross correlation analysis, only 234 events have XCC > 0.7 and can be classified into families (5%). Whilst these families only represent a small fraction of the total seismicity, they very clearly distinguish the three drumbeat phases (fig 4.10). The early-August drumbeats are defined by several families, whereas only the later phase of drumbeats can exclusively defined by a single family (family 9). The $K_{1,2}$ values illustrate the different signal envelopes and particularly the shift in the last drumbeats phase to lower amplitude, 'double-pulsed' signals which appear to have two peak components and a more emergent onset (fig B.4). There is a marked increase in the fundamental frequency between the early and late drumbeat phases from 2.6 to 4.1 Hz. This trend is reflected in a decrease in the average amplitudes and increase in event duration. This is seen in the changing shape of the K curves in figure 4.10.

4.3.4 Episode 4: October 2013

This episode of drumbeats is characterised by a single day of seismicity. Manual inspection of the waveform data showed that 9th October contained some very intense repeating seismicity (fig 4.13). The catalogue picks looked sparse, and so I manually picked the 24hr sequence to ensure all events could be analysed. The re-calculated periodicity for these manual picks, peaks at over 10 - the largest value seen in this thesis and comparable to well studied April 2015 drumbeats (Bell et al., 2017). When cross correlated, however, the events are remarkably dissimilar. From the 981 manually picked events, not a single event could be placed into a family. The Q_{ARMA} values are well constrained with a mean value of 7.89 - a comparable value to other drumbeat LPs in this study. The spectral peak frequencies, however, do not show neatly constrained, monotonic peak frequencies but are typically between 3.0 and 5.0 Hz.

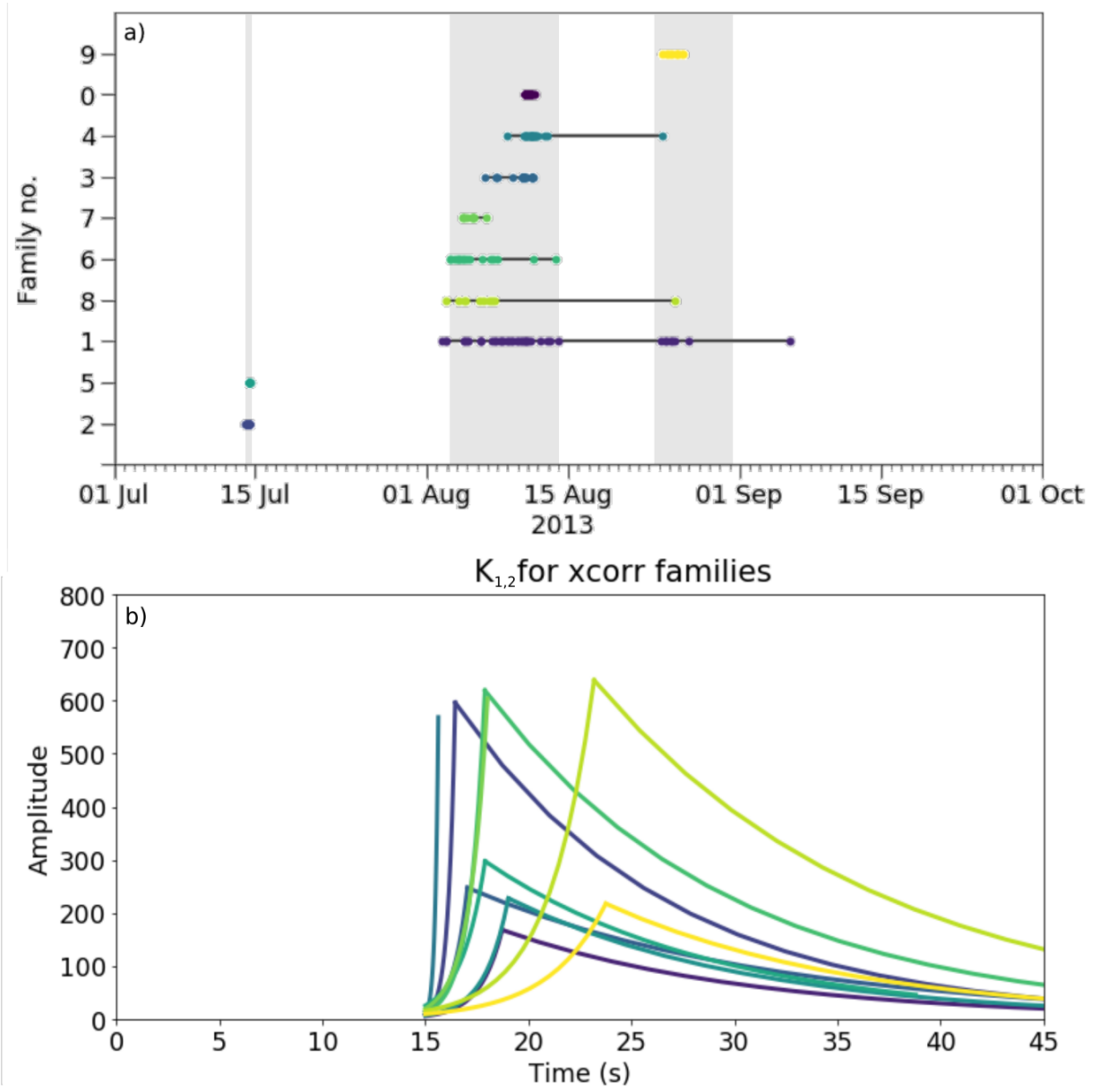

Figure 4.10 Episode 3: family and $K_{1,2}$ analysis, July - September 2013. *a)* The cross correlation returns 10 families, *b)* and the K_1 and K_2 curves calculated from the stacked event representing each family. The colours in both panels correspond to one another. Grey panels correspond with figure 4.9 and show episodes of drumbeat seismicity.

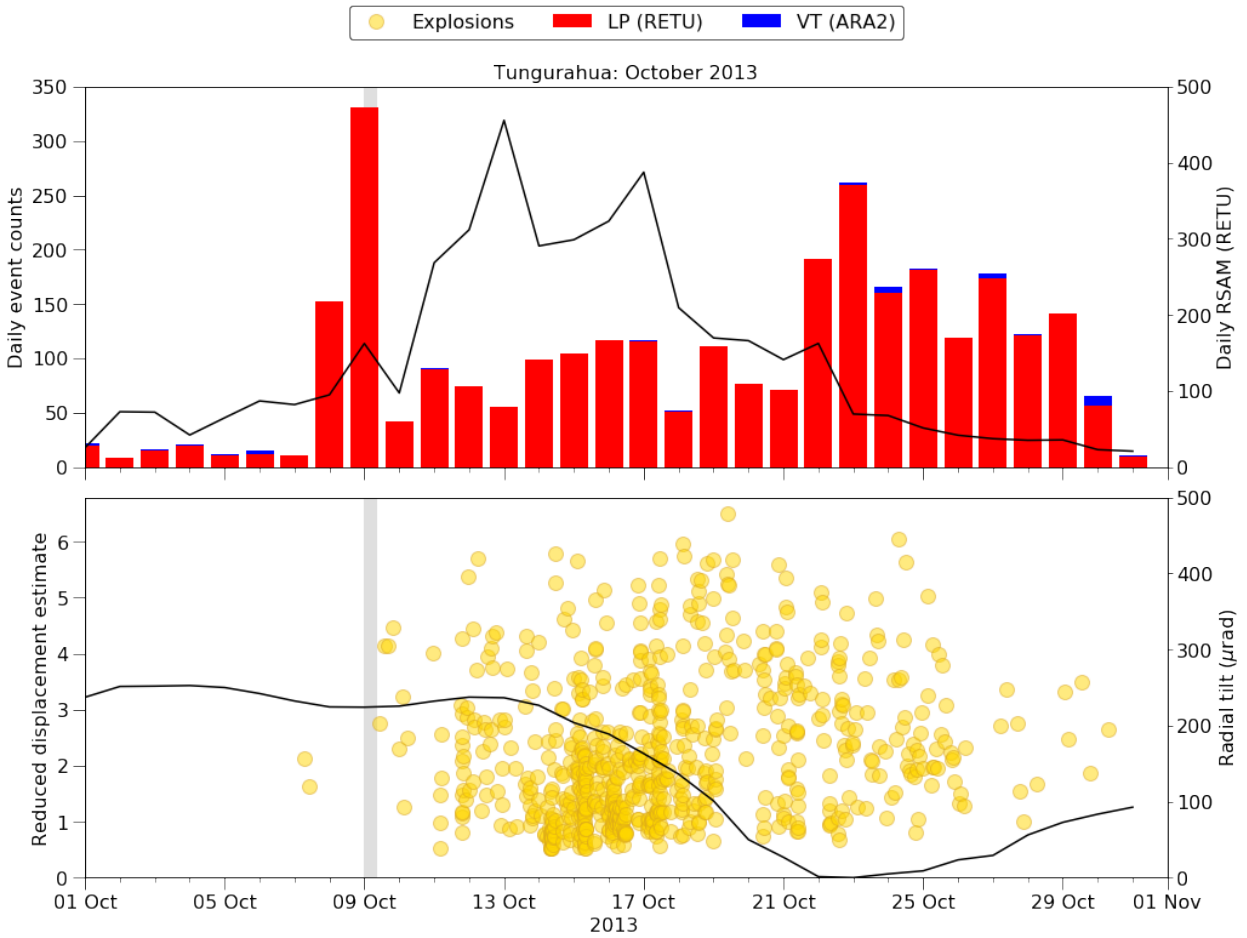

Figure 4.11 Episode 4: October 2013, summary of activity. Daily seismic event counts from the catalogue are shown in the bars; red shows LPs recorded at RETU, blue shows VTs recorded at ARA2. The daily RSAM is marked in a black solid line. The bottom panel shows explosions in yellow with the radial tilt signal from station RETU in a solid black line. The grey shading in both panels, marks the episode of drumbeat seismicity.

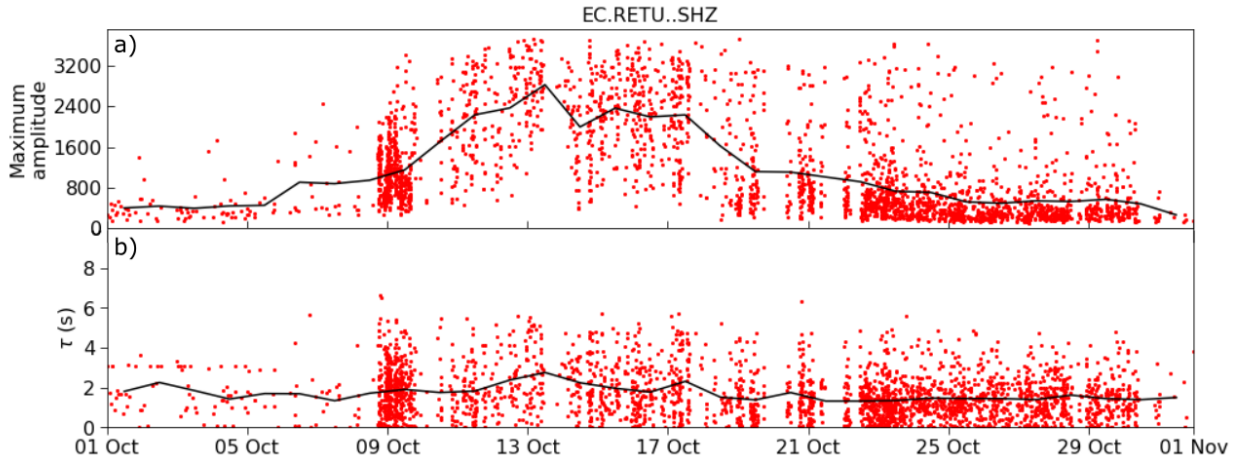

Figure 4.12 Episode 4: Drumbeat seismicity at RETU, 9th October 2013. Red marks show manually picked events, and *a)* shows maximum event amplitudes and *b)* the signal duration, *tau*. A moving average is plotted in black.

This single episode of drumbeats, however, appears to launch a new phase of explosive activity at Tungurahua, after several weeks of repose. 702 more explosions are recorded in the following 21 days. Activity reports note a increase in SO_2 flux from 87 t/d to over 4000 t/d. This episode of explosions was also coincident with a deflation signal in the radial tilt recorded at RETU. Using the catalogue picks, I examined the continued seismicity in October. Due to the number of explosions, the signal is often clipped. However, from the events that are well recorded, I note that LPs between 10th-20th October are longer in duration (+1.6 s), associated with lower frequencies (>2.5Hz) and larger amplitude. This transition in the amplitude and duration is reflected by the larger K_1 values and smaller K2 values after 10th October (figs 4.12, B.5).

4.3.5 Episode 5: February - May 2014

Following three months of repose, activity resumed at Tungurahua in February 2014 with one of the largest explosions recorded in terms of infrasonic power (fig 4.14). This also marked the return of periodic seismicity. Two episodes of drumbeats are recorded in late February

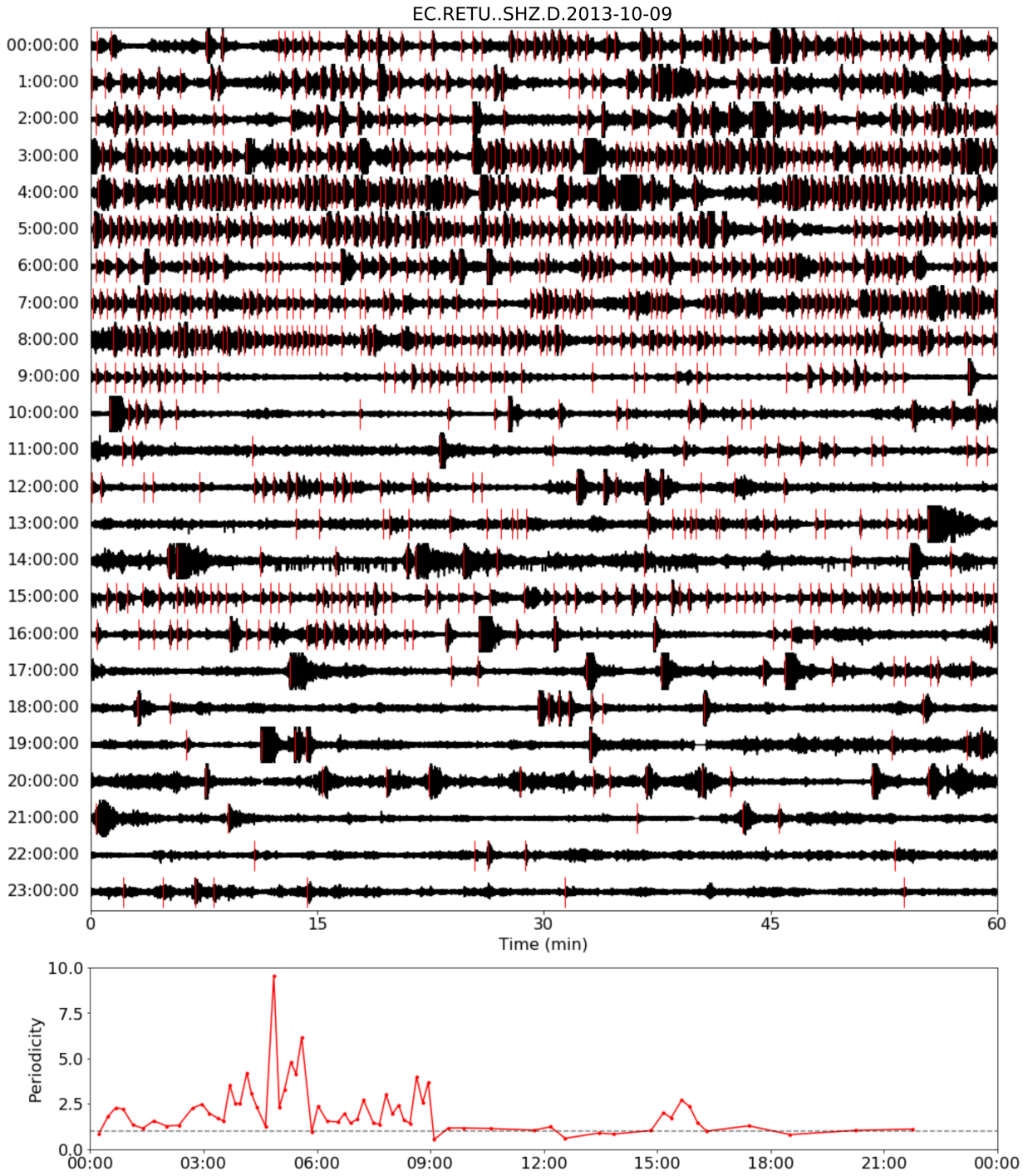

Figure 4.13 Episode 4: intense repeating drumbeat seismicity at RETU, 9th October 2013. Red marks show manually picked events. In the bottom panel is periodicity calculated in fixed width bins of 15 events.

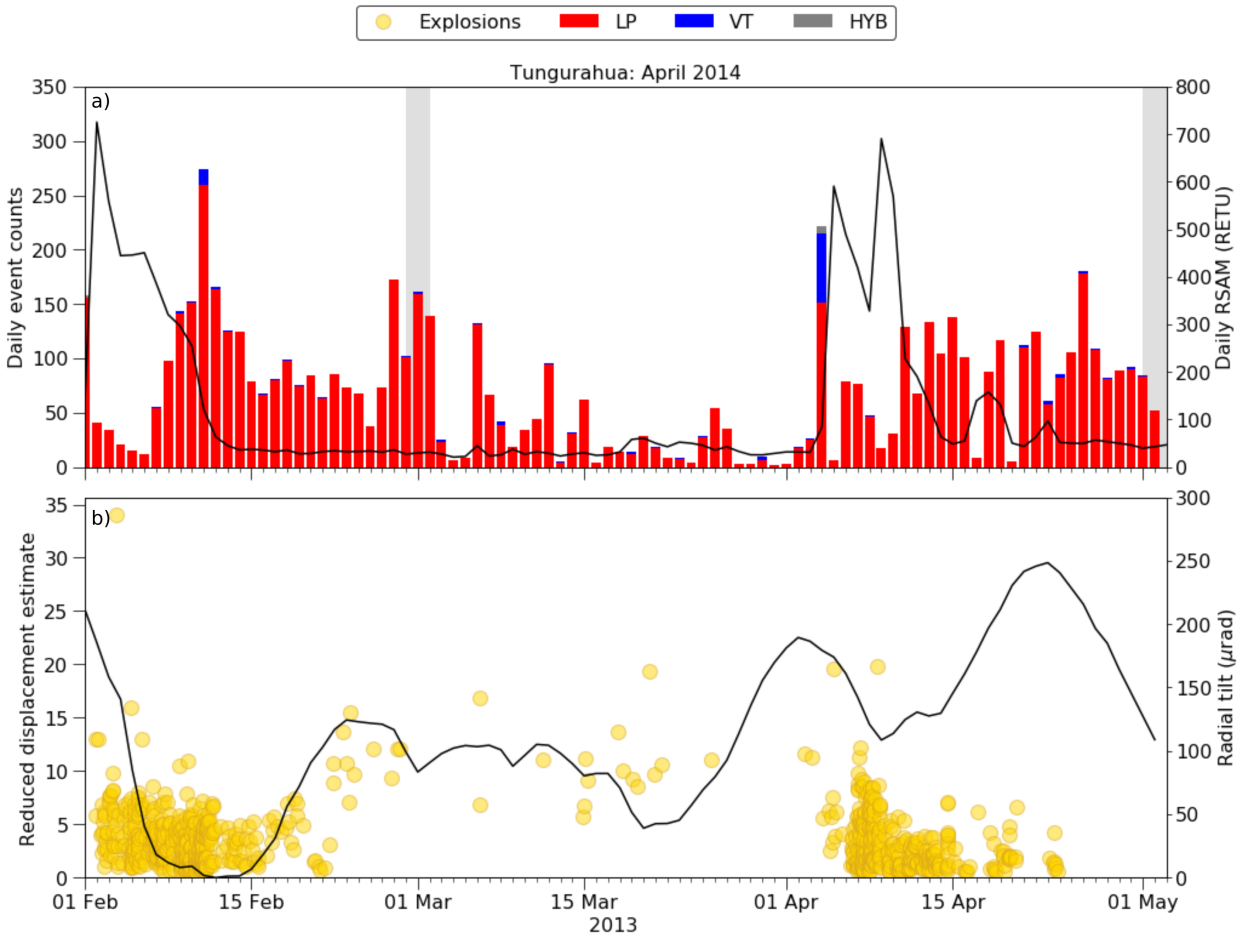

Figure 4.14 Episode 5: February - May 2014, summary of activity at Tungurahua. *a)* Daily seismic event counts are shown in the bars; red shows LPs recorded at RETU, blue shows VTs and HYBs recorded at ARA2. The daily RSAM is marked in a black solid line. *b)* Explosions are shown in yellow with the radial tilt signal from station RETU in a solid black line. The grey shading in both panels, marks the episode of drumbeat seismicity.

and early May, both following a series of significant explosions, preceding a period of relative quiescence and during a deflation in the tilt signal (fig 4.14). I used manual picks in the short

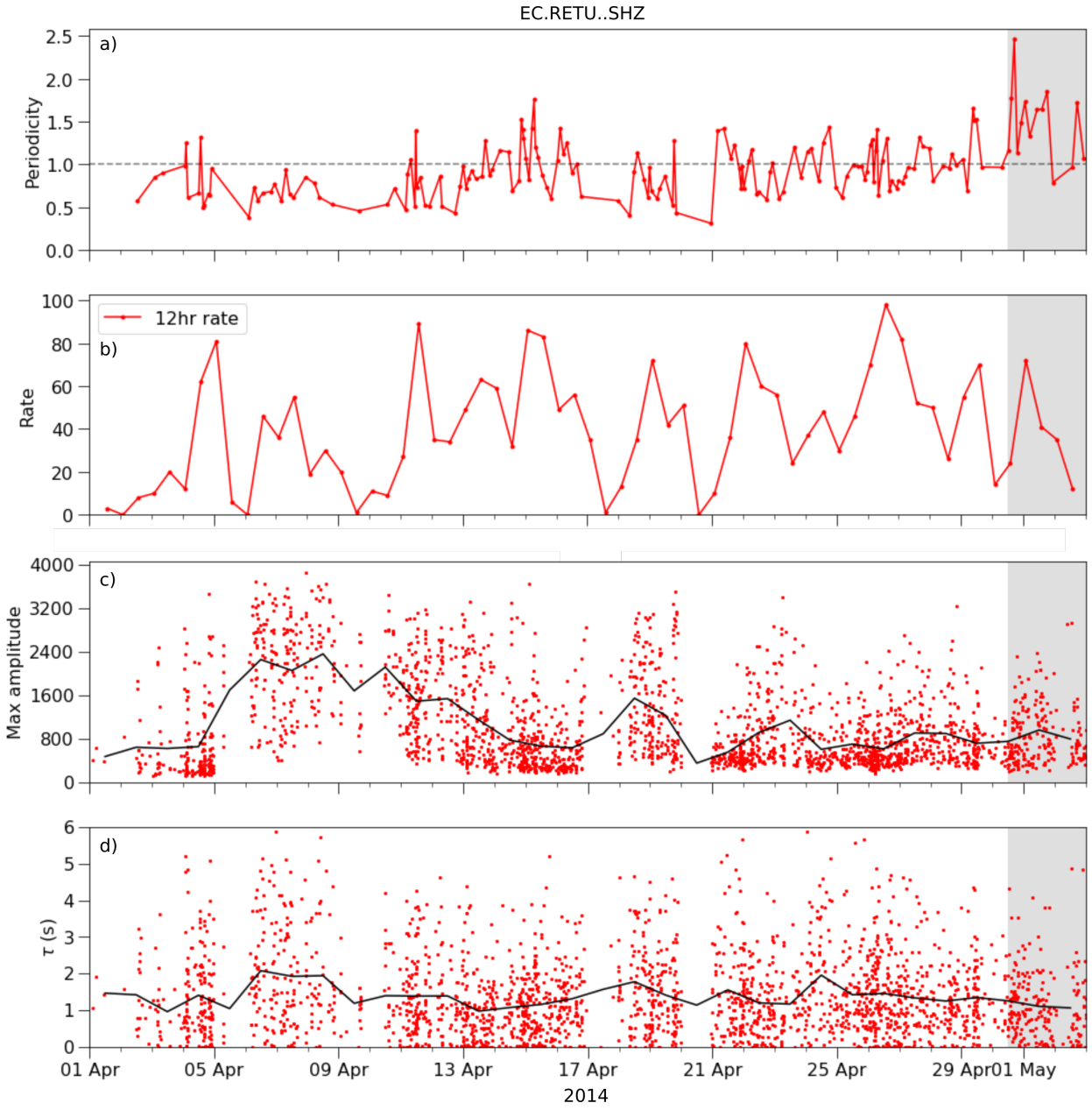

Figure 4.15 Episode 5: evolution of seismicity, April 2014. In all panels, grey shading marks where drumbeats are identified. All picks were STA/LTA picks and only those within the grey panels were manually picked. Panel *a)* Periodicity calculated in windows of 15 events, *b)* average event count over 12hr windows, *c)* maximum amplitude of individual events and moving average value and *d)* duration of events, τ (s) with moving average.

episodes of clear drumbeat seismicity and STA/LTA picks in eight weeks between the two. The May drumbeats show very well constrained spectral contents, peaking at 2.9 Hz and when cross correlated fall into just one family. The drumbeat episode in February do not neatly organise into families although the event durations, amplitudes and Q_{ARMA} values are comparable to those in May. From 21st April to the drumbeats on 1st May, the STA/LTA picked events become increasingly periodic, as the overall event rate decreases and event duration decreases (fig 4.15).

4.3.6 Episode 6: October 2014

This penultimate episode of periodic seismicity was another instance where drumbeats appear and disappear within a matter of hours. Unlike episode 2, in this sequence there is a high amplitude LP event, followed by an intense sequence of decelerating LP events that remain persistently periodic for approximately 12 hours. This episode occurred in a period of relative quiescence at Tungurahua and cross referencing with acoustic records, the catalogue and surface observation reports, confirm that this was just a very high amplitude LP and not any record of an explosion. However, this isolated burst did occur just weeks after the last of the cyclical explosive phases in 2014 and during a significant period of deflation in the tilt signal at RETU (fig 4.1). I manually picked 234 events across the 12 hour period to ensure the most confidence in first arrival pick times (fig 4.16). These events are characterised by a lower Q_{ARMA} value than previous drumbeat phases, with a mean values of 5.82. Spectrally, these events are very similar with peak frequencies limited between 2.0 and 4.0 Hz throughout the episode. The cross correlation does not return a single family, however, on inspection of the cross correlation matrix, $\sim$26% of XCC values are $>$0.5. From this, I suggest that this episode is not a sequence of identical repeating events, but is better described as quasi-similar repeating events.

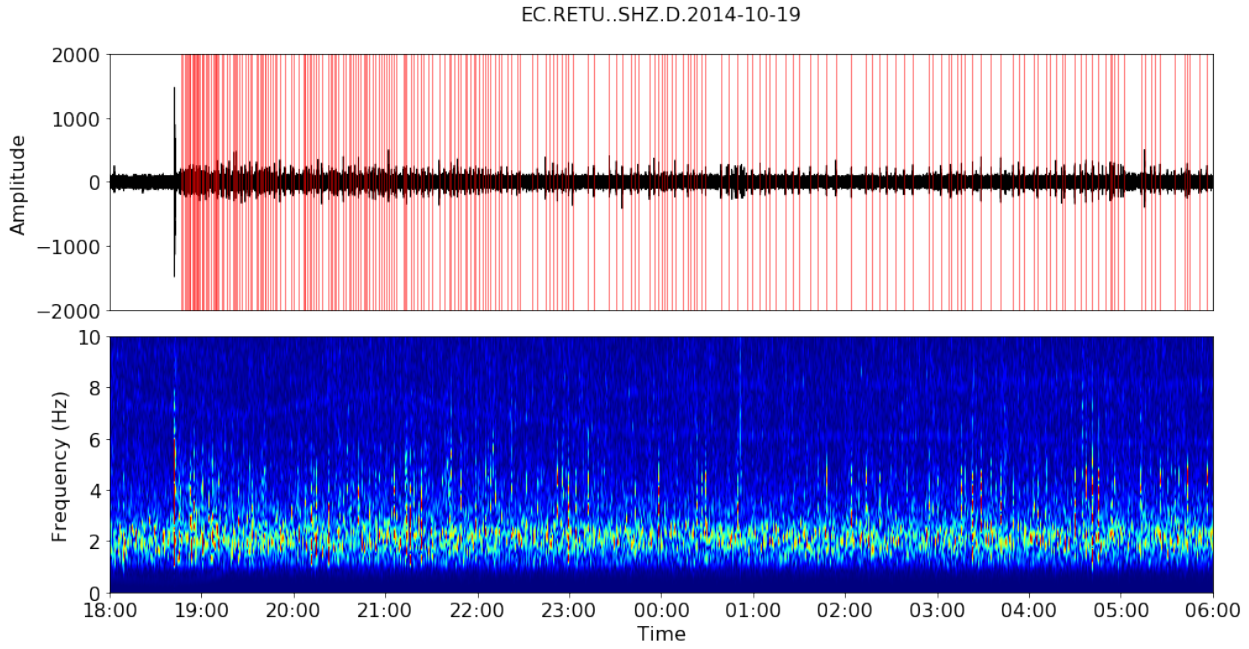

Figure 4.16 Episode 6: decelerating periodic LP seismicity, October 2014. Red marks show manually picked events. The top panel shows the raw signal from RETU, filtered between 1 and 10Hz, whilst the bottom panel shows the spectrogram.

4.3.7 Episode 7: August - October 2015

The catalogue periodicity search isolated five separate phases of highly periodic LP seismicity in 2015. Two of these episodes in April and November, account for the largest daily rates of seismicity recorded at Tungurahua. Both episodes of unrest are analysed in detail in (Bell et al., 2017) and (Butcher et al., 2020) respectively. As such, I focussed attention here on the remaining three episodes of periodic seismicity identified in August and October to complete the records. Unlike the cyclical activity in 2013 and 2014, these drumbeat episodes occurred sporadically and in between explosions, although the repose periods are much less well constrained (fig 4.17). I manually picked 2421 events across the drumbeat phases, to ensure the best possible accuracy for waveform analysis. The station RETU is affected by outages and noisy spikes through the August and early-October phase. There is a marked increase in the dominant spectral peak frequency from August to November. The isolated

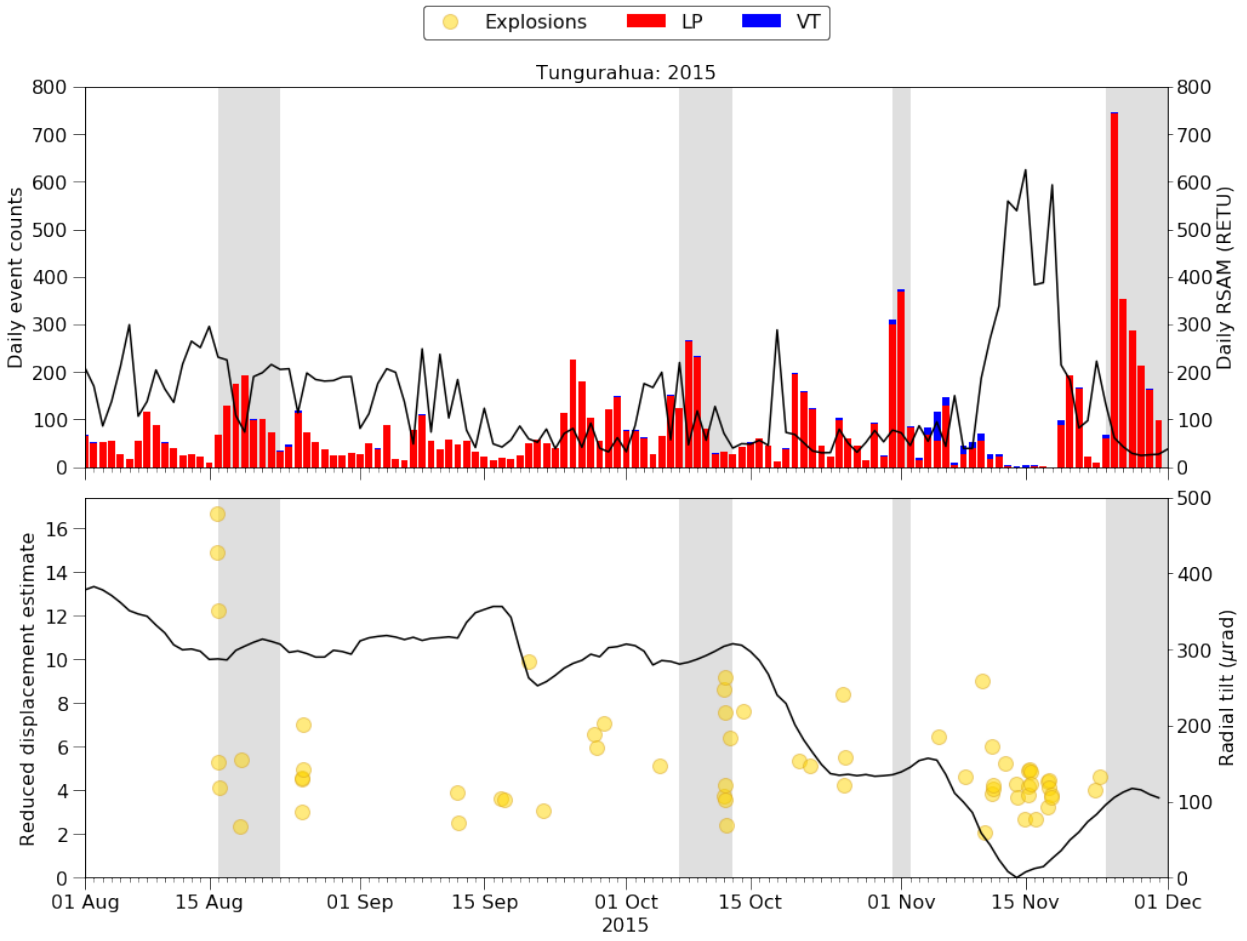

Figure 4.17 Episode 7: August - November 2015, summary of activity at Tungurahua. Daily seismic event counts are shown in the bars; red shows LPs recorded at RETU, blue shows VTs recorded at ARA2. The daily RSAM is marked in a black solid line. Explosions are shown in yellow with the radial tilt signal from station RETU in a solid black line. The grey shading in both panels, marks the episode of drumbeat seismicity.

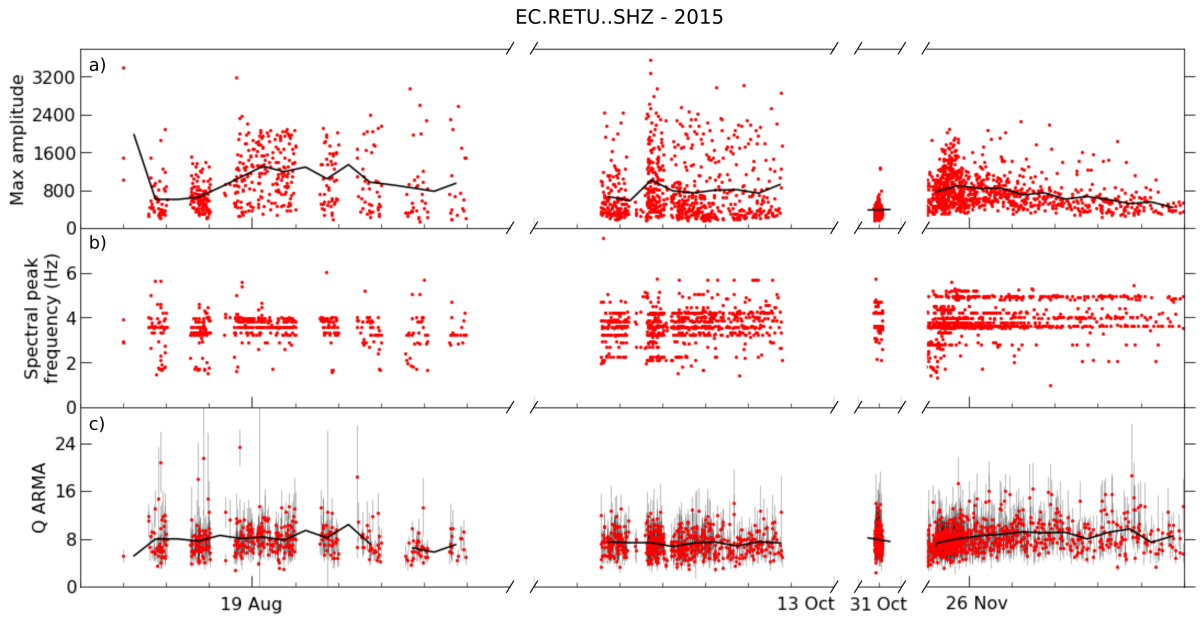

Figure 4.18 Episode 7: waveform analysis of events, August - November 2015: *a)* Maximum amplitude, *b)* Spectral peak frequency (Hz), *c)* Q_{ARMA}. Daily moving averages are plotted in a solid black line.

episode of drumbeats on 31st October are notably lower amplitude than at any other point, and although short, show a slowly decreasing Q_{ARMA} trend (fig 4.18).

Of the seven episodes from 2012 - 2015 this is undoubtedly the phase with the most similar waveforms, according to the cross correlation and families (fig 4.19). 1007 events can be classified into 23 families. From the strikingly similar events on 31st October, over 70% are allocated to families. The largest family (family 0) spans all four of the drumbeat phases identified in late 2015. However, it should be noted in family 0, only three events (1.3%) belong to the late November drumbeats and these generally map very separately to the three previous phases of drumbeats. The late October drumbeats also separated well into their own families, where as the August and early-October events appear to be much more similar in their waveforms.

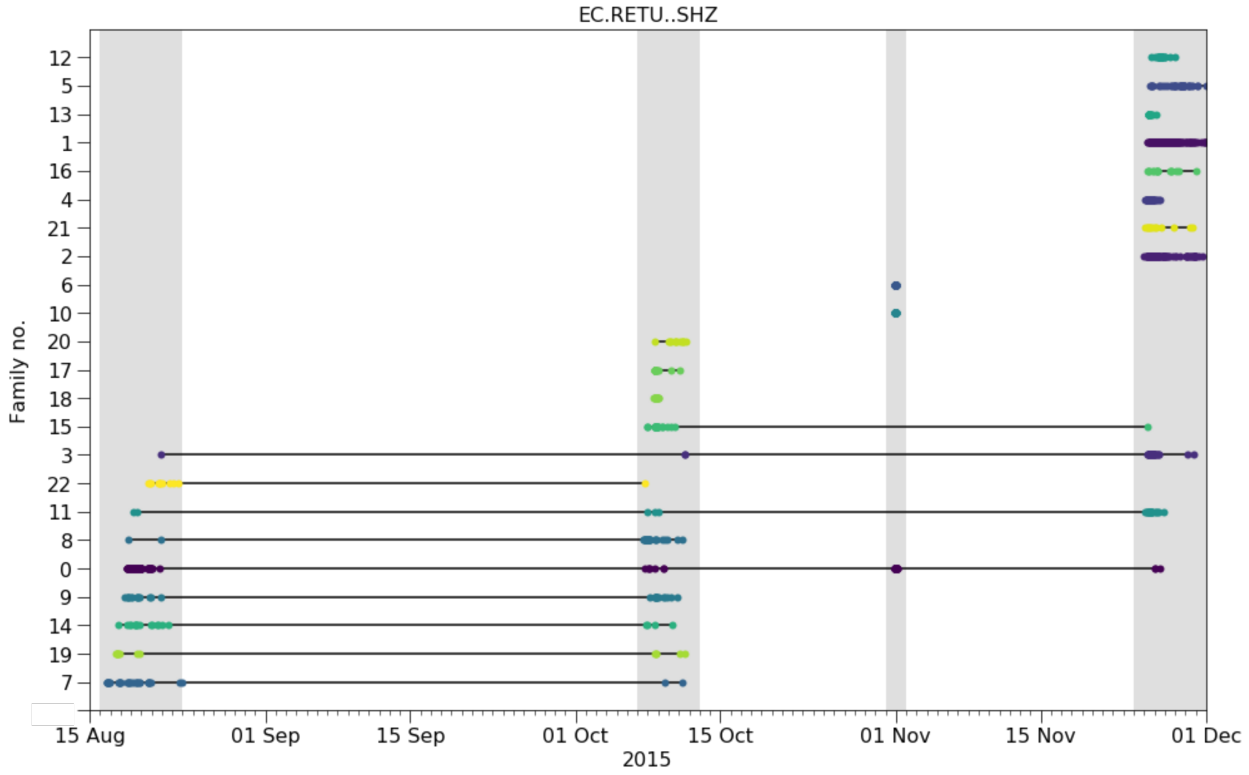

Figure 4.19 Episode 7: cross correlation analysis, August - November 2015. Grey panels mark the episodes where drumbeats were manually picked.

4.4 Discussion

The seven episodes of drumbeat seismicity, each highlight important stages in the dynamic state of the shallow conduit at Tungurahua. Broadly speaking, these demonstrate three distinct styles of seismicity. Firstly, early seismicity before December 2012 is erratic, shows limited repeatability and does not correspond well to explosive activity. Then in the transition to cyclical Vulcanian eruptions in 2013-2014, seismicity becomes much more predictable, and drumbeats occur before and after major explosions. And finally, in the closing stages of the eruptive phase, the seismicity corresponds to several 'failed' explosions and an overall slowing down of the system. Here I discuss the signal properties in each and suggest the likely state of the conduit and driving source mechanism.

4.4.1 Erratic seismicity

The eruption style at Tungurahua in 2012 was markedly different to any other period examined in this chapter. For instance, the explosions: these were smaller in their infrasonic power, and occurred more frequently with a more uniform distribution throughout the year, compared to the episodic explosions in 2013 and beyond (fig 4.1). The radial tilt at RETU also varied by <150 μrad prior to 2013, whereas thereafter, it was frequently reported to fluctuate between 500 and 1000 μrad. Hidalgo et al. (2015) defines Period 3 from December 2011 - September 2012 as generally '*low explosive activity*' (LEA) and distinct from cyclical explosions in 2013.

This pattern is reflected in the characteristics of the drumbeats. In March and May 2012, the drumbeats identified are relatively dissimilar to one another. There are no strong correlations or consistencies in the signal properties. The peaks in periodicity are isolated rather than sustained, and typically only last for a few hours. Beyond the few instances where the inter-event times are periodic, the signal processing suggests it is unlikely that these are similar, repeating drumbeat LPs caused by the same recharging source mechanism. This is certainly true in contrast to very refined examples at Mount St Helens or Soufrière Hills Volcano (Green & Neuberg, 2006; Iverson, 2008). In terms of the timeline of activity at Tungurahua, these LPs also appear to be disconnected to any explosions or long lasting trends seismicity. The peak frequencies, durations and Q_{ARMA} values associated with these events are comparable to those in December 2012 and later in 2013. As such, I have some confidence that they are the generated at a similar depth and pressure, or by similar fluid interactions (Kumagai & Chouet, 2000). However, without any strongly defining waveform characteristics and only quasi-periodic behaviour, I can only loosely speculate that these LPs are a shallow process likely related to explosive activity. The most significant detail to take, is how remarkably different the seismicity is to any other episode.

4.4.2 Repeated fracturing and sealing of a conduit plug

The second episode of drumbeats analysed in this study, identifies a shift to a new regime of seismicity that extends until 2014. This is in agreement with the timeline of activity presented by Hidalgo et al. (2015) which defines the start of Period 4, '*high explosive activity*' (HEA) in December 2012. Here I dissect Episodes 2 - 6 of drumbeat LPs and relate these to the eruptive processes to demonstrate that drumbeats are inherently linked to the rupture and resealing of a conduit plug.

Chugging and choked flow

The drumbeat episode in Episode 2 is a clear example of where LPs may be considered precursory seismicity (Chouet et al., 1994). Although only brief, the accelerating rate of LPs up to an explosion on 14th December 2012 is comparable to precursory swarms also observed in 2013 at Tungurahua (Bell et al., 2018), Volcán de Colima (Varley et al., 2010a) and Soufrière Hills Volcano (Hammer & Neuberg, 2009). The explosion generated a PDC and an ash-bearing column of emissions over 7 km above the height of the crater. The 102 events picked in the 90 minutes prior to the explosion show remarkable similarity to one another when cross correlated. These events are likely generated by the same repeating source associated with the imminent failure of the conduit plug prior to the explosion. The large explosion at 19:37 on 14th December 2012 (fig 4.8) is followed by several days of explosions and what is thought to be open-system venting of ash and gas. Typically open-vent degassing has been observed at very well studied, open systems such as Kilauea and Stromboli and is often associated with well constrained very long-period events (VLPs) and infrasonic harmonic tremor (Chouet et al., 2010; Chouet et al., 2003; Fee et al., 2010a). However, if the explosion on 14th December did not result in a complete plug rupture, rather a partial plug fracturing and there remains a constriction in the conduit, the episodic harmonic tremor captured on the 19th - 21st December may be more like a choked flow

regime or chugging, such as that described at Tungurahua in 2006 (Ruiz et al., 2006). Similar episodes of degassing explosions have been recorded at Reventador (Lees et al., 2008), Fuego (Lyons et al., 2010) and Sangay (Johnson & Lees, 2000). Notably the study of Sangay and Karymsky volcanoes distinguish two different styles of harmonic tremor, as either short impulses (< 1 minute) associated with individual explosions, or more sustained periods of tremor linked to multiple events. Chugging has been recorded before at Tungurahua, during a deployment of broadband seismo-infrasonic stations in 2004 (Ruiz et al., 2006). The chugging observed was rare, but pulses were short and did not show clear gliding tremors as has been observed in similar studies (Hotovec et al., 2013; Johnson & Ripepe, 2011). The brief, isolated event in December 2012, with short and long pulses and bursts of harmonic and gliding frequencies, was perhaps unique in this study but not unexpected in the longer timeline of this eruptive phase.

Cyclical drumbeats

Episode 2 also marks the start of a pattern that persists through the episodic Vulcanian eruptions in 2013 and 2014, whereby periodic drumbeats are recorded immediately before and after periods of intense explosions. The accelerating rates of drumbeat LPs on 14th December 2012 illustrate a sequence of precursory events. Whereas, the drumbeats analysed in Episode 2 (December 2012), Episode 3 (August 2013) and Episode 5 (February and May 2014) all occur immediately after significant explosions and typically show a decelerating trend in rate. Typically the rate of drumbeats decreases such that it appears the sequence breaks down and returns to background, pre-explosion levels of seismicity. Within each episode, there are further complexities which can be related to the dynamics in the shallow conduit.

In December 2012, there is a single initial explosion that generates a PDC, followed by 4 days of continuous explosions and open-system degassing (section 4.4.2) and then 12 days of periodic drumbeats which breakdown and subside to pre-eruptive, background seismicity

rates. By background seismicity, I infer from the periodicity returning to ∼1 that inter-event times are randomly distributed.

The three bursts of drumbeats in Episode 3 are also neatly defined by the signal characteristics and draw parallels with the timeline of Episode 2. The sequence also begins with one large triggering explosion, accompanied by a series of accelerating rates of precursory LPs, followed by 13 days of continuous smaller explosions, and then 12 days of drumbeats. The accelerating rate of LPs up to the explosion on 14th July 2013 are well documented (Bell et al., 2018). In this study, I demonstrate that the signal characteristics in the precursory drumbeats are very different from the post-explosive drumbeats in August. In Episode 2, I can only speculate on the dynamic conduit processes, whereas in Episode 3 there is more information from field studies at the OVT and deformation data. Petrological studies of ejecta have shown the 14th July 2013 explosion was a plug rupture event. Although the explosion was associated with fresh magma ascent, the conduit was sealed with a cooled crystalline plug from a previous pulse of magma related to earlier explosions in May 2013 (Gaunt et al., 2020). Despite this, throughout the explosive phase and the drumbeats, the radial tilt signal at RETU still suggests ongoing inflation in the shallow edifice. The final episode of drumbeats in late-August 2013 were concurrent with a short deflation signal in the tilt. This mirrors previous observations that tilt and seismicity cycles occur out of phase relative to one another (Marsden et al., 2019; Mothes et al., 2015). The signal characteristics, and specifically the $K_{1,2}$ values that define the signal envelope, illustrate the shift in LP seismicity from the beginning to the end of August (fig 4.10).

In Episode 5, the timeline is a little less comparable to the previous instances. Once again, in February 2014 there was a single large initial explosion following a long period of repose. This was succeeded by 15 days of continuous smaller explosions, and followed by a short 3 day sequence of drumbeats, in parallel with a small deflation in the tilt signal (fig 4.14). The drumbeat sequence in May 2014 was preceded by 9 days of increasingly quasi-periodic seismicity and during a much more significant deflation signal (>150μrad) in the

tilt. In each of these instances the decelerating drumbeat phase post-explosion are markedly different to the accelerating precursory drumbeats.

The post-explosive drumbeats may be associated with a settling or sealing process in a conduit plug (fig 4.20). It is thought the Vulcanian cycles in 2013 and 2014 are controlled by repeated crystallisation and densification of magma in the conduit, forming a vertically stratified, tight seal (Clarke et al., 2015; Hall et al., 2015). Magma in the conduit continues to degas in this sealed closed-system and building towards over-pressure, until a new pulse of magma ascends and triggers critical over-pressurisation and plug rupture (Gaunt et al., 2020). Similar cycles have been described at Galeras, Colombia (Bain et al., 2019; Stix et al., 1997) and Soufrière Hills Volcano, Montserrat (Druitt et al., 2000). Following several days of open-system explosions, as magma ascent rate decreases, the eruption begins to stall and there is a period of overlap where some degassing continues but the magma begins to crystallise and form a proto-plug. Within this proto-plug, there may be fractures into which gases can escape the system although less freely than during the explosive phase. I suggest the drumbeat LP seismicity is caused by the fluid resonance of persistent degassing through an increasingly closed and crystalline plug. As the proto-plug seals and becomes increasingly impermeable, there are less transient fractures in the plug in which gas and volatiles can resonate and fewer LPs are generated. This persists until the plug is fully sealed, LPs cease and the tilt signal continues to show an inflationary signal as pressure builds beneath the plug.

I suggest this seismicity is associated with the plug and very shallowest depths in the conduit, perhaps only in the top 0.5 - 1 km (Gaunt et al., 2020). This is why there is such an overwhelming record of events from the very closest station RETU and little recorded elsewhere on the more distant, broadband network. Q_{ARMA} values of these drumbeat LPs are typically between 7 and 12 across the four years of study. These values are aligned with studies at Kilauea where Sompi analysis of LP events estimates Q in the range 10-20 (Kumagai et al., 2005). Modelled on a fluid filled crack, it was suggested these Q values

indicate a bubbly water or steam was the likely resonating fluid. Kumagai et al. (2005) also cite an earlier study which determines a similar source mechanism, but an average Q value of 8.2 (Saccorotti et al., 2001) and suggest this may be inaccurate as Q is calculated from the whole signal as opposed to only the coda tail. In this study, I followed Cusano et al. (2008) and calculate Q from 2 s after the pick time so as to only consider the coda tail. However, findings from the $K_{1,2}$ values suggest perhaps the emergence of the LP events in these sequences may longer than 2 s (fig B.3, B.4). Furthermore, I used automated picking methods which carry an additional error. As a result, the Q_{ARMA} values lie closer to those from (Saccorotti et al., 2001) perhaps due to signal processing rather than a different resonating medium.

Previous studies of deformation cycles have suggested that increases and decreases in tilt are not simply signals of inflation and deflation, but the result of shear stress in the conduit margins (Neuberg et al., 2018). Although it is also important to note that topographical effects can cause an inflationary process to appear as deflation signal in tilt data (Cayol & Cornet, 1998). Just as interpreting the seismic record is complex, understanding sequences of deformation with limited data is also difficult and can vary from one system to the next. The tilt cycles at Tungurahua can be particularly inconsistent between 2012-2016 and appear to deviate from expected trends of inflation-deflation. For example, during the July 2013 explosive phase, tilt continued to increase despite suggested models of depressurising after plug failure (Gaunt et al., 2020). Bell et al. (2017) demonstrates that brief periods of decrease in the tilt signal are also synchronous with peaks in SO_2 flux. If the post-explosion drumbeat LPs are considered the last phases of degassing, then this is also the very last depressurising before sealing of the plug and hence concurrent with localised minima in the tilt signal and peaks in the SO_2 flux. Figure 4.20 illustrates this idealised model of tilt and drumbeat seismicity relative to plug rupture and resealing.

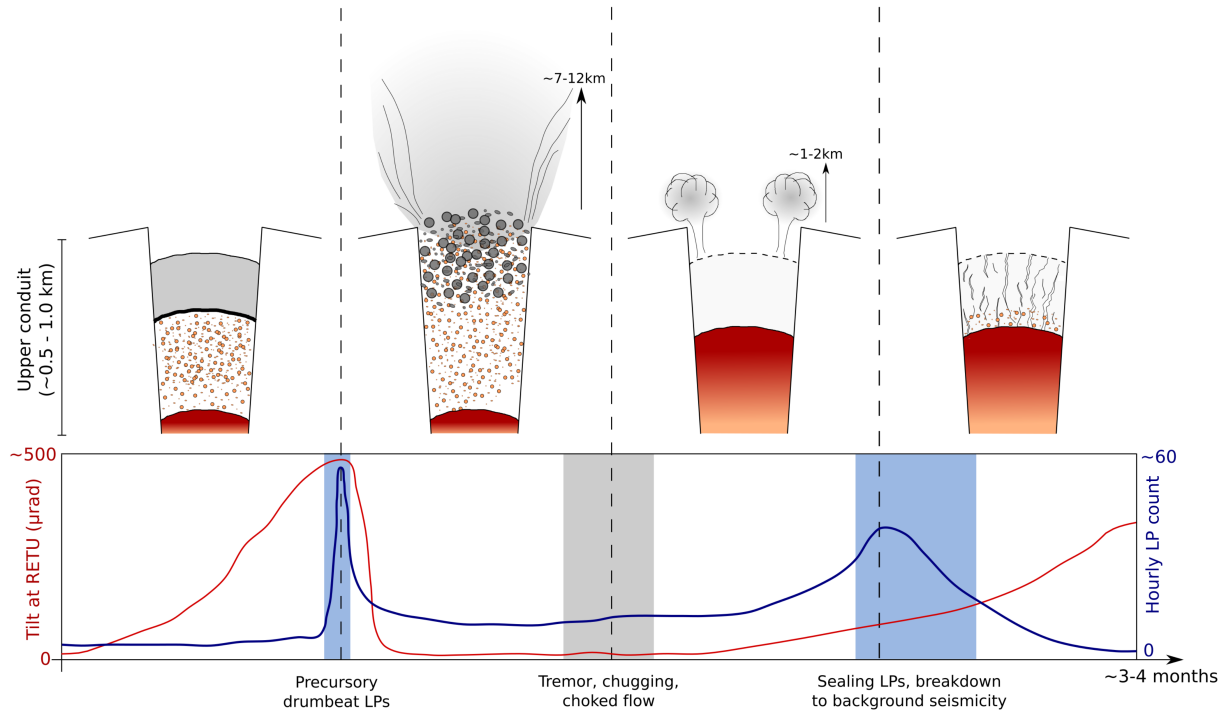

Figure 4.20 Schematic diagram illustrating the origins of seismicity in cyclical Vulcanian eruptions. Initially, a strong impermeable plug seals the top of the conduit. Magma ascent and exsolution of volatiles increases pressure beneath the plug, causing an inflation signal in the tilt. This continues until critical overpressure causes the plug to fail. A short sequence of rapidly accelerating rates of drumbeat LPs occur as a precursor to the plug failure and explosion, associated with resonating gases in an increasingly fractured plug. Rapid decompression causes fragmentation of magma in the conduit and a deflation signal in the tilt. This first explosion is typically the largest, and smaller explosions and emissions continue in a partially open system. If the entire plug is not ruptured, this is where restrictions in the conduit may generate tremor, chugging and choked flow. As magma in the upper conduit cools, densification begins to create a new upper conduit plug. Passively degassing magma in the shallow conduit interacts with complex fracture networks in the plug, generating the post-explosion drumbeat LPs. The plug continues to cool and seal, allowing less and less volatiles to escape, and increasing the pressure, mirrored by a slowly increasing tilt signal. Drumbeat LPs subside to background seismicity levels. Adapted from (Gaunt et al., 2020).

False precursors

It is important to note that not every one of the ∼3 monthly cyclical Vulcanian explosions in 2013-2014 is associated with this model sequence of seismicity. This may be related

to the ascending magma and its composition and how able it is to degas, or perhaps a result of how much plug material was fractured and ejected in the previous cycle. Certainly some episodes of drumbeat LPs identified in this study are anomalous and do not fit the model. Episode 4 (October 2013) demonstrates a single day of periodic LPs and the highest periodicity calculated in the entire four years, yet there was no post-explosion drumbeat phase (fig 4.11). The brief episode of decelerating drumbeats in Episode 6 (October 2014) are reflective of an entirely different process. These drumbeats are not associated with any kind of explosive activity and the signal properties, including a lower Q_{ARMA} value are indicative of a different resonating media (Kumagai & Chouet, 2000). Numerical simulations in Kumagai and Chouet, 2000 suggest that Q_{ARMA} values in the order of 10^2 are unlikely to be associated with magma. However, even small changes in this range can suggest significant changes in the ratio of gas, ash or water vapour, and in turn a changing process. This is a reminder that even very striking or periodic drumbeats should be carefully analysed in the context of the surrounding days of seismicity and any other available geophysical monitoring data; as not all all drumbeats are precursory to an explosion.

4.4.3 'Switching off' at Tungurahua

Drumbeat seismicity in 2015 at Tungurahua has been well studied (Bell et al., 2017; Butcher et al., 2020) but when compared to the drumbeats in 2012 - 2014, is markedly different. The nature of the eruptions are different to the cyclical phases in 2013 and 2014. Bell et al. (2017) includes a detailed analysis of periodic LPs but notably only associated with minor explosions, ash emissions but no lava extrusion. Similarly Butcher et al. (2020) (and chapter 5 in this thesis) describes a decelerating sequence of LPs following a 'failed' attempt at an eruption. The drumbeat phases in Episode 7 of this study (August - November 2015) do not correlate with significant changes in the tilt or marked explosions. The event signals themselves, however, show consistent Q_{ARMA} values with previous drumbeat phases,

and much more constrained bands of dominant spectral peak frequencies (fig 4.18). As such, I suggest drumbeat seismicity during 2015 is still likely the result of resonating gas in the fractured upper conduit. However, the occurrence of the drumbeats and explosions is much less cyclical and so there must be a change in the dynamic conditions in the shallow conduit. I suggest that the ∼3 month repeating cycles of Vulcanian eruptions in 2013-2014 are controlled by an optimal combination of steady magma ascent and a low permeability plug that efficiently seals the conduit (Gaunt et al., 2020; Hall et al., 2015). And so the shift in 2015 may be due to the strength of the plug, the composition of the shallow magma, the amount or rate at which new magma ascends, or a reflection of the state of stress in the system (Cassidy et al., 2018; Roman & Cashman, 2018).

To demonstrate the transition of seismicity behaviour, I ran cross correlation and family analysis for all 15,385 events used in this study, including a mixture of STA/LTA automatically picked events and manually picked events. I then classified families using the same thresholds as described in section 4.3. In total 1648 events in 57 families are extracted to describe the four years of seismicity (fig 4.21). Nearly half of these are attributed to seismicity in early 2012 and also include events from the duration of the study period. From 2013 onwards, however, seismicity is increasingly characterised by independent families, unique only to that episode. Particularly from 2015, where with the exception of a handful of events, seismicity is entirely independent from previous years. This might imply that the disconnected and dissimilar seismicity in early 2012 (Episode 1) describes a more generic degassing process in the upper conduit which is applicable to many swarms of LPs observed, even if they are not distinctly periodic. The specific and very constrained drumbeat episodes in 2015 (Bell et al., 2017; Bell et al., 2018; Butcher et al., 2020; Marsden et al., 2019) are characteristic of unique source mechanisms, rather than a generalised or ongoing process.

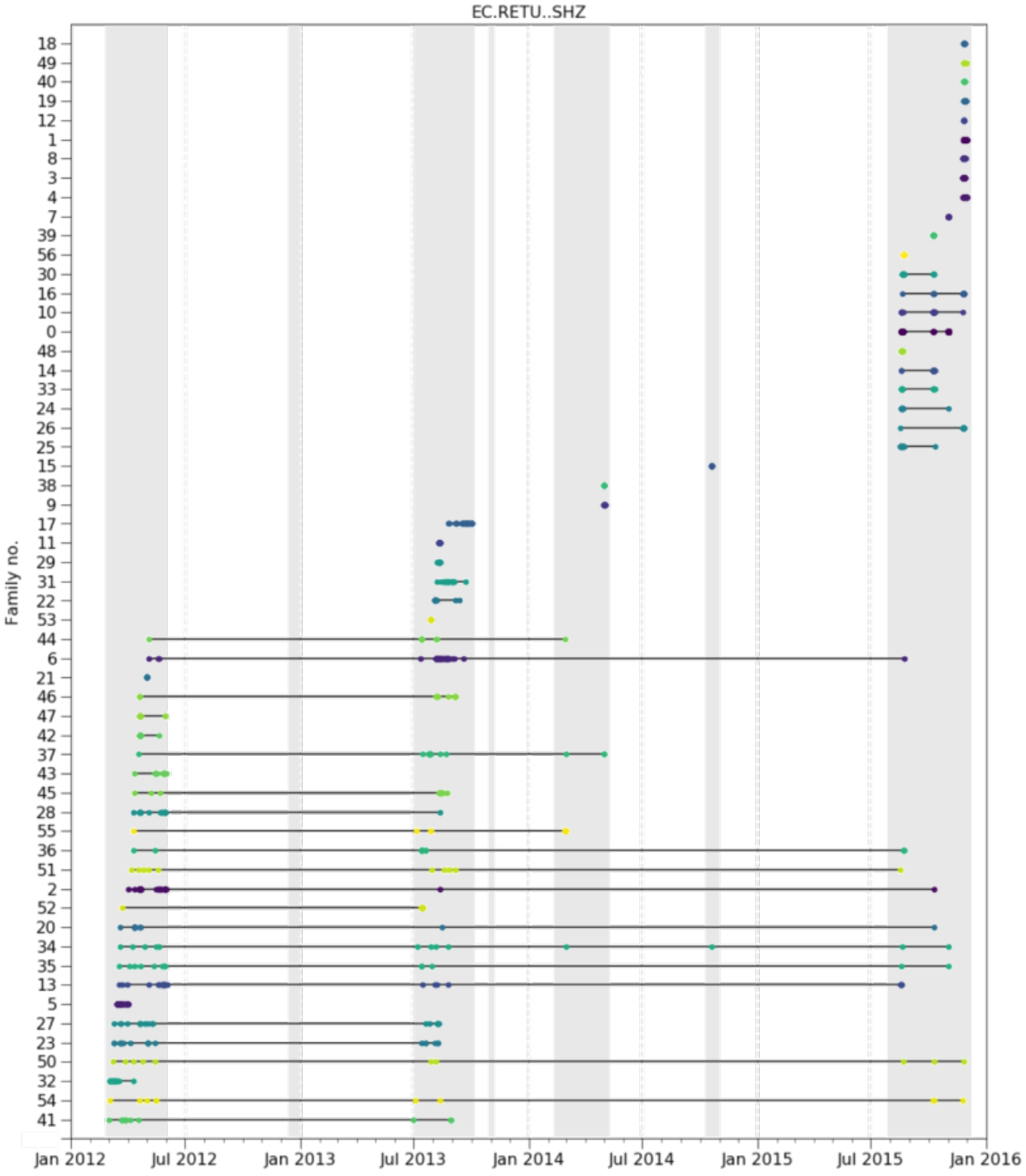

Figure 4.21 Full cross correlation and family analysis for 15,385 events between 2012 and 2015. 57 families are extracted and numbered from largest (0) to smallest (56) and plotted in chronological order of appearance. Grey shading shows the seven episodes analysed in this chapter.

4.4.4 LP seismicity in forecasting eruptions

By taking a broader view of the periodic seismicity at Tungurahua, I can more carefully interpret drumbeat LPs and consider whether they are a useful tool for forecasting eruptions. In hindsight, during the repeating Vulcanian eruptions, patterns of periodic LPs are clear and informative. There was a marked shift in 2015, however, and thereafter LPs did not follow an idealised pre- and post- explosion model. Drumbeats in this period were not indicative of imminent activity. Between the isolated drumbeats on 31st October 2015 and the decelerating sequence in November 2015 there was a significant volcano tectonic (VT) swarm. 207 VTs are recorded in November 2015 accounting for 16% of all catalogued VTs between 2012 and 2016. An InSAR study attributed this swarm to a shallow, lobe-shaped area of magma storage beneath the western flank (Hickey et al., 2020). Then the seismicity at the end of November 2015 suggests a 'failed' eruption where the conduit material was simply not subject to enough pressure, either from fresh magma recharge or exsolution of volatiles, to cause failure in the upper conduit (Butcher et al., 2020). And finally, in the final explosive phase in February 2016, there was significant LP seismicity and tremor, but no periodic episodes. Whilst there were violent explosions and several PDCs in 2016, reports from OVT also describe a process of 'boiling over' and more sustained lava effusion than in previous episodes (IGEPN, 2016b). For these three very different eruptive episodes to occur consecutively, and after such cyclical and predictable activity there had to be a change in the dynamics in the shallow conduit. The ability to degas, conduit geometry and magma storage are cited as some of the reasons for transitions from explosive-effusive eruption styles (Cassidy et al., 2018). Perhaps additional magma storage, associated with the VT swarm in November 2015 and rapid deflation in the tilt signal in early 2016 is indicative of a larger depressurising in the plumbing system (Cannata et al., 2015). This study shows that not all major plug failure events are preceded by rapid accelerating drumbeats. However, the lack of periodic seismicity in 2016 may suggest the sealing of a plug was not a crucial

component of this eruption and perhaps why the system then appeared to stall and settle into a phase of quiescence. Prolonged tremor following the initial explosion in February is more characteristic of open-system venting (Ruiz et al., 2006).

Currently, LP seismicity is only clearly recorded at short period station RETU as the station lies only 2 km from the crater rim. With additional stations around the crater, I would be able to more confidently constrain depths and even estimate source mechanisms. Installing monitoring equipment on the flanks of a volcano with such steep relief and at significant altitude comes with logistical concerns. However, this study highlights that in order to confidently use LP seismicity as a measure for imminent activity and to understand the shallowest conduit processes, better network coverage is needed. Tungurahua has been quiet for over five years now, but perhaps this approach can be adopted at analogous volcanoes such as Karymsky Volcano (Johnson & Lees, 2000) and Arenal (Zobin et al., 2019).

4.5 Conclusions

This study details seven key episodes of drumbeat seismicity at Tungurahua. Using these, I have defined three different scenarios in which the drumbeat LPs relate to the shallow conduit dynamics. From spectral analysis and Q_{ARMA} values, I infer the LPs are likely generated by a resonance of a steam-gas mixture in the fractured upper conduit. Inconsistent and erratic seismicity in early 2012 is associated with lower-level eruptions and degassing. I have also presented a three-stage model for pre- and post-explosion drumbeats during cyclical Vulcanian eruptions, related to the failure and resealing of an upper conduit plug. And finally I have demonstrated the 'breakdown' of activity at the end of 2015 where drumbeats are associated with failed or unsuccessful explosions. By using automated picking methods and manually verifying the results, I have generated an extended catalogue of LP events, to further our understanding of seismicity at Tungurahua.

In the event of a resumption of seismicity at Tungurahua, the findings from this study

could inform decision making in hazard assessment. Any increase in seismicity should be investigated, however, we now have examples of 'false precursors' where drumbeats are not associated with explosions. Seismicity should be carefully interpreted in conjunction with available geophysical monitoring data, particularly as the tilt data has been demonstrated as a key indicator in the shallowest conduit processes. The signal processing workflow could be used to quantify new earthquake signals and determine their likely source process. New events can also be cross correlated with the the extended catalogue, generated in this study, to investigate the resumption of isolated and specific source processes described in 2015. I hope the approach to waveform analysis and generalised plug models presented here could easily be applicable to interpret repeating LP seismicity at similar intermediate-composition volcanoes.

Summary of findings

In this chapter I have applied the methodology described in chapter 3 to seismic records from 2012 - 2016 at Tungurahua. I specifically address research questions

3. What can we learn about the shallow dynamics at Tungurahua and Cayambe volcanoes, from analysis of the seismicity?

4. With better characterisation techniques, can volcano-seismic events then be used to interpret episodes of unrest at poorly monitored volcanoes?

5. What is the significance of periodic, drumbeat LPs?

Here, I have isolated seven episodes of periodic drumbeat seismicity which in turn, characterise three different eruption styles. I have demonstrated particularly, how drumbeat LP seismicity relates to models of sealing magma plugs, well-established previously by geochemical studies.

By identifying new patterns in drumbeat LP seismicity at Tungurahua, and inferring shallow conduit processes, this chapter also begins to answer research question 5.

6. Can this detailed volcano-seismic analysis better inform hazard assessment?

Developing our understanding of the historical processes at Tungurahua can act to inform hazard assessment and decision making in the event of future seismic unrest.

5 | Drumbeat LP "Aftershocks" to a Failed Explosive Eruption at Tungurahua Volcano, Ecuador

Preface

In chapter 4 I identified episodes of drumbeat LPs at Tungurahua, for some of which the rates of seismicity considerably accelerate and decelerate. In section 2.2.4, figure 2.4, I also illustrated examples of LP swarms from around the world, plotted with respect to their earthquake rates and amplitudes through time. Accelerating rates of earthquakes have frequently been modelled as 'precursors' to eruptions, although as explored in the previous chapter, these sequences can also be 'false precursors'. In this chapter, I explore the importance of seismicity rate. In particular, I expand on the findings of Episode 7 (chapter 4) and investigate a striking sequence of drumbeat LPs that are recorded at RETU in November 2015, with a decelerating rate of earthquakes. I develop the methodology in chapter 3 and further answer research question 1, by using a Bayesian approach to model temporal patterns in the seismicity. I address research questions 4 and 6 and demonstrate that rates of drumbeat seismicity can be informative for shallow conduit dynamics. Here I propose a model for a 'failed' explosive episode at Tungurahua.

This chapter was published in *Geophysical Research Letters* in 2020 (https://doi.org/10.1029/2020GL088301) and is included here without further editing. As such there may be a small amount of repeated information in the data and methods sections of the chapter. As this was published as a short format paper, limited to only four figures, I also include some of the supplementary figures and further discussion in a post-script.

5.1 Abstract

Highly periodic, repetitive long-period (LP) earthquakes, known as 'drumbeats', have been observed at a range of volcanoes, typically during the ascent of degassed magma. Accelerating rates of drumbeats have been reported before explosions, and potentially offer forecasts of future activity. However, the broader phenomenology of drumbeats is poorly understood. Here we describe an episode of over 900 LP earthquakes recorded in November 2015 at Tungurahua Volcano, Ecuador, that we believe are associated with a failed explosion. Rates of LP drumbeats accelerated for 10 hours, consistent with an Inverse Omori's Law. Before any explosion occurred, seismicity decreased following Omori's Law, over a further six days. Despite earthquake rates decelerating, amplitudes, spectral peaks, Q values and periodicity remain constant, suggesting there is little change in the source process with time. We argue that the decelerating seismicity is a result of progressive reduction of gas flux, unable to provide sufficient overpressure for explosion.

5.2 Plain Language Summary

When a volcano is erupting, small earthquakes from the volcano can be used to infer what internal processes may be occurring. Earthquakes that are very similar to one another and repeat at consistent intervals are known as drumbeat earthquakes. These are of interest in volcanic systems as it implies the earthquakes are generated by a single, repeating source.

Previous studies of drumbeat earthquakes at Tungurahua Volcano, Ecuador, have described these earthquakes occurring closer together in time and accelerating up to an explosion. In this case, we identify a sequence of drumbeats where the rate accelerates, and without any explosion, decelerates again. We suggest these earthquakes are generated by gas flux which is slowing down. This gas originates beneath a plug at the top of the conduit. We use statistical models to estimate when the volcano may have exploded if the earthquakes had continued to accelerate, and quantify the subsequent deceleration in earthquake rate.

5.3 Introduction

Active arc volcanoes of andesitic-dacitic composition are often sources of rich seismic data. Signals at these volcanoes are often dominated by long-period earthquakes (LPs), commonly associated with processes occurring in and around the magma column. Understanding these signals could be key to improving our ability to forecast volcanic activity. LPs are characterised by frequencies between 0.5 and 5.0Hz, emergent onsets, and missing clear S wave arrivals (Chouet et al., 1994). They often begin with a mixed frequency onset, followed by low frequency coda that decays in amplitude with time. This characteristic shape has been modelled as a two part process with an initial excitation trigger and subsequent resonance (Chouet, 1996). These are some of the features that have been used to distinguish different categories of volcano seismic events, attributed to different source processes (Chouet & Matoza, 2013). Swarms of periodic, highly similar, repeating LPs occur in a phenomenon known as drumbeats. Drumbeat seismicity is commonly associated with degassed magma ascent, however, the broader phenomenology of drumbeats is still poorly established. Locating LPs is generally a very difficult process, however, with one or two stations, careful analysis of the waveforms and their frequency content can tell us about an evolving source mechanism.

Drumbeat earthquakes are best known from the dacite spine extrusion episode at Mount St. Helens between 2004 and 2005. Iverson (2008) approximated long term steady-

state behaviour and slowly changing drumbeat rates and amplitudes with frictional stick-slip at the conduit margins. However, drumbeat seismicity is known to display a variety of characteristics from many arc volcanoes. Drumbeat seismicity at Soufrière Hills Volcano appeared in pulses lasting several hours (Green & Neuberg, 2006). These pulses were associated with brittle failure of ascending magma at conduit margins (Neuberg et al., 2006). The behaviour of drumbeats observed at Tungurahua alone is varied. One study examined a six-day episode of steady-state, repeating LPs in 2001 where the Q factors of individual earthquakes were changing through time (Molina et al., 2004). This shift was modelled with repetitive injections of increasingly ash-laden gas. Repeated low frequency (1-3Hz) pulses are recorded in both the seismic and infrasonic record for episodes in 2004 (Ruiz et al., 2006). In July 2013, accelerating drumbeats merged into tremor before large explosions (Bell et al., 2018). A further study identified the incremental breakdown of an episode of drumbeat LP seismicity during April 2015 (Bell et al., 2017). Building on previous models at Soufrière Hills, a more developed plug model argued that LPs were triggered by gas escape and shear failure in the conduit margins with magma ascent.

Accelerating seismicity, has been related to material failure in the Failure Forecast Method (FFM) (Main, 1999; Voight, 1988). New statistical methods allow analysis of point process data, revealing properties of precursory sequences. Improved methods help to quantify data, identify changes and understand underlying processes. We can examine seismicity rates with relationships such as the Modified and Inverse Omori's Laws. By contrasting accelerating and decelerating seismicity with models and examining this 'mirrored' effect we can investigate the significance of failed explosions, better understand the physics of the process and develop forecasting statistics.

Here we describe a six day sequence of accelerating and decelerating drumbeat LP earthquakes at Tungurahua during November 2015 associated with a 'failed' explosive eruption. We use a Bayesian gamma point process model (Bell et al., 2017) to examine the acceleration of seismicity rate, and the subsequent decreasing rate of seismicity. We find

that the drumbeats both accelerate and decelerate according to a power law with an exponent value, $p = 0.96 \pm 0.51$ and $p = 0.97 \pm 0.12$ respectively. Despite prolonged decaying temporal rates of seismicity, the earthquakes show strong similarity with families persisting across the six day sequence and amplitudes unchanging. This suggests a slowing rather than a breakdown of the driving source mechanism following a failed eruption.

First we introduce the activity and data recorded at Tungurahua during November 2015. We then present the seismic data, along with the statistical methods for analysis. We model the data using a Bayesian point process methodology, testing different rate models and estimating parameter posterior distributions. We analyse earthquake properties including waveform similarity, families and Q factor values. We finally present a model for accelerating and decelerating drumbeats, and discuss the implications this has for magma ascent dynamics at Tungurahua.

5.4 Data & Methods

5.4.1 Tungurahua

Tungurahua is a 5,032m high andesitic stratovolcano in the Central Cordillera of the Ecuadorian Andes (Hall et al., 1999). The most recent phase of activity occurred between 1999 and 2016 with notable sub-Plinian activity in 2006 (Mothes et al., 2015). Unrest at Tungurahua was typically associated with high rates of LP seismicity. Between the major explosive episodes of 2014 and 2016, heightened seismicity accompanied deformation and repeating tilt cycles (Bell et al., 2017; Marsden et al., 2019; Neuberg et al., 2018). This study focuses on an episode of drumbeats during one such cycle in November 2015. The drumbeats persisted for six days and did not culminate in any explosion. There was then a repose period of three months before the final explosions in February 2016. Drumbeat seismicity persisted for several weeks in April 2015 and was accompanied by small explosions and ash emissions

(Bell et al., 2017). Whilst in October and early November 2015, small pulses of drumbeat seismicity emerged and ceased over just a few hours or days and are as yet unstudied (fig 5.1).

5.4.2 Monitoring data

The Instituto Geofísico de la Escuela Politécnica Nacional (IGEPN) maintain a volcano monitoring network on Tungurahua. The network includes short period and broadband seismometers, DOAS gas flux stations, infrasound stations, tiltmeters, GPS, cameras and acoustic flow monitors. From a seismic network of 11 stations, IGEPN maintain a catalogue of detected, classified, and where possible, located events. Over 90% of events were recorded at RETU, a short period seismometer at elevation over 4000m, approximately 2000m from the crater rim. This proximity means the signal to noise ratio (SNR) is high and many small, shallow events are recorded. We manually picked 932 events from 25 - 30 November 2015 for this study, representing all detectable events at RETU. These events were only visible at the one station and with emergent onsets and no clear S-phases, locating the events was not possible. As the seismicity is only recorded at this uppermost station, we believe these LPs are associated with shallow processes in the top 2000m of the conduit (Bell et al., 2018). The similarity of the waveforms indicates that they are all closely co-located within a small depth range. Given this co-location, we use the maximum amplitudes of individual events as a relative comparison for magnitude. 615 of the manually picked events appear in the IGEPN catalogue. However, there are only 20 events which are located and have estimated magnitudes, all of which are less than magnitude 1.5, and carry large uncertainties. The seismicity on 25 November is the first clearly identifiable sequence of LP events as in the preceding days, the signal at RETU is dominated by emission tremor.

Details of surface observations and ash column heights are extracted from daily reports produced by the Observatorio del Volcán Tungurahua (OVT) (https://www.igepn.edu.ec/),

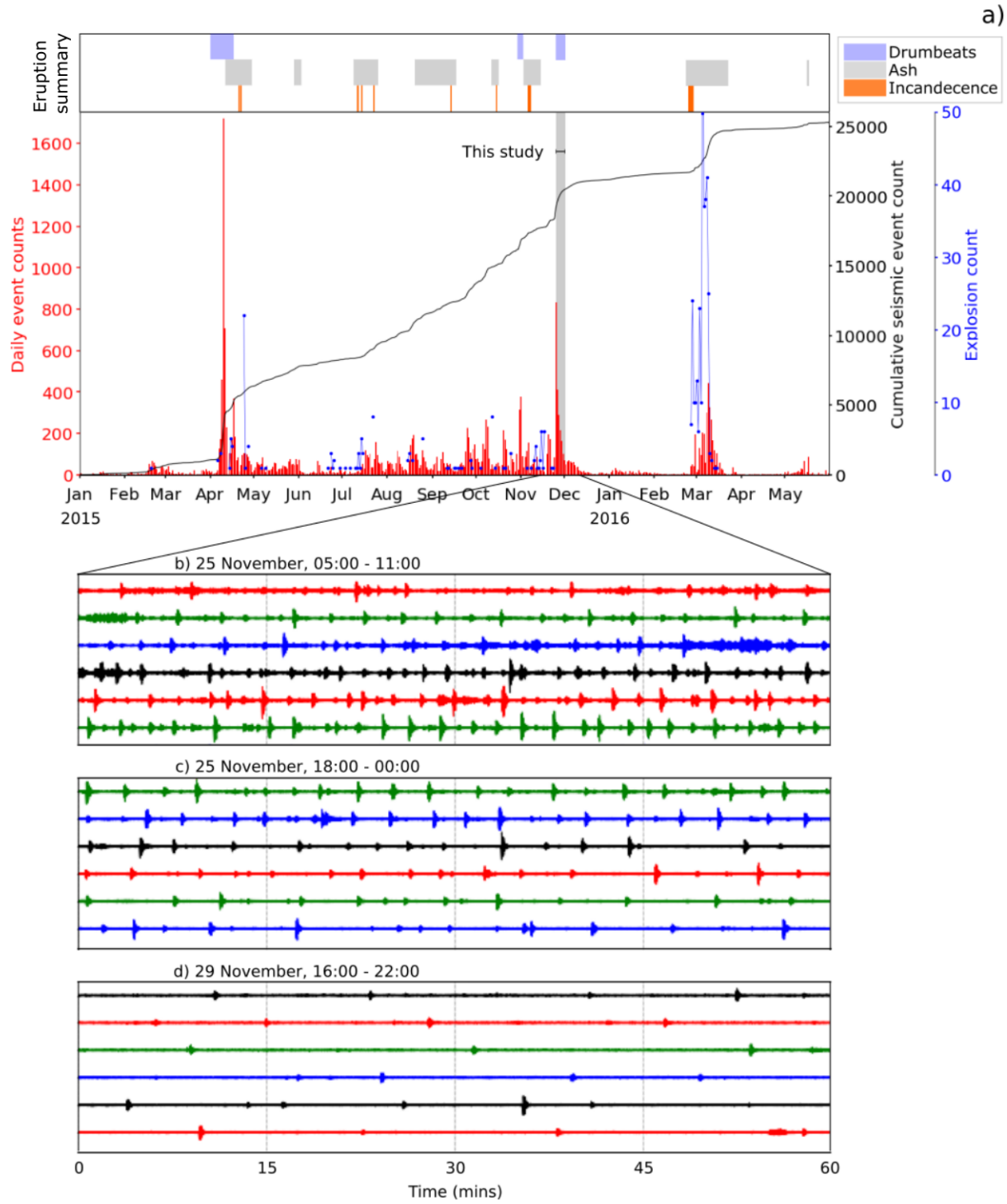

Figure 5.1 *a)* Seismicity at Tungurahua 2015-2016. Red bars show daily event counts, blue dots mark daily explosions, black line shows cumulative seismicity, grey shading marks period of interest for this study. Top panel marks surface observations - blue shows known episodes of drumbeats, grey shows ash ejection and orange are sightings of incandescent glow in crater. *b)* Accelerating drumbeats, 25 November. *c)* Decelerating drumbeats, 25 November. *d)* Penultimate day of drumbeats, 29 November. All 6hr extracts from RETU. All times are local.

and used in conjunction with the seismic data for temporal analysis. Explosion counts and radial tilt measurements at station RETU are also collected from IGEPN catalogues.

5.4.3 Methods

The seismic data are initially processed using the ObsPy toolkit (Krischer et al., 2015). 30 second duration waveforms are sliced and bandpass filtered between 1 and 40Hz. The maximum amplitude of each event is extracted. Fast Fourier Transform (FFT) of each signal is calculated to generate a periodogram. We find the power spectral density (PSD) for frequencies sampled at an interval of 0.01Hz and extract the maximum value as the fundamental peak frequency.

The Q factor for each event is calculated using an auto-regressive moving average (ARMA) technique, adapted from *Seismo-Volcanalysis* software (Lesage, 2007). The Q factor is a non-dimensional number that describes how quickly or slowly wave energy dissipates and is often strongly linked to the fundamental peak frequency. Auto-regressive methods have been successfully used to analyse changing LP frequency contents (Kumagai & Chouet, 1999; Lokmer et al., 2008). The approach is similar to the commonly used Sompi method (Hori et al., 1989). A signal is composed of a number of individual harmonic decaying oscillations. Each component can be represented in complex frequency space and quantified by a peak frequency (f, Hz) and growth rate (g, s^{-1}). (Kumazawa et al., 1990). We generated cumulative *f-g* diagrams for all filters between 2 and 30 and points that cluster around a pole at the spectral peak are used to calculate Q (Eq 5.1) (Cusano et al., 2008). In this automated adaptation of the ARMA method, a hierarchical clustering method is used to automatically select points in the complex frequency space (Eads, 2008).

$$Q = \frac{-f}{2g} \tag{5.1}$$

We determine the maximum cross correlation coefficient between 0 and 1, for all pairs

of events in our catalogue and use a threshold value to group events into families (Park et al., 2019; Waite et al., 2008; Yukutake et al., 2017). Following previous studies, including that of LP drumbeat seismicity in April 2015 at Tungurahua, the threshold is set at 0.7 (Bell et al., 2017; Petersen, 2007; Thelen et al., 2011).

We also calculate earthquake inter-event times (IETs) and their periodicity to highlight times of pronounced drumbeat activity. Bell et al., 2017 defines periodicity as the ratio between the mean, μ, and standard deviation, σ, of IETs. Events randomly distributed in time, with an average rate, λ, will have a probability density function such that $\frac{\mu}{\sigma} = 1$. Clustered events have periodicities less than 1, whereas periodic events have periodicities greater than 1.

Finally we considered models for the accelerating and decelerating components of the drumbeat episode. Previous studies of accelerating seismicity have modelled rates using power, exponential and hyperbolic relationships (Bell et al., 2018; Ignatieva et al., 2018). In accelerating and decelerating components we opted to model the event rates using an exponential relation (Eq 5.2) as a function of time, t, where λ is the rate parameter and k is a scaling parameter. We also modelled the sequences as a power-law relationship. Again, these are defined by a scaling parameter, k and a power exponent, p. For the decelerating event rates this is the Modified Omori's Law (Eq 5.3) and for the accelerating rates, an Inverse Omori's Law (Eq 5.4) .

$$n(t) = ke^{\lambda t} \tag{5.2}$$

$$n(t) = k_1(t - t_f)^{-p_1} \tag{5.3}$$

$$n(t) = k_2(t_f - t)^{-p_2} \tag{5.4}$$

We model the drumbeat sequence as an inhomogeneous Gamma process (Bell et al., 2018). We define the point of maximum seismicity as, t_f, separating the accelerating and decelerating components. We use a Bayesian approach with PyMC3 implementation (Salvatier et al., 2016). We use Markov Chain Monte Carlo (MCMC) to sample the posterior distributions of model parameters. We run 5000 iterations. We provide initial estimates for parameters p, t_f and k. The prior distribution and rate parameters used are detailed in tables B.1 and B.2.

5.5 Results

Across the six day period from 25-30 November we see an initial increase in the rate of seismicity before a rapid deceleration. The peak in event rate occurs at 10:00 on 25 November (fig 5.2). During the drumbeat episode the radial tilt increases and decreases in a range of 10 μrad.

5.5.1 Drumbeat Onset

The first 10 hours of the drumbeat sequence is markedly different from the activity observed thereafter. In the first 10 hours, the event rate increases, the individual event amplitudes increase slightly and the seismicity becomes increasingly periodic (fig 5.2). The point process modelling shows the accelerating rates of seismicity can be defined by a power law (fig 5.3a). The best fitting exponent, $p = 0.96 \pm 0.51$. The best fit value for t_f is 0.53 ± 0.16. The t_f value gives a 'hind-cast', indicating when an eruption may have occurred, if drumbeats continued to accelerate. The point process model finds t_f and the possible eruption at approximately 12:43pm. This is nearly three hours after the peak rate of seismicity and onset of the deceleration.

Through this sequence, the Q factor shows little to no change. A few events before 10:00 on 25 November are included in families that persist through the episode, but there are

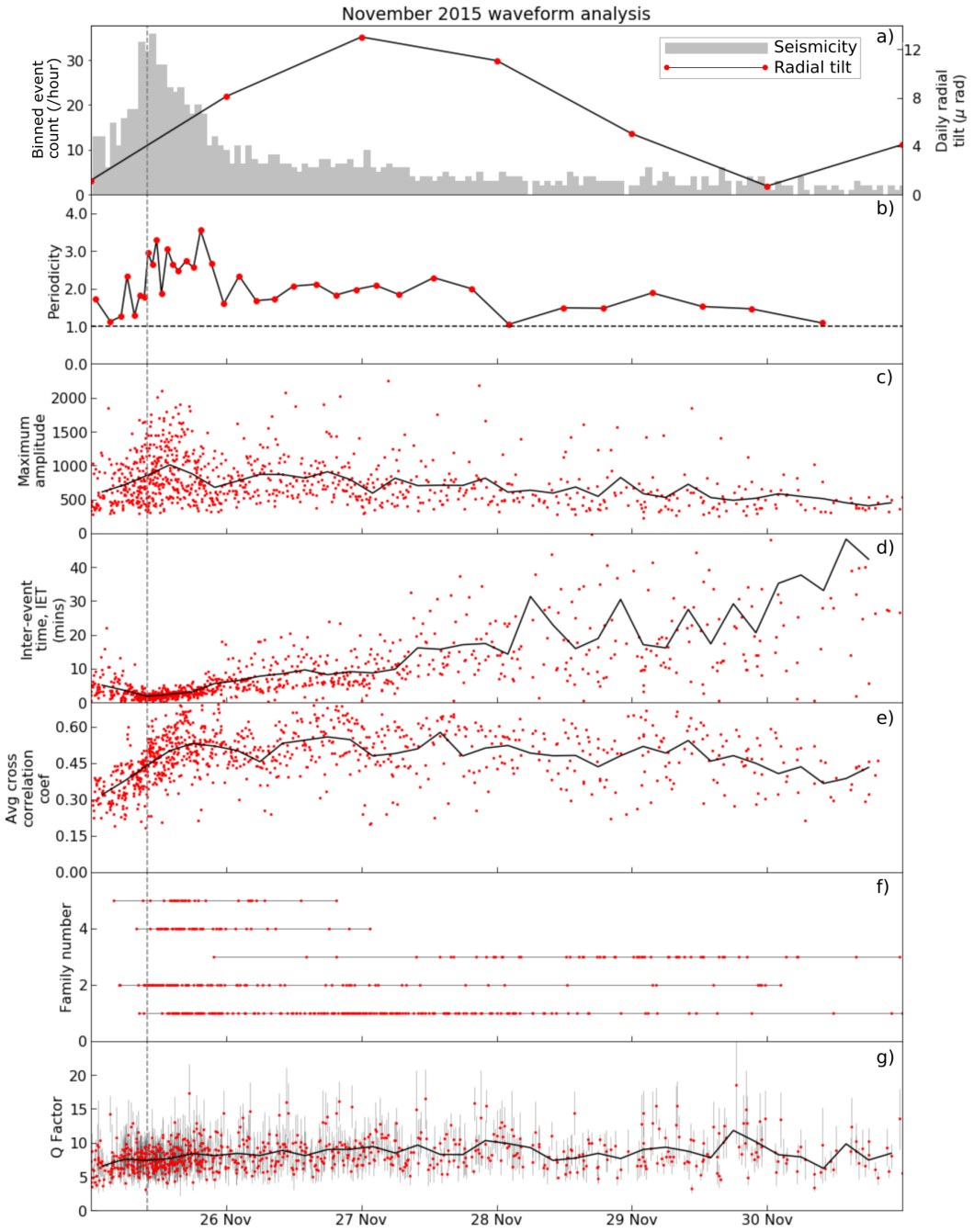

Figure 5.2 *a)* Hourly seismic event count, and radial tilt at station RETU. *b)* Periodicity for 25-event windows. Black dashed line at periodicity = 1. *c)* Absolute maximum amplitude of individual events (red circles). 4hr non-overlapping windowed averages (solid black lines). *d)* Inter-event times (mins). *e)* Average value of cross correlation coefficient for each event with next 10 events. *f)* Five largest families of events in episode, ranked in order of size, representing 43% of all picked events. *g)* Q factor. Grey error bars indicate standard deviation amongst points selected for pole. Vertical grey dashed line in all panels marks the exact peak in seismicity.

no families that exclusively represent events prior to 10:00. This suggests that accelerating events before 10:00 are not generated by a distinct source that differs to that active later in the episode. There is no specific activity from the surface observations that can be pinned to the change in seismicity at 10:00. From 18:00 on 24 November to 18:00 on 25 November there were observations of energetic gas and steam emissions between 300 and 800m. Notably this was with no ash content, but for the majority of the day the summit remained obscured by cloud (IGEPN, 2015).

5.5.2 Drumbeat 'Aftershocks'

During the afternoon of 25 November, the earthquake rate decreases rapidly whilst the periodicity remains greater than 1. Event amplitudes and the Q factor show no systematic change with time (fig 5.2). The average cross correlation coefficient also remains stable through the sequence, but begins to decrease after 12:00 on 29 November, and fewer events after this point are grouped into families. Unlike previous studies of event families, where systematic shifts in families correspond to physical changes in activity (Bell et al., 2017; Green & Neuberg, 2006; Thelen et al., 2011), there is no chronological variation in the families identified here. The largest family contains 177 events, representing 20% of all picked events in the sequence, and persists across all six days, of both accelerating and decelerating seismicity. There is strong waveform similarity between families, as the master events also show high cross correlation coefficients with one another (fig B.6).

The decrease in seismicity rate is well modelled by a power law. The best fit parameters are calculated where $p = 0.97 \pm 0.12$ (fig 5.3). The power-law exponent is consistent with the Omori's Law relationship where $p = 1$ and so the rate of earthquakes is inversely proportional to the period of time since the peak of activity. Previous studies examining tectonic aftershock sequences using modified Omori's law have found p values between 0.6 and 1.8 (Holschneider et al., 2012; Wiemer & Katsumata, 1999). Tectonic aftershock se-

quences are typically described as clustered, whereas seismicity here is quasi-periodic. The exponential model provided a less successful fit (fig B.7, tables B.1 and B.2).

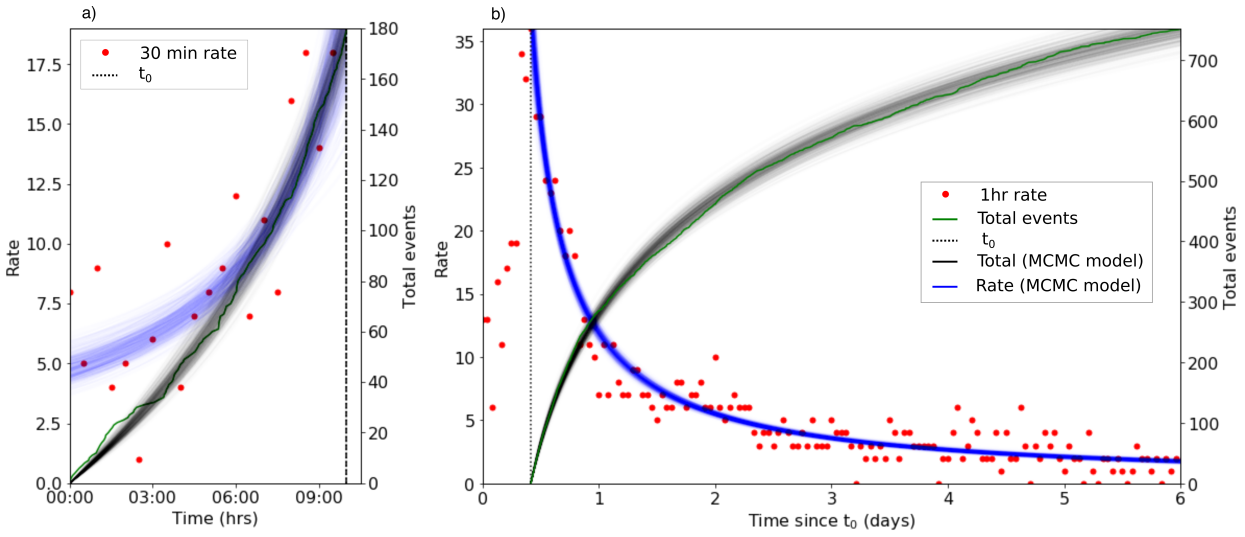

Figure 5.3 a) Accelerating and b) decelerating components of the seismic episode using power law model. Red circles show event rates. Green marks true total event count. Blue and black lines show rate and total seismic counts respectively, from 500 samples from posterior distributions.

5.6 Discussion

The surface observations, tilt data and seismicity analyses allow us to build a conceptual model for the process generating this seismicity. The point process modelling reveals two distinct phases of accelerating and decelerating seismicity. The accelerating drumbeats follow a power-law increase, according to the Inverse Omori's Law (Eq 5.4) with exponent $p = 0.96 \pm 0.51$ (table S2). Hind-cast values for t_f suggest that had seismicity continued to accelerate this may have culminated in an explosion nearly three hours later. This is comparable with the accelerating LP drumbeats prior to a large explosion in July 2013 at Tungurahua where the exponent is $p = 1.05$ (Bell et al., 2018). Five minute real-time seismic amplitude (RSAM) was calculated for 00:00-10:00 25 November for comparison. Unlike July 2013, amplitudes of

individual events in this study do not accelerate to the same degree, but through the majority of the drumbeat episode, they do generate RSAM values in the same range ($\sim$ 50-150) (fig 5.6) (Bell et al., 2018). The decelerating phase closely mirrors the acceleration, as point process modelling fits the Modified Omori's Law (Eq 5.3) with an exponent, $p = 0.97 \pm 0.12$.

Drumbeats that show short inter-event times and similar waveforms require a single, rapidly recharging, non-destructive source process (Neuberg et al., 2000). Families of events persist through the phases of accelerating and decelerating rates of seismicity. High periodicity, and unchanging Q factors and amplitudes also persist throughout, suggesting the seismicity is likely generated by the same source location and process through the full episode.

The Q factor of individual waveforms can be used to determine the composition of resonating fluids generating LPs. Q values in the literature can vary from 3-300 (Molina et al., 2004). Although the Q values in November 2015 do not show a clear increase or decrease, they are consistently in the range 3-15, which fit well with a high gas fraction CO_2 or SO_2 water (Kumagai & Chouet, 2000). This is unlike the dusty-ash-gas mixture examined in Molina et al. (2004) where Q systematically increases from 200-500. This also corresponds well with the daily records, that on 25 November steam and gas emissions continue but notably, without any ash.

A common component of models for LP drumbeats is a process of loading and release. However, the controlling mechanisms proposed have included stick slip processes (Iverson, 2008), magma failure (Green & Neuberg, 2006; Tuffen et al., 2003) and gas escape and depressurisation (Bell et al., 2017). A plug model is illustrated in Bell et al. (2017) and plug sealing and destruction cycles during 2013-2014 at Tungurahua are well documented (Hall et al., 2015). Although these drumbeats follow a period of small explosions, and there is no evidence that a plug was destroyed following April 2015 drumbeats (Bell et al., 2017). Instead, we consider the plug as an intermittently permeable barrier with fracture networks and transient pathways to allow gas, ash and magma to ascend through it. The driving pro-

cess is ascending magma in the conduit, which is degassing, and there is a decelerating force that leads to longer loading and failure cycles at a plug in the upper conduit. Irrespective of the physics of the excitation mechanism in this episode, we can put constraints on the nature of the loading process.

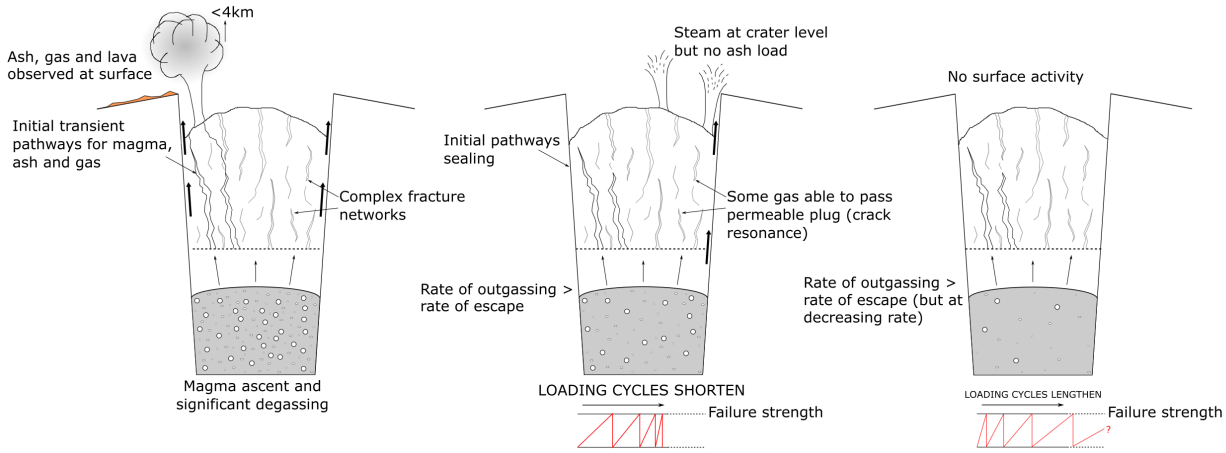

Figure 5.4 Schematic model for conduit processes before drumbeat seismicity, during initial onset and then decay

We propose a model for the timeline of events in November 2015. During 11-17 November initial magma ascent in the conduit, as detected in the inflation signal at RETU, caused depressurisation and fragmentation leading to minor explosions and ash emissions (Cassidy et al., 2018). In the plug, there were persistent pathways for gas and ash escape, without increasing overpressure in the conduit. Observations of incandescent blocks on the flanks suggests magma was extruded. We assume this initial ascent was an aseismic process (Neuberg et al., 2006; Salvage & Neuberg, 2016). Following the explosions, there was a further period of repose in surface activity (IGEPN, 2015) but the radial tilt still increases, indicative of ongoing magma ascent (fig B.8). By 25 November, the radial tilt increase slows and we observe increasing rates of drumbeats. This timing in the tilt cycle is the same as the April 2015, though different to most in which SO_2 flux and seismicity peaks occur during minima in tilt inflation cycles (Bell et al., 2017). As the tilt cycles and episodes of seismic

unrest are out of synchronisation with one another, this suggests there was something unusual about the episodes of drumbeats in April and November 2015. Outgassing was ongoing and building pressure beneath the plug as the rate of release exceeds the rate at which it can freely escape. Each time the failure strength was surpassed, escaping gas interacts with this complex fracture network and generated LP events. Between 00:00 and 10:00 on 25 November the accelerating rate of LP drumbeats, suggests there was an increase in the gas accumulation and hence the loading rate. This overpressure, however, was insufficient for an explosion. Seismicity persisted as outgassing continued but at a decreasing rate, and there was a decreased loading rate. The time to reach a failure strength increased, and so the repose period between events remained cyclic but increasing. The loading rate and seismicity decreased as a power law relationship until a state of equilibrium and repose. As the body was not ascending at this stage or under any further external pressures, we assume the plug was in a steady state. We suggest degassing continued at a reduced rate, but we cannot be certain for how long.

The next paroxysm in February 2016 included some of the most violent activity in the whole eruption, with pyroclastic flows and over 130 explosions in the first week of March (IGEPN, 2016a). It is therefore significant that we see heightened seismicity and acceleration up to a failed explosion, before several months of quiescence. This provides valuable insight into forecasting potential explosions using seismicity at intermediate composition volcanoes. The power law fit during the accelerating seismicity indicated an eruption time at 12:43 on 25 November, by which time the seismicity rate had already decreased 30% from the peak rate.

Subsequent deformation analysis has used InSAR to examine inflation on the western flank during the first three weeks of November 2015, prior to the onset of drumbeat LP seismicity. The most likely source model identified was an inclined body of shallow, short-term, pre-eruptive magma storage (Hickey et al., 2020). This shallow magma storage may have contributed to processes in the conduit prior to drumbeat LPs.

5.7 Conclusions

The analysis of the November 2015 drumbeats contributes to the narrative of the final years of activity in the 1999-2016 eruption at Tungurahua. Although the sequence overall shows similarities with the drumbeats observed in July 2013 and April 2015, the driving mechanism and subsequent surface activity is likely different. Across accelerating and decelerating phases, the earthquake signals show minimal changes in their properties including Q factor and amplitudes, suggesting the source process is unchanging. Q values are consistent with LP excitation by a gas rich mixture as opposed to magma or ash-gas mixtures.

We suggest that the observation can be explained by a model involving ascent of a degassing magma body. We initially see acceleration of drumbeat LP events and an increasing rate of loading on the plug. Insufficient overpressure from gas flux causes an increasing repose time in loading-failure cycles at the plug and hence a decreasing rate of seismicity. We believe this is a ‘failed’ explosive event, followed by several days of drumbeat LPs where magma in the conduit continues to degas.

This work contributes to further understanding the broader phenomenology of drumbeat seismicity and their source processes. This last instance of degassing is key to bringing the conduit into a state of equilibrium before several months of quiescence. Future work will look to extend these analyses to quasi-periodic seismicity throughout 2015 and into the final explosive eruptions during 2016. For volcanic hazard analysis, it is important to highlight that high rates of seismicity are not necessarily a precursor to substantial explosions. Careful analysis of the seismicity rate and individual event properties, alongside the surface observations show these drumbeats are part of a complex process.

Post-script

This chapter was written as a short format manuscript, and so here I discuss further some of the implications of the findings from this research. I also discuss some of the figures that were in the supplementary material of the original publication.

5.7.1 The 'switching off' of Tungurahua

In this section I want to briefly expand on how this research develops from the findings of the previous chapter. In chapter 4, I proposed a cyclical model for drumbeat seismicity that relates to the rupture and resealing of an upper conduit plug (fig 4.20). This correlates to a continued slow ascent rate of degassing magma in the conduit, demonstrated in the cyclical tilt signal at RETU. This is an idealised model which is fully realised in a handful of drumbeat LP episodes, although as demonstrated, some episodes show variations from this cycle. The drumbeat LPs in November 2015, described in this chapter, are significant as they are the last periodic earthquakes to be recorded at Tungurahua to present day and they do not clearly follow this idealised model of plug rupture. In the discussion section, I suggested that there was insufficient overpressure underneath the magma plug to cause failure and ejection of the plug from the conduit. Further to the model proposed in chapter 4 (fig 4.20 and illustrated further in fig 5.5), I suggest what we see here, is a small sub-section of the idealised plug cycle. We still see magma degassing and a process of crack resonance in a fractured upper conduit plug. However, there is one or more conditions which is different in November 2015 to the conduit conditions during the periodic Vulcanian plug-rupture cycles. This could relate to a number of factors. As suggested in the previous chapter, the sealing magma plug is likely composed of the slowly ascended magma from the previous explosive cycle, which has cooled, densified and vertically stratified (Gaunt et al., 2020). Perhaps due to the time it took to cool, or the composition of the magma in the previous ascent cycle,

the plug formed prior to November 2015 was not as mechanically strong or impermeable and therefore the conditions were not adequate to generate critical overpressure. It could also be a result of the previous three months of activity. As demonstrated in section 4.3.7, there was a sustained three month period from August-October 2015 with a number of episodes of LP seismicity associated with degassing. Perhaps the magma in the shallow conduit has sufficiently degassed more slowly through 2015, such that there is no further pressure driven from the exsolution of volatiles beneath the plug, and resulted in this failed eruption. One study also identifies an inflationary signal in the deformation data beneath the western flank, during early November 2015, likely associated with shallow magma storage (Hickey et al., 2020). This is in turn associated with a small swarm of VTs from the unconsolidated flank. Perhaps pressure is relieved in the conduit as remaining shallow magma is re-routed and able to find equilibrium in this additional area of storage. It may be a combination of all three conditions suggested here that mean there is insufficient pressure to generate the large explosion and plug failure in the idealised model. Without petrological and textural studies from field samples of the plug material that was later ejected in 2016, this is only speculative. The seismicity alone cannot tell us whether the plug material was mechanically less strong, or more permeable; we can only relate the seismic observations to a model. What is significant is that at the end of this episode of seismicity, there was insufficient pressures in the system to cause substantial seismicity or deformation in the shallow edifice; so much so, Tungurahua remained in quiescence for a further three months. Perhaps the plug conditions were different to the 2013 Vulcanian cycles, as with the resumption of explosive activity in 2016, there was no associated periodic seismicity and the explosions ended the eruptive phase entirely.

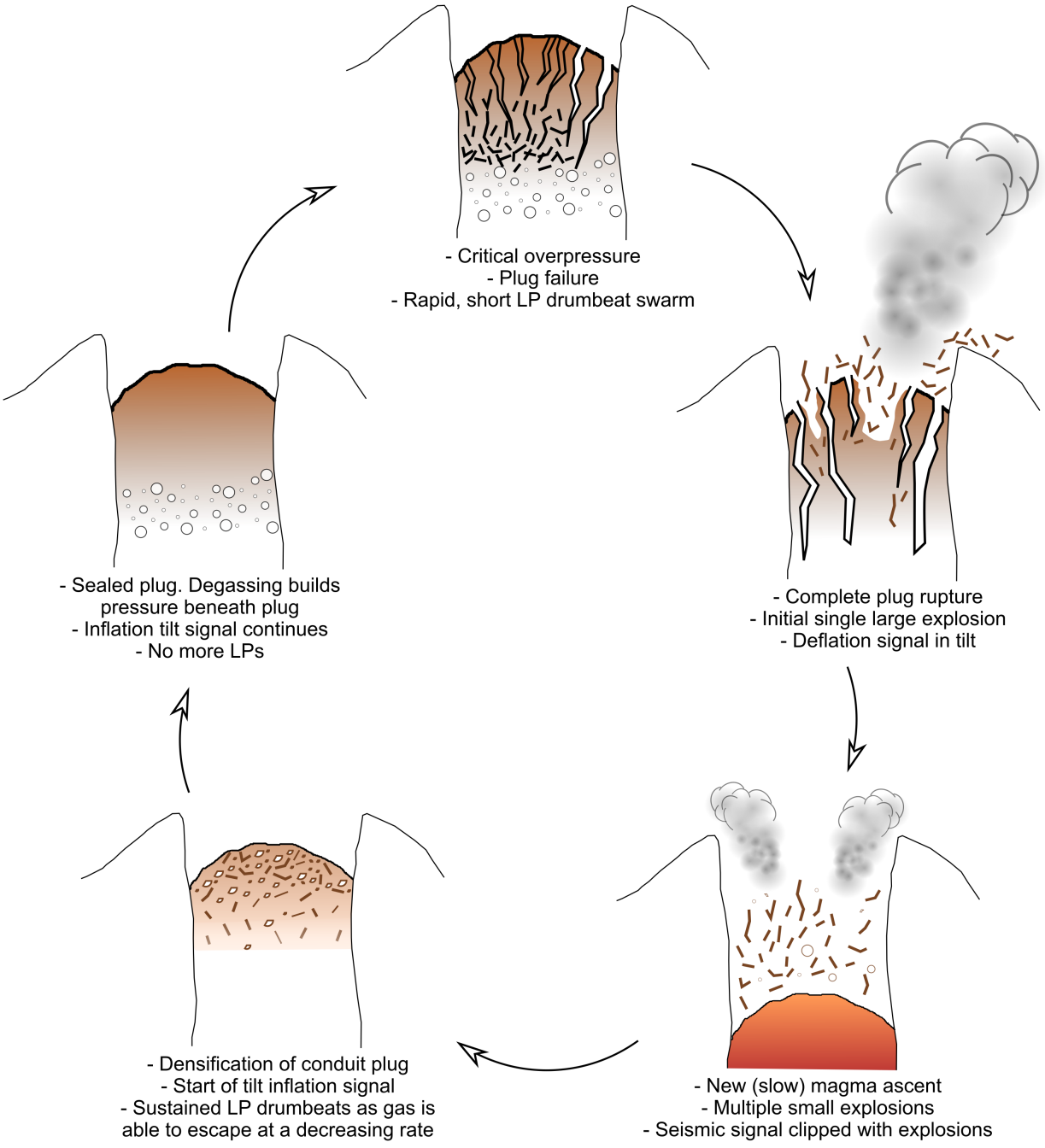

Figure 5.5 Cartoon illustrating the idealised plug rupture and resealing cycle as illustrated in chapter 4. One or more conditions relating to the conduit or magma, mean this controlled periodic plug cycle does not occur in November 2015.

5.7.2 The use of Bayesian statistics alongside the signal processing routine

The research in this chapter also expands the signal processing workflow defined in the methodology, to consider a Bayesian statistical approach to quantify seismicity. As discussed in the manuscript, accelerating rates of LP drumbeats were identified prior to the intense Vulcanian explosion in July 2013. These were also modelled using an MCMC approach to hindcast the eruption time and demonstrate the potential for these types of methods in real-time seismic monitoring. In this chapter, I have taken this one step further and combine MCMC methods with the signal processing routine, to generate a thorough suite of metrics to quantify the behaviour of the seismicity. The detail that comes from the signal processing alongside the Bayesian statistical approach could be decisive in real-time monitoring. For example, by also considering the amplitude of the earthquakes, using 5 minute RSAM, figure 5.6 illustrates how very different the accelerating seismicity was in July 2013, relative to November 2015. Clearly in hindsight, these two episodes relate to very different processes. The July 2013 explosion was one of the most powerful recorded in recent history at Tungurahua, whereas the November 2015 unrest represents only a failed attempt at plug rupture (fig 5.5). However, in real time these metrics could be decisive. This point processing method could readily be incorporated into the signal processing routine. Ultimately the only input is a catalogue of earthquake times, which if being updated in real-time can easily translate into inter-event times (IETs) and binned event rates. With relatively small numbers of data points (in the order of $\sim 10^2$), 5000 iterations can be computed in seconds. If executed in real time, for example every 5 or 10 minutes, then the best fit parameters from the previous model can be used to inform and update the priors for the next model. In turn a forecast peak seismicity or eruption time could be monitored.

In addition to hindcasting eruption times from accelerating rates of seismicity, the MCMC approach and power-law model provide an excellent fit to quantify the decelerating

rates of seismicity in this episode. Again, this is an analysis tool that could be incorporated into long-term retrospective studies of seismicity. The idealised plug-rupture model (figures 4.20 and 5.5) includes a period of decelerating rates of LPs during plug resealing processes. Although overall trends of decelerating LP seismicity were observed in a number of the seven episodes of periodic unrest, none were so clearly defined and prolonged as this sequence. The Modified Omori's power-law is a good basis fit for this sequence, but there is scope to consider exponential (fig B.7) and hyperbolic models in other episodes.

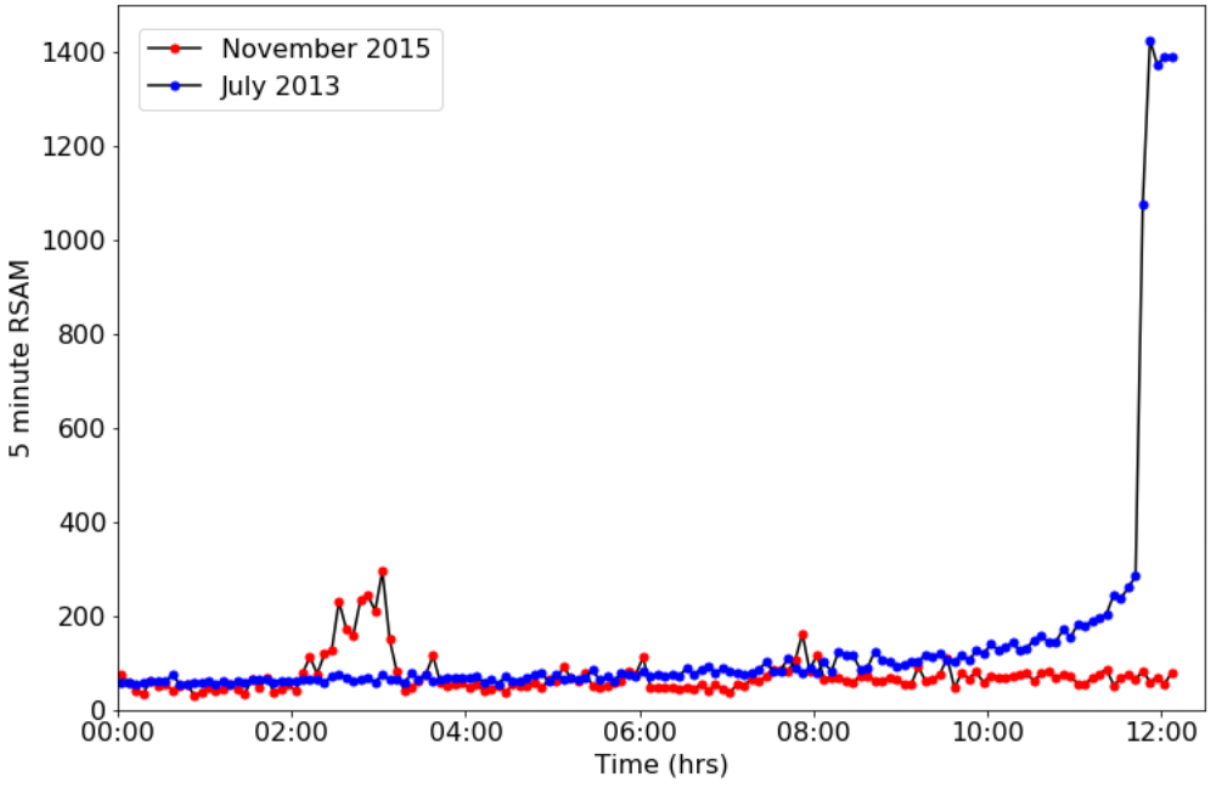

Figure 5.6 5 minute RSAM during drumbeats during 14 July 2013 Bell et al., 2018 and 25 November 2015 (this chapter). Both events initiated at 00:00hrs.

5.7.3 Further observations of accelerating and decelerating seismicity at Tungurahua

As is demonstrated in the July 2013 sequence of drumbeats (Bell et al., 2018), there is great potential and promise that accelerating seismicity could forecast explosion times and are therefore often considered precursors. In contrast, the findings in this chapter also demonstrate an example of where a false-warning may have been issued if real-time point process modelling had been ongoing and these had been interpreted as precursory LP drumbeats. In chapter 4, I present another example of precursory seismicity, where there is a short accelerating sequence of drumbeat LP earthquakes prior to an explosion (episode 2, section 4.3.2). This explosion was much smaller (in terms of estimated displacement and infrasonic measurements) than the July 2013 explosion, however, it does appear to initiate the first of the Vulcanian cycles described in chapter 4 (figs 4.20 and 5.5). Hidalgo et al. (2015) also cite December 2012 as the start of a new period and style of eruption at Tungurahua, and so it is significant that we see an episode of accelerating drumbeat LPs prior to an eruption. I have subsequently applied the point process modelling techniques described in this chapter to this short episode of unrest in December 2012. The exponential fit is plotted in figure 5.7 and the prior parameters and best fit values are detailed in tables 5.1 and 5.2. This episode of unrest was much shorter than either the sequence in July 2013 (Bell et al., 2018) or November 2015 as in this chapter; there was only 90 minutes between the first identified LPs to the explosion. As a result, there are fewer earthquakes and so even considering a 5 minutes binned event rate, there are limited and much more scattered data points to fit the point process model to. The same number of iterations are run for this sequence as November 2015 (5000), however, there is more uncertainty in the exponential best fit as illustrated by the spread in figure 5.7 and the errors in table 5.2. There is approximately a 5 minute offset between the explosion time and peak seismicity, and the range in rate shown in figure 5.7 is $\sim 33\%$. This is an example of where real-time temporal modelling with Bayesian

statistics has the potential to identify precursory seismicity, however, given the uncertainty in the model, there would be challenges to translate this to successful hazard assessment.

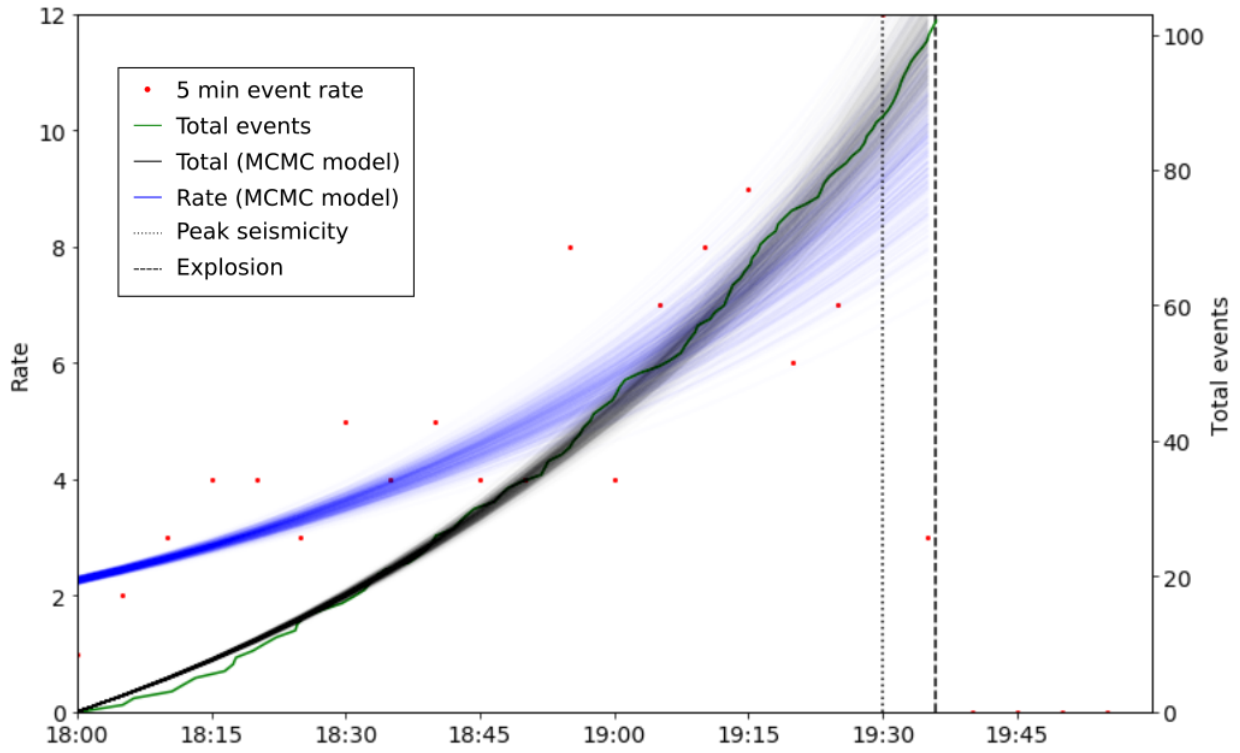

Figure 5.7 Episode 2: December 2012. Point processing to fit the accelerating sequence of events, 14th December 2012. Exponential model fit. Red circles indicate 5 minute event rate, solid green line shows the true total event count. 5000 iterations of MCMC generate simulations of rate (blue) and total (black) events. Black dotted line indicates the peak rate of seismicity and black dashed line shows the true time of eruption.

The previous chapter only really considers episodes where periodicity is consistently greater than 1.5, whereas these accelerating and decelerating rates of seismicity may occur outside the seven identified episodes. This is particularly the case if we believe these accelerating sequences are inherently related to the rupture and resealing of a magma plug, respectively. Some of the cyclical eruptions in 2013-2014 did not correspond to a prolonged periodic seismic episode. As much as the periodicity uses the inter-event times (IETs) to identify swarm and periodic episodes, perhaps the first derivative of a series of IETs could

be used to quantify the rate of change and identify episodes where there is consistent acceleration or deceleration.

Parameter	**Prior distribution**	**Prior parameters**
λ	Half-normal	$\sigma = 25.5$
k	Uniform	$630 < x < 670$

Table 5.1 Episode 2: December 2012. Exponential MCMC model prior parameters

Parameter	**Best fit value**	**Error**
λ	22.21	± 1.46
k	650.8	± 11.5

Table 5.2 Episode 2: December 2012. Exponential MCMC model best fit parameters and standard errors

5.7.4 Summary of findings

This chapter extends the methodology defined in chapter 3 and takes further steps to answer research questions 1 and 2.

1. How can we better quantify volcano-seismic events with limited data?
2. And can this be streamlined into a unified signal processing routine, for adaptation around the world?

Specifically research question 1 emphasises the need for methods suitable for limited-data. The point process modelling is a more advanced statistical technique that can be applied to any earthquake catalogue. It has been demonstrated in both this chapter and in a previous publication, to work on a catalogue of events with single station and single component data. In turn, I have also been able to develop some of the models from chapter 4 which describe the

shallow conduit dynamics at Tungurahua. This is particularly important for understanding the state of the conduit at the end of this most recent eruptive phase and as such, specifically addresses research question 3.

3. What can we learn about the shallow dynamics at Tungurahua and Cayambe volcanoes, from analysis of the seismicity?

This is also an important observation of drumbeat LP seismicity and contributes further to answering research question 5:

5. What is the significance of periodic, drumbeat LPs?

On initial inspection of the waveform, it appears a striking and isolated episode of unrest, however, it draws parallels with previous studies about pre- and post-explosion drumbeats. By further documenting the characteristics of the seismicity in this drumbeat LP episode, I have contributed further to our understanding of drumbeat seismicity and the associated source processes.

6 | Evolution of seismicity during a stalled episode of reawakening at Cayambe Volcano, Ecuador

Preface

One of the problems highlighted in the literature review in chapter 2, is that volcanic seismicity studies generate models that are very specific and particular to one system. And so in this chapter, in order to compare and evaluate some of my findings from Tungurahua, I examine the seismicity at neighbouring volcano, Cayambe. In particular, I focus on the VT swarm in 2016 - 2017 in which uncharacteristically high rates of earthquakes were recorded. This swarm presents an interesting opportunity to study seismicity that does not directly correspond to explosive activity. Cayambe also faces similar challenges as Tungurahua and has a limited capacity of seismic monitoring. Here I address research question 2 and apply the earthquake analysis methodology in chapter 3 to further understand the internal dynamics. In this chapter I begin to investigate research question 6 and consider dynamic and static triggering processes at Cayambe volcano, as the VT swarm also commenced just 8 weeks after the M_w7.8 Pedernales earthquake in 2016. This theme is explored further still in chapter 7. Finally, in order to answer research question 5, I demonstrate how careful analysis

of the seismicity can distinguish magmatic and hydrothermal LP earthquakes. I also make recommendations for incorporating these techniques into monitoring and hazard assessment in the future at Cayambe.

This chapter was published in *Frontiers in Earth Science* in 2021 (https://doi.org/10.3389/feart.2021.680865) and is included here without further editing.

Abstract

Cayambe Volcano is an ice-capped, 5790 m high, andesitic-dacitic volcanic complex, located on the equator in the Eastern Cordillera of the Ecuadorian Andes. An eruption at Cayambe would pose considerable hazards to surrounding communities and a nationally significant agricultural industry. Although the only historically documented eruption was in 1785, it remains persistently restless and long-period (LP) seismicity has been consistently observed at the volcano for over 10 years. However, the sparse monitoring network, and complex interactions between the magmatic, hydrothermal, glacial, and tectonic systems, make unrest at Cayambe challenging to interpret. In June 2016 a seismic 'crisis' began at Cayambe, as rates of high frequency volcano-tectonic (VT) earthquakes increased to hundreds of events per day, leading to speculation about the possibility of a forthcoming eruption. The crisis began two months after the M_w7.8 Pedernales earthquake, which occurred on the coast, 200 km from Cayambe. Here we show that the 2016 seismicity at Cayambe resulted from four distinct source processes. Cross correlation, template matching, and spectral analysis isolate two source regions for VT earthquakes - tectonic events from a regional fault system and more varied VTs from beneath the volcanic cone. The temporal evolution of the LP seismicity, and mean Q value of 9.9, indicate that these events are most likely generated by flow of hydrothermal fluids. These observations are consistent with a model where a new pulse of magma ascent initially stresses regional tectonic faults, and subsequently drives elevated VT seismicity in the edifice. We draw comparisons from models of volcano-tectonic

interactions, and speculate that static stress changes from the Pedernales earthquake put Cayambe volcano in an area of dilation, providing a mechanism for magma ascent. Our findings provide a better understanding of 'background' seismicity at Cayambe allowing faster characterisation of future crises, and a benchmark to measure changes driven by rapid glacial retreat.

6.1 Introduction

6.1.1 Motivation

Seismic records at active volcanoes can be a rich and informative dataset for monitoring and understanding internal processes. The characteristics of a seismic signal can be indicative of the source process that generated it (Chouet & Matoza, 2013; McNutt & Roman, 2015; Zobin, 2012). If recorded across multiple stations then the locations of the earthquakes can be used to infer the source mechanism (Lehr et al., 2019; Woods et al., 2018). The rates at which earthquakes occur can also indicate whether a source mechanism is constant and stable or evolving. Accelerating sequences of earthquakes have been linked to material failure and can be significant in forecasting eruption (Bell et al., 2018; Boué et al., 2015; Voight, 1988). Whilst very long term, constant and sometimes periodic earthquake rates may suggest a stable or resonating process (Park et al., 2019). The emergence of new swarm seismicity including spasmodic bursts may suggest a change in the stress regime, and may be associated with fluid migration, or rock fracturing (Hill et al., 2002a; Hotovec-Ellis et al., 2018). Understanding and characterising different types of volcano-seismic events allows us to attribute them to specific processes, and can be particularly important in hazard assessment and forecasting. This is particularly the case at volcanoes which have been dormant. When there is not an extensive historical record of seismicity at a volcano, recognising patterns may help to identify signs of 'reawakening' (White & McCausland, 2019).

Interpreting patterns of seismicity in terms of volcanic processes and evolving unrest can be challenging. Earthquakes in volcanic regions can originate from a number of different sources, and may be independent from processes that may drive new eruptive activity. Active fault systems, hydrothermal systems and permanent glacial cover can add another element of complexity to geophysical monitoring at volcanoes (Cusano et al., 2008; Jónsdóttir et al., 2007). Particularly within the tropics, small, high altitude glaciers can respond to small changes in climate on short timescales, and may be susceptible to significant impacts from El Niño and La Niña years (Basantes-Serrano et al., 2016; Ceballos et al., 2006). Whilst it is known that equatorial glacier retreat has been ongoing for 150 years, this has accelerated in the last 30 years and should be closely monitored at active volcanoes (Manciati et al., 2014). Glaciers on a volcano can act as a constant supply of fluid to alter and weaken the edifice (Carrasco-Núñez et al., 1993) and so increasing retreat may lead to an acceleration of these processes. In the event of a volcanic eruption, glacier melt waters can contribute to disastrous debris flows, such as those seen at Nevado del Ruiz in 1985 (Huggel et al., 2007) and Nevado del Huila in 2007 (Worni et al., 2012). Several large non-cohesive lahars involving glacial melt, have been mapped in the valleys surrounding Mt Rainier, where runouts extend over 100 km (Hoblitt et al., 1998).

6.1.2 Cayambe Volcano

Cayambe Volcano is in the north of the Eastern Cordillera of the Ecuadorian Andes, just 60 km north of the capital Quito. The complex is a notably large volcanic centre, with a peak elevation of 5790 m. Above 4800 m the volcano is covered in a 22 km^2 ice cap, which in places is as thick as 100m (Detienne et al., 2017; Guillier & Chatelain, 2006). Tephrochronology studies have revealed previous explosive activity in the last 4000 years, including pyroclastic flows, lava dome extrusions and collapse events (Samaniego et al., 1998). Hydrothermal alteration of flank deposits and thawing soils from glacial retreat act

to destabilise the western slopes of Cayambe. Small perturbations in the system, for example, from a magmatic intrusion or seismic event, could lead to catastrophic failure and significant landslides (Detienne et al., 2017; Hoblitt et al., 1998). This would pose a threat to the town of Cayambe, population 20,000, that sits just 15 km west of the volcano (Samaniego et al., 1998). Mass debris flows and lahars descending the eastern flanks of Cayambe could also easily damage the Trans-Ecuadorian oil pipeline and major highways to the oilfields in northeastern Ecuador (Schuster et al., 1996). Whilst there has only been one historically documented eruption at Cayambe (1785-1786), it has been persistently restless in the last 20 years and mountaineers regularly report sulphur smells from the upper flanks. The 1785 eruption is thought to have been a Vulcanian type eruption ∼VEI 1-2 (Bernard & Samaniego, 2017; Global Volcanism Program, 2013b), similar to the Cotopaxi eruption of 2015 (Bernard et al., 2016) and those seen at Tungurahua in 2014 (Hall et al., 2015).

Activity at Cayambe is monitored by the Instituto Geofísico de la Escuela Politécnica Nacional (IGEPN), the national geophysical monitoring agency of Ecuador. In 2016, IGEPN detected a seismic crisis at Cayambe. Swarms of high-frequency volcano-tectonic (VT) events in June and September were recorded by three seismometers on the flanks of Cayambe volcano. These swarms involved daily earthquake rates significantly above previously recorded baseline seismicity. These swarms included two events of magnitude 3.3 and 3.7 during November, the largest two VT events of the year at Cayambe (Global Volcanism Program, 2013b; IGEPN, 2016b), and raised speculation about the possibility of an imminent eruption. In this study we characterise the seismicity during 2016 at Cayambe and try and to quantify the differences between the events of the seismic crisis and typical baseline seismicity in the preceding years. Subtle changes in the character of the waveforms can be indicative of a changing source or path process. Previously, detailed retrospective studies of temporal and spatial patterns in seismicity, have revealed key characteristics in eruption styles at comparable andesitic volcanoes, including Volcán de Colima (Zobin et al., 2015), Redoubt Volcano (Buurman et al., 2013) and Soufrière Hills Volcano (Neuberg et al., 2006).

Also of note, on 16th April 2016, two months before the onset of seismic unrest at Cayambe, the M_w7.8 Pedernales thrust earthquake struck the coast of Ecuador, 200 km from Cayambe (Heidarzadeh et al., 2017; Nocquet et al., 2017; Yoshimoto et al., 2017). This event caused MMI intensity III to IV ground shaking around Cayambe, and was followed by seven M_w >6.0 events in the following three months (USGS, 2021). Tectonic earthquakes can generate both permanent static changes and temporary dynamic changes in the stress field (Manga & Brodsky, 2006). Static changes are a direct result of slip on the earthquake fault and crustal deformation and are more prevalent closer to the earthquake epicentre. Whilst dynamic stress field changes are related to passing teleseismic surface waves and can effect distances much further from the earthquake (Prejean et al., 2004). Stress changes from tectonic events are known to be able to trigger both eruptive activity and seismic activity at volcanoes (Hill & Prejean, 2015). However, distinguishing between causation and correlation is complex, particularly if there are limited records of historical earthquakes or eruptions (Prejean & Hill, 2018). Here we investigate the relationship between the Pedernales earthquake in April 2016 and unrest at Cayambe that commenced in June 2016.

The permanent ice cap on Cayambe presents a further potential complexity for hazard assessments from seismic records. Studies further south in the Chilean Andes have shown icequakes to be much more common than previously thought (Lamb et al., 2020). These can be generated by basal slip on the glacier, slip at fractures within the glacier or the resonance of fluids within glacier cracks. Icequakes observed at Cotopaxi volcano, Ecuador and Katla volcano, Iceland, show waveforms that look very similar to long period (LP) earthquakes (Jónsdóttir et al., 2009; Métaxian, 2003). We refer to LP events as low frequency emergent signals, often associated with fluid movement, including magma emplacement and hydrothermal systems (Varley et al., 2010a; Woods et al., 2018). Therefore being able to clearly distinguish between the two phenomena is key to reducing uncertainty in hazard assessment. This is particularly the case when we cannot confidently constrain depths and locations to separate sources.

Here we introduce the seismic data records during the 2016 crisis. We then describe the template matching process used to expand the catalogue of picked events. We detail the different methods used to quantify sequences of significant events throughout the year. We then present an interpretation of the seismic swarms that occurred during 2016. Our results identify a stable source of long period seismicity, likely associated with a shallow hydrothermal system. We also demonstrate the two VT swarms to be separate populations, from both local tectonic and volcanic sources. We draw comparisons between the seismic observations and models of reawakening volcanoes, and speculate the significance of the Pedernales event prior to activity at Cayambe in 2016. Finally we discuss the wider implications of a seismic crisis like this for hazard assessment in the future.

6.2 Data & Methods

6.2.1 Monitoring Data

The volcanic complex at Cayambe is defined by 3 cones, and bound by a significant regional fault to the north east, the 'La Sofía-Río Chingual' fault. Old Cayambe is a basic-andesitic stratovolcano that is more than 250,000 years old. It has mostly been eroded and the more recent Nevado Cayambe, a composite cone, has been built in its place, and over the eastern flanks (Samaniego et al., 1998). There has been a permanent geophysical monitoring network on Cayambe volcano since 1988, maintained by IGEPN (Guillier & Chatelain, 2006). Initially a single station on the northern flank, the network is now three stations, with telemetry to IGEPN in Quito. The seismic network includes one three-component broadband seismometer (Trillium Compact 120), CAYA, and two short period seismometers (L4C), CAYR and ANGU, each sampling at 100 Hz (fig 6.1). There was also a short temporary deployment of seismometers between 1997 and 1998 (Guillier & Chatelain, 2006; Guillier et al., 1999). Station CAYA is positioned between the Nevado Cayambe cone and the La

Sofía-Río Chingual fault, whilst ANGU and CAYR are positioned close to the edge of the glacier line on the western flanks. For this study, we have access to 366 days of data from station CAYA in 2016, and data from January 2015 through to December 2017 at station CAYR to specifically examine the LP seismicity. Waveform data from station ANGU are unavailable during July-September 2016 and the station was upgraded from a short-period to a broadband instrument in December 2016. As such we are only able to use data from January-November in 2016.

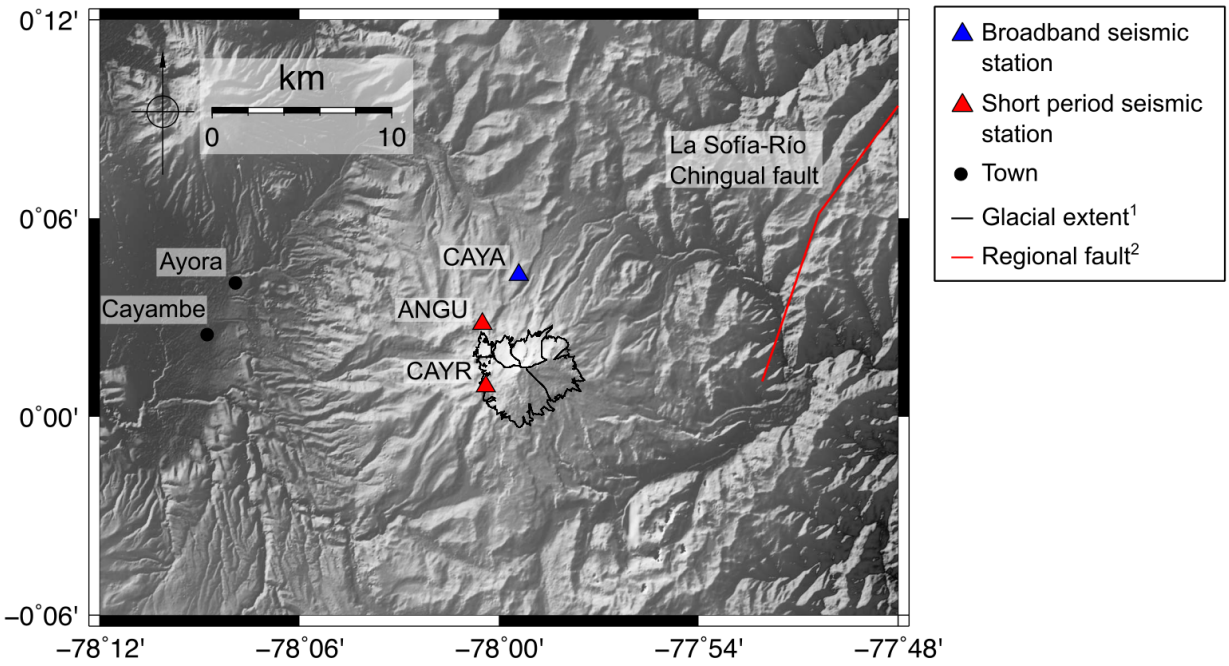

Figure 6.1 Permanent geophysical monitoring network installed on Cayambe Volcanic Complex. [1]Glacier extent from GLIMS Database (Cogley et al., 2015), [2]Regional fault data from Active Tectonics of the Andes (ATA) (Veloza et al., 2012)

6.2.2 Signal processing

Seismic data are analysed and processed using the ObsPy toolkit (Krischer et al., 2015). Our initial analysis uses a catalogue of manually picked and categorized events, provided by IGEPN. Events in the catalogue are labelled broadly as either LP, VT, hybrid (HYB) or tec-

tonic (TECT) events. We remove tectonic events by cross referencing the IGEPN Cayambe catalogues with IGEPN catalogue data for nearby Reventador volcano and a national tectonic events catalogue to ensure there are no falsely identified events. We filter the data between 1 and 40 Hz. After the catalogue is updated, we create a 30 second event waveform for analysis, slicing 5 seconds before the picked P- phase arrival and 25 seconds afterwards. Station CAYR lies much closer to the summit of Nevado Cayambe (∼2.5 km) and exhibits a much higher signal to noise ratio (SNR). As a result, over 80% of picked events in the catalogue are identified at CAYR (fig 6.2). The IGEPN catalogue also includes some located VT events. These are used to map and interpret some of the significant swarms in 2016.

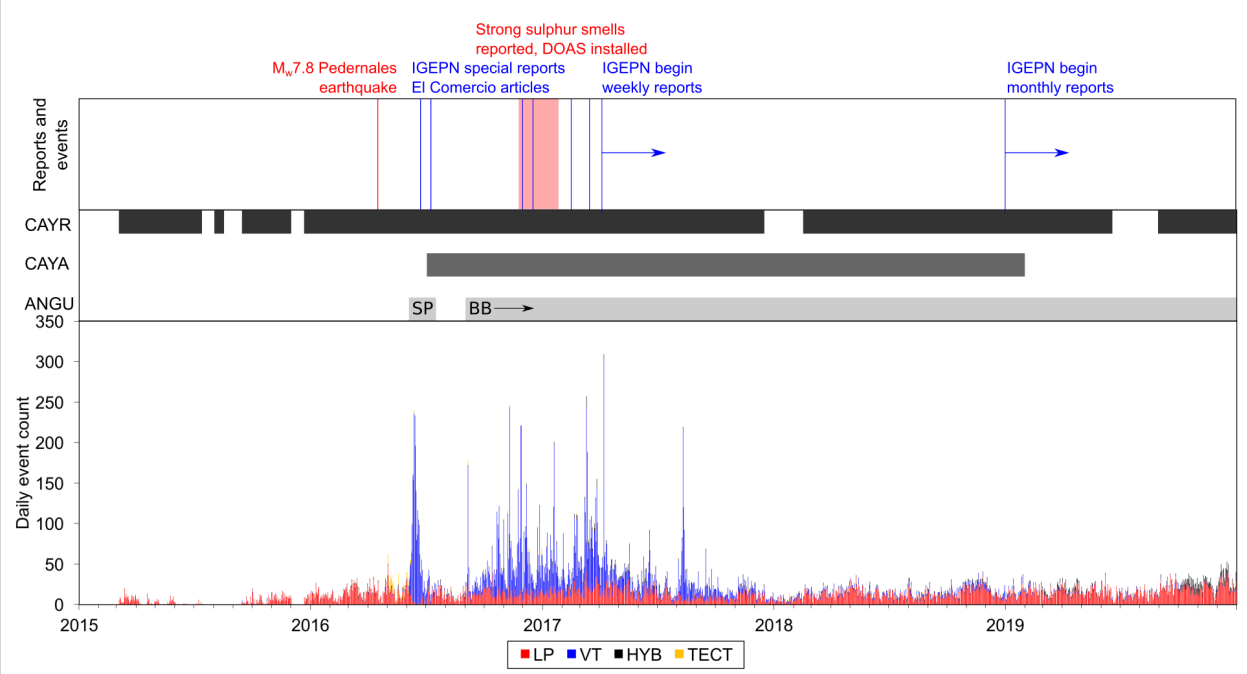

Figure 6.2 Summary of seismicity at Cayambe, 2015-2019. Top panel identifies key milestones in the monitoring, including reports from IGEPN and El Comercio (national Ecuadorian newspaper). The middle panel indicates when the three stations were active. SP = short period, BB = broadband. Bottom panel shows daily seismic event counts.

First, using catalogue picks at station CAYR, we run a cross correlation analysis. Each event is cross correlated with every other event, generating a cross correlation coefficient (XCC) between 0 and 1 as well as and the shift, in seconds, required to align the two picks at the maximum coefficient. The coefficient can be considered a measure of similarity (Petersen, 2007; Thelen et al., 2011; Waite et al., 2008). We set a minimum coefficient threshold of 0.7 to group events into families (Bell et al., 2017; Butcher et al., 2020; Park et al., 2019). The event with the most coefficients greater than the threshold is selected as the master event of the first family and every event with a coefficient greater than the threshold is included in the family. This is repeated until the families are too small to be considered significant. We set a minimum requirement of 20 events to be considered a family. The master event from each family is then used in a template matching method to extend the catalogue (Gibbons et al., 2007; Park et al., 2019). The master event is cross correlated with the signal for each whole day, and when a cross correlation threshold is exceeded, an event is picked. We then consider patterns within and across the families identified from the cross correlation analysis. The master event of each family is cross correlated with every other master to determine which families might be closely related. Every event in a family is shifted in time to align with the point of maximum cross correlation and stacked. These stacked events are then also cross correlated.

For each event, we determine the Q factor of the signal. The Q factor has been used in volcano-seismology studies to quantify and group event types (Lokmer et al., 2008; Molina et al., 2004). Q describes how quickly energy in a signal is attenuated, either as a result of a source or path process, and can be used as a metric to identify patterns of change in series of earthquakes (Rossing & Fletcher, 2004). Q and the interpreted attenuation is often empirically related to resonance in a fluid filled crack model (Kumagai & Chouet, 1999; Lipovsky & Dunham, 2015). This value can be calculated by a number of different methods and reported values for Q vary between $10^0 - 10^3$ (Lipovsky & Dunham, 2015; Molina et al., 2004). This range is validated by a series of synthetic tests for fluid-filled cracks where the

fluid compositions are varied (Kumagai & Chouet, 2000). In any one study, however, only one method is used to calculate the Q value for an event. These broad ranges in Q values can in turn lead to very different interpretations of the seismic event sequences. We apply three different approaches to calculate Q for each event and compare the output. We will use these Q values as a tool to distinguish earthquake events associated with different processes.

The decay method is used in a comparative study across Mt Etna, Colima and Campi Flegrei volcanoes (Del Pezzo et al., 2013; Elmore & Heald, 1985). The method relies on decay time, τ, defined as the time taken for the squared amplitude of the waveform to decay to less than $\frac{1}{e}$ of the squared maximum amplitude (eq 6.1). This calculates the Q_{decay} value for the oscillations of a single frequency, and so assumes the waveform spectra is dominated by a single peak frequency, f_0 (Rossing & Fletcher, 2004). As such, this method works consistently for LP type events, and specifically single frequency tornillos or on infrasound data, but is less robust with broadband signals.

We also apply the bandwidth method, which is closely related to the decay method. It relies on identifying the bandwidth of the spectral peak frequency, δf. The bandwidth is the difference between the high and low corner frequencies of the power spectral density (PSD). Q_{band} for this spectral peak is then defined as the ratio between the spectral peak and it's bandwidth (Elmore & Heald, 1985) (eq 6.2). This method is presented using smoothed spectra for the analysis of tornillo infrasound events at Cotopaxi Volcano in 2015 and 2016 (Johnson et al., 2018). In this study the bandwidth, δf is calculated for the single largest spectral peak. We do not apply smoothing to avoid imprinting any interpretation on the spectra.

Finally, we apply an auto-regressive moving average (ARMA) methodology to determine Q_{ARMA}, as described in Lesage, 2009. The ARMA approach assumes a signal is a superposition of many individual harmonic decaying oscillations, each defined by their own frequency, (f, Hz) and decay rate (g, s^{-1}). We consider all AR filters from 2 to 50 and plot cumulative *f*-*g* diagrams (Lesage, 2008). The method is automated to identify points in the

complex frequency space that cluster at a pole around the spectral peak (Butcher et al., 2020). This method is closely related to the Sompi method which uses eigen-decomposition to identify poles and calculate Q_{ARMA} (Hori et al., 1989; Kumazawa et al., 1990) (eq 6.3).

$$Q_{decay} = 2\pi f_0 \tau \tag{6.1}$$

$$Q_{band} = \frac{f_0}{\delta f} \tag{6.2}$$

$$Q_{ARMA} = \frac{-f}{2g} \tag{6.3}$$

For each event, we also identify the peak spectral frequency from the periodogram of the signal, and the maximum absolute amplitude of every event. On single station records, with limited data we have to consider maximum amplitude as a proxy for magnitude and gather information about amplitude ratios between stations.

In order to identify clustered swarms of events, and locate any episodes of periodic activity we calculate the inter-event times (IETs) and periodicity (Bell et al., 2017). This is done for the whole catalogue initially and then within families and by event type. The periodicity is the ratio between the mean and standard deviation of the inter-event times. This is a useful tool to identify swarms and periodic episodes as it assumes events are randomly distributed and so have a ratio and periodicity equal to 1. Clusters and swarms will have a periodicity much lower than 1 and periodic episodes of drumbeat-like, repeating seismicity will have periodicities much greater than 1.

6.3 Results

6.3.1 Located events

Due to the sparse monitoring network on Cayambe, only 179 of the 11,990 VT events in the IGEPN catalogue are located, and even then with significant uncertainties. Despite this, the

locations identify at least two distinct VT clusters throughout the year (fig 6.3). Manual inspection of the records show the events group broadly in 4 very distinct time intervals, with little overlap: June, July, September and November-December. We use these locations to aid our interpretations from the individual event analysis. The June events are widely spread over the north and eastern flanks, whilst the November events are much more concentrated near upper reaches of the Nevado Cayambe cone. The network geometry is such that the shallowest events are best captured by short period station CAYR on the highest flanks of the Nevado Cayambe, and is the most reliable station in the network.

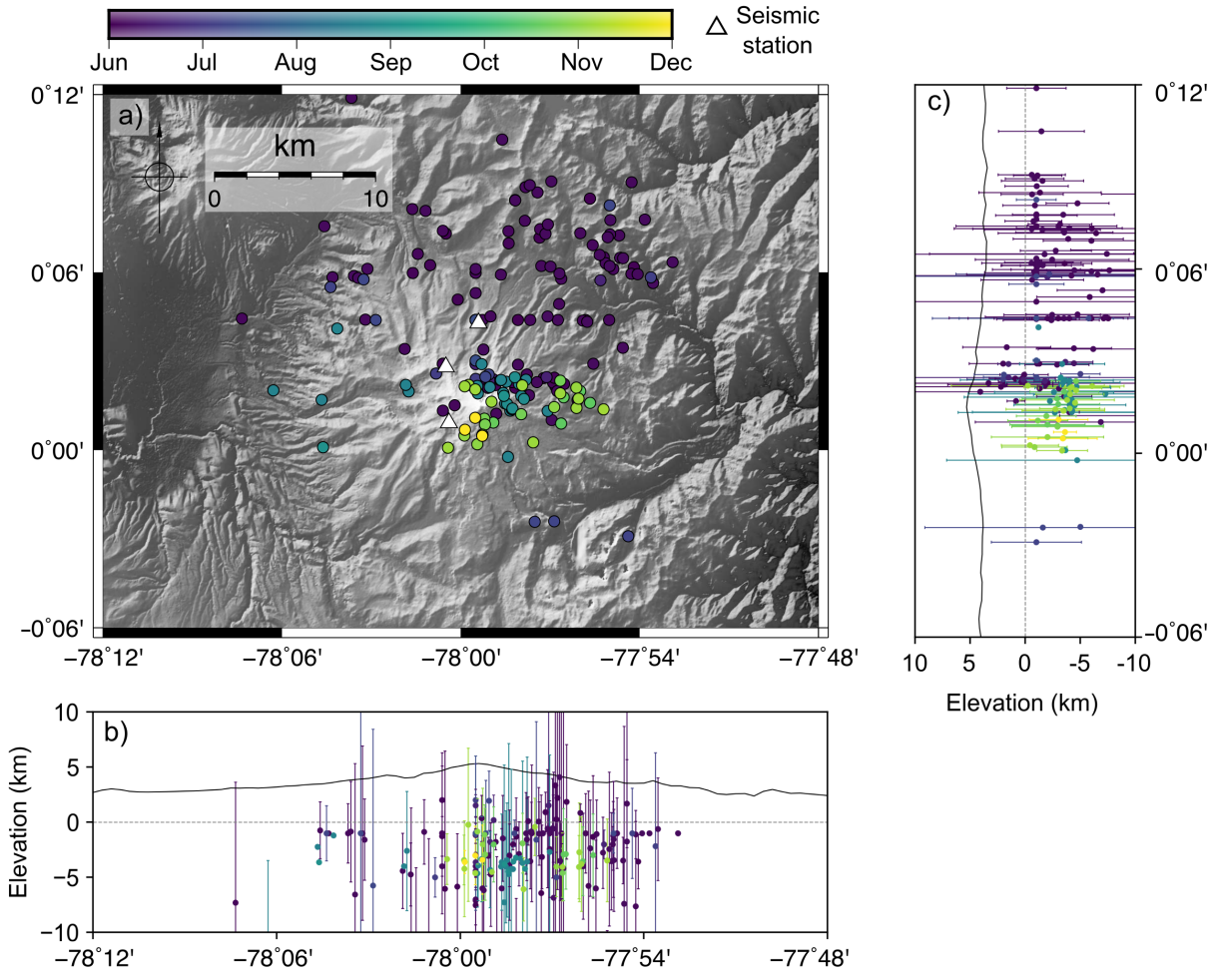

Figure 6.3 Located VT events in the IGEPN catalogue during 2016 showing *a)* locations and b) depth uncertainties.

6.3.2 Catalogue overview

From the total 11,990 events in the catalogue in 2016, 9848 events are recorded at station CAYR, of which 46% are labelled as LPs, 48% as VTs, and the remaining 6% as hybrids (HYB) and tectonic events (TECT). This is in stark contrast to 2015 where 98% of events recorded were labelled as LP, although there are significant data gaps. The cross correlation analysis generated 31 unique families of greater than 20 events (fig 6.4). Despite the catalogue containing almost an equal split of LP and VT events, only 84 LP events were grouped in two families representing more long term, background LP seismicity spanning the whole year. The remaining 29 families represent 1545 VTs - 7 of which highlight a short VT swarm in June and 21 families span more long term VT seismicity from September to December. The event labels are assigned from the IGEPN catalogues. Due to the number of events to analyse in this episode, I do not manually review the associated event labels. As such there is some uncertainty associated with the classification of these events.

We use the master events from the 31 families to conduct template matching and identify any events not originally picked in the IGEPN catalogue. An additional 3853 events are identified by this template matching method, extending the catalogue to 13,683 events in 2016. In particular the template matching identifies 364 new LP events - more than 4 times as many LPs than were in the original 2 LP families. The template matching identifies a further 1378 VT events in the June swarm and 2111 VT type events from September to December 2016. The template matching expanded the reach of some VT swarm families but no single family contains events in both June and November, showing a strong distinction between the source processes in each case. We also use the located VT events in the catalogue to verify the master events of the families. The located events in June and July correspond well with families 0, 6, 9, 10 and 23 (fig 6.6a). Whilst the master event of family 20 shows an XCC > 0.85 with a located VT event and occurs within just 20 minutes (fig 6.6c). This suggests family 20 represents an isolated repeating source mechanism between the two large

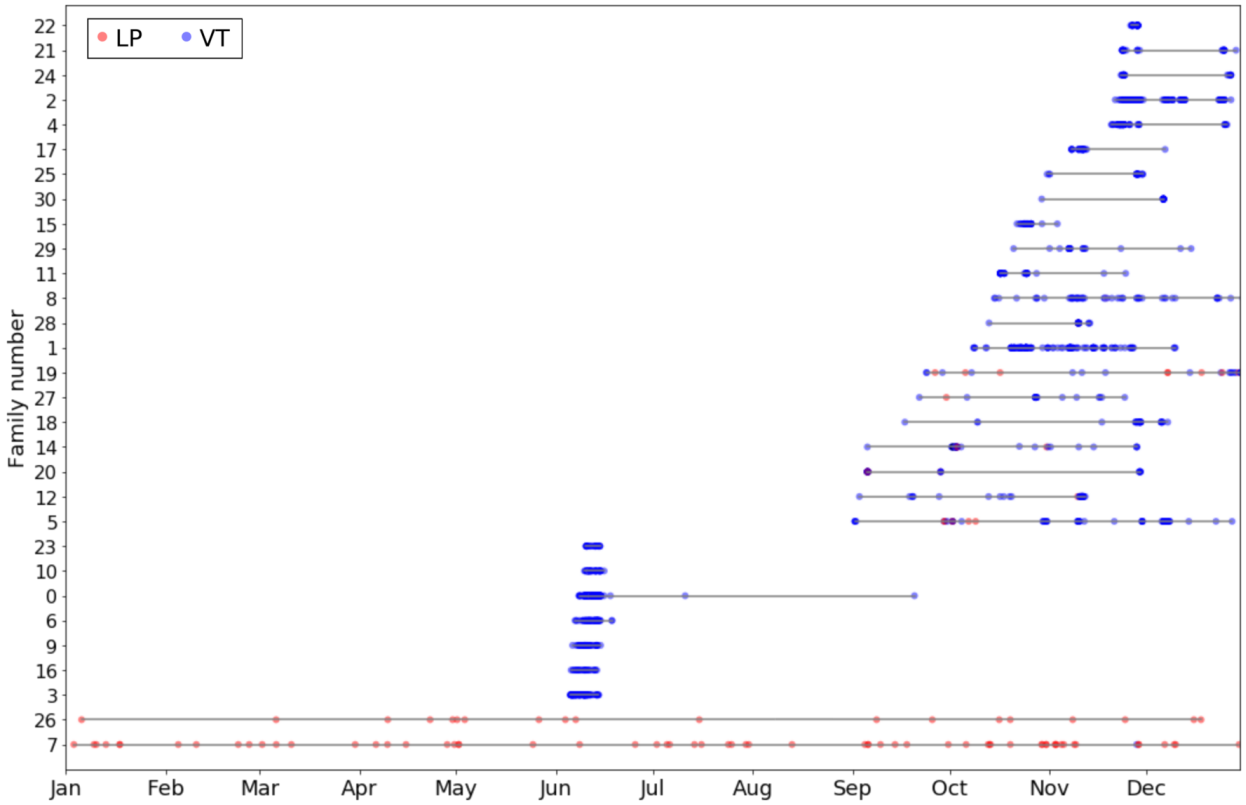

Figure 6.4 Families extracted from cross correlation analysis of the initial 9484 catalogue picks at CAYR. Individual events coloured by their label, red shows LPs, blue shows VTs. Families numbered in order of size largest to smallest. Classification labels are from IGEPN catalogues.

swarms in June and November.

Figure 6.5 shows seismic event characteristics through 2016. All event types have a near exponential distribution of inter-event times (t), as the periodicities remain close to 1 (Bell et al., 2017). The periodicity is calculated in fixed windows of 15 events, and so during swarm activity in June and December there are isolated incidents where seismicity is either clustered (periodicity <1) or cyclical (periodicity >1), but at generally low levels.

In general the LP events show a consistent peak frequency at 2.1 Hz. As expected this is lower than the VT events, but particularly in October-December when the VT events have a consistent peak frequency at 5 Hz. The June swarm VT events have uncharacteristically low spectral peak frequencies, less than 2 Hz and less than the background LPs. Thorough

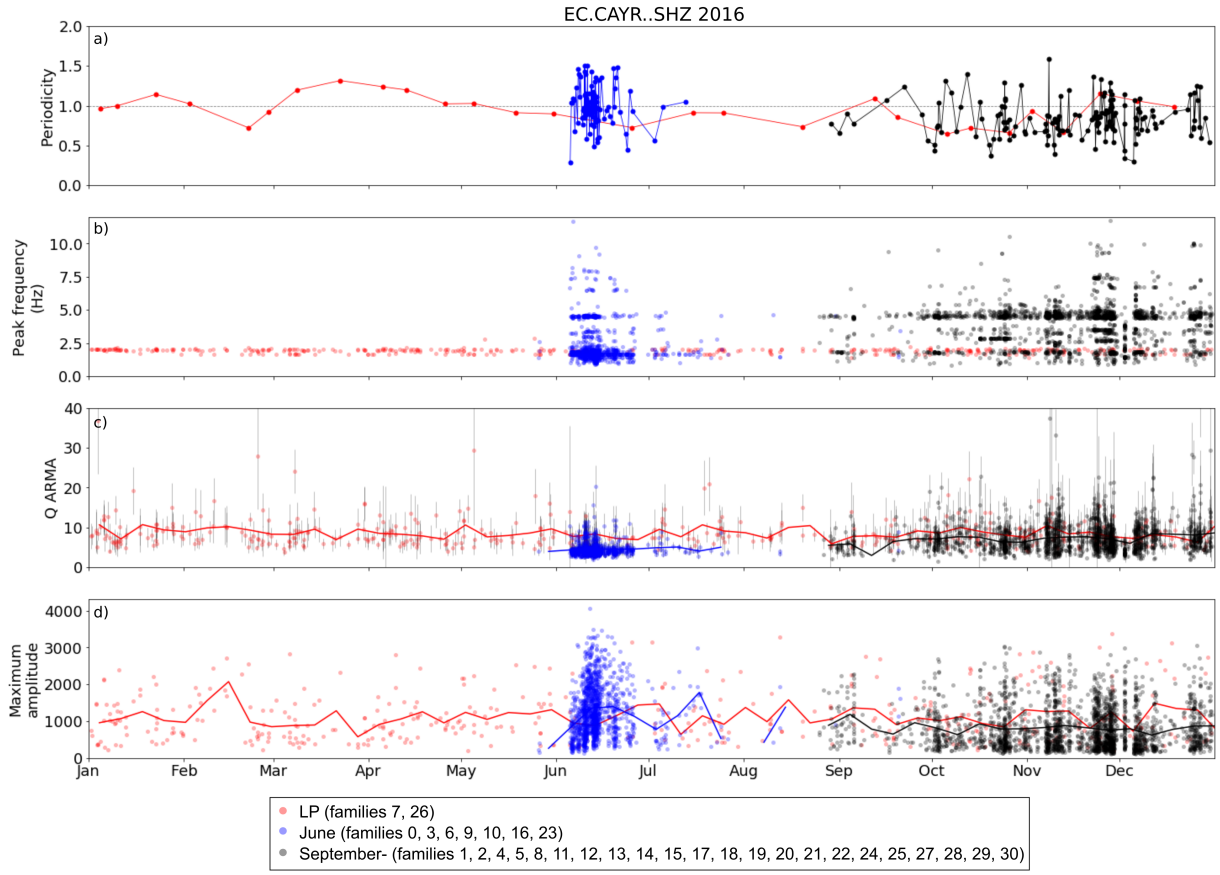

Figure 6.5 Individual event analysis from all catalogue and template matched events on station CAYR that were successfully grouped into families. Red shows year long LP events from families 7 and 26. Blue shows VT swarm events in June from families 0, 3, 6, 9, 10, 16 and 23. Black shows all other VT swarm families from September onwards. Moving averages are calculated for windows of 7 days. *a)* Periodicity calculated in fixed bins of 15 events, *b)* Peak spectral frequency (Hz), *c)* Q_{ARMA}, *d)* Absolute maximum amplitude.

inspection of the June events show that they have typical spectral contents expected for VTs, between 1.0 and 15.0 Hz. This highlights how using a single peak frequency value as a defining characteristic can be misleading.

The Q values by all three methods return values across multiple orders of magnitude. A comparison for all three methods on the same family is shown in figure 6.4. This output from the three separate methods can lead to spurious interpretations and conclusions, and so for consistency we refer only to Q_{ARMA}. The Q_{ARMA} values are calculated by an automated

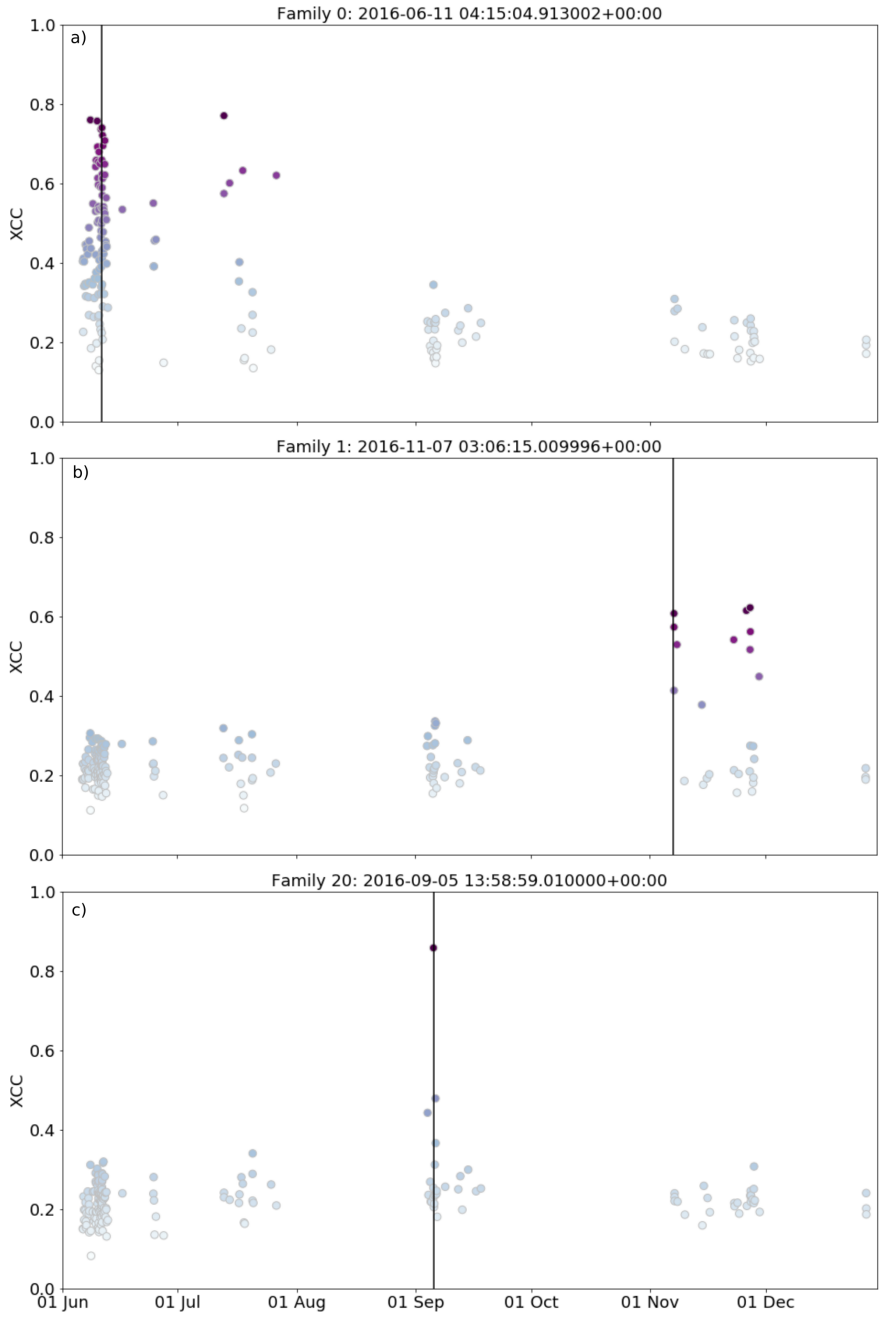

Figure 6.6 Cross correlation coefficients for located events with master events. Masters are as labelled in main text: *a)* Family 0, *b)* Family 1, *c)* Family 20. Vertical line in all panels marks the time of the located event.

clustering algorithm and so the standard error from the clustered poles is used to plot the error bars in figures 6.5c, 6.7f and 6.7l.

6.3.3 Persistent LP seismicity

The catalogue shows a consistent level of baseline LP seismicity in 2015–2017 (fig 6.2). In 2016, LPs make up 46% of identified events at CAYR. However, from the cross correlation and family analysis, only 2 LP families emerge (families 7 and 26, fig 6.4). The template matching expands the catalogue of LP picks (fig 6.7g-l), an additional 209 events are added to the 64 catalogue events, taking family 7 to 273 events. The XCC values show how each of the LPs are remarkably similar to one another, likely hinged on the dominant monochromatic peak frequency at 2.1 Hz. The family persists across the whole year without any significant interruption, for example during swarm VT activity. The dominant feature of the signal is the single frequency onset at 2.1 Hz. Both the peak frequency and spectrogram (fig 6.8b and 6.8c) illustrate the uniform spectral signature. The master and stacked events of families 7 and 26 are also very similar and likely suggest the same source. It is important to note at this stage, I do not merge the families 7 and 26, so as to not lose any detail identified by the template matching or cross correlation process.

Unlike some of the higher frequency events, these LP events are poorly recorded on stations ANGU and CAYA. In particular the high frequency response from ANGU impedes how well the LP waveforms and spectra are recorded (fig 6.9c). Given the sensitivity of the cross correlation method, we expand the template matching search for LPs into 2015 and 2017 but only with station CAYR. Even beyond 2016, metrics such as the spectral peak frequency and Q_{ARMA} show very little variation. The temporal analysis shows these LP families have a periodicity average at 1.1, suggesting an exponential inter-event time (t). Short episodes of clustered or cyclical seismicity are generally artefacts as a result of the chosen window length. The event rate is low compared to VT swarm event counts, just 1-2

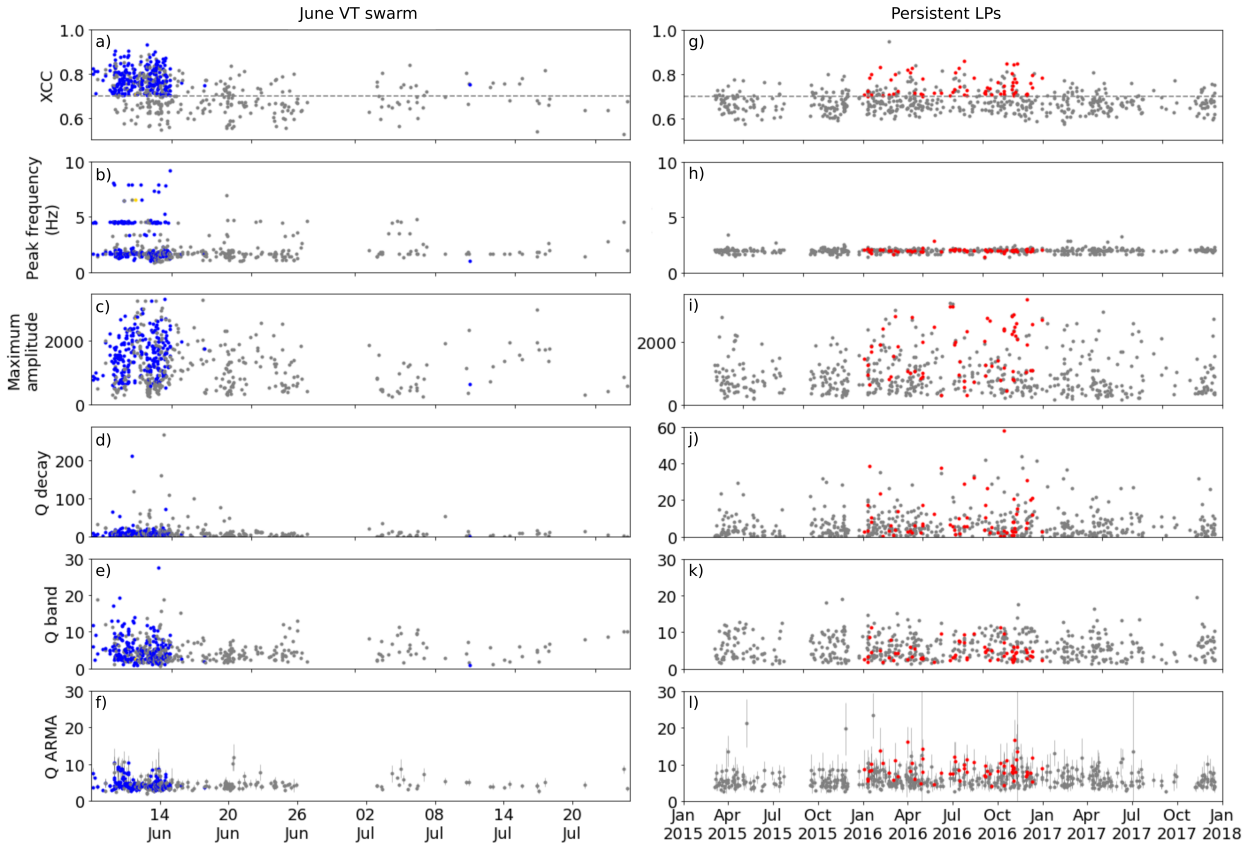

Figure 6.7 Panels *a)* to *f)* show individual event analysis for family 0 and panels Panels *g)* to *l)* show the results for family 7. Blue markers show VTs, red markers show LPs and grey indicate new unclassified events found by template matching (XCC $\geq$0.5). *a)* and *g)* cross correlation coefficient with master event, *b)* and *h)* peak spectral frequency, *c)* and *i)* maximum amplitude, *d)* and *j)* Q_{decay}, *e)* and *k)* Q_{band}, *f)* and *l)* Q_{ARMA} method.

events per day.

In addition to the repeating LP seismicity classified by cross correlation, some less consistent low-frequency events were identified in the data. These events are much longer (1-5 minutes in length) and have highly harmonic frequencies (fig 6.8d-g). Due to the varying lengths of these events, they are not classified into families successfully. They are identified throughout the year, although more are located in October and November. Single frequency events with long coda and distinct Hilbert transform envelopes are often referred to as tornillos (Fazio et al., 2019; Narváez et al., 1997). Some of the identified events

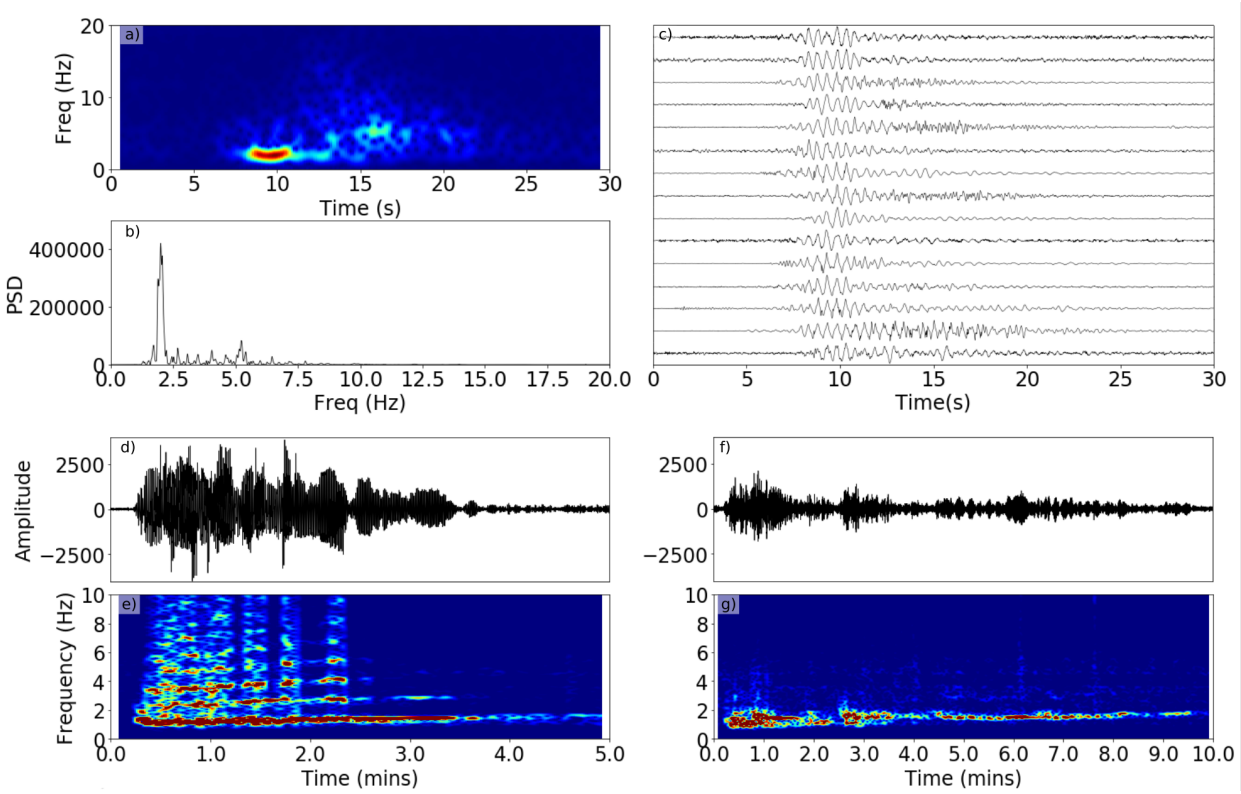

Figure 6.8 Long period seismicity identified at Cayambe. Panels *a)* to *c)* show LP seismicity from master event of family 7: *a)* spectrogram, *b)* power spectral density (PSD), *c)* sample of 15 characteristic events. Panels *d)* to *g)* show a sample of the harmonic events identified: *d)* spectrogram and *e)* PSD for an event with integer harmonics and *f)* spectrogram and *g)* PSD for a long harmonic sequence.

match this description; however, many show interesting characteristics such as strong integer harmonics (fig 6.8d and 6.8e). Sequences of these tornillo-type events can appear to merge and generate long episodes, which may be considered harmonic tremor (fig 6.8f and 6.8g). Particularly in fig 6.8e and 6.8g, when fundamental peak frequency increases through time, this may be an example of a short burst of gliding tremor (Almendros et al., 2014).

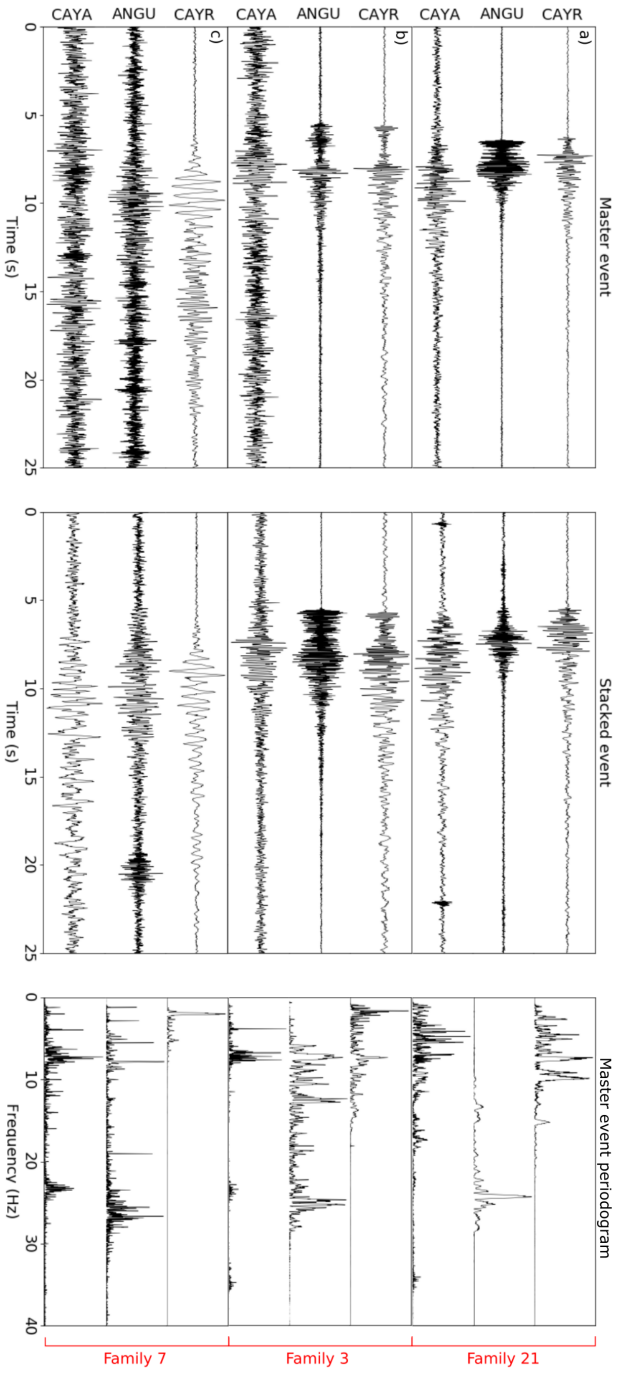

Figure 6.9 Event records across the network. Subplots *a) b)* and *c)*, families 21, 3, and 7 are shown at stations CAYR, ANGU and CAYA. The master event as located at CAYR is shown on the other 2 stations and stacked events are calculated from picks within the respective families.

6.3.4 June 2016 distal swarm

The cross correlation analysis picks out seven distinct families in June 2016. The largest family found contains 229 events, all occurring between 8th and 17th June (fig 6.7a-f). However, applying the template matching method identifies an additional 346 events and extends the duration of the family to 26th July. This family is characterised by short (<15s), high frequency, VT events. They have a distinct signal envelope, clearly showing P- and S-phase arrivals. Three spectral bands emerge around 1.6 Hz, 4.5 Hz and 7.9 Hz and are the peak frequency in 44% of events in the seven families which represent seismicity in June (fig 6.7b, 6.10). When the master and stacked events of each family in the June swarm are cross correlated with one another, they show high correlation values (fig 6.11a), suggesting a highly repeatable source and path. Due to the way families are extracted and because one event can only belong to one family, it is possible to have multiple families which represent similar events, and possibly from the same source. Q_{ARMA} shows very small errors compared to some other swarms and families (fig 6.7l, fig 6.11). The June swarm events are clear on both CAYR and ANGU, although ANGU shows a particularly high frequency response. These events are harder to see at CAYA but, when stacked, do show an improved signal to noise ratio (fig 6.9b).

6.3.5 September 2016- proximal swarms

From September onwards, the families extracted from the cross correlation method persist longer than those in June. Some VT swarm families even contain a small number of events identified as LPs by the IGEPN, although in any family these amount to no more than 8% of the total events. These LP events were manually checked and verified to ensure the labelling is as accurate as possible. These families represent VT events which are more LP-like in their signal properties, and so are not well suited to these rigid classification labels. They have a more emergent onset, and less distinct P- and S- phase arrivals but a high peak

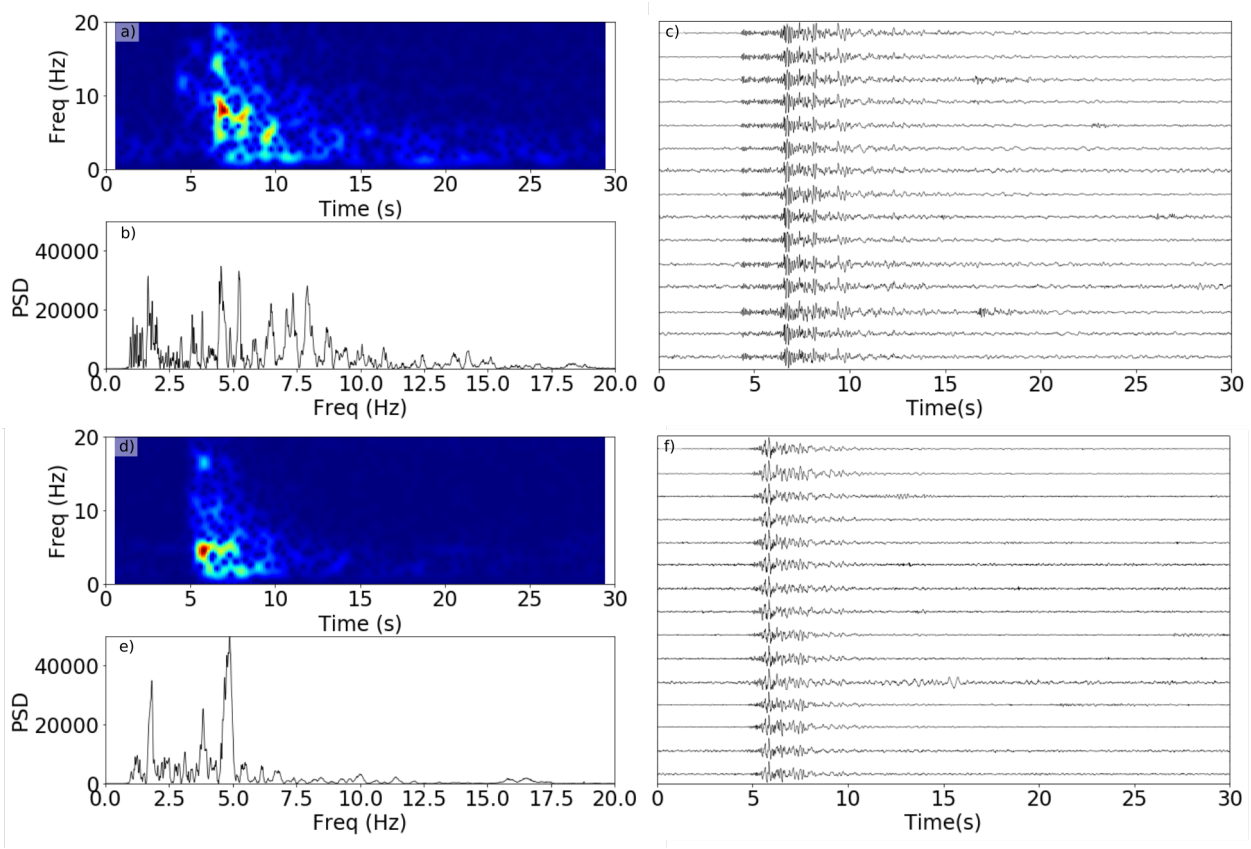

Figure 6.10 Catalogued VT seismicity at Cayambe. Panels *a)* to **c)** show VT seismicity from family 0, June 2016,: *a)* spectrogram, *b)* power spectral density (PSD), *c)* sample of 15 characteristic events. Panels *d)* to *f)* show VT seismicity from family 5, September 2016: *d)* spectrogram, *e)* power spectral density (PSD), *f)* sample of 15 characteristic events.

frequency and more broadband spectra (fig 6.10). Some families correspond to events which occur exclusively within a single day, whereas others represent more long term recurring events over several months (fig 6.4). Unlike the June families in which the families were all very cohesive and self similar with high cross correlation values, the November swarms show very little similarity to one another (fig 6.11b). The Q_{ARMA} values show the events from September onwards have a typically higher Q_{ARMA} value and peak frequency, than those in the June swarms (fig 6.7, fig 6.12).

Two significant located VTs occurred during November - a M3.3 event at 13:32 on 14th November, and a M3.6 event at 22:30 on 27th November. These are the two largest

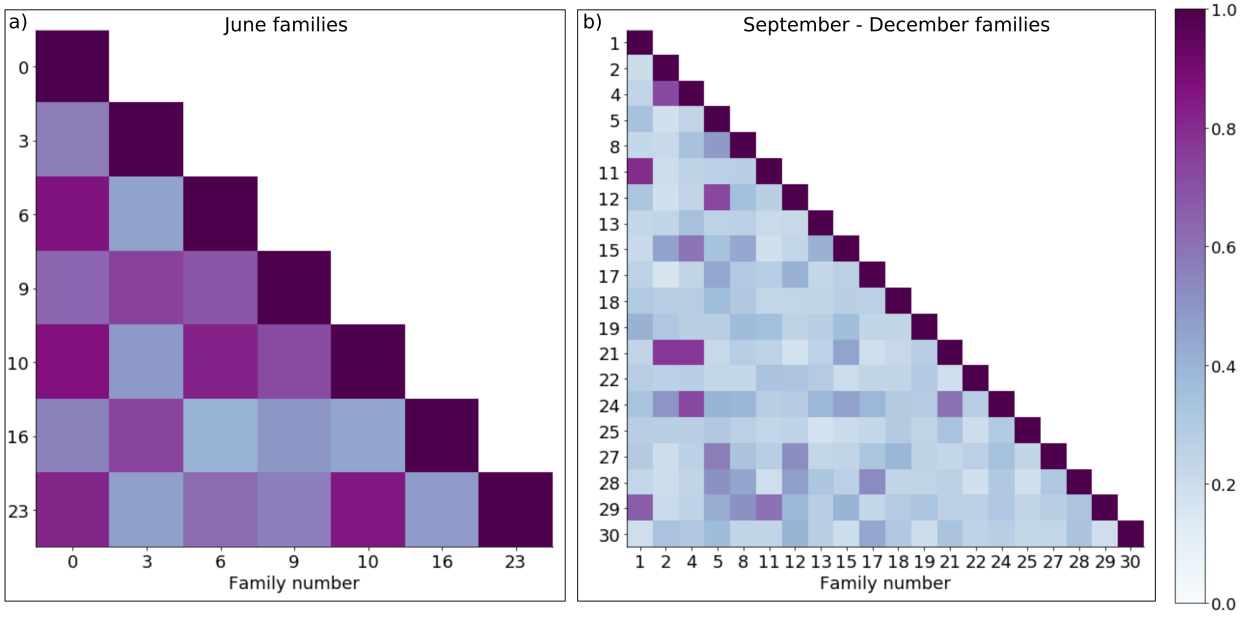

Figure 6.11 Cross correlation matrix of the stacked events for families during *a)* June and *b)* September - December 2016.

VT events at Cayambe during 2016. We manually pick events immediately before and after each of these M>3 events to be sure we have an accurate picture of all seismicity which may be associated. We carefully model the rates of events following the M3.6 and M3.3 events; however, there is not a clear mainshock-aftershock pattern that can be modelled by a power (Modified Omori) or exponential relationship (Bell et al., 2018; Utsu et al., 1995). Family 1 groups a number of events around 14th November. However, it is unlikely that Family 1 exclusively represents this slip event as Family 1 spans October to December, indicative of a longer term process. For the slightly larger event on 27th November, however, there was more of a significant visible response in the seismic record. From the cross correlation of events at CAYR, there are a handful of families, which cluster events specifically on the days around 27th November (families 2, 22, and 25), suggesting these are generated by a repeating, similar source. We manually pick events at CAYR between 22:00 27th November and 02:00 28th November. In the hour immediately after the M3.6 event, there are 118 short

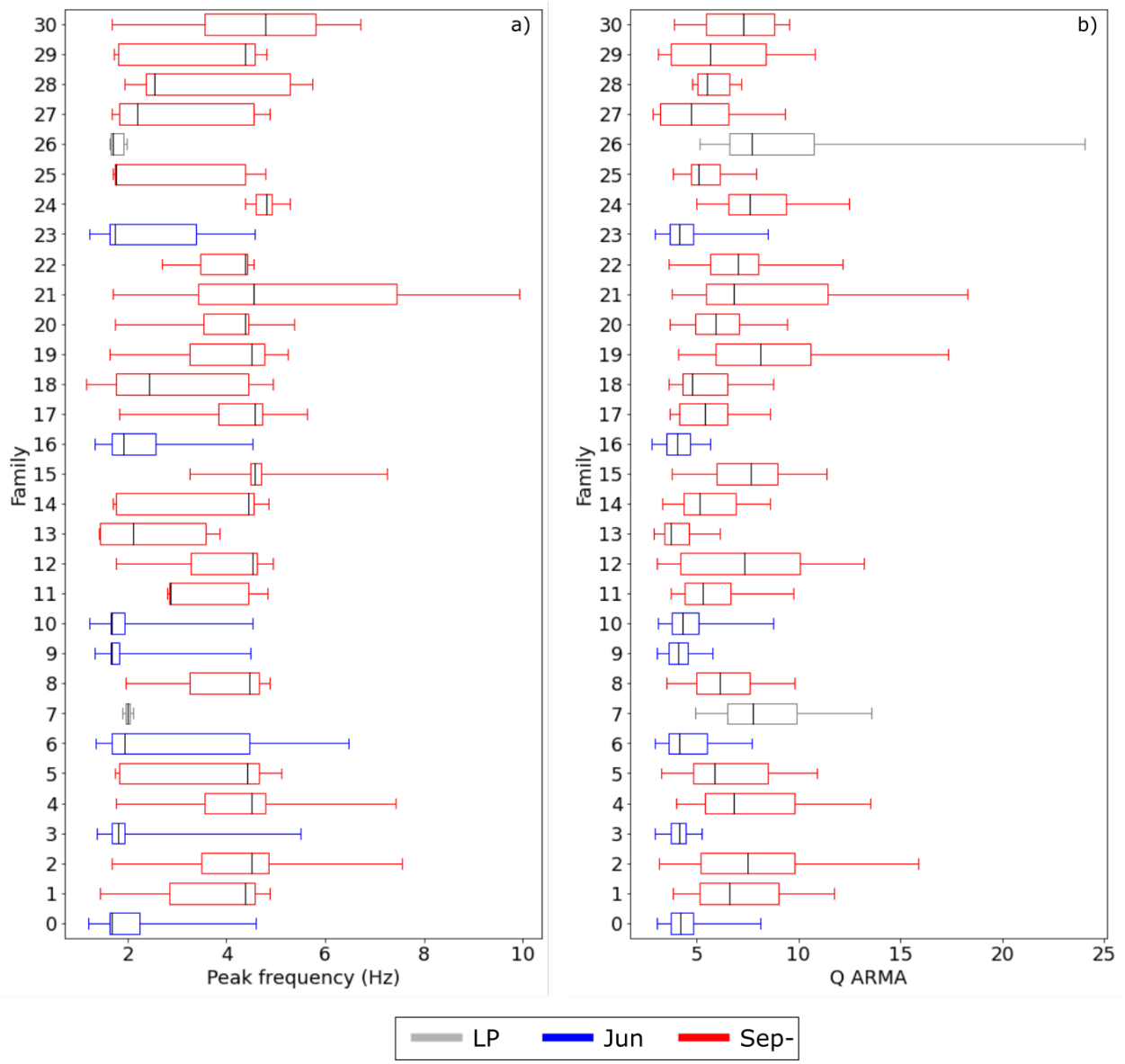

Figure 6.12 Distributions of *a)* peak frequency and *b)* Q_{ARMA} in each family. Solid black line shows the mean, box length shows the inter-quartile range and whiskers show 5th and 95th percentile values. Blue indicates families representing the June swarm, red shows families from September onwards and grey shows the two LP swarms.

high-frequency VT type events. Rather than aftershocks, these may be small repeating events from the same source as the M3.6 event. There are similar instances of isolated days, particularly in December, where recurring VTs from the same family show periodicity >1.5.

6.3.6 M_w7.8 Pedernales earthquake

The M_w7.8 Pedernales thrust earthquake occurred at 23:58:37 UTC approximately 200 km west of Cayambe, on 16th April 2016. The high amplitude surface wave arrivals can be clearly seen on all three stations after 00:00:00 on 17th April 2016. Within the surface wave arrivals at ANGU, a series of high frequency spikes can be seen in the spectra between 20 and 30 Hz (fig 6.13). We manually pick these high frequency spikes within the 5 minutes after 23:58:37UTC. However, station ANGU appears to have a defect and records recurring high frequency response between 20-30 Hz even during events known to be predominantly low frequency (fig 6.10c, 6.13). As these events cannot be identified at stations CAYA or CAYR, we rule out any possibility that they are dynamically triggered events.

As well as looking within the surface wave arrivals, we look for changes in average seismicity rate in the 24 hours following the Pedernales event, for larger scale changes. We manually picked events as the catalogue only contained 5 event pick times, but visual observations of the file showed there were likely more. We picked at station CAYR, as this had the best signal to noise ratio. Overall there is a decreasing rate of seismicity through the 24 hour period following the earthquake, from 30 events per hour, to less than 15 (fig 6.2).

6.4 Discussion

6.4.1 The meaning of Q

The Q values returned by all three methods span two orders of magnitude, which raises questions about the suitability of each approach. All methods were developed and tested for the purpose of low frequency seismicity, and specifically LP events generated by a resonating fluid filled crack (Kumagai & Chouet, 1999, 2000). These methods are hinged on the spectral peak frequency of a monochromatic or harmonic signal (Lipovsky & Dunham, 2015). As

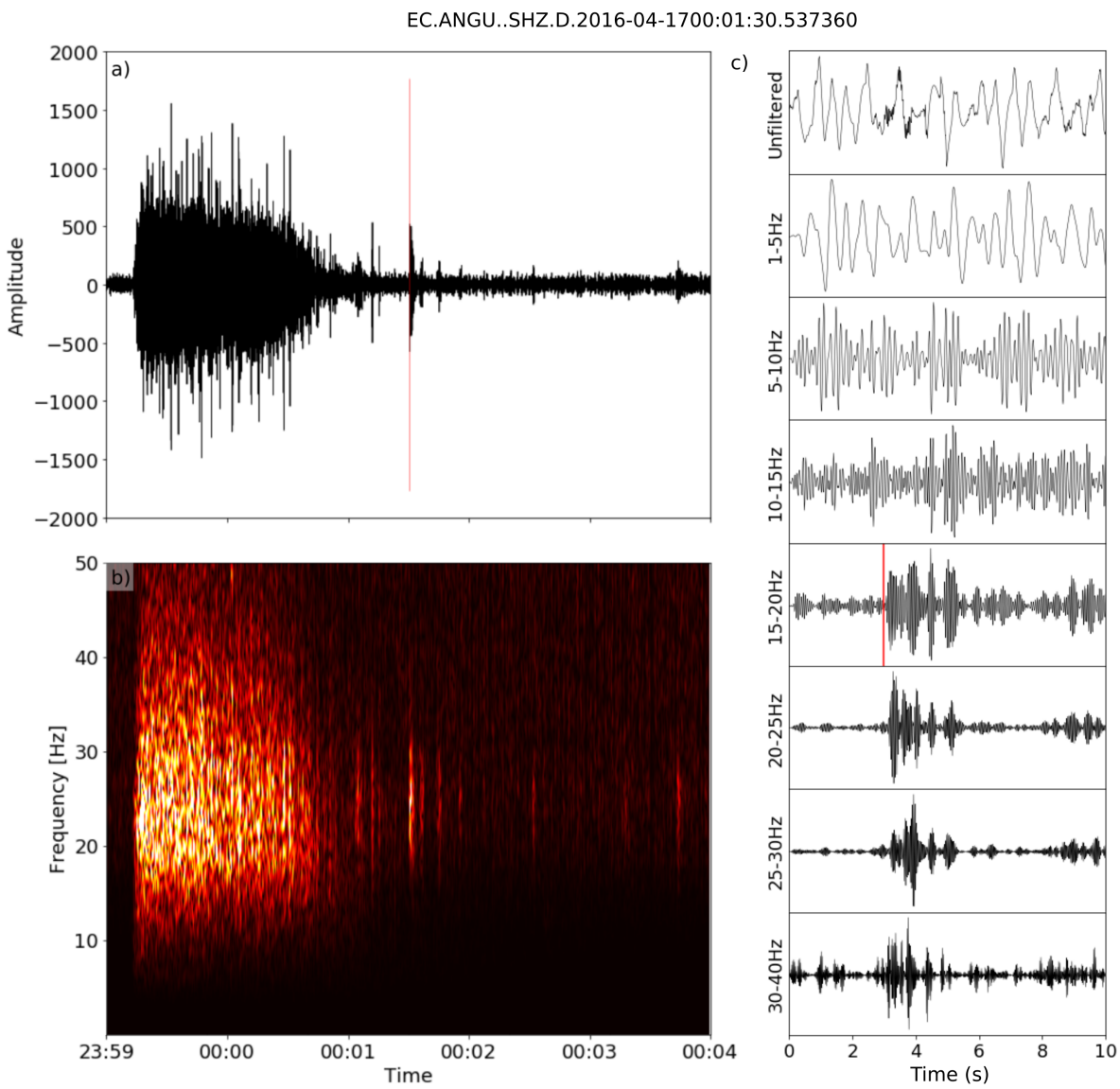

Figure 6.13 High frequency instrument response at ANGU. When the signal clips at ANGU, there is high frequency component which is amplified. *a)* Pedernales earthquake, *b)* Spectrogram and *c)* ANGU at the red pick time as filtered through bands with increasing frequencies.

such, the results of the Q analysis on broadband VT seismicity are not meaningful in a physical sense. Particularly in the case of Q_{band} - a metric based on a single peak frequency in a broadband VT spectra, tells us very little. However, we can use Q_{decay} as a quantifiable metric to describe the signal envelope. Determining a signal envelope that can be used to distinguish event types is often a subjective matter, as a certain degree of smoothing must be included. One more quantified approach is to define a relationship between the peak amplitude of a signal and a minimum 'threshold' (Lees et al., 2008). The Q_{decay} approach determines how quickly the signal amplitude decreases to $\frac{1}{e}$ of the maximum. This decay time, τ, shows a significant difference between the VT swarms in September and the persistent LP seismicity (fig 6.14). It is important to note again that in the short term, values may be comparable, but over longer periods of time, changes in Q may also be due to changes in source-receiver path.

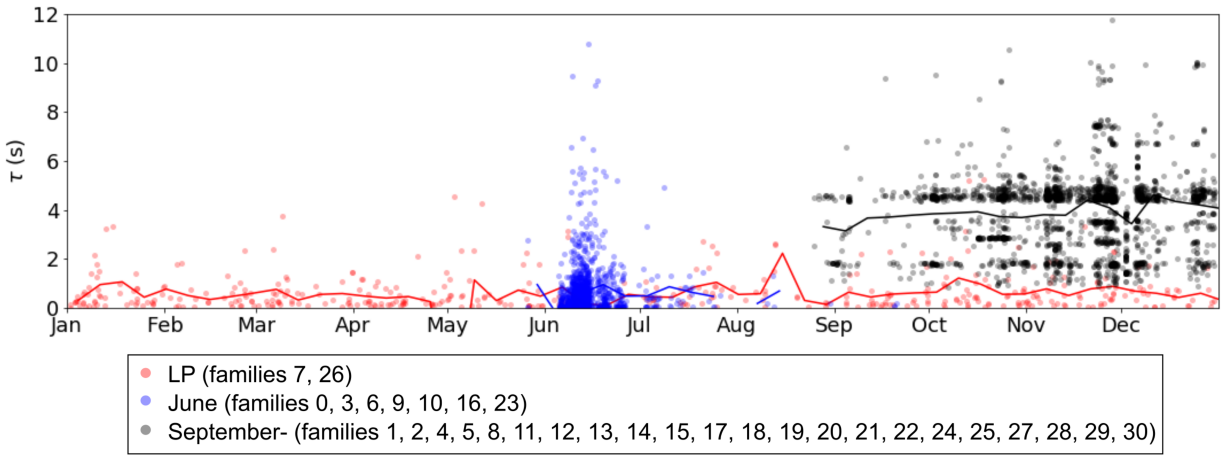

Figure 6.14 Event 'durations' defined by the τ parameter in the Q_{decay} method. Events are separated into three broad populations identified by families: red marks persistent LP seismicity, blue marks the June VT swarm events, and black the VT swarm from September onwards.

The Q_{ARMA} method is also reliant on quantifying the growth rate (g) of a singular fundamental frequency (f). However, if there are insufficient points clustered at a pole at the peak spectral frequency, a Q_{ARMA} value is not calculated. This reduces the number of

erroneous Q values generated for broadband VTs. With this in mind, we use Q_{ARMA} as the primary Q metric for interpreting this sequence of seismicity. For the analysis of LP seismicity this brings this study in line with previous efforts to monitor changes in Q across a series of unrest (Métaxian, 2003; Molina et al., 2004). And for VT events, if a Q_{ARMA} value is calculated it is a function of the most dominant frequency with a broadband signal and used for comparison purposes, but not to interpret a physical process.

6.4.2 VT swarms in 2016-2017

The temporal and spectral analyses do an excellent job to help quantify the different types of seismicity observed throughout one year at Cayambe. The two swarms in June and September onwards are related to two very distinct processes. The June swarms show clear separation between P- and S- phase arrivals, and have a distinct signal envelope in comparison to other families of VT events, where the signals are more emergent. Whilst there is significant uncertainty in the depth and magnitude estimates, the locations detailed in the IGEPN catalogue all show the June swarm events to be in the northern and eastern flanks of the volcano - quite separate from those later in the year. The high XCC of events in the June swarm, but dissimilarity to the September swarms suggests they have different source mechanisms. The events in June 2016 show a very different spectral signature to those later in the year, with much lower peak frequency and Q_{ARMA} values. This may be the result of both source and path effects. Unconsolidated or hydrothermally altered flank deposits can act to extend the coda of failure events (Bean et al., 2014), which for proximal VT swarms may generate an increased Q value compared to a distal VTs. However, the disparity may also be dependent on depth and proximity relative to station CAYR. This June swarm was more likely associated with movement from the regional fault line along 'La Sofía-Río Chingual'. The Chingual fault is a major regional fault that extends 70 km from Cayambe, north through the Andes into Colombia (Alvarado et al., 2016; Eguez et al.,

2003; Ferrari & Tibaldi, 1992) (fig 1). As a named fault it is frequently cited in relation to earthquakes and volcanic systems in the region (Guillier & Chatelain, 2006; Samaniego et al., 2005; Yepes et al., 2016). Although it should be noted that the local tectonics in this region are complex and many smaller faults are not well constrained (Tibaldi et al., 1995). The last major tectonic earthquakes to occur in this region were in 1987 (M6.9 and M6.7), however several smaller thrust and right lateral strike slip events have occurred since (Guillier & Chatelain, 2006; Kawakatsu & Cadena, 1991; USGS, 2021). Unlike some of the swarm activity later in the year, these events are well recorded across all three permanent stations. Particularly at station CAYA, which lies closer to the Río Chingual and 5 km north of the Nevado Cayambe central crater.

The seismicity from September onwards, however, is more likely to originate from beneath the Nevado Cayambe central cone. The locations of the events are much closer to the central cone and to the south and west flanks. The events from the catalogue and subsequent template matching search show a more emergent signal envelope than those in June, with no clear separation between P- and S- phase arrivals. These events have higher peak frequencies overall and higher Q_{ARMA} values. These VT events are quite LP-like in this respect. Whilst some families (15, 17, 22) represent events exclusive to just a few days, the majority span more than 3 months, indicative of a long term source process. Expansion of the template matching into 2017 shows a number of these families persist to the end of VT swarm activity in September 2017. However, unlike in June, the families are all quite dissimilar to one another suggesting there are multiple sources or the source is more heterogeneous or changing. The VT families after September 2016 are also less clear at station CAYA unless tens or hundreds of events are stacked, suggesting the origin is perhaps closer to the central cone and stations ANGU and CAYR. We believe these proximal VTs in late 2016 may be associated with progressive magma ascent and the formation of a proto-conduit (Fournier, 2007; White & McCausland, 2019). Whilst some families of events represent seismicity from a single day and perhaps correspond to a single rupture event (fig 6.6c), more long term

persistent proximal VTs indicate an ongoing shallow process.

6.4.3 Origin of LP seismicity

The long period seismicity is informative as a baseline measure of day-to-day activity at Cayambe. Each event from both the catalogue and the template matching shows remarkable similarity throughout the year with a strong single peak frequency at 2.1 Hz and no strong additional harmonics. The LP events have typical durations between 10 and 15 seconds, and so cross correlation calculated in 10 second windows captures a thorough representation of the whole signal for these specific events. The LP seismicity is not well recorded on either ANGU or CAYA, and with no visible distinction between P- and S- phases, locating or magnitude estimating these events is not possible. Given these events are so well captured at only station CAYR, we suggest they are likely of a shallow source very close to CAYR within the Nevado Cayambe cone.

We consider all the possible source mechanisms for the persistent, repeating, LP seismicity in this episode of unrest at Cayambe. Low frequency, and in particular repeating low frequency seismicity have been described and modelled around the world. Minakami et al. (1951) first identified similar repeating events at Usu Volcano by manually measuring and matching peaks in the waveforms. These C-type earthquakes were attributed to a repeating source mechanism. Since these early efforts to categorise and interpret sequences of LP seismicity, a diverse range of LP seismicity has been described, and as such, there are many well established models for source mechanisms. Initial understanding of LP seismicity stemmed from studies of tremor and an idealised monochromatic or harmonic resonance process (Chouet, 1981). LP seismicity is inherently related to fluids and pressure changes and therefore their presence in the record is of interest for volcanic monitoring and forecasting. Generally, it is accepted that LPs are associated with the resonance of a fluid filled crack (Chouet, 1988).mThis has been extensively modelled by varying the crack media and investi-

gate changes in the resultant waveform (Kumagai & Chouet, 2000). Further theoretical work has sought to model the initial excitation mechanism of the resonance process. For example, with the the transportation of magma, flow-induced oscillations may excite a resonance mechanism (Julian, 1994). Whilst other studies have linked LP seismicity with the tensile hydraulic fracturing of rock (Bame & Fehler, 1986; Fournier, 2007; Lipovsky & Dunham, 2015). It is important also to consider that the volcanic edifice is very heterogenous and LP seismicity may be the result of failure in unconsolidated materials rather than fluid presence (Bean et al., 2014).

In this particular study we have a relatively small number of events that are captured clearly on just one station, and therefore can only make speculative suggestions around the source mechanism involved. Previous studies of LPs in volcanic systems have presented models of cyclical, periodic repeating events generated by magma emplacement and conduit processes (Bell et al., 2018; Petersen, 2007). Whereas episodes of LP seismicity from stick-slip glacial sources have shown swarm like behaviour correlating with periods of snow fall (Allstadt & Malone, 2014). The LPs at Cayambe demonstrate neither of these extremes, and have an average periodicity $\sim$1, suggesting a constant average event rate and exponentially distributed inter-event times. The LP event rate is also low compared to observations of seismicity at similar intermediate arc volcanoes. At Tungurahua volcano, hundreds of events per hour were recorded during activity in 2015 (Bell et al., 2017) and prior to explosions at Volcán de Colima, LP seismicity rate was in the range of hundreds of events per day (Varley et al., 2010b). However, although neighbouring and compositionally similar, these are two very active volcanoes. Rates of seismicity in the order of 10^0-10^1 per day are more closely aligned with Puracé, Colombia (Arcila & Arcila, 1996) and Kawah Ijen, Indonesia (Caudron et al., 2015) which like Cayambe, have not experienced recent explosive activity. Even in a scenario where LP seismicity is believed to be caused by glacial slip as opposed to volcanic processes, such as at Cotopaxi volcano, events were recorded at a rate of 60 events per hour (Métaxian, 2003). In the four instances where periodic LPs from the families are

detected, the average rate at Cayambe is just one event per day. The LP event distributions in frequency and magnitude are also largely unaffected by the swarms in June and September, and show no change following the Pedernales M_w7.8 earthquake.

A study on Cotopaxi Volcano, Ecuador, used Q values to establish whether LP earthquakes were glacial or volcanic in origin (Métaxian, 2003). Using ARMA methods from the signal waveforms and estimating Q from the impedance contrast of ice and water, Q values 1-3 were identified as being glacial. However, in the records at Cayambe, the LP events generate Q_{ARMA} values with a mean value 9.9. We use the same procedure (Aki et al., 1977) and consider a water-andesite contact with approximate andesite bulk density and V_p values of 2800 kgm^{-3} and 3000 ms^{-1} respectively, where Q is approximately 9.5.

If we believe the LPs are associated with a hydrothermal system, then we may anticipate long term trends in the seismicity, and so we extend the template matching to identify LPs in 2015 and 2017 (fig 6.7g-l). The rate of seismicity is unaffected by continued VT swarm activity in 2017. Key identifying metrics including Q_{ARMA}, peak frequency and high XCC values suggest these are from the same source as the 2016 LPs. Studies of Glacier 15α on Antisana volcano note that it is a good analogue for other glaciers in the Eastern Cordillera in Ecuador. This is due to their position on the equator, and direct exposure to the humid winds from the Amazon basin immediately to the East (Manciati et al., 2014). Unlike volcanic glaciers closer to the tropics, that are subject to extremes in climate such as El Niño and La Niña (Ceballos et al., 2006), the equatorial glaciers do not experience extremes of seasonality in precipitation, winds or temperature (Basantes-Serrano et al., 2016; Manciati et al., 2014). As such we might expect sub-glacial hydrothermal systems to be relatively consistent all year, rather than pronounced seasons of glacial unloading and meltwater recharge (Jónsdóttir et al., 2009). If the LP seismicity is related to hydrothermal interactions beneath the glacier, it is important to understand how these react - if at all - to external volcanic or tectonic seismicity.

Harmonic and tornillo-type seismicity was not easily identified and sorted by cross

correlation. This is likely due to the duration of the events, and inconsistent peak frequency of these signals. The cross correlation method is applied over a fixed length, 10 second window for all events. This is suitable to capture similarities in VT and LP events that are up to 30 seconds in length for example, but does little to define events that last several minutes. In the harmonic seismicity, we see some examples of gliding frequencies and sequences of discrete events with different peak spectral frequencies (fig 6.8d-f). If a harmonic signal has only one very dominant spectral peak, this frequency can very significantly control the envelope and duration of the signal. This will limit the effectiveness of a simple, sliding window, cross correlation method, even with a very low detection threshold. As such these low frequency harmonic events should be carefully monitored, as they may be missed by automatic classification methods. Processes such as the harmonic product spectrum (HPS) (Roman, 2017) or a simple automated search for strongly peaked frequencies should be used to identify longer episodes of seismicity. Tornillo events and harmonic tremor at active volcanoes can be indicative of very shallow fluid processes and are often indicative of imminent activity (Arámbula-Mendoza et al., 2016; Hellweg, 2000; Hotovec et al., 2013). Highly monochromatic tornillo events at Galeras Volcano, Colombia, showed strong correlation between event duration and the time until eruption (Narváez et al., 1997). Whilst very long period (VLP) and LP events at Cotopaxi and Tungurahua, Ecuador were attributed to resonance of gas and ash filled cracks (Molina et al., 2008; Molina et al., 2004). These observations of tornillos are all quite different to the tornillo and harmonic seismicity documented here at Cayambe. The tornillo signals at Cotopaxi and Tungurahua were generally all very similar to one another, consistent or sequential in their dominant forcing frequency, and occurred during heightened activity or eruptions. The varied character of the harmonic seismicity at Cayambe, however, suggests this is not a stable or well established source process; without locations it is not possible to confirm whether these are from multiple sources. The first documented strong sulphurous smells near Picos Jarrín on the southwestern flanks of Cayambe, are in a Special Report on 1st December (IGEPN, 2016b). However, without any quantified constraints on

gas flux, we cannot be certain of the origin of this very heterogeneous harmonic seismicity. Due to the duration and pulsed like nature of some of the harmonic signals, they may also be classified as harmonic tremor (Arámbula-Mendoza et al., 2016; Bell et al., 2018). It is important to consider that anthropogenic sources such as nearby helicopters are known to generate harmonic tremor, and must be carefully identified and excluded from analysis - although this is often at much higher frequencies >10 Hz (Eibl et al., 2015)

6.4.4 Dynamic and static triggering

Large tectonic earthquakes cause stress changes in the crust, that may subsequently interact with volcanic systems. The stress change may be large and temporary (dynamic triggering) or small but permanent (static triggering) (Hill et al., 2002b; Manga & Brodsky, 2006). This relationship is complicated and causality versus coincidence is frequently debated (Lemarchand & Grasso, 2007). We use the seismicity rate as an indicator for dynamic triggering, given there is no eruption in this sequence. Clear evidence for dynamic triggering can be seen in Bell et al. (2021a). An approximate calculation using distance and average wave speed will indicate a window at which the tectonic surface waves would arrive at the target location. Bell et al. (2021a) show evidence of volcanic activity within a window of minutes. As static stress changes creates a permanent change of state in the crust, changes in the volcanic system may occur over a longer period of days or weeks. Following the Pedernales M_w7.8 earthquake, manually picked events at station CAYR do show a decreasing rate overall. It is significant that there is no dramatic increase in LP seismicity, as previous dynamic triggering studies have linked tectonic earthquake surface wave arrivals to instability in shallow magma storage (Lemarchand & Grasso, 2007; Lin, 2017; Walter et al., 2007). Although there are many more contributing factors, it has been shown that often shallow fluid storage does not necessarily make a volcanic system more susceptible to dynamically triggered activity (Prejean & Hill, 2018).

Given the first VT swarm begins at Cayambe just 7 weeks after the Pedernales earthquake, we speculate whether a small static stress change in the crust may have played a role in the resumption of activity. One study by Walter and Amelung (2007) presents a model for triggering of eruptions at arc volcanoes following megathrust earthquakes. Four case studies are presented from Sumatra, Kamchatka, Alaska and Chile, where a subduction earthquakes occurs within 200 km normal to a volcanic arc. Elastic numerical modelling of the volumetric strain demonstrates that each of these volcanic arcs would likely have been in a dilational area of volumetric expansion. This may in turn cause small static changes in the stress field and perhaps promote new eruptions. For example, a magma reservoir in an area of dilation can experience overpressure driven by magma mixing and exsolution of volatiles (Sparks et al., 1977). We believe the geometry of this model is paralleled at Pedernales and Cayambe. Further to this, Béjar-Pizarro et al. (2018), model the stress change from the CMT focal mechanism of the Pedernales mainshock, and suggest that Cayambe lies in a region of 'high level potential activation' where induced normal stress ($\Delta\sigma$) < 0.1 bar (fig 6.15).

6.4.5 Reawakening dormant volcanoes

The sudden increase in seismicity at Cayambe has implications for long term forecasting, particularly given there is no record for recent eruptions. One possible model for the reawakening of dormant stratovolcanoes presents a 4-stage process (White & McCausland, 2019). Different phases of characteristic seismicity can be attributed to each stage - from deep seismicity, to distal VT events, to vent clearing and then finally shallow repetitive seismicity ahead of an eruption. The study presents this model exemplified on volcanoes across timescales from days to years. Stage 1 including deep seismicity is associated with lower crustal magma storage. As is the case on many volcanoes, the limited three station network on Cayambe, and in turn the uncertainty in depth estimates mean it is not possible

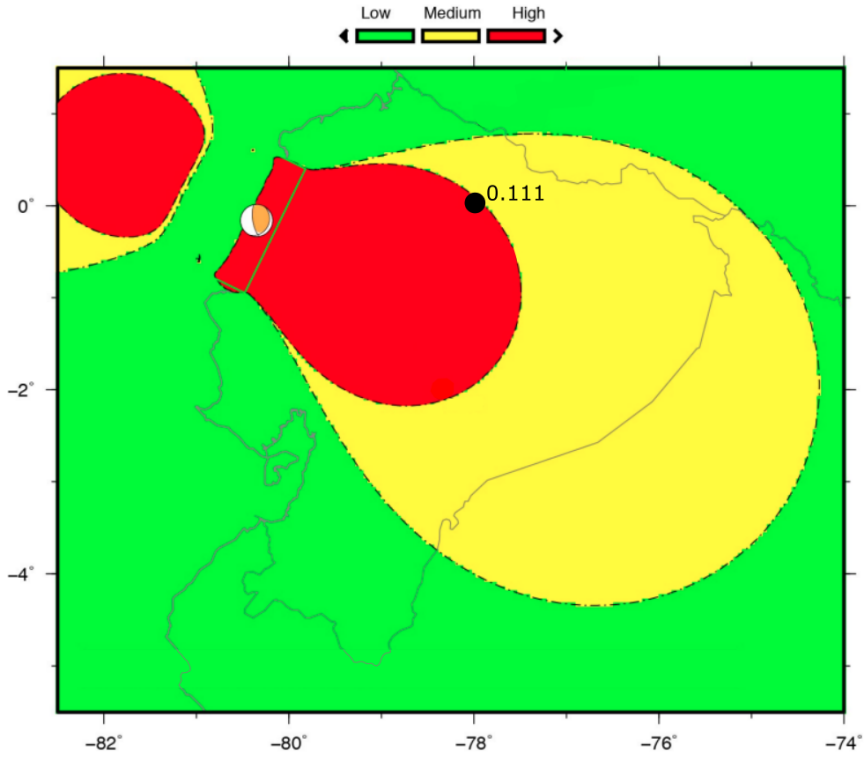

Figure 6.15 Adapted from Béjar-Pizarro et al. (2018). Coulomb3 model to show the static stress change, from the Global CMT solution for the Pedernales earthquake. Cayambe is marked with a black circle in the high risk zone, and the induced normal stress is shown.

to constrain with confidence any VT seismicity between 10 and 40 km depth. However, it is possible that the variety of seismicity recorded at Cayambe in 2016 and 2017 may be indicative of some stage 2 and 3 reawakening, described in this model.

The VT swarm during June 2016 may be considered distal seismicity and is consistent with the stressing of a regional fault system, described in stage 2 of White and McCausland (2019). We speculate that the M_w7.8 Pedernales earthquake generated a small static change in the stress field at Cayambe (fig 6.16). This may have promoted a new pulse of magma to ascend (Walter & Amelung, 2007), or perhaps pressurized local aquifers and allowed slip along a pre-stressed fault (Coulon et al., 2017; White & McCausland, 2016).

The subsequent VT swarm from September 2016 onwards recorded events located

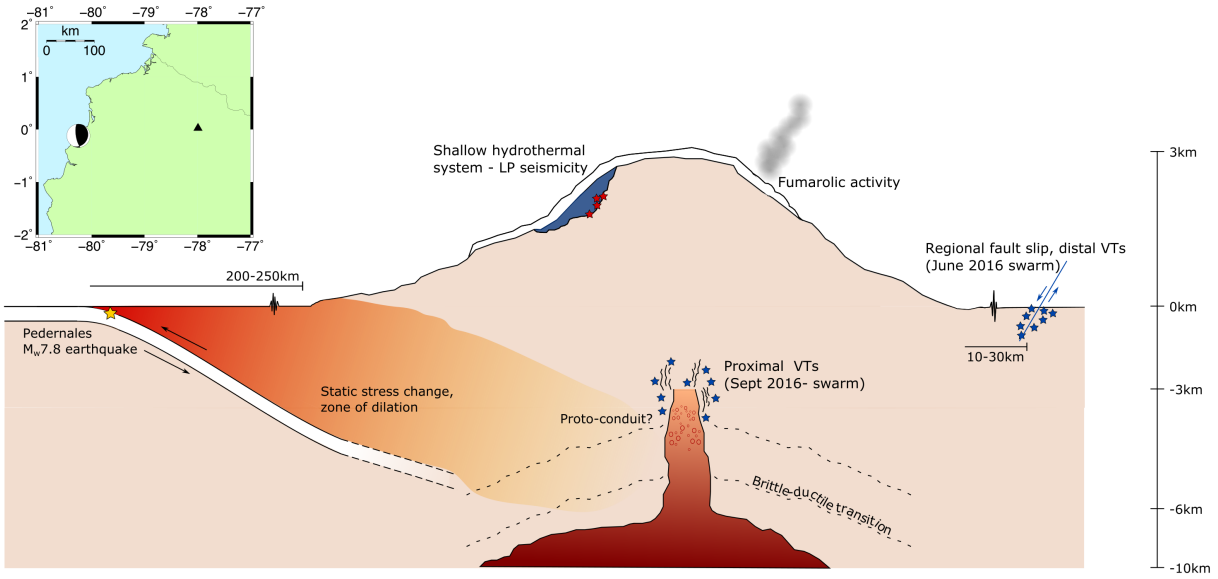

Figure 6.16 Schematic diagram of seismicity at Cayambe in 2016-2017, adapted from the crustal stress model presented in Walter and Amelung (2007). Map inset shows CMT focal mechanism for the M_w7.8 Pedernales earthquake (Dziewonski et al., 1981; Ekström et al., 2012) and relative location to Cayambe. Vertical scale on right, only an indicator of magmatic processes and not applicable for subduction depths.

within the Nevado Cayambe cone, and may be considered proximal VTs. If the distal VTs were associated with a new pulse of magma, then the proximal VTs may document the progression of ascent and possibly the formation of a proto-conduit. Repeated long-term families of VTs may indicate repeated rupture and sealing events of the brittle-ductile transition (Fournier, 2007), whilst isolated families may be indicative of individual rock fracturing episodes to accommodate ascent of magma and gases (Hill et al., 2002b). VT events that could not be classed into families may also be the spasmodic and irregular VT seismicity described in White and McCausland (2019) and associated with rupturing the brittle-ductile seal. We do not see accompanying low frequency seismicity at this stage, although this is possibly due to limitations in the network. The model for new activity at Cayambe is not wholly reliant on a new pulse of magma. It is also possible that a dilational

regime in the crust prompted further exsolution of volatiles in pre-existing magma storage (Sparks et al., 1977). This is an option explored in a similar model in Roman and Cashman (2018).

The next stages of the awakening are vent clearing and shallow repeating seismicity, as magma reaches the shallowest point in the conduit and eventually the surface. Evidence from the seismic record, however, does not suggest Cayambe volcano reached this stage in 2016-2017. The LP seismicity in particular is not typical or indicative of these late stages of reawakening. Empirical calculations of acoustic impedance between magma-rock contacts would suggest Q values for these types of LPs should be an order of magnitude higher (Kumagai & Chouet, 2000; Métaxian, 2003). We also might expect these events to have larger amplitudes and more prominent cyclical trends as magma ascends and interacts with the conduit margins (Bell et al., 2018; Butcher et al., 2020; Iverson, 2008). Whilst we may speculate some harmonic tremor and isolated tornillos are coincident with records of sulphurous smells up on the flanks of Cayambe (IGEPN, 2016b), they are not characteristic of rapid magma ascent or gas venting processes in the latter part of stage 3 and stage 4 of the model (Arámbula-Mendoza et al., 2016; Hotovec et al., 2013). During the crisis, IGEPN reported deformation data but neither GPS or tiltmeter readings suggested any change beyond the margin of any instrumental uncertainty, $\pm$ 7 mm (IGEPN, 2016b). This further supports the idea that whilst there may have been magma ascent, it was not particularly rapid or shallow enough to cause significant flank deformation. The VT swarms show a decreasing rate until the end of 2017 (fig 6.2). There has since been no significant increase in the rate of LP seismicity, indicative of further magma ascent and a transition to stage 3 (White & McCausland, 2019). Whilst it is possible that exsolved gases in an ascending magma body will act to increase volumetric expansion, exsolution of water will act to stall ascent as the viscosity of magma increases (Dixon et al., 1995). It is possible that exsolution of water played a role, or simply the static stress field change was not enough for a magma pulse to ascend to the surface at Cayambe.

We suggest the persistent LP baseline seismicity recorded during 2016 and 2017 is of hydrothermal origin (fig 6.16). As such any increase in LP seismicity with a significantly different envelope, Q_{ARMA} or spectral signature; coupled with an increased in volcanic VT type events should be carefully monitored. Harmonic tremor and tornillo events should also be carefully monitored, coupled with DOAS measurements to identify significant changes in degassing. Periodically running cross correlation analyses and updating master event signals is important to trace subtle changes in seismicity and incorporate more recent events into the monitoring and interpretations. The 4-stage process (White & McCausland, 2019) presents observations of the model in action across time scales from 3-4 months at Mt St Helens (Thelen et al., 2011) to nearly 4 years at Mt Sinabung (McCausland et al., 2019). It is therefore not unusual to observe this slow transition across a period of several years. The models for reawakening are not necessarily linear and if the process of reawakening did stall in 2017, then any resumed activity may include stage 2 distal VTs as well as more stage 3 shallow LPs and VTs (Roman & Cashman, 2018).

6.4.6 Implications for the future

Low latitude glaciers are rapidly shrinking (Thompson et al., 2011). Evidence from analogue glaciers on Antisana suggests that whilst glacial retreat has been ongoing for over 150 years, this has accelerated in the last 30 years, as a result of anthropogenic climate change (Manciati et al., 2014). Studies in Iceland have shown that unloading effect from ice retreat can impact stress conditions within a volcano (Sigmundsson et al., 2010), and cause long term changes to failure conditions in shallow magma storage. Rapid unloading may then promote further magma ascent and impact pre-stressed faults in the volcanic edifice. Station ANGU, although with it's defective instrument response, is installed on the very edge of the western reaches of the summit glacier. Carefully monitoring for any changes here may be particularly important. Even very localised slip may have further implications for secondary hazards from

the glacier itself. Furthermore, in terms of hazard assessment, there are immediate hazards present from ice retreat and rapid glacier melt, particularly during an eruption (Tuffen, 2010). It is estimated around 4.2 km^2 of ice was lost during the 1985 eruption of Nevado del Ruiz, contributing to devastating secondary lahars (Ceballos et al., 2006). In the short term, increased meltwater also has the potential to interact further with hydrothermal systems, increasing pore pressure. If we consider Cayambe Volcano to be reawakening, where the next stage includes further magma ascent and shallow storage then additional meltwaters could lead to potentially very dangerous phreatic activity. Using the existing network, close monitoring of the LP seismicity could be crucial. Due to the unique positioning of glaciers in the Ecuadorian Andes, Cayambe is not subject to seasonal extremes in climate and so the record of seismicity from the hydrothermal system is consistent all year round. Slight changes in the Q_{ARMA} value, or spectral signature could then be indicative of a change to what appears to be a very stable hydrothermal system in balance through 2016 and 2017. All of these recommendations for monitoring signal properties, can only be reliably determined from one station. An extended network of seismometers on Cayambe would allow for greater accuracy in locating events, to underpin interpretations from the event characteristics.

6.5 Conclusions

This study identifies several unique subsets of volcanic seismicity, observed at Cayambe during the seismic crisis of 2016. We explore the potential for reawakening at a volcano that has been seismically restless for 20 years but last erupted in 1785. The seismic crisis at Cayambe volcano occurred just 3 months after the M_w7.8 Pedernales earthquake, 200 km west on the Ecuador coastline. We draw comparisons from models of dynamic and static triggering of volcanic eruptions to the seismicity documented in 2016 and 2017. Should the seismicity have been generated by a new pulse of magma beneath Cayambe volcano, then the process of reawakening is likely ongoing, although slowed or stalled currently. Given

the potentially vulnerable state of the glacier, the unknowns around eruption dynamics and significant populations living within the immediate vicinity, Cayambe remains a dangerous volcano. We believe that using the metrics presented in this study, however, it is possible to carefully monitor the seismicity on the existing permanent network, and quickly identify when earthquake signals are evolving.

Summary of findings

In this chapter I have explored VT swarm seismicity at Cayambe, in contrast to LP drumbeat seismicity at Tungurahua. This further expands the use of the methodology presented in chapter 3 and takes steps to answer the research questions

3. What can we learn about the shallow dynamics at Tungurahua and Cayambe volcanoes, from analysis of the seismicity?

4. With better characterisation techniques, can volcano-seismic events then be used to interpret episodes of unrest at poorly monitored volcanoes?

By examining a contrasting and previously dormant volcano, I have been able to test the capabilities of the methodology to consider a more varied earthquake catalogue. I have also begun to distinguish seismicity relating to persistent, ongoing eruptions, and seismicity associated with the reawakening of volcanoes that have long been quiescent. In turn, this contributes significantly to our understanding of seismicity in forecasting volcanic activity and should inform future hazard assessment accordingly, and specifically answers research question

6. Can this detailed volcano-seismic analysis better inform hazard assessment?

Finally, I have also addressed the relationship between the M_w7.8 Pedernales earthquake and volcanic unrest. Here I have begun to examine the complex relationship between tectonic and volcanic processes and develop further answers relating to research question

7. Is there any evidence for volcano-tectonic interactions at Tungurahua and Cayambe?

This is explored further in the next chapter.

7 | Discussion

In chapters 4, 5 and 6 I have presented three specific studies of volcanic seismicity at Tungurahua and Cayambe. These provide robust evidence that support the signal processing methodology and seismic analysis that is possible with limited data. In this chapter, I detail exactly how the research questions from chapter 2 have been addressed. In particular I focus on the comparisons that can be drawn from Tungurahua and Cayambe volcanoes and the scope to apply this research at analogue systems. As laid out in the introduction, I address some of the differences between persistently active systems, compared to reawakening volcanoes, and how this is demonstrated in the seismicity. Finally I present some ideas for further research beyond the thesis.

7.1 Evaluating the success of the methodology to characterise seismicity

The literature review in chapter 2 identifies the need for a robust signal processing routine to analyse seismicity at poorly monitored volcanoes. Whilst the methods presented in chapter 3 were developed and tested against synthetic waveforms, the real challenge was to determine how usable these were against real volcano-seismic data. Particularly given the station outages and data gaps that have been demonstrated in this research, this further highlights the need for analysis techniques that are not dependent on extensive networks of seismometers. When the methodology is applied to data from both Tungurahua and Cayambe, I am

able to present new, quantified seismic characteristics and describe seismic phenomena which have not been published in the literature. These metrics allow us to reliably and quantitatively compare seismicity from different volcanoes, and in turn might help us to understand fundamental internal volcanic processes. As such, I think I have confidently answered research questions 1 and 2. The results from characterising the seismicity in three different scenarios at Tungurahua and Cayambe, go on to inform idealised models of the eruption processes. Particularly at Cayambe, where there are additional external complexities that can influence the seismic record, it is significant that the analyses presented in this thesis can successfully characterise the LP seismicity and distinguish different sources. At Tungurahua, where drumbeat LP seismicity has been studied before, the approach taken in this thesis sheds light on long-term important features of drumbeats in cyclical vulcanian explosions. The methods were tested in two extremes of data: at Tungurahua where very similar LPs need careful quantifying and characterisation, and at Cayambe where the catalogue includes a mixture of VT and LP seismicity.

The workflow presented in this thesis also acts to unify a quantitative method to analyse seismic signals. Prior to this research, methods to characterise volcanic earthquakes were inconsistent and sometimes conflicting, and I hope the signal processing routine here can be used as a framework to adopt in future studies. As discussed in section 3.4, across multiple studies there are variations of the Q methods used interchangeably, which can result in misleading interpretations and incomparable results. By testing all three approaches, I can demonstrate the stability of the Q_{ARMA} approach for large datasets and extract a meaningful metric, τ from the Q_{decay} method to quantify the signal duration.

There are still limitations to the analysis, which can be considered for future work. Physically, the Q factor relates to a single frequency resonator and hence, best quantifies LP seismicity that is particularly monochromatic (Rossing & Fletcher, 2004). A Q value associated with a VT earthquake corresponds to the spectral peak frequency only, but has no physical relationship the source mechanism or resonator. This means in a catalogue with

a mixture of VT and LP events, although the Q factor can be used as a distinguishing feature, for VTs it is more of an informative measure about the dominant peak frequency rather than a tool for interpreting a physical process or medium.

One of the other issues addressed in chapter 3 is the parameter tuning required for both the STA/LTA picking and the cross correlation method. Before running analysis on several months or years of data, it is necessary to test the success of automatic picking on a handful of days and alter the STA/LTA search criteria accordingly. Whilst this picking method could be easily expanded to search several stations in a network simultaneously, this would rely on the user tuning the parameters for each station relative to the signal to noise ratio. Similarly, in order to select a suitable search window for the cross correlation analysis, there needs to be a cursory search to examine the typical durations of the earthquake signals. Perhaps for implementation on a large scale this is something that could be automated and optimised.

The methods presented in this thesis successfully characterise seismicity with limited data. Obviously, where possible, the more data that can capture these volcanic-earthquakes the better. Ideally in order to complement the findings from limited permanent monitoring, a temporary deployment of a well-planned broadband array, from which depths and focal mechanisms could be calculated, would add some confidence and additional details to the interpretations that can be made from single station analysis. Going forward it would be interesting to test the methodology on even more varied earthquake catalogues that include more examples of hybrids, tornillos and harmonic and gliding tremor.

7.2 Understanding eruption dynamics

In this section, I evaluate how the findings from this thesis contribute to our knowledge of unrest at intermediate-composition arc volcanoes. I refer back to some of the earlier questions laid out in the introduction and first consider seismicity relating to persistently

active systems, and then reawakening systems after a period of quiescence. To some extent, the findings in this thesis present the two scenarios as extreme end-members on a spectrum of volcanic-seismicity. Tungurahua exhibits continued episodes of very periodic repeating LPs, where seismicity is sustained over a 17 year period. Whilst Cayambe exhibits a mixture of LP, VT and tornillo-like seismicity in an almost unexpected swarm, lasting just longer than a year. I then subsequently related these two contrasting styles to two very different dynamic models of the shallow conduit. Here I explore these two models in the context of the literature, and how the research in this thesis has contributed to our understanding of eruption processes. I present a selection of analogous systems which may benefit from the seismic analysis and models presented for Tungurahua and Cayambe, and further our understanding of these internal processes. Finally, I go on to examine whether there are comparisons to be drawn from these two end-member scenarios, if not in their present day states, but historically.

7.2.1 Persistent unrest and the associated seismicity

Tungurahua's explosive 17 years of unrest (1999-2016) was one of the longest eruptive phases for any Ecuadorian volcano in living memory. Therefore, it is important to understand how the shallow conduit dynamics are able to sustain such persistent unrest, and what can be learned from the seismicity in this period. Specifically this section will then evaluate how successfully these findings go to answering research questions 3 and 5.

In chapters 4 and 5, I have presented models for a sealing conduit plug, which is inherently connected to shallow stored magma. This shallow magma plug is thought to control explosions and subsequently, the seismicity at Tungurahua. Sealing conduit plugs and their role in vulcanian style eruptions have been frequently described in the literature (Diller et al., 2006), although often in relation to the geochemistry and texture of the plug materials (Cassidy et al., 2015; Clarke et al., 2007; Preece et al., 2016). Petrological studies

like these give a more detailed insight to the pressure conditions associated with magma plug emplacement and eventual rupture (Bain et al., 2019). The process of plug formation is complex, and dependent on factors including magma composition and its ability to degas both vertically and laterally into permeable conduit margins, magma ascent rate, and strain exerted at the conduit margins (Diller et al., 2006). These processes have been simulated in laboratory analogue experiments, to further understand how degassing magma, behaves in a conduit (Del Bello et al., 2015). However, there is limited published material on LP seismicity accompanying plug processes. In both chapters 4 and 5, I have identified specifically, periodic LP drumbeats that are attributed to gas interactions in a fractured plug, before and after rupture. To my knowledge, this is the first time that periodic LP seismicity has been connected with conduit plug processes in this way. The question that remains, is whether these LP drumbeats are unique to a process at Tungurahua, or they simply have not yet been explored in other volcanoes. It is important to address this in order to contextualise the findings in this thesis.

If we look at some other examples of LP seismicity identified early in this thesis (fig 2.4) they are modelled in relation to eruption processes, but not explicitly to a plug model as is described here. For example, the extrusion of more silicic spines at Mt St Helens (MSH) were modelled as a stick-slip frictional process that is able to generate highly repeatable drumbeat LP earthquakes (Iverson, 2008; Thelen et al., 2011). From the Q factor, cross correlation and temporal analysis, I have established that the LP seismicity at Tungurahua is not comparable to the MSH stick-slip model, particularly given there is no field evidence of a similar ongoing process. Studies from Soufrière Hills Volcano (SHV), Montserrat, consistently refer back to a model involving strain and shear failure at the conduit margin from viscous, plug-forming magma. This includes studies in deformation (Green et al., 2006), seismicity (Hale, 2007; Neuberg, 2000) and petrology (Clarke et al., 2007). These models suggest that shearing at the conduit margin causes brittle failure of the magma, generating LPs and an increasing tilt signal (Neuberg et al., 2000). At SHV,

the tilt cycles and swarms are very periodic and cyclical and so this model appears suitable. Previous studies have attempted to apply this shearing model and correlate tilt cycles with LP seismicity at Tungurahua (Marsden et al., 2019; Neuberg et al., 2018), however, as established here, the occurrence of periodic LP swarms and tilt cycles have been inconsistent and often out of phase with one another. Particularly given the altitude of station RETU and it's sensitivity to the shallowest processes, it appears more likely that the tilt signal from here relates to a shallow inflation rather than a larger shearing process.

Some specific studies have examined plug processes in relation to acoustic and infrasonic data (Johnson & Lees, 2000; Traphagan & Lees, 2020). Prolonged, energetic and pulsed degassing associated with acoustic emissions known as chugging (so called because of its similarity to a steam train) has been previously observed at Tungurahua (Ruiz et al., 2006). Although we do see some evidence for harmonic tremor and possible chugging-type events where there is open-system venting, this again does not correspond with the more commonly occurring cyclical seismicity here. The closest example in the literature to the findings in this thesis, is a long term seismicity study at Santiaguito volcano in Guatemala (Gottschämmer et al., 2021). This particular study takes a similar approach to examine more than two years of seismicity and corresponds the findings to explosive activity. However, the focus is predominantly a different process relating VTs and harmonic gliding tremor to lava dome collapse.

Each of the examples in figure 2.4 are modelled as isolated instances where one LP swarm relates to a specific source mechanism. This was highlighted in the literature review and research questions in chapter 2, that there is a need to understand the significance of LP drumbeats and if they relate to a more universal source process. I suggest that the LP drumbeat seismicity and accompanying processes of magma-plug rupture and resealing are not necessarily unique to Tungurahua. Repeated failure and healing of magma has been demonstrated in laboratory conditions as an important control in pressurising the shallow conduit and regulating explosive eruptions (Kendrick et al., 2016; Lamur et al., 2019).

However, without long term specific investigations into periodic volcanic seismicity, such episodes of unrest have not been analysed and described in the literature. Of the LP swarms described in chapter 2.2 (fig 2.4) very few are long term studies that would necessarily identify sustained cyclical patterns of persistent seismicity. Those that are, including repeated but varying LP swarms at Volcán de Colima, are explicitly attributed to a variability in the plug characteristics, magma rheology and ascent rate (Varley et al., 2010a; Varley et al., 2010b). Any long term trends in LP swarm seismicity at Augustine Volcano are attributed to much deeper processes and are therefore not comparable. The results in chapter 4, particularly, are the first time periodic drumbeat LPs have been presented as a persistent repeating process over several years and attributed to a longstanding magma plug model, rather than an isolated phenomena dependent on a very unique or specific source mechanism. I suspect that the network geometry on Tungurahua (fig 2.8) favours such clear recordings of LP seismicity, that dominate the earthquake catalogues; that may not be the case on other volcanoes, and perhaps this is why similar periodic LP swarms have not been recorded and interpreted.

By further understanding the importance of LP seismicity, and particularly such characteristic, periodic repeating LP seismicity, and how this relates to shallow conduit processes, future monitoring efforts can be informed accordingly. Figure 7.1 summarises the processes associated with shallow persistent volcanic seismicity. The relationship between persistent LP seismicity and shallow conduit processes are novel contributions to the science and have scope to be adapted and considered at comparable volcanoes. At intermediate composition volcanic systems, where sealing conduit plugs are thought to be a controlling factor in the eruption process, there should be a greater focus on monitoring LP seismicity. Extensive retrospective studies, as in this thesis, could pick out long-term trends that may have previously been overlooked, where only individual swarms have been considered. This is particularly the case at volcanic systems where erupted plug products have already been analysed in terms of the petrology and geochemistry and field samples can be pinpointed to specific explosions,

and in turn seismicity (Del Bello et al., 2015; Preece et al., 2016). If it is possible, then there may be benefits to re-considering station locations to be positioned closer to the active vent and sensitive to the shallowest activity. Or alternatively, undertaking a cursory initial investigation with a temporary seismic array to quantify shallow LP seismicity, as recommended previously. This would act to consolidate the findings here and accurately correlate seismic and petrological interpretations to further understand shallow plug processes.

7.2.2 Lessons from reawakening processes

The model of persistent seismicity in a well established conduit at Tungurahua, is presented in contrast to the reawakening swarm seismicity at Cayambe. This is highlighted by the schematic in figure 7.2, illustrating the different conditions associated with two different types of seismicity. In chapter 6, the model that is repeatedly referenced and structures the discussion, is for the reawakening of dormant stratovolcanoes, where dormant is defined as any period >20 years (White & McCausland, 2019). Cayambe has been dormant for over 200 years, and so whilst this meets the criteria for the model, 200 years is still a relatively short period of inactivity on volcanic timescales. There is limited information about the last eruption in 1785; reports suggest there was still fumerolic activity ongoing as late as 1802 (Detienne et al., 2017). Field campaigns have focussed on debris flows (Detienne et al., 2017) and dating deposits from a longer period of late Holocene eruptions (Samaniego et al., 1998). Furthermore, with such a limited record of seismicity, there have been no tomographic studies to infer possible magma storage depths, such as those at Tungurahua (Molina et al., 2005). As such, there is significant uncertainty about the deeper magmatic sources and plumbing system at Cayambe.

It is the rate of seismicity and the earthquake waveform characteristics that confirm the significance of the 2016-2017 swarm at Cayambe. Although there is substantial uncertainty in the calculated depths of the VT swarms, this establishes that distal seismicity played a

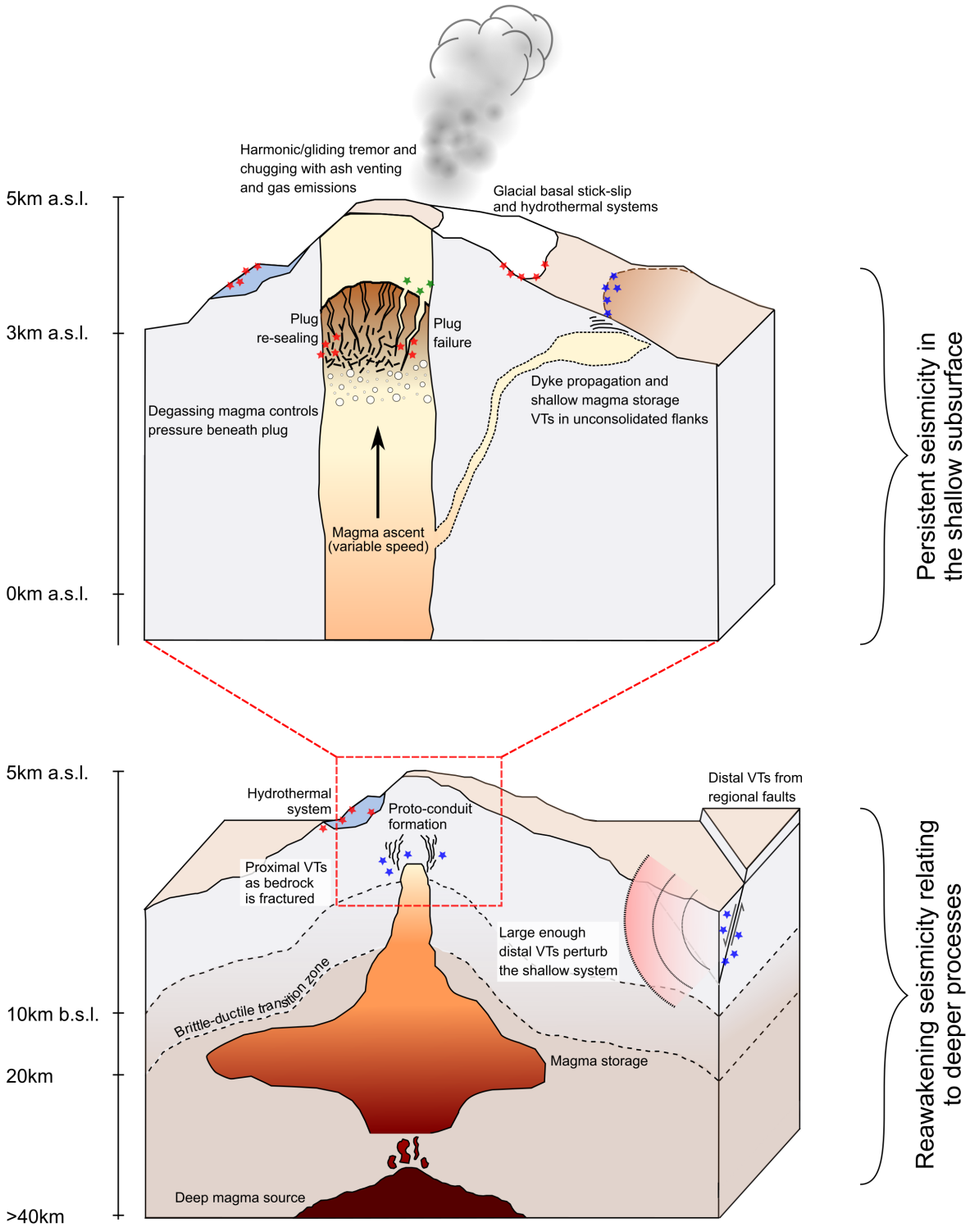

Figure 7.1 Schematic diagram to summarise the sources of seismicity and how these relate to eruption processes as discussed throughout the thesis. The top panel shows a closer view of the very upper conduit, whilst the bottom panel considers deeper processes.

key role in the unrest and reawakening at Cayambe. By determining the low (9.5) Q factor associated with LP seismicity which indicates hydrothermal activity, this in turn provides further evidence of a shallow heat or pressure source consistent with new magma ascent (Métaxian, 2003). The reawakening at Cayambe is described as 'stalled' because there was no evidence of the shallowest LPs associated with vent clearing (in the top 1 km of the conduit) and rapid boiling of brine-filled lenses (White & McCausland, 2019). This is likely because there was not an adequate pressure change or driving mechanism for the magma to continue its ascent into the shallow edifice. This may also relate more closely to the magma properties and the ability for volatiles to exsolve, rather than the pressure in the surrounding crust (Dixon et al., 1995). A number of the exemplar, dormant volcanoes discussed in White et al. (1998) including Sinabung (McCausland et al., 2019) and Shishaldin (Petersen, 2007) demonstrate complex timelines of reawakening with periods of inactivity and quiescence that last decades. Prior to this research, there was no published material on the 2016 volcanic swarm at Cayambe. The findings in this thesis not only contribute to the narrative of what might be a significant reawakening at the volcano, but should act to inform future hazard assessment.

7.2.3 Analogous volcanic systems

It is at this stage we can start to draw some comparisons from processes at Tungurahua and Cayambe. Clearly, persistent seismicity and reawakening processes occur at different depths and at different stages in the development of a volcanic conduit (fig 7.1). However, there are similarities in the dynamics of a 'failed' explosion in the magma plug, and a 'stalled' ascent of magma, where a vent cannot be cleared to the surface. This furthers the discussion about the sensitivity and optimal conditions required for eruptions to commence and persist, as introduced in chapter 6. Both are examples where there were inadequate conditions for the next stage of the eruption to progress. At Tungurahua, we have some confidence that this

process is associated with a sealing conduit plug and insufficient pressures to cause the plug to rupture and fail (fig 5.4). In contrast, at Cayambe this may be a similar but deeper process where there was insufficient pressure to continue vent-clearing. The specific differences in the processes are reflected in the disparity in the seismicity. To understand how the findings from this thesis are more universally applicable, we must look to volcanic systems beyond Ecuador.

Given the systems at Cayambe and Tungurahua cannot be directly compared in their present day conditions, I have used the 'VOLCANS' software (Tierz et al., 2019) to identify more suitable analogous volcanic systems. VOLCANS uses records from the Global Volcanism Programme and suggests comparable volcanoes on the basis of factors such as rock geochemistry, eruption style and tectonic setting. This method introduces a certain element of bias, in that very understudied volcanoes with limited records will not be recommended by the programme. It also does not account for how well monitored a volcanic system is. It provides a good initial list of suggestions. However, I carefully selected from this list systems which have similar external factors as those at Cayambe, such as proximity to society and glacier cover. For example, Mount Hood, Oregon, where the last known eruption occurred in 1866 (Cameron & Pringle, 1987). Mount Hood is also a snow capped stratovolcano, with a weak unconsolidated edifice from previous collapse events, and lies within 80 km of the city of Portland (population >600,000) (Global Volcanism Program, 2013d). As such, this is a good candidate for comparing reawakening processes described at Cayambe. In order to carefully monitor the whole Cascades range, and further hazards from the Pacific North West tectonics, there is a significant seismic monitoring network near Mount Hood (Moran, 2004). Petrological analysis from the deposits of previous eruptions have suggested that although more silicic lava dome type eruptions were common, they were possibly promoted by recharge of more basaltic magma and subsequent mixing and therefore more comparable to Cayambe (Koleszar et al., 2012). Because there is such an extensive seismic network in place, previous studies have been able to estimate magnitudes and locations of significant earthquake

swarms and suggest the seismicity is generally tectonic and there is currently no evidence of volcanic reawakening (Jones & Malone, 2005). In the event of a reawakening process at Mount Hood, however, there is sufficient monitoring from the USGS that deep and distal seismicity (stages 1 and 2 of the reawakening model) would rapidly be detected. Therefore the single station workflow for analysis is not necessary to influence decision making and hazards assessment at Mount Hood, although some techniques in the signal processing such as the Q factor and $K_{1,2}$ values may help to distinguish certain clusters or sources mechanisms. Particularly given the proximity to major plate boundaries, it is important to be aware of the potential for static triggering to promote new magma ascent. The potential for volcano-tectonic interactions is perhaps lower at Mt Hood as USGS catalogues only identify six earthquakes $M_w 6.0>$ since 2000, all of which are approximately 500 km from the volcano. This is perhaps beyond the range of effects for static triggering processes, however, dynamic stress changes may be important. These are also typically strike slip events associated with the Juan de Fuca plate, as opposed to thrust events from subduction. As explored a little in chapter 6 (and appendix A), it is unclear whether these are more or less likely to trigger volcanic activity. There are still lessons about slow or subtle reawakening processes, that can be learned from carefully comparing the activity at Mount Hood and Cayambe.

In contrast, Atitlán volcano, Guatemala is another andesitic stratovolcano with steep relief and unconsolidated flanks, that last erupted in 1853 (Global Volcanism Program, 2013a). This again has a comparable eruption timeline and period of dormancy to Cayambe volcano, and a good candidate to consider what reawakening and the associated seismicity might look like. Historically eruptions have been described as explosive and vulcanian to sub-plinian in nature (Haapala et al., 2005). Whilst there is no summit glacier to complicate matters, Atitlán does form part of the Guatemalan arc and the region is subject to frequent thrust earthquakes from the subduction of the Cocos plate. The unstable slopes of Atitlán are vulnerable to debris flows and secondary triggered lahars from both regional earthquakes as well as heavy rains and storms (Luna, 2007). In the event of a new erup-

tion at Atitlán, lahars are predicted to be, by far the most dangerous potential hazard to nearby communities (Haapala et al., 2005). Unlike the well funded and coordinated USGS efforts at Mount Hood, there is limited capacity for geophysical monitoring and there are no dedicated seismic stations at Atitlán (Instituto Nacional de Sismologia Vulcanologia Meteorologia e Hidrologia (INSIVUMEH), 2021; International Seismological Centre (ISC), 2021). The nearest active, permanent station is in Guatemala city (∼80 km). There have been some temporary stations deployed at nearby Volcán de Fuego since the June 2018 paroxysm (Diaz-Moreno et al. 2020; Calder, *per comms.*), however these data will likely be dominated by seismicity from Fuego itself. As such, the single station analysis techniques presented in this thesis would be more appropriate to the monitoring capabilities here. A retrospective study of any available seismic data, using the methods presented in this thesis could describe the behaviour of the seismicity at Atitlán for the first time. If possible, this is a volcanic system that would benefit from a short temporary deployment of seismometers to further understand the current state of the system and to look for any indicators of a reawakening process analogous to Cayambe. Crucial lessons could be learned from careful monitoring of seismicity at both of these systems, to inform decision making.

To draw comparisons from the persistent seismicity and shallow conduit plug proposed at Tungurahua, we might look to somewhere like Galeras volcano, Colombia. Galeras is a predominantly andesitic stratovolcano with a recent history of explosive activity that has been extensively studied both in terms of the petrology and seismicity (Bain et al., 2021; Gil Cruz & Chouet, 1997). There have been dedicated studies to examine how degassing and seismicity processes correlate (Fischer et al., 1994), describe sealing conduit plug formation (Bain et al., 2019) and to further understand the significance of frequent tornillo earthquakes (Fazio et al., 2019; Narváez et al., 1997). Since 2014, however, Galeras has been in a period of relative quiescence (Global Volcanism Program, 2013c). Perhaps still more active than the quiescence described at Tungurahua, as the national monitoring agency, Servicio Geologico Colombiano (SGC), have reported on fumerolic activity extending <700m above the height

of the crater. There have been no further reports of eruptions since 2017. Long term seismic-tomographic imaging that could clearly identify a shallow conduit and magma storage during years of activity (2001-2007) could not distinguish the same conduit-shaped, seismic anomaly in later years (2015) (Koulakov & Vargas, 2018). This in turn may suggest a 'switching off' of the shallow magma plumbing system at Galeras, similar to that experienced at Tungurahua. Five years of inactivity at Tungurahua is a very short period of time on geological timescales, and so it is hard to say with confidence that the system is completely dormant and no longer considered a hazard. By paying close attention to analogous systems such as Galeras, where a very similar internal system has been described, we can adapt and interpret more carefully the models proposed in this thesis. Equally, the signal processing routine can be retrospectively applied to historical seismic records at Galeras to quantify past seismicity to determine whether seismicity and known explosive episodes correlate. This would consolidate the theories proposed for mechanisms at Tungurahua and inform future hazard assessment at both systems.

7.2.4 Tungurahua and Cayambe as comparable systems

Although these two systems have been examined as two end-member scenarios for seismicity an unrest in the present day, here I consider both systems in a longer volcanic timescale and the implications for our understanding of conduit processes. This is particularly important as Tungurahua has remained quiet for over five years and we begin to imagine what a reawakening process might look like, and if it is comparable to unrest seen at Cayambe. On the longest of timescales, both Tungurahua and Cayambe have been defined by major explosion and collapse events which have lead to the partial-destruction and rebuilding of the main edifice (Le Pennec et al., 2008; Samaniego et al., 1998), and so we know that each system is capable of suitable overpressure and explosive activity. However, to get a better understanding of the possible parallels that can be drawn between Tungurahua and Cayambe,

we need to look at more recent histories. There have been more extensive field campaigns undertaken at Tungurahua and so there is more certainty around the late-Holocene eruptive activity than at Cayambe. For instance, the present day cone Tungurahua III (3000 years BP) has been defined by two eras: a construction phase, of mostly strombolian eruptions and lava flows (up to 1470 years BP) and an explosive phase defined by PDCs (up to present day) (Hall et al., 1999). In the most recent history, eruptions at Tungurahua have been defined by approximately one eruptive phase per century, with confirmed eruptions in 1641-1646, 1773-1781, 1886-1888, 1916-1918 and then the resumption of activity in 1999-2016. In this most recent eruptive phase, explosions began in October 1999, however, tremor was identified as early as 1993 (Le Pennec et al., 2012; Ruiz et al., 2006). This should be considered when we consider the next stages of reawakening at Cayambe, and that a six year delay between the onset of seismicity and first explosions is not unprecedented. It is not thought that the resumption of magma ascent and explosions in the late 1990s at Tungurahua, was triggered by any tectonic earthquakes as is suggested here for Cayambe, and the earlier eruptive phases pre-date widespread seismic monitoring. The M_w8.8 Esmeraldas earthquake occurred in 1906 just 100 km further north than the Pedernales 2016 earthquake (Kanamori, 1977). However, this was 10 years prior to the 1916 eruptive phase at Tungurahua and any connection between the two can only be assumed as coincidental, without further evidence.

Going forward then, might we expect explosive activity at Cayambe within six years of 2016 seismicity? As laid out in this discussion here, any further seismicity indicative of imminent eruptive activity would look more like the persistent shallow LPs, rather than the deep reawakening VTs. There is limited information on what the tremor was like in 1993 at Tungurahua (Ruiz et al., 2006), but tremor has not yet proven to be significant in the reawakening seismicity. The timeline of events at Tungurahua may be a good indicator of a cyclical reawakening-active-quiescence process (fig 7.2), however it is important to remember that this is based on a number of assumptions and limited data. The pattern of one eruption per century is only really based on these five observations, and the 1999 eruptive phase that

lasted 17 years (23 years if we consider the precursory seismicity in 1993) is much longer than the 2-3 year eruptions recorded in historical documents. In order to sustain such a long eruptive phase, perhaps the internal processes between 1999 and 2016 at Tungurahua were very different to episodes earlier than 1918. As speculated previously here, perhaps due to magma ascent rate and composition, the cyclical plug rupturing and sealing process was able to control conduit pressures and sustain seismicity and accompanying explosions for a much longer total eruptive phase. We do not have such detailed and extensive records of eruptions at Cayambe, with only the one historically documented eruption in 1785. Tephrochronology studies identify major explosive episodes in the last 4000 years with repose periods between 600 and 1000 years (Samaniego et al., 1998). These are longer eruptive and repose cycles than documented at Tungurahua, but following the same logic, Samaniego et al. (1998) suggests the last eruptive phase at Cayambe is still likely ongoing and the 1785 eruption was simply the most recent eruption in this phase. At this point then it is important to distinguish that the reawakening processes discussed in this thesis consider dormancy for periods of tens to hundreds of years, rather than considering whole eruptive phases lasting thousands of years. Figure 7.2 illustrates a cycle of reawakening-persistent seismicity using the findings in this thesis and historical records at Tungurahua and Cayambe. The two systems may be more comparable than initially appears, if we consider they are currently at different stages within this overarching cycle.

As I alluded to in chapter 6, volcanic-tectonic interactions are complex and need to be addressed on a case-by-case basis. It is unclear from the limited data points that we have to reference, how large tectonic earthquakes would interact with the timeline in figure 7.2. How a tectonic earthquake affects a volcano is also likely dependent on the state of the volcano itself. This in turn may relate to where on the timeline the system exists - dormant, reawakening, or persistently active. If we believe that the two volcanoes are in two very different stages of this longer cycle of reawakening, this provides further support as to why each volcano did not demonstrate the same reaction to the M_w7.8 Pedernales earthquake.

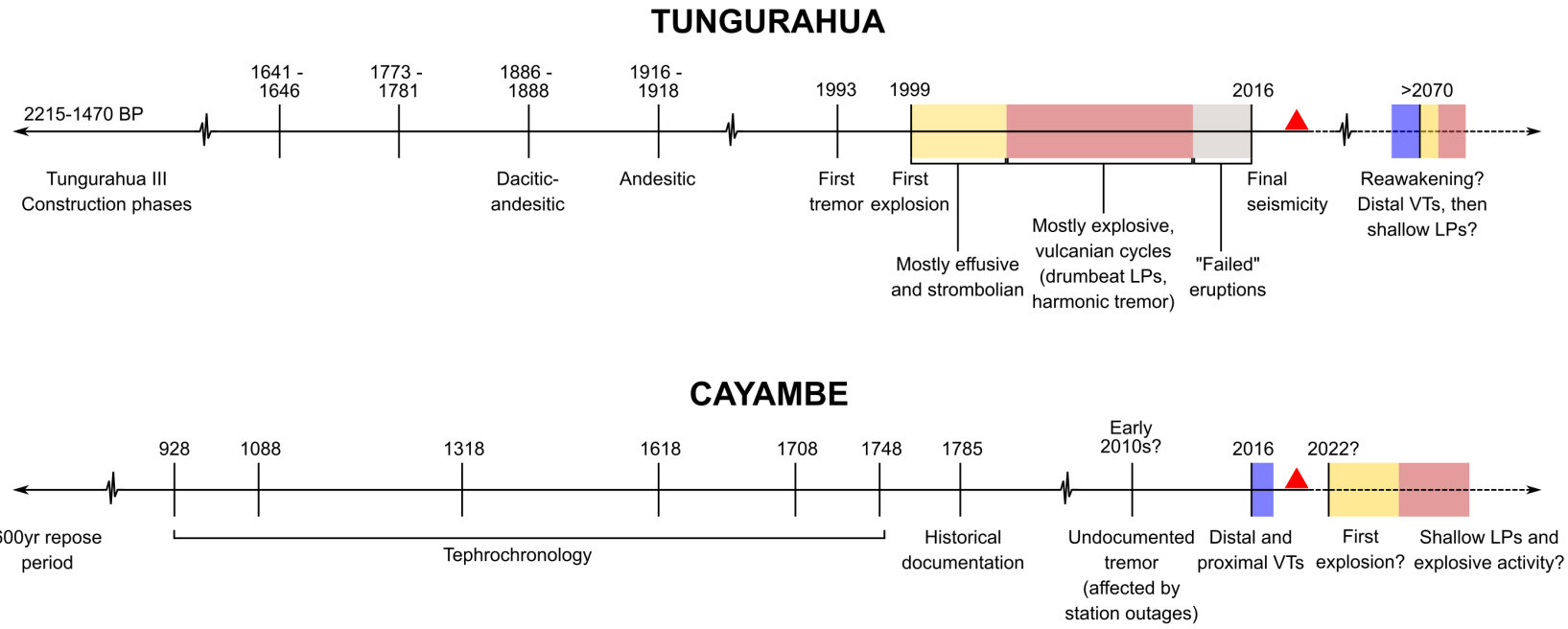

Figure 7.2 Schematic timeline of eruption styles and seismicity at Tungurahua and Cayambe. Red triangle indicates present day, and different eruption processes and associated seismicity are labelled accordingly. By comparing the two timelines, we can appreciate the cyclical nature of the eruption processes in intermediate-compositions, and how the dynamics at Tungurahua and Cayambe may be analogous but at different periods of time.

By looking again at analogous volcanic systems, a longer history should be considered to determine whether long-term dynamic state is a contributing factor in the susceptibility to triggering.

7.3 Scope for further work

This thesis presents some clear evidence to address the research questions laid out in chapter 2, however, it also poses some further questions which could motivate future research. Firstly, whilst IGEPN do a fantastic job of running geophysical monitoring networks across 20 active volcanoes, this research highlights how frequently seismometer outages and faults occur. Whilst the signal processing routine was developed with single station and single component analysis in mind, even the most reliable seismometers such as RETU and CAYR falter during crucial episodes of unrest. The high frequency response at ANGU confirms that the station data is generally unreliable. This supports a bid to deploy a short temporary seismic array on Cayambe and perhaps another active Andean volcano. If with more reliable seismic waveform data, the methodology and interpretations presented in this thesis could be replicated at Cayambe and another proximal system, this would further support the case to re-assess the current monitoring network. Particularly at Cayambe volcano where the research in this thesis highlights the potential secondary hazards from an unexpected eruption. Reproducible results with a temporary seismic network would also consolidate some of the models in this thesis. It would also highlight the potential for monitoring and the detailed analysis that could exist for currently unmonitored systems, such as Atitlán.

In appendix section A.3.1 I present a very cursory initial investigation into peak dynamic strain at Tungurahua volcano. In order to conduct a more statistically robust analysis, I would like to expand this study to include more volcanoes and tectonic earthquakes. The only requirement for a candidate volcano would be a single operating broadband seismometer. There is sufficient monitoring on Guagua-Pichincha, Cotopaxi, Chiles-Cerro Negro and

Reventador to investigate the PDS, and each of these systems have demonstrated swarm-type seismicity in recent years (fig 1.1). I would look to use a ranked estimated maximum ground motion method (appendix section A.3.3) to consider, the largest 50 or 100 earthquakes, rather than a sample of 13. There is scope to expand this work even further by more accurately calculating the surface wave magnitude, as opposed to using a more crude estimate. When multiple candidate volcanoes at different phases of eruption are considered, the findings will hopefully answer some of the outstanding questions about optimal conditions for volcanic triggering. A large scale and more robust study would also have further implications for considering volcano-tectonic interactions at other intermediate-composition arc volcanoes around the world.

8 | Conclusions

This thesis presents a new, unified methodology for the analysis of seismic signals. It will benefit volcanoes that are subject to limited monitoring and has the advantage of relying only on single station, single component data. However, it can also be readily adopted for volcanoes monitored with multiple stations and I envisage this being a useful approach at many at other volcanoes globally. I have addressed the differences between the Q factor methods commonly used in the literature and automated the auto-regressive moving-average (ARMA) approach such that it can return results for thousands of earthquake signals in seconds. Furthermore I have automated functions to quantify the rise and fall time of an emergent signal ($K_{1,2}$). Going forward, there is flexibility to update the signal processing routine as required for the capabilities and data availability at a volcano; this includes new methodologies, such as the Bayesian approaches in chapter 5. The signal processing routine has been proven to work in conjunction with gas flux and tilt data, as well as long-term catalogue statistics, to inform a more well-balanced interpretation of unrest. In the development stages, it was successfully tested against synthetic waveforms and subsequently applied to real and varied volcano-seismic catalogues and waveform data from Ecuador.

By using the methodology, I have generated robust and reliable signal metrics to characterise earthquake data at both Tungurahua and Cayambe. In turn, I have proposed two different models for seismicity associated with persistent and reawakening processes. Firstly, I have identified long term trends in persistent, periodic LP seismicity at Tungurahua between 2012 and 2016. The analysis of seven periodic 'drumbeat' episodes like this, together,

is the first of its kind. The findings in this chapter demonstrate a cyclical pattern in the seismicity controlled by the repeated rupture and resealing of an upper conduit plug. This model has been speculated previously at Tungurahua from the study of ejecta deposits, however, this is the first time that the seismicity has been connected with the process. Drumbeat seismicity is associated with plug rupture and resealing in four of the seven episodes identified and plays an important part in defining and understanding the persistent unrest between 2013 and 2015. In turn, this cyclical pattern in drumbeat seismicity is inherently related to the occurrence of explosive vulcanian eruptions. The signal characteristics, extracted by the methodology, distinguishes three separate styles of unrest at Tungurahua. Specifically, the cross correlation analysis identifies a marked shift in the signal frequency, envelope and duration of earthquakes from pre-2012 strombolian activity, to vulcanian plug-rupture cycles in 2013, to drumbeats in November 2015.

A Bayesian statistical approach highlights significant episodes of drumbeats and quantifies the temporal rates and patterns in drumbeat seismicity. This focuses on the very last part of the idealised cycle proposed for vulcanian eruptions, with decreasing rates of seismicity during plug resealing, and increasing rates of seismicity prior to initial failure. Again, this is the first time that different episodes of drumbeats have been considered like-for-like and in the same source mechanism, rather than as isolated episodes. By using a Markov chain Monte Carlo (MCMC) approach, I have demonstrated that decreasing rates of seismicity can be modelled by a power law with an exponent close to 1, and drawn similarities with statistical models of tectonic mainshock-aftershock sequences. I have also applied the method to examine accelerating episodes of LPs and highlighted the need for care and consideration when labelling volcanic-seismicity as 'precursory'. In two of the seven periodic episodes identified in December 2012 and July 2013, increasing rates of drumbeat LPs were identified prior to explosions, although these were significantly different in terms of the explosion energy and subsequent PDC run-out. In this instance, I have demonstrated that careful use of temporal statistics alongside the results of the signal processing methodology, could be used

for successful real-time hazard assessment. In contrast, however, I have also raised the issue of 'false precursors'. An MCMC model is used to hind-cast an eruption in November 2015 and demonstrated the first example of a 'failed explosion' at Tungurahua. Careful analysis of the temporal patterns in seismicity has helped us to understand the fragile state of the conduit dynamics towards the end of the recent eruptive phase at Tungurahua.

This model of persistent seismicity is in contrast to unrest at Cayambe volcano. I have built upon models of reawakening processes at dormant volcanoes and infer the 2016 seismic crisis was related to the stalled ascent of new magma. By determining typical Q values 9.9, I have demonstrated that LP seismicity is caused by the resonance of a fluid in a hydrothermal system, and ruled out glacial basal-slip as a seismic source mechanism. This chapter further tested the capability of the methodology incorporating a more varied catalogue of earthquake types. Cross correlation analysis clearly distinguished distal VTs associated with slip on regional faults, and proximal VTs beneath the main cone that are more likely linked to the movement of magma itself. Furthermore, I considered models of static triggering to infer that a dilational stress change in the regional crust equivalent to 0.1 bar as a result of the M_w7.8 Pedernales earthquake, may have been sufficient to promote magma ascent and the 2016 unrest. I have also demonstrated that despite experiencing a similar static stress change as Cayambe, Tungurahua was unaffected by the Pedernales earthquake. This has contributed further to our understanding of the delicate and dynamic relationship between large magnitude tectonic earthquakes and active volcanoes.

At the time of writing this thesis, both volcanoes remain in a period of quiescence. In the instance of a resumption of seismic unrest, the findings in this thesis will help to quickly determine the significance of the seismicity being recorded. This is true both at Cayambe, Tungurahua and to some extent, applicable to our understanding of analogous intermediate-composition arc volcanoes globally. By understanding the internal processes during previous episodes of activity, a more informed judgement can be made about the likely ongoing source process. This in turn will also help to inform hazard assessment and

ensure that local communities are safely and carefully advised and assisted. With a more unified and collaborative approach to understanding the fundamental processes associated with volcanic seismicity, we will be better prepared in the next instance of unrest.

APPENDICES

Appendix A

Investigating volcano-tectonic interactions and triggering processes

Preface

In the the main thesis chapters I have quantitatively characterised the seismicity and in turn, proposed models for the shallow conduit dynamics at both Tungurahua and Cayambe volcanoes. In this section, however, I turn my attention to focus more specifically on research question 7. Here I consider triggered volcanic activity at both Tungurahua and Cayambe, as well as implications for further studies. The Ecuadorian Andes are subject to frequent large tectonic earthquakes, as are so many intermediate-composition arc volcanoes globally. Understanding the complex relationship between volcanic activity and earthquakes can develop our understanding of the seismicity explored in this thesis and further still, inform future monitoring and hazard assessment. Significantly, this frames some of the research in this thesis in a broader context, and examines the case-study volcanoes as more than just isolated systems, but comparable analogues for similar volcanoes.

This chapter has been written in the style of a short, letters-style manuscript, with intention for submission following the thesis. This is an initial investigation which proposes some further research questions for beyond the scope of this thesis. As it is an incomplete study, it is included here as an appendix. I elaborate further on some of these ideas in section, 7.3.

A.1 Introduction

Arc volcanoes are frequently subject to large mega-thrust earthquakes from adjacent subduction zones. Large tectonic earthquakes act to deform the crust locally, but also generate significant surface waves which travel the world (Peng et al., 2011). Both of these can potentially interact with magma plumbing systems and act to encourage or halt volcanic activity (Hill et al., 2002b). In chapter 6 I present a model suggesting static stress changes within the crust due to a large regional tectonic earthquake, may have acted to promote magma ascent or reactivation at Cayambe volcano. Here I explore some of the factors to be considered in volcano-tectonic interactions and any further evidence for triggered activity at both Cayambe and Tungurahua.

This research was further motivated by discussions about dynamically triggered seismicity in the Galápagos archipelago (Bell et al., 2021, *in-press*). Sierra Negra entered a new eruptive phase in 2018 (Bell et al., 2021b) and has remained restless since. This most recent investigation shows evidence for dynamically triggered seismicity in the passing surface wave train of large tectonic earthquakes.

Here I present some initial thoughts and discussion centred on the M_w7.8 Pedernales earthquake, deemed responsible for the reawakening at Cayambe. I then introduce a method to calculate the peak dynamic strain (PDS) and identify candidate tectonic events for triggering seismicity at Tungurahua volcano. I present some initial results and evidence for triggering, and pose further plans for investigation.

A.2 Motivation

A.2.1 Understanding triggering processes

We can think of triggering processes as relating a source (the tectonic earthquake) and a receiver (a critically stressed fault, a volcano, a geyser or hydrothermal system). Triggering processes are most commonly examined in relation to earthquake and aftershock sequences (Elst & Brodsky, 2010; Hill, 2008; Peng et al., 2010). This is perhaps because there are less unknowns with numerically modelling a single fault plane geometry as opposed to a complex magmatic plumbing system (Uchide et al., 2016). Triggering studies relating to earthquake-earthquake interactions, also often rely on optimal conditions at the receiver. In order to be susceptible to triggering, a fault must be pre-stressed sufficiently so that a small perturbation in the stress field can cause failure (Brodsky & Elst, 2014). Other factors such as the geometry of the source and receiver have been shown to influence the optimal conditions for triggering. For example, in studies of coulomb stress failure, the orientation, depth and mechanism of a fault (normal, reverse, strike-slip) can influence the pattern and area affected. Similarly, studies have shown a variation in susceptibility to failure from either Love or Rayleigh waves (Hill, 2008). Defining optimal conditions in a volcanic system is much more complicated. Pore fluid pressures have often been cited as a controlling factor in susceptibility to triggering in volcanic systems (Aiken & Peng, 2014). Sensitivity to triggering may also be dependent on pressure in shallow magma storage, magma rheology and volatile contents (Hill et al., 2002b). In terms of the source-receiver geometry, the orientation of the dominant pressure gradient relative to the orientation of weak edifice scars, regional faults and dykes can all also limit sensitivity to triggering (Prejean & Hill, 2018). The magnitude of stress and strain perturbations also vary with depth (Gomberg & Bodin, 1994). For very well studied earthquakes and faults, such as the 1992 M_w 7.3 Landers earthquake, fault models up to 15 km depth can be used with some degree of confidence (Wollherr et al.,

2019). Even with the very best tomographic imaging and petrological studies of ejecta, it is difficult to accurately determine the size and importantly, the connectivity of a magmatic plumbing system beneath a volcano. As such, when considering a volcano as the receiver in a triggered system, accurately determining the point of failure is almost impossible. We can, however, broadly model the stress and strain tensors and make inferences about triggering, like those proposed in chapter 6.

As introduced in section 6.4.4, changes in stress in the crust encompasses both static and dynamic processes. Static stress changes in the crust causes permanent deformation and typically affects an area equivalent to one or two fault lengths (Aiken & Peng, 2014; Hill et al., 2002b). Dynamic stresses, however, may be experienced much further away and cause large but temporary changes in the crust (Prejean et al., 2004). Studies have also shown that dynamic effects may continue long after the initial surface waves have passed a receiver, either due to cascading triggering processes in aftershock sequences (Brodsky, 2006) or as surface waves pass multiple times around the world (Peng et al., 2011). This may be as long as hours or days. As discussed in Prejean and Hill (2018), by considering longer time frames, it becomes harder to distinguish causation from coincidence and there is more opportunity to draw false correlations. Again, the literature tends to focus on earthquake-earthquake dynamic triggering as opposed to earthquake-volcanic dynamic triggering (Brodsky et al., 2000; Gomberg & Johnson, 2005). This is likely due to the number of uncertainties in volcanic susceptibility.

A.2.2 Static triggering and the M_w7.8 Pedernales earthquake

The model presented in chapter 6 is adapted from Walter and Amelung (2007) and suggests static stress changes in the crust as a result of the Pedernales earthquake, placed Cayambe in a regional dilational regime. In this thesis, I suggest that a relaxation in the crust at Cayambe, promotes the ascension of a new pulse of magma and commences a re-awakening

process. This model is suitable for Cayambe as the focus of the Pedernales earthquake was <200 km to the north-west and numerical models in Béjar-Pizarro et al., 2018 infer that small but long-lasting changes to the state of stress in the crust would extend this far. This stress change would also have affected Tungurahua volcano, which lies within a comparable distance to Pedernales, $\sim$ 250 km. Therefore, it is appropriate to examine the data and assess whether a static stress change in the crust influenced activity at Tungurahua. The Pedernales earthquake also struck at an important point in the timeline of activity at Tungurahua. The earthquake occurred approximately 8 weeks after the final explosions at Tungurahua, and 3 weeks after the alert status at Tungurahua was also reduced to 'low'. Unlike at Cayambe, there was no significant reactionary swarm seismicity indicative of triggered activity. There was a small episode of unrest in mid-May, around 4 weeks after the Pedernales earthquake. In this small episode are five days where between 40 and 80 LP earthquakes are recorded per day and visual observations of fumerolic activity (IGEPN, 2016a). There is a similar short LP swarm in September 2016 that also last approximately 7 days, with comparable LP earthquake rates, also associated with fumerolic activity (fig 2.7). However, each of these swarms were small numbers of LP events relative to both historic LP rates at Tungurahua, and the VT swarm triggered at Cayambe. Beyond these two small swarms in May and September 2016, there is no other significant unrest documented at Tungurahua to present day. This would suggest that a dilational stress regime in the crust did not affect Tungurahua in a way to promote activity, as it may have at Cayambe volcano (Béjar-Pizarro et al., 2018). If we consider again our source-receiver model for triggering activity, it is possible that there was not 'optimal conditions' for triggering at receiver, Tungurahua, in 2016. This could be for a number of reasons. At Cayambe, I suggest that a magma reservoir undergoing dilation may drive magma mixing and further exsolution of volatiles (Sparks et al., 1977; Walter & Amelung, 2007). However, if the explosive episode in February 2016 at Tungurahua caused plug rupture and a complete evacuation of shallow magma storage, it could be that there simply was not enough magma to be perturbed by the Pedernales earthquake (Aiken & Peng,

2014). As explored in chapter 4, there are no drumbeat LPs associated with explosions in 2016. This suggests that shallow conduit dynamics associated with this final eruption were very different to those in 2013 - 2015. Perhaps with no immediate influx of ascending magma, and a slowly sealing upper conduit plug, conditions were not primed for triggering by the Pedernales earthquake in 2016. Particularly then following the 'failed' explosions in late 2015 (chapter 5), where I suggest the conduit dynamics had changed since 2013 - 2014 and it is likely that there was not sufficient pressure for explosions to occur (Cassidy et al., 2018). This optimal state for triggering could also be related to the magma composition, volatile contents, pressure gradient in shallow storage or a change in the deeper origins of the magma (Edmonds & Woods, 2018).

Inspection of the radial tilt data at RETU, suggests a continued and significant inflation signal even after the February 2016 explosions and the Pedernales earthquake. Much like the seismicity records at RETU, where the station is installed high on the flanks of Tungurahua, it is very sensitive to the shallowest dynamics. This might suggest that a very shallow source continues to be pressurised during 2016 but there is a disconnect between deep and shallow plumbing systems, which have distinct triggering thresholds.

The lack of triggered seismicity at Tungurahua following the Pedernales earthquake, does not invalidate the result from Cayambe, but confirms the two volcanoes were in very different dynamic states in April 2016. This also consolidates some of the differences between Tungurahua and Cayambe, that I begin to establish in the previous chapters. It also confirms some of the complexities that are associated with triggering activity at volcanoes. Due to the conditions at Tungurahua, even the 0.1 bar induced normal stress modelled by Béjar-Pizarro et al. (2018) was not adequate to reactivate the system. This poses two questions - has Tungurahua sufficiently 'switched off' such that even a M_w7.8 earthquake within 250 km could not perturb the system? And has Tungurahua ever shown signs of triggering, even when it was persistently active?

A.3 Data & Methods

A.3.1 Dynamic triggering

To further investigate a longer timeline, and to compliment the findings of chapter 4, I consider the potential for dynamically triggered seismicity at Tungurahua volcano. For now, I only examine Tungurahua as figure 6.2 illustrates that there are more significant data gaps at Cayambe; although I discuss the scope for further investigations into dynamic triggering across Ecuador in section 7.3. Tungurahua is also a very good candidate system to examine dynamic triggering as it is well known there is likely shallow magma storage for many years, and a good monitoring network high on the flanks which is sensitive to these most shallow changes. During the 17 years of activity at Tungurahua, 260 M_w >7.0 earthquakes occurred globally, including the Great Tohoku Earthquake in 2011 and the Boxing Day Sumatran Earthquake in 2004 (USGS, 2021). For this reason, again, it is important to distinguish between causality and coincidence, as with such a high number of tectonic earthquakes and volcanic eruptions it would be easy to draw false correlations (Prejean & Hill, 2018). Previous statistical studies have attempted to demonstrate correlations between tectonic earthquakes and volcanic activity (Avouris et al., 2017), however, this is likely to be biased at Tungurahua given the length of this most recent eruptive phase, and therefore inappropriate. Rather than speculatively looking at selected tectonic earthquakes, I here present a systematic investigation by considering the peak dynamic strain (PDS) experienced at Tungurahua, due to surface wave arrivals from distant tectonic earthquakes. This is a cursory initial investigation, to develop the some of the research, but should be expanded into a much larger study beyond this thesis (section 7.3).

A.3.2 Peak dynamic strain (PDS)

To calculate the peak dynamic strain at Tungurahua, before and after the tectonic earthquake, I follow the method proposed in Hill et al. (1993). Tungurahua, has five operational broadband stations which are sensitive to lower frequencies (<0.5Hz) and suitable for examining very long period surface wave arrivals (fig 2.8). In particular, I use data from station BULB as it has the highest signal to noise ratio and is the least prone to battery failure and outages (Hernandez, *per comms.*). However, in later investigations this could easily be expanded to examine the rest of the network.

A.3.3 Identifying tectonic events

In order to initially identify global tectonic earthquakes which may have affected Tungurahua volcano, I run a search for all earthquakes >M_w6.5, with a focus <50 km depth, from 2008 to present day (USGS, 2021). RETU data is readily available from 2008 onwards and given this thesis focuses on unrest from 2012, I do not search for any earlier events. I remove all events within 300 km radius of Tungurahua as we wish to consider the effects of dynamic triggering. Previous studies have suggested that up to 200 km from the source, static stress changes in the crust may also influence volcanic activity (Béjar-Pizarro et al., 2018; Walter & Amelung, 2007). However, I do include the M_w7.8 Pedernales earthquake as this is of particular interest in the timeline of activity. For each earthquake I determine the epicentral distance from Tungurahua, Δ, and retain only events in the range $20° < \Delta < 160°$, as per International Seismological Centre (ISC) convention (Bondár & Storchak, 2011; Kayal, 2008). It is suggested that beyond 160° surface wave amplitudes increase unexpectedly (Kárník et al., 1962). Using estimated surface wave magnitude (M_s) values I calculate the estimated maximum horizontal ground movement, A (μm), for surface waves with a period,

T, 20s (eq A.1).

$$M_s = log\left(\frac{A}{T}\right)_{max} + 1.66log\Delta + 3.3 \quad \text{(A.1)}$$

This is a crude approximation in order to identify candidate events for triggering. True surface wave modelling would be more appropriate in a large scale study to calculate M_s (section 7.3). I then use the estimates for maximum horizontal ground movement to rank the tectonic earthquakes from smallest to largest. This catalogue is the basis for candidate event selection. I systematically remove any events where aftershocks are included as separate events to a larger mainshock, as I want to consider only the mainshock impact initially. Examination of the ranked events suggested that many of the largest estimates were from thrust events located along the west coast of South America, associated with the subduction of the Nazca Plate. In order to generate a representative catalogue of different source mechanisms and locations relative to Tungurahua, I hand pick a selection of events with lower estimated maximum ground motions to analyse, in addition to the top ranked earthquakes. The earthquakes are plotted in figure A.1 and detailed in table A.1. I also try to define a catalogue of candidate events that are well distributed across the timeline of activity at Tungurahua (fig A.2). I choose two very deep earthquakes ($\geq$150 km, events 9 and 11) to contrast with the shallower tectonic events. I also include the complex 'triple' earthquake sequence from the Solomon Islands in 2013, where there are three consecutive earthquakes with thrust, normal and strike-slip source mechanisms within 60 minutes (table A.1, events 6, 7, 8). The shortlisted 13 events then represent a range of source mechanisms, strike orientations relative to Tungurahua, epicentral distances, depths and magnitudes. For each earthquake, I calculate approximately the time at which the surface waves would pass Tungurahua and examine the waveforms from broadband station, BULB (fig 2.8). For the raw waveform at station BULB, I deconvolve the instrument response and rotate to consider the radial and transverse components of the signal. I then resolve the maximum velocity according to all three components. The peak dynamic strain experienced at BULB is calculated as the maximum velocity, V, divided by the apparent propagation speed, C, of the

incoming surface wave (eq A.2). I use an approximate speed 4 kms^{-1} for Rayleigh waves (Elst & Brodsky, 2010).

$$PDS = \frac{max(V)}{C} \tag{A.2}$$

I also plot the spectrograms at RETU and BULB, 30 minutes either side of the incoming surface wave in order to manually inspect for evidence of dynamically triggered events. Given shallow volcanic seismicity is captured best at station RETU, I then also plot the RSAM, tilt and event counts for 12 hours, 3 days and 7 days before and after the incoming surface wave arrivals. Taking longer windows allows us to measure any long term changes in the activity at Tungurahua as a result of the tectonic event. However, looking at longer windows introduces more room to interpret coincidental activity, and so great care must then be taken in the analysis.

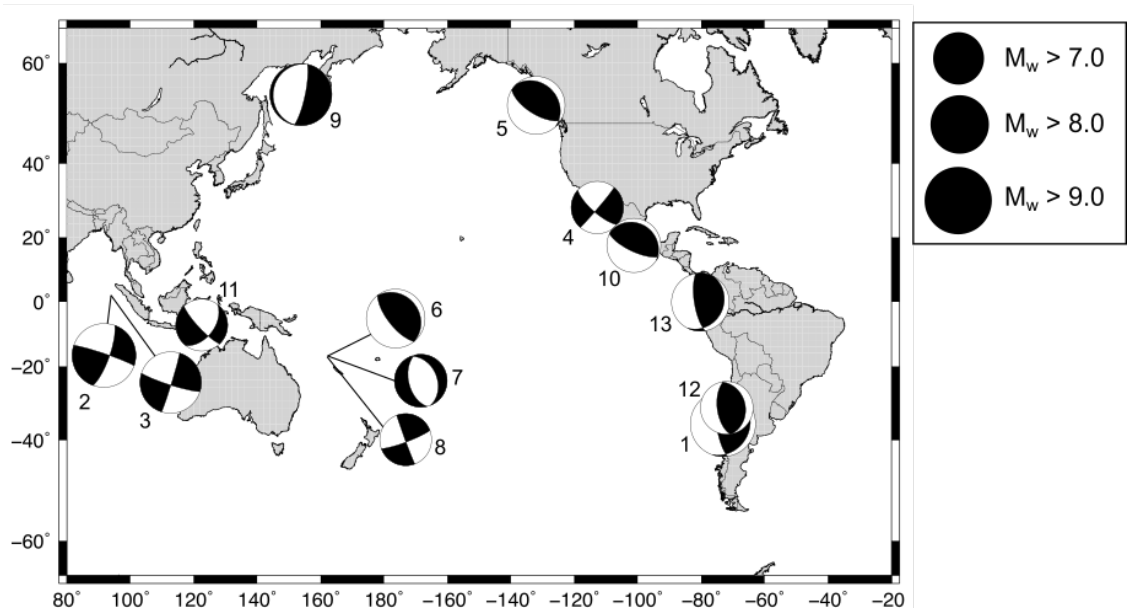

Figure A.1 Map illustrating candidate events used to determine peak dynamic strain. CMT solutions from the global CMT catalogue (Ekström et al., 2012). Event numbers correspond to table A.1.

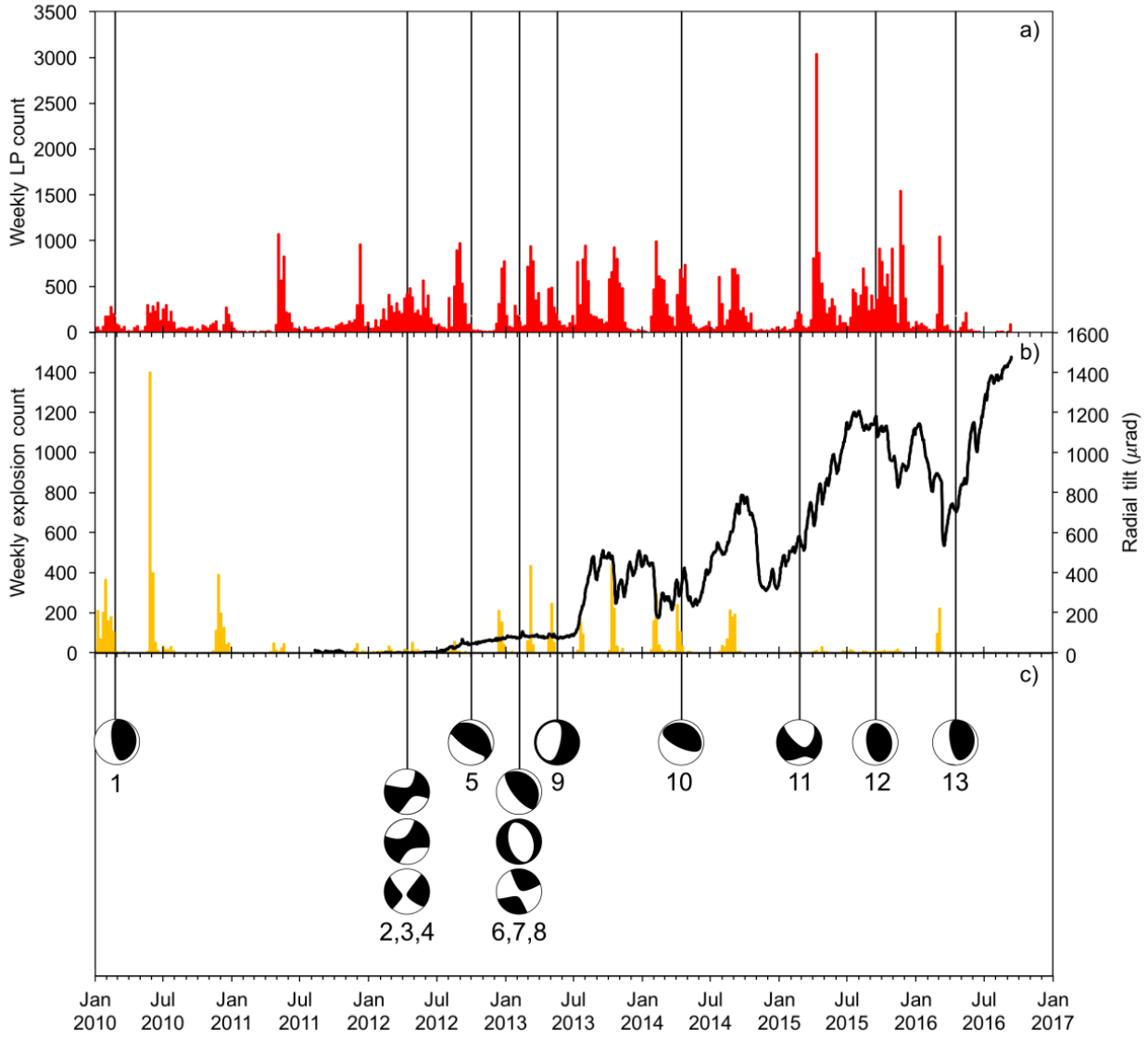

Figure A.2 Timeline adapted from fig 4.1 illustrating candidate events used to determine peak dynamic strain. *a)* Weekly LP seismic event counts at RETU from the IGEPN catalogue, *b)* Weekly explosion counts and tilt at RETU, *c)* CMT solutions from the global CMT catalogue (Ekström et al., 2012). Event numbers correspond to table A.1.

	DateTime (UTC)	**Location**	**Lat**	**Lon**	**Distance (km)**	**Depth (km)**	$\mathbf{M}_w$	**Δ (°)**	**Az (°)**
1	2010-02-27T06:34:11	Offshore Bio-Bio, Chile	-36.122	-72.898	3895.3	22.9	8.8	35.03	172.18
2	2012-04-11T08:38:36	Off the west coast of northern Sumatra	2.327	93.063	19066.5	20.0	8.6	171.47	84.10
3	2012-04-11T10:43:10	Off the west coast of northern Sumatra	0.802	92.463	19001.5	25.1	8.2	170.89	94.10
4	2012-04-12T07:15:48	Baja California, Mexico	28.696	-113.104	49867.0	13.0	7.0	44.85	314.98
5	2012-10-28T03:04:08	Haida Gwaii, Canada	52.788	-132.101	7811.9	14.0	7.8	70.25	328.83
6	2013-02-06T01:12:25	75 km W of Lata, Solomon Islands	-10.799	165.114	12856.7	24.0	8.0	115.62	257.28
7	2013-02-06T01:23:19	112 km WSW of Lata, Solomon Islands	-11.183	164.882	12876.6	10.0	7.1	115.80	256.83
8	2013-02-06T01:54:14	33 km NW of Lata, Solomon Islands	-10.499	165.588	12809.2	8.8	7.0	115.20	257.67
9	2013-05-24T05:44:48	Sea of Okhotsk	54.892	153.221	12474.3	598.1	8.3	112.18	330.84

	DateTime (UTC)	**Location**	**Lat**	**Lon**	**Distance (km)**	**Depth (km)**	$\mathbf{M}_w$	Δ (°)	**Az** (°)
10	2014-04-18T14:27:24	33 km ESE of Petatlan, Mexico	17.397	-100.972	3239.6	24.0	7.2	29.13	311.33
11	2015-02-27T13:45:05	130 km N of Nebe, Indonesia	-7.297	122.535	17491.7	552.1	7.0	157.31	247.00
12	2015-09-16T22:54:32	48 km W of Illapel, Chile	-31.573	-71.674	3422.0	22.4	8.3	30.77	168.68
13	2016-04-16T23:58:36	Pedernales	0.3819	-79.922	263.4	20.6	7.8	2.37	321.42

Table A.1 Candidate events used for dynamic triggering analysis at Tungurahua

A.4 Results

The estimated ground displacement, actual ground displacement and PDS values are detailed in table A.2. Particularly for events which fall outside the initial conditions (depth <50 km, $20° < \Delta < 160°$) there is a clear discrepancy in the displacement and PDS values generated. For example, where event 13 occurs <300 km from Tungurahua, there is a large disparity between the estimated and true maximum ground displacement. Similarly for event 11 where the earthquake focus is >150 km, the surface wave approximation generates a large disparity in the estimated values. Previous studies of earthquakes being dynamically triggered have suggested a dynamic strain threshold in the order of 10^{-6} must be passed (Gomberg et al., 2001). However, statistical modelling has suggested that threshold may even be as low as 10^{-9} (Elst & Brodsky, 2010). On this basis, some of the candidate earthquakes where strain is $< 10^{-6}$, are unlikely to generate enough dynamic strain to trigger failure. As discussed previously, however, the receiver in this model is not a pre-stressed tectonic fault, but a volcano. And internal conditions such as the state of the conduit, and shallow magma storage will affect susceptibility to triggering, in addition to surpassing a strain threshold (Prejean & Hill, 2018). For the majority of earthquakes considered in this precursory investigation, there is no substantial evidence for dynamic triggering. Some earthquakes do show potential signs of volcano-tectonic interactions which should be investigated further.

Despite being the largest earthquake analysed, the M_w8.8 Bio-Bio earthquake in 2010 (event 1) exhibits no obvious dynamic triggering within the passing surface wave train. One study of dynamic triggering in a tectonic setting suggests that triggered events may occur up to 10 days after the passing surface waves (Brodsky, 2006). However, in the 7 days before and after the earthquake, the station RETU is poorly operating and no volcanic-earthquakes can be clearly identified. This the first of many instances where the signal quality is compromised and in turn, provides further justification for a larger scale study across multiple volcanoes and networks.

	DateTime (UTC)	**Location**	**Est. amp (cm)**	**PDS (x10^{-7})**	**Max. amp (cm)**
1	2010-02-27T06:34:11	Offshore Bio-Bio, Chile	1.73	4.50	1.20
2	2012-04-11T08:38:36	Off the west coast of northern Sumatra	0.078	0.64	0.26
3	2012-04-11T10:43:10	Off the west coast of northern Sumatra	0.031	0.28	0.18
4	2012-04-12T07:15:48	Baja California, Mexico	0.018	0.051	0.031
5	2012-10-28T03:04:08	Haida Gwaii, Canada	0.054	0.12	0.023
6	2013-02-06T01:12:25	75 km W of Lata, Solomon Islands	0.038	0.027	0.016
7	2013-02-06T01:23:19	112 km WSW of Lata, Solomon Islands	0.0047	0.027	0.016
8	2013-02-06T01:54:14	33 km NW of Lata, Solomon Islands	0.0038	0.027	0.016
9	2013-05-24T05:44:48	Sea of Okhotsk	0.079	0.26	0.074
10	2014-04-18T14:27:24	33 km ESE of Petatlan, Mexico	0.0589	0.14	0.026
11	2015-02-27T13:45:05	130 km N of Nebe, Indonesia	0.0023	0.0093	0.0011
12	2015-09-16T22:54:32	48 km W of Illapel, Chile	0.68	2.40	0.51
13	2016-04-16T23:58:36	Pedernales	15.11	34.2	4.80

Table A.2 Results of peak dynamic strain analysis for tectonic events interacting at Tungurahua volcano

The Sumatran strike-slip earthquakes in 2012 (events 2 and 3) were not initially included when ranking estimated maximum ground motion as they lie beyond the epicentral distance threshold at >160°. However, they form an interesting sequence of events where the two large Sumatran earthquakes (M_w 8.6 and 8.2 respectively) are followed by a M_w 7.0 strike slip event in Baja, Mexico, less than 24 hrs later (event 4). There is no evidence from the broadband data at BULB that there are dynamically triggered volcanic earthquakes within the passing surface wave train. Yet 4 hrs after the Baja earthquake, there is a large high amplitude clipped signal at RETU, which in chapter 4 was established as an explosion event that commenced a sequence of drumbeat LPs that last several hours (fig 4.3). The explosion is not the first in this time frame - the catalogue details eleven explosions on 9th April, two on 10th, one on the 11th, this particular explosion on 12th April and one more on 13th April. This is however, the first recorded instance of drumbeat seismicity.

There are visible volcanic earthquakes coincident with tectonic surface wave arrivals during the Okhotsk, Petatlan and Illapel earthquakes (events 9, 10 and 12) (figs A.5, A.6, A.4). These all correspond to periods of heightened activity at Tungurahua, particularly Petatlan which occurs during an explosive sequence in Episode 5 (chapter 4) and Illapel during quasi-periodic seismicity in Episode 7. These three instances are also periods where the signal quality at RETU is frequently out or compromised with noisy artefacts.

One study of dynamic triggering in geothermal and volcanic regions, quantifies a β-statistic to determine local seismicity rates before and after a large tectonic earthquake (Aiken & Peng, 2014). In figure A.3 I show the hourly RSAM, tilt data and catalogue event counts for 7 days either side of the Illapel earthquake. The inconsistencies in the RETU signal this time are clear in the fluctuating RSAM and so from this data alone, I cannot confidently determine a β-statistic. Overall the seismicity rate is low (<5 earthquakes per hour) although there is a marked upturn in seismicity rate coincident with a significant deflation signal (>80μrad) approximately 4 days after the tectonic earthquake. Tilt data measurements are crude as there is only a single value that can be extracted per day, but

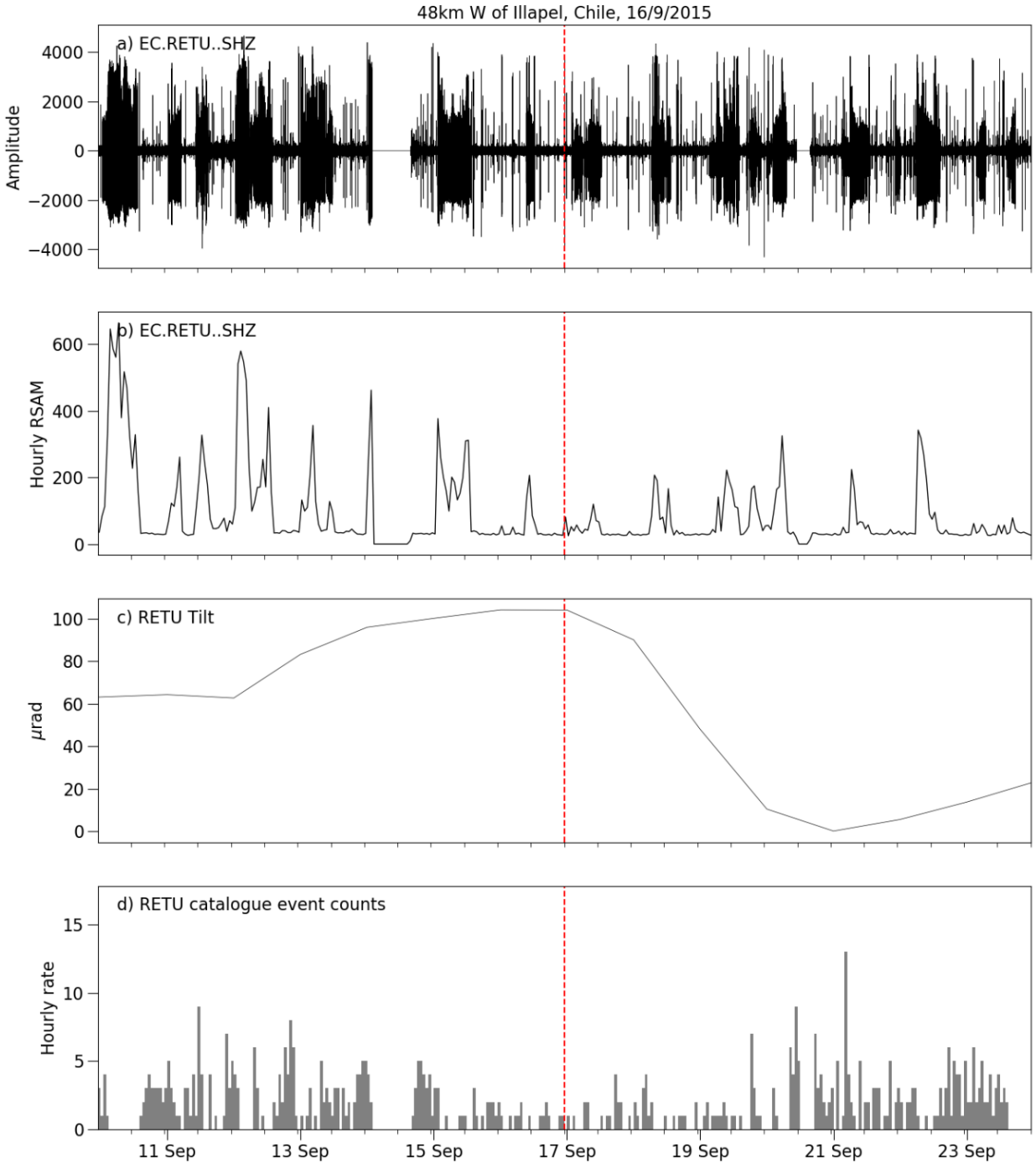

Figure A.3 Summary of activity at Tungurahua ±7 days from Illapel earthquake (event 12, table A.1) *a)* Raw waveform data at RETU, *b)* Hourly RSAM from RETU, *c)* Tiltmeter data from RETU and *d)* Histogram of hourly seismic event counts from IGEPN catalogues.

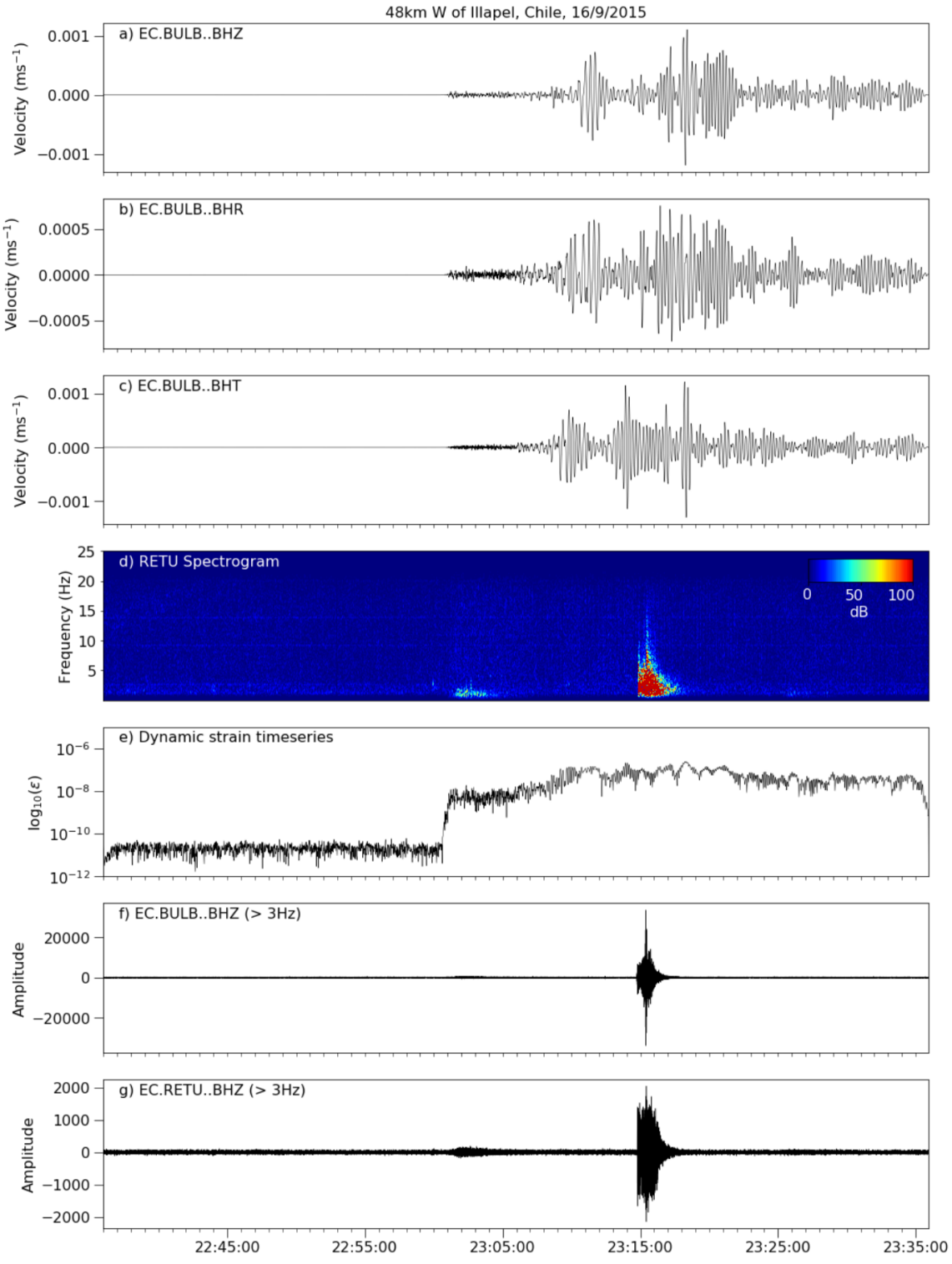

Figure A.4 Peak dynamic strain (PDS) at Tungurahua following the Illapel earthquake. Showing seismographs from *a)* BULB vertical, *b)* radial and *c)* transverse components, *d)* spectrogram from RETU, *e)* calculated peak dynamic strain at BULB, and seismographs for *f)* BULB and *g)* RETU bandpass filtered >3Hz.

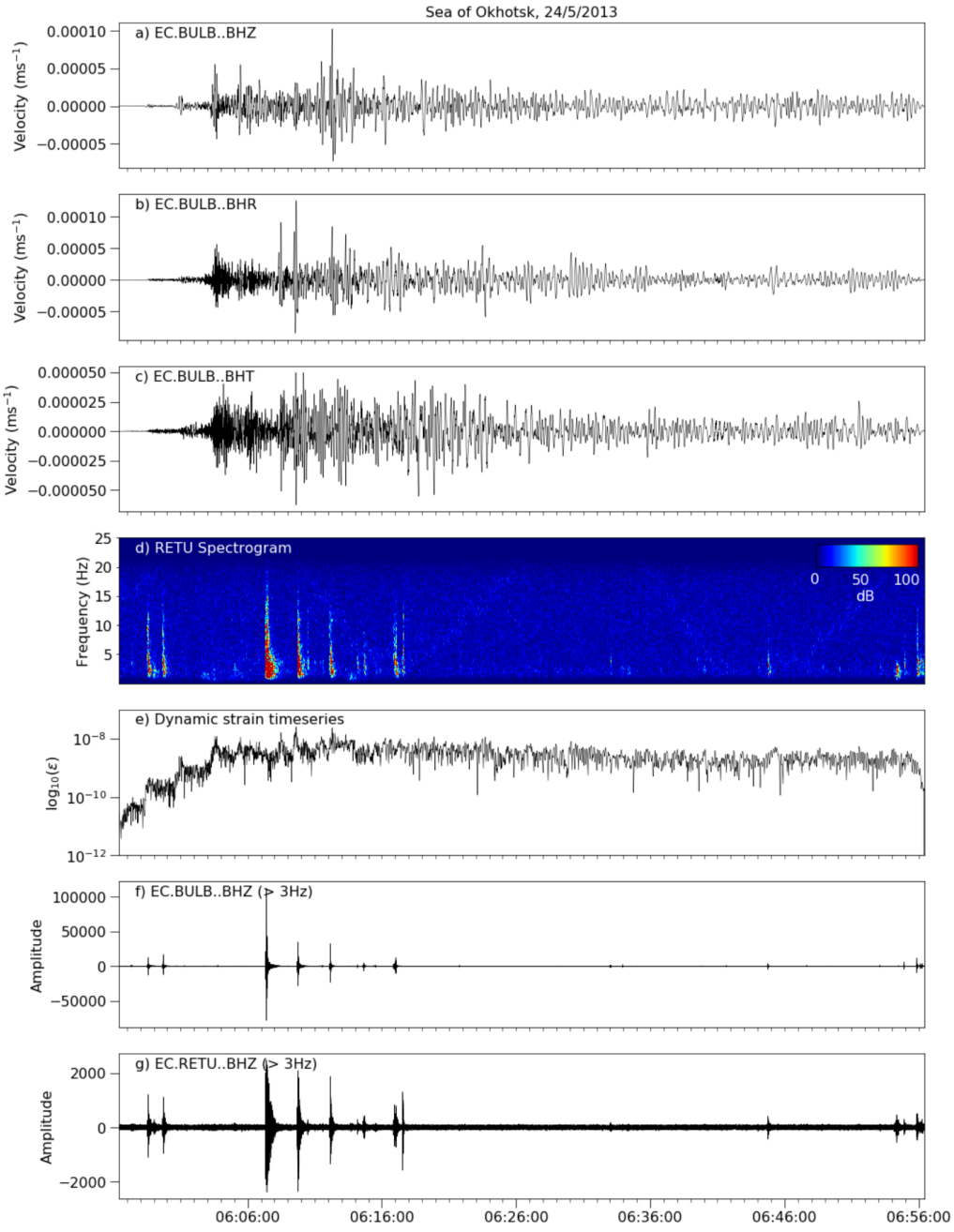

Figure A.5 Peak dynamic strain (PDS) at Tungurahua following the Okhotsk earthquake. Showing seismographs from *a)* BULB vertical, *b)* radial and *c)* transverse components, *d)* spectrogram from RETU, *e)* calculated peak dynamic strain at BULB, and seismographs for *f)* BULB and *g)* RETU bandpass filtered >3Hz.

the Illapel earthquake does occur around the peak in this particular inflation cycle. This would invite a more detailed further study in future, perhaps using InSAR data to more

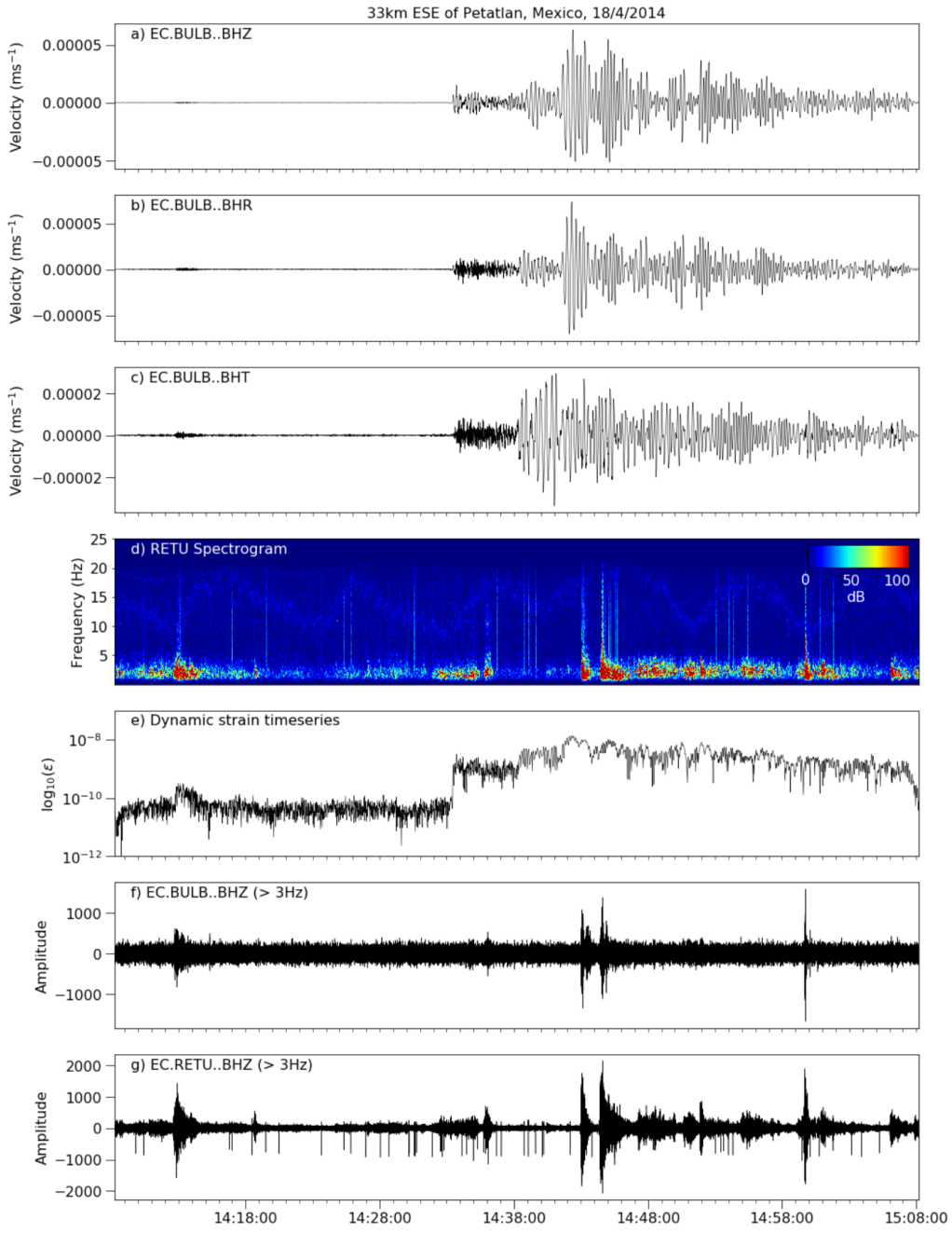

Figure A.6 Peak dynamic strain (PDS) at Tungurahua following the Petatlan earthquake. Showing seismographs from *a)* BULB vertical, *b)* radial and *c)* transverse components, *d)* spectrogram from RETU, *e)* calculated peak dynamic strain at BULB, and seismographs for *f)* BULB and *g)* RETU bandpass filtered >3Hz.

accurately determine any deformation on the very high flanks of Tungurahua. I would also like to manually pick earthquakes from the signal at RETU during this 14 day period to ensure a robust catalogue of events is analysed. This sequence is comparable to the explosion cycles described in chapter 4 or more likely the failed explosive episodes in chapter 5 as there are only 2 small explosions recorded in IGEPN catalogues for this time period, that do not correlate to the event shown in figure A.4.

A.5 Discussion

From this initial investigation there is no single earthquake which confidently provides clear evidence for dynamic triggering. Certainly not as convincingly as te static triggering model described at Cayambe in chapter 6. However, there are potentially triggered episodes and reasons to investigate further, particularly the Petatlan and Illapel earthquakes (events 10 and 12 in tables A.1 and A.2). These are both thrust earthquakes, occurring to the north and south of Tungurahua respectively, but the strike of each earthquake are almost perpendicular to one another, posing two different orientations relative to Tungurahua. The larger M_w8.3 earthquake at Illapel generates a PDS and maximum ground motion that are each an order of magnitude larger than those associated with the M_w7.3 Petatlan earthquake. They each occur during two contrasting styles of eruption at Tungurahua and hence possibly two different dynamic states in the conduit. Particularly for the Petatlan earthquake which occurs during the more predictable and repeatable cycles of Vulcanian explosions in 2014, it is possible that even though the peak dynamic strain was less here than during other earthquakes considered, there may have been 'optimal' conditions in the shallow edifice to promote the next explosive episode. Whereas in 2015 for the Illapel earthquake, there were a handful of small subsequent explosions in the passing surface wave train. Despite the fact the earthquake produced a larger strain at Tungurahua, it may not have been enough to fully trigger an explosive episode if the shallow edifice was not primed to do so. I would like

to look at both of these events in a much more detailed study using more station data and the β-statistic (Aiken & Peng, 2014).

I would also like to contrast the potentially triggered seismicity from these two thrust earthquakes, with strike-slip tectonic earthquake interactions. The double Sumatran earthquake sequence followed by the Baja, Mexico earthquake occur immediately before an episode of drumbeat LPs. Significantly, the Sumatran earthquakes should not have been included in the initial search for candidate trigger earthquakes according to the threshold parameters defined by Kárník et al. (1962) as they lie more than 160° from Tungurahua. The PDS and maximum ground deformation from the Baja earthquake is lower than those of the Sumatran earthquakes, but the focus is much closer to Tungurahua. I would need to investigate more sequences of tectonic earthquakes in short succession but at different source locations in order to determine the most influential parameter. No other strike-slip tectonic earthquakes in this small study appear to trigger any volcanic activity at Tungurahua. As such, I would also like to explore further to determine whether this is related to more shear, strike-slip events not being as successful as trigger sources, or if this related to sub-optimal conditions in the receiver at the time.

Ultimately, from 13 candidate earthquakes, there are 3 which show potential for volcano-tectonic interactions, however a much larger study is required to confidently model a triggering process at Tungurahua. This would require using more station data and a better catalogue of volcanic earthquakes in order to determine long term temporal statistics before and after the tectonic earthquake. As established by previous studies, the relationship between volcanic systems and large tectonic earthquakes is complicated (Uchide et al., 2016) but this initial investigation and the findings in this thesis suggest that Tungurahua is a good candidate volcano to explore this question.

A.6 Conclusions

By examining the static and dynamic stress and strain models for Tungurahua, this chapter takes significant steps to specifically answer research question

7. Is there any evidence for volcano-tectonic interactions at Tungurahua and Cayambe?

Whilst the evidence is compelling that a static stress change from the Pedernales earthquake was a crucial component in the reawakening at Cayambe, it is striking how unaffected Tungurahua appears to be. Yet all other evidence suggests Tungurahua is an excellent candidate system to study dynamic triggering. This poses further questions about how long lasting the on going quiescence at Tungurahua might be. If Pedernales and no earthquake since has shown any effect then perhaps the 'switching-off' in 2016 was more than a temporary dynamic change to the internal system. The initial results in this chapter are promising and suggest there is scope for evidence of triggering, which can be consolidated with a further, more robust, statistical study.

In terms of research questions 1 and 6, it is important to understand how triggered seismicity can be identified through routine signal processing, and how it may affect decision-making in hazard assessment. If a volcanic system is in an 'optimal' position to be triggered, for example, with stored shallow magma approaching critical overpressure, then dynamic triggering from a large tectonic earthquake may act to accelerate the process of an explosion. In a period of very cyclical, repeating episodes of Vulcanian explosions, an explosion may occur sooner than expected and so rapid action will have to be made to communicate imminent risks to the surrounding communities.

Appendix B

Supplementary figures

B.1 Chapter 4: Supplementary figures

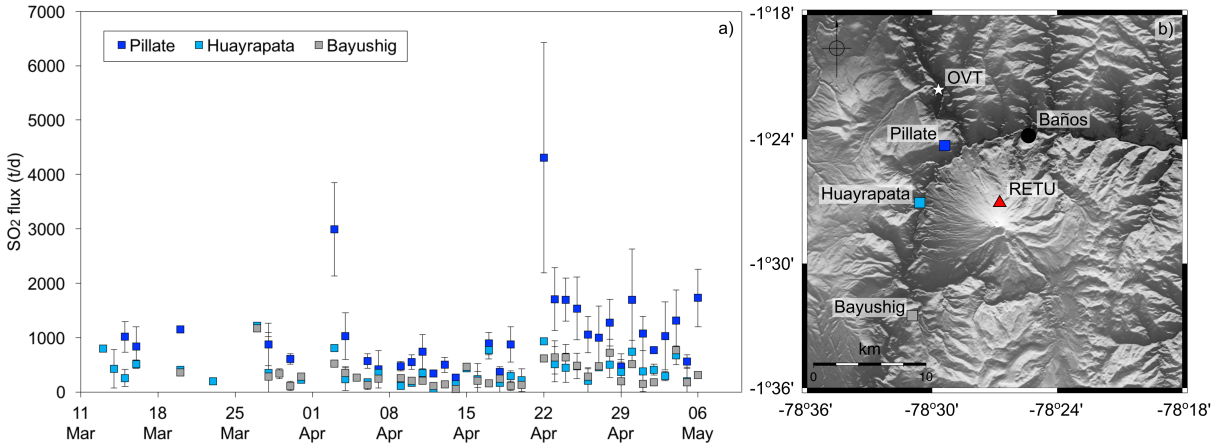

Figure B.1 Episode 1: SO_2 flux, *a)* Flux values and errors in tonnes per day, at three DOAS stations, *b)* Map indicating the three DOAS station locations, in addition to short period seismometer, RETU (red), local observation station, OVT (white) and the town of Baños (black).

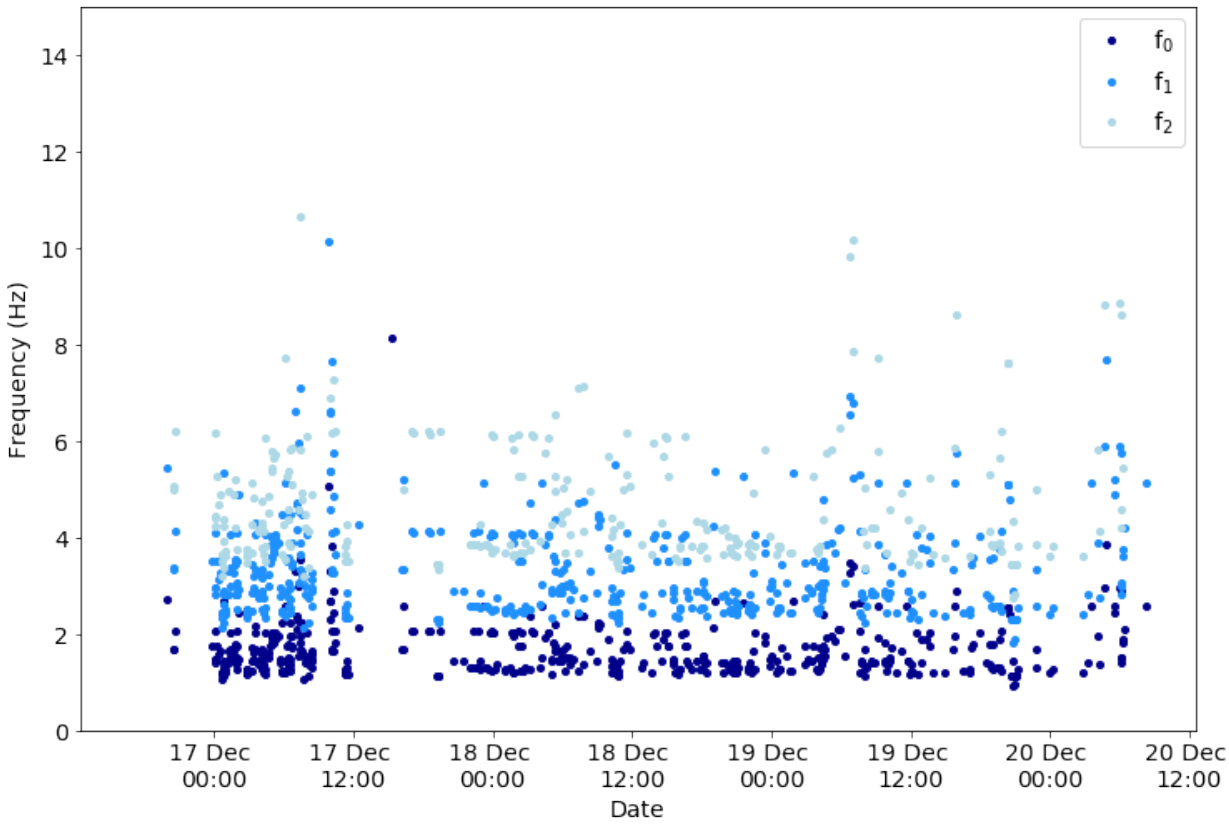

Figure B.2 Episode 2: December 2012. Fundamental and harmonic frequencies identified by harmonic product spectrum (HPS) method. 489 minute slices were identified between 12:00 16/12/2012 and 12:00 20/12/2012.

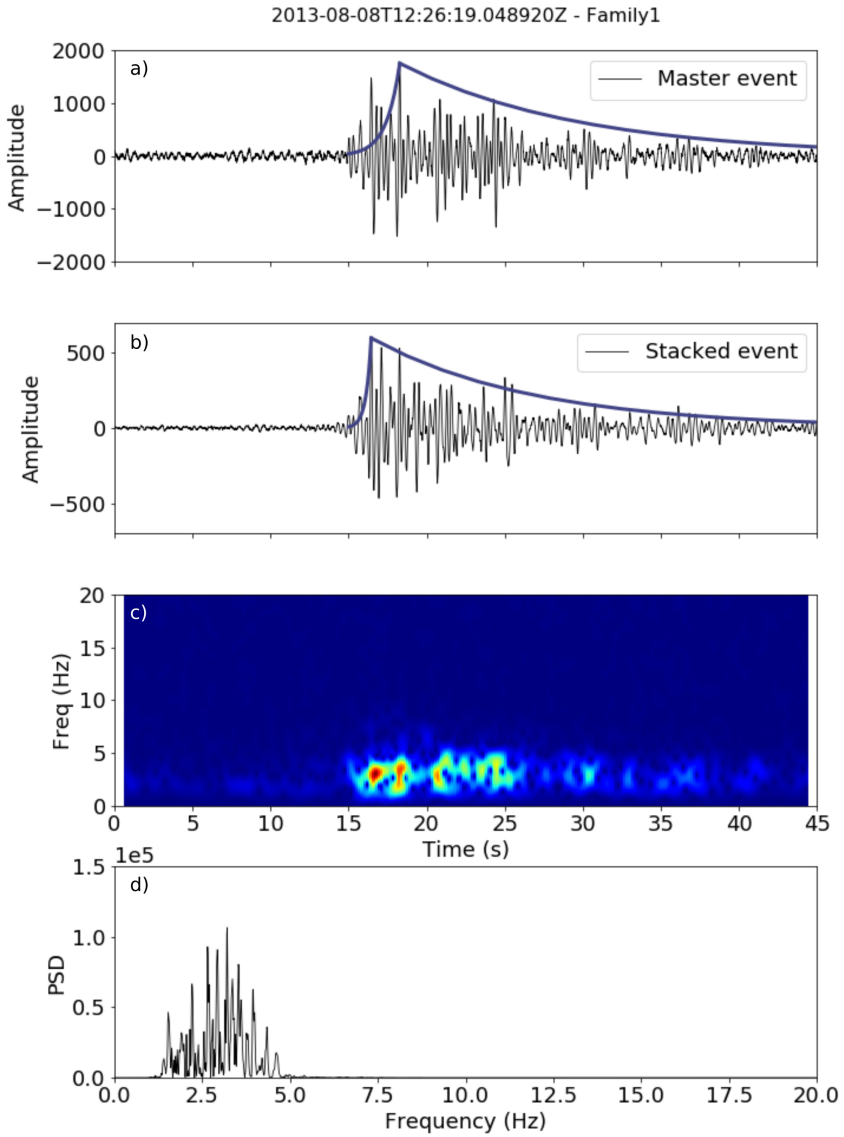

Figure B.3 Episode 3: July - September 2013. Family 1 from the cross correlation analysis. *a)* Master event, *b)* Stacked event from all events in the family, *c)* Spectrogram, and *d)* periodogram of the stacked event. The K_1 and K_2 slopes for each event are marked on panels *a)* and *b)*. Colours of K in this figure and figure B.4 correspond to 4.10.

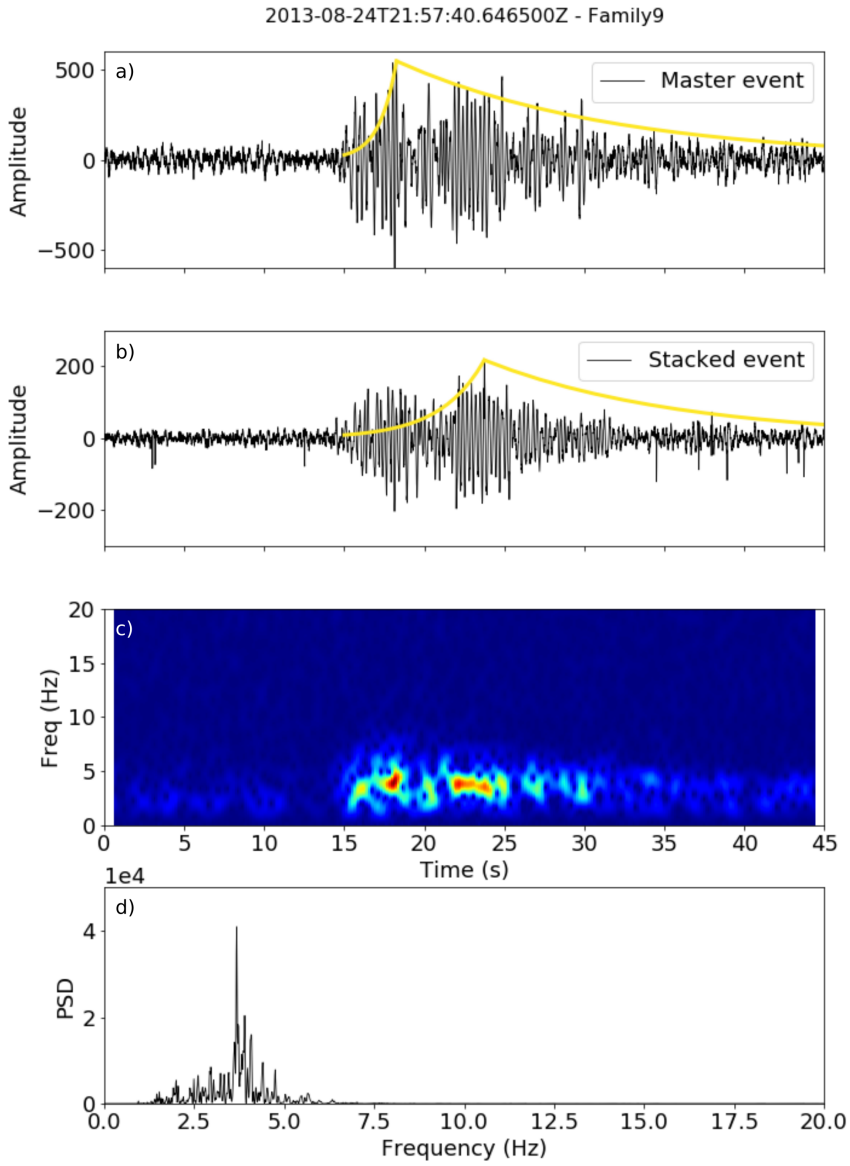

Figure B.4 Episode 3: July - September 2013. Family 9 from the cross correlation analysis. *a)* Master event, *b)* Stacked event from all events in the family, *c)* Spectrogram, and *d)* periodogram of the stacked event. The K1 and K2 slopes for each event are marked on panels *a)* and *b)*. Colours of K in this figure and figure B.3 correspond to 4.10.

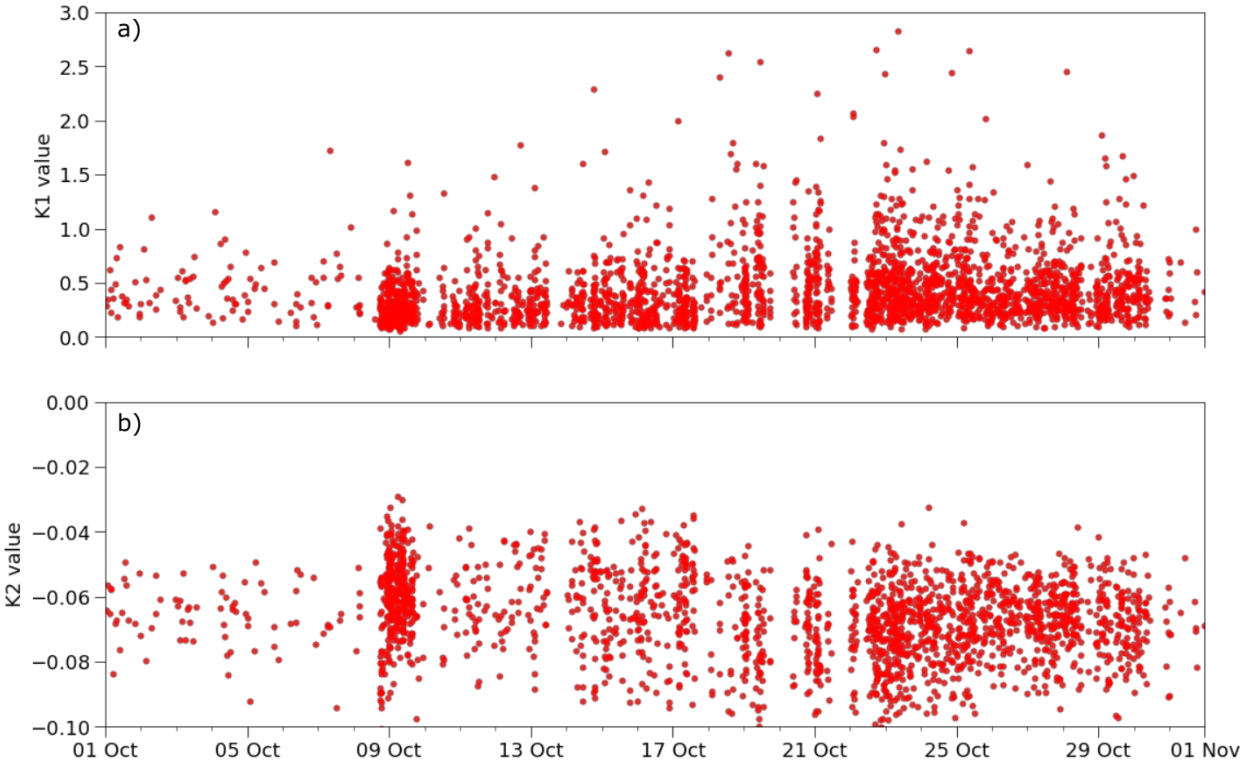

Figure B.5 Episode 4: October 2013, $K_{1,2}$ analysis. Individual events are marked with red circles, *a)* shows K_1 values, and *b)* the K_2 values.

B.2 Chapter 5: Supplementary figures

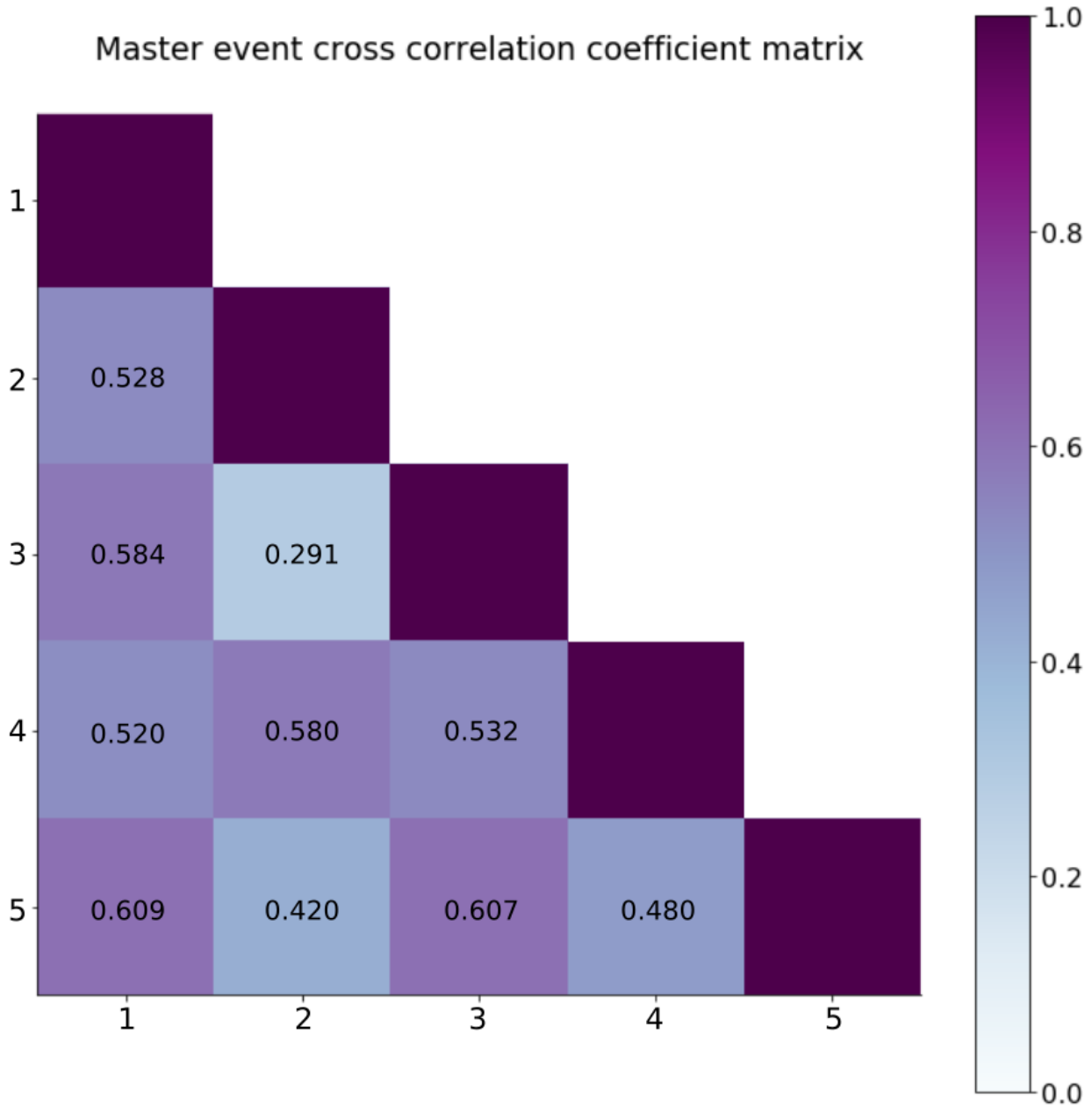

Figure B.6 Cross correlation coefficient matrix for the master events of the 5 largest families in the study.

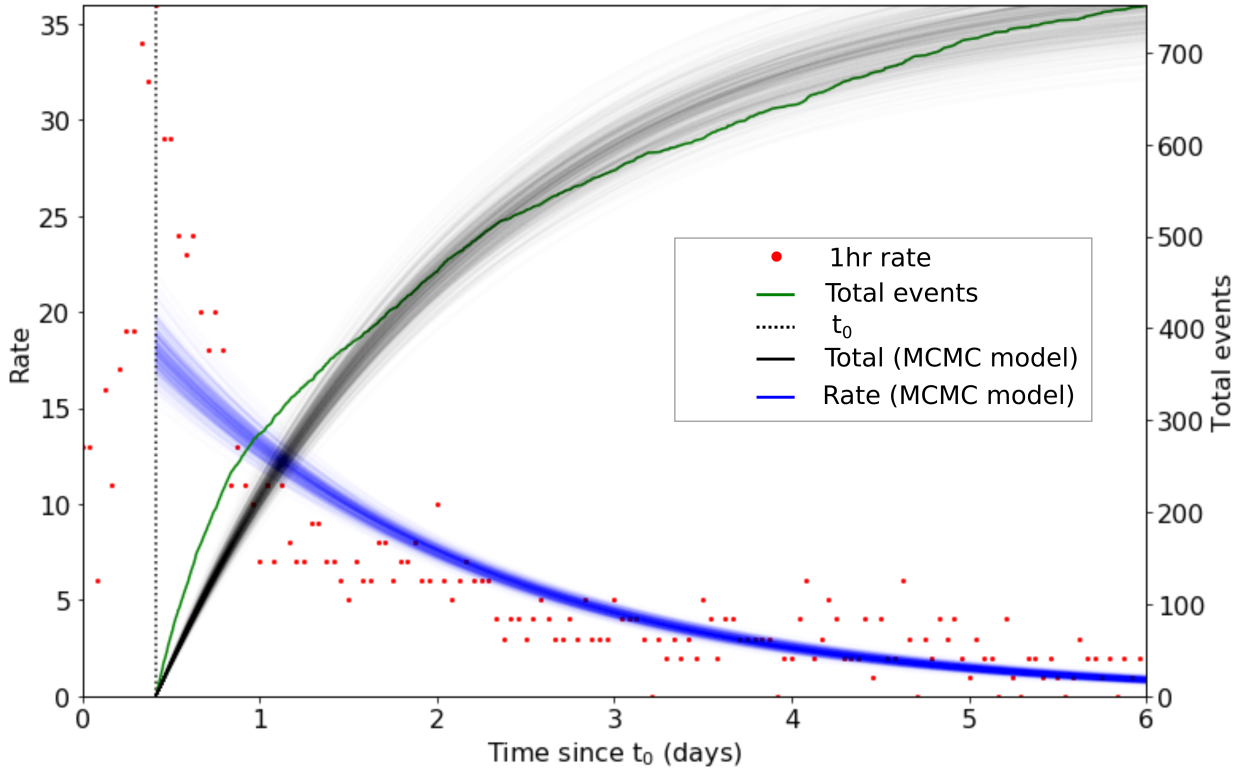

Figure B.7 Exponential model fit for decelerating drumbeat seismic episode. Red circles show event rates. Green marks true total event count. Blue and black lines show rate and total seismic counts respectively, from 500 samples from posterior distributions.

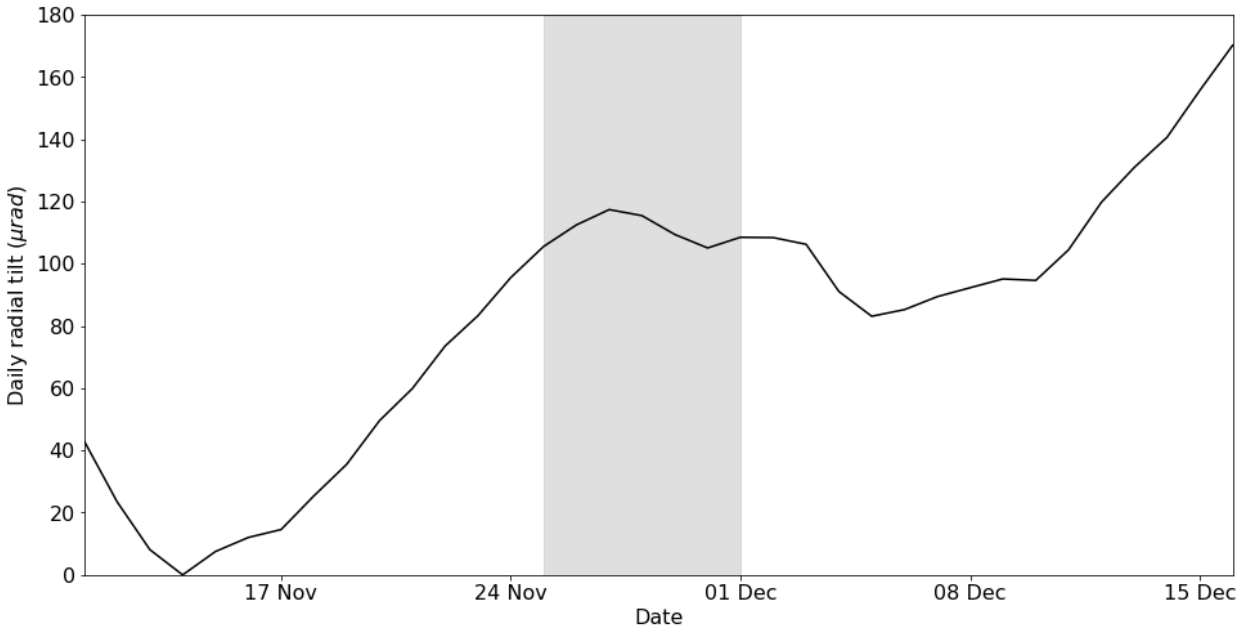

Figure B.8 Radial tilt measurements for station RETU, 11 November - 16 December. Study period marked in shaded window. Two inflationary signals occur outside the study period - one before and one after.

	Parameter	Prior distribution	Prior parameters
Inverse Omori's Law	p	Lognormal	$\mu = 0.1$
	t_f	Exponential	$\lambda = 0.01$
	k	Exponential	$\lambda = 0.01$
Modified Omori's Law	p	Lognormal	$\mu = 1.0$
	t_f	Lognormal	$\mu = 0.3$
	k	Exponential	$\lambda = 0.01$

Table B.1 Prior distribution estimates and parameter information for point process modelling

	Parameter	Best fit value
Inverse Omori's Law	p	0.96 ± 0.51
	t_f	0.53 ± 0.16
	k	123 ± 43.9
Modified Omori's Law	p	0.97 ± 0.51
	t_f	0.53 ± 0.16
	k	237 ± 40.8

Table B.2 Best fit values for model parameters after point process modelling

Appendix C

Working Python code

C.1 Q factor

The function `samples_analysis` takes a catalogue of pick times and slices whole day files into individual 30s traces, sliced 5s before the pick and 25s after. The function `qarma` calculates the Q_{ARMA} values and `qrun` can be executed over thousands of individual traces.

```
import numpy as np


def arma(sample):
    resamp = 25
    P_min = 2       #AR filters
    P_max = 20
    q_min = 0
    q_max = 3
    pickpt = 5      #Signal is pre-prepared with pick time at 5s


    signal = sample
    rs = signal.resample(resamp)
    ana_signal = rs.data[int((2.+pickpt)*resamp):] #Slice 2s after pick point
    pas = 1.0/(rs.stats.sampling_rate)
```

```
# Define poles (p) and zeros (q)
P_min = P_min
P_max = P_max
q_min = q_min
q_max = q_max

# Window the signal
r = 0.1
wt = tukey(len(ana_signal),alpha=r)
ana_sig = ana_signal*wt

# Calculate normalised autocorrelation
ac = np.correlate(ana_sig, ana_sig, mode='same')
acnorm = ac/np.amax(ac)

# Prepare empty arrays for f and g output values
arr_dim = int((q_max+q_min)*(P_max+P_min)*20)
freal = np.zeros((1, arr_dim))
g = np.zeros((1, arr_dim))
Q = np.zeros((1, arr_dim))
n_pole = 1

def get_ar(autocor, p, q):
    option = 1 # Return all roots
    middle = np.ceil(len(autocor)/2.0)
    matautocor = np.zeros((p, p))
```

```
for k in range(p):
    matautocor[k,:]=autocor[int(middle-q-k-1):int(middle-q-k+p-1)]
secondmember=autocor[int(middle+q):int(middle+q+p)]
coeffilterAR=np.linalg.solve(matautocor,secondmember.conj().transpose())
coefpolyno=np.append((np.array([1])), -coeffilterAR)
polesAR=np.roots(coefpolyno)
nbroot=np.size(polesAR)
if q==0:
    for k in range(nbroot):
        if np.absolute(polesAR[k]) > 1.6:
            print('Some poles outside the unit circle')
        else:
            pass
else:
    pass


if option == 2:
    realroot = np.zeros((nbroot,1))
    cplxroot = np.zeros((nbroot,1), dtype=complex)
    nrealroot = 0
    ncplxroot = 0
    for k in range(nbroot):
        if np.isreal(polesAR[k]) == True:
            realroot[nrealroot] = polesAR[k]
            nrealroot+=1
        else:
            cplxroot[ncplxroot] = polesAR[k]
```

```
                ncplxroot+=1
        realroot = realroot[0:nrealroot]
        cplxroot = cplxroot[0:ncplxroot]
        rootcplexsconj = np.zeros((int(ncplxroot/2), 1), dtype=complex)
        for k in range(0, ncplxroot, 2):
            rootcplexsconj[int(k/2.0)] = cplxroot[k]
        rootcplexsconj = np.concatenate(rootcplexsconj)
        if len(realroot) == 0:
            filter_ar = rootcplexsconj.conj().transpose()
            polesAR = filter_ar
        else:
            realroot = np.concatenate(realroot)
            filter_ar =np.append(rootcplexsconj.conj().transpose(), \
            realroot.conj().transpose())
            polesAR = filter_ar

    else:
        pass
    return(polesAR)

for q in range(q_min,q_max):
  for p in range(P_min,P_max):
    # Calculate ARMA filters for the normalised autocorrelation given a p and z
    filter_ar = get_ar(acnorm,p,q)

    # Calculates the corresponding complex frequencies
    x=filter_ar.real
```

```
        y=filter_ar.imag
        r=np.sqrt(x**2+y**2)
        theta=np.arctan2(y,x)

        # Find any values outside the unit circle
        h1 = np.where(theta <= 0.0)
        h2 = np.where(r >= 1.0)
        h3 = np.append(h1, h2)
        h = np.unique(h3)

        theta_ = np.delete(theta, h)
        r_ = np.delete(r, h)

        nb_p = len(theta_)

        # Frequency and Quality Factor
        f = theta_/(pas*2*pi)
        qf = theta_/(2*(1-r_))



        freal[0][n_pole-1:n_pole-1+nb_p] = f
        Q[0][n_pole-1:n_pole-1+nb_p] = qf
        g[0][n_pole-1:n_pole-1+nb_p]=-(1-r_)/(pas*2.0*pi)
        n_pole = n_pole + nb_p

    # Delete empty values at the end of the lists
    f_ = np.delete(freal[0], np.where(freal[0] == 0))
```

```
g_ = np.delete(g[0], np.where(freal[0] == 0))
q_ = np.delete(Q[0], np.where(freal[0] == 0))

# Calculate Q from pole clustered points around spectral peak
freq, psd = periodogram(ana_signal, fs=1./pas, nfft=10000, scaling='density')
peak = freq[np.argmax(psd)]
peakmin = peak-0.2
peakmax = peak+0.2
flim = f_[np.where((f_ < peakmax) & (f_> peakmin))]
glim = g_[np.where((f_ < peakmax) & (f_> peakmin))]
qlim = q_[np.where((f_ < peakmax) & (f_> peakmin))]
data = np.column_stack((flim, glim))
thresh = 0.1
try:
    clusters = hcluster.fclusterdata(data, thresh, criterion="distance")
    mode = max(set(list(clusters)), key=list(clusters).count)
    count = np.where(clusters==mode)
    if (len(count[0])) > 10:
        flimclust = flim[np.where((clusters==mode))]
        glimclust = glim[np.where((clusters==mode))]
        qlimclust = qlim[np.where((clusters==mode))]
        qavg = []
        for i in range(len(qlimclust)):
            q = -flimclust[i]/(2*glimclust[i])
            qavg.append(q)
        Q = np.mean(qavg)
        qerror = np.std(qavg)
```

```
        else:
            Q = -999.99
            qerror = 0.0
    except:
        Q = -999.99
        qerror = 0.0

    return(Q, qerror)

def qrun(startday, endday, startyear, endyear, stationname, data_loc, picks_num, \
sample_loc, pick_len, pickpt, output_loc):
    samples, picks_ = samples_analysis(startday, endday, startyear, endyear, \
    stationname, data_loc, num2date(picks_num), sample_loc, pick_len)
    tot = len(picks_)
    print(tot, 'events extracted')

    # Output results
    outfile = open(output_loc, 'w')
    outfile.close()
    print('---Starting Q Factor Analysis---')
    print(len(picks_num))
    for i in range(len(picks_num)):
        fs = 100.0
        sl = int(fs*(pickpt+2))
        x = (samples[i].data - np.mean(samples[i].data))[sl:]
        f, p = periodogram(x, fs=fs, nfft=10000, scaling='density')
        pf = f[np.argmax(p)]
```

```
        qarma, qarma_error = arma(samples[i])
        outfile = open(output_loc, 'a')
        outfile.write("%s\t" % i)
        outfile.write("%s\t" % picks_num[i])
        outfile.write("%s\t" % qarma)
        outfile.write("%s\n" % qarma_error)
        outfile.close()

    return()
```

C.2 Cross correlation and families

The cross correlation analysis is run using the ObsPy function `xcorr_pick_correction` which returns the absolute maximum XCC value and associated shift. Again, the inputs are samples prepared with the function `samples_analysis` which slices a whole day waveform into a 30s event trace, 5s before the pick time and 25s after. The function `xcorr` calculates the cross correlation values and initiates the matrices, and `xcorr_run` is used to execute over the whole catalogue of earthquake times and sample traces.

```
def xcorr(picks_, samples, matrix, shifts, faulty_inds):
    totvals = (len(matrix)*(len(matrix)+1))/2.
    for i in range(len(matrix)):
        print('Progress: ', i, '/', len(samples))
        rowlen = len(matrix)-i
        rowtri = (rowlen*(rowlen+1))/2.
        progress = ((totvals-rowtri)/totvals)*100.
```

```
        print('Processing row ', i, '(',np.round(progress, 2), '% complete)')
        pick1 = picks_[i]
        trace1 = samples[i]
        for j in range(i, len(matrix)):
            pick2 = picks_[j]
            trace2 = samples[j]
            try:
                pick_corr, value = xcorr_pick_correction(pick1, trace1, pick2,\
                trace2, t_before=2.4, t_after=4.5, cc_maxlag=5.0)
                if value >1.0001:
                    faulty_inds.append([i,j])
                    matrix[i][j] = np.nan
                    shifts[i][j] = np.nan
                elif pick_corr >5.0001:
                    faulty_inds.append([i,j])
                    matrix[i][j] = np.nan
                    shifts[i][j] = np.nan
                else:
                    matrix[i][j] = value
                    shifts[i][j] = pick_corr
            except:
                matrix[i][j] = np.nan
                shifts[i][j] = np.nan
    return()


def xcorr_run(output_loc, picks_, samples):
```

```
matrix = np.zeros((len(samples), len(samples)))

shifts = np.zeros((len(samples), len(samples)))

faulty_inds = []

print('********** Cross correlation analysis **********')

xcorr(picks_, samples, matrix, shifts, faulty_inds)

matrix_trans = matrix.T

fullmatrix = matrix+matrix_trans

del matrix

del matrix_trans

matrix_save = fullmatrix.copy()

shifts_trans = shifts.T

fullshifts = shifts+shifts_trans

del shifts

del shifts_trans

shifts_save = fullshifts.copy()

np.savetxt(str(output_loc)+'matrix.txt' fullmatrix)

np.savetxt(str(output_loc)+'shifts.txt', fullshifts)

np.savetxt(str(output_loc)+'faultyinds.txt', faulty_inds)


np.fill_diagonal(fullmatrix, 1)

nan_color = 'white'

color = cm.BuPu

color.set_bad(nan_color,1.)

fig = plt.figure(figsize=(12, 12))

ax = fig.add_subplot(111)

cax = ax.matshow(fullmatrix, vmin=0, vmax=1, cmap=color)

fig.colorbar(cax)
```

```
ax.xaxis.tick_bottom()
ax.yaxis.tick_left()
ax.spines['top'].set_color('w')
ax.spines['right'].set_color('w')
ax.set_xlabel('Event number')
ax.set_title('Cross correlation coefficient matrix')
plt.savefig(str(output_loc)+'matrix.png')

print('********** Family extraction **********')
# Family analysis
np.fill_diagonal(fullmatrix, np.nan)
tot = len(matrix)
families = [[0, 0, 0, 0, 0, 0, 0, 0, 0, 0]]
count = 0
thresh = 0.7
masters = []
while len(families[-1]) > 9:
    matrix_mod = []
    for i in range(len(fullmatrix)):
        row = fullmatrix[i]
        modcount = []
        for j in range(len(fullmatrix[i])):
            if fullmatrix[i][j]>thresh:
                modcount.append(fullmatrix[i][j])
            else:
                pass
        mod = len(modcount)
```

```
            matrix_mod.append(mod)
        master = np.argmax(matrix_mod)
        family_events = []
        for i in range(len(fullmatrix[master])):
            if fullmatrix[master][i] > thresh:
                family_events.append(i)
            else:
                continue
        for val in family_events:
            fullmatrix[val] = np.nan
            fullmatrix[:,val] = np.nan
        families.append(family_events)
        masters.append(master)
        count+=1
        print('Family', count, 'extracted')
fam = families[1:-1]
if len(fam) == 0:
    print('No families found')
else:
    print('In total', len(fam), 'families were found.')
    print('The largest family has', len(fam[0]), 'events in it.')
    unfound = (np.count_nonzero(~np.isnan(fullmatrix))/(len(fullmatrix)* \
    len(fullmatrix)))*100
    print("%.2f" % unfound, '% of events could not be put into families.')
print('There were', len(faulty_inds), 'instances where either xcc>1 or \
shift>5s, so no value is stored')
```

```
    output = str(output_loc)+'familyinfo.txt'
    outfile = open(output, 'w')
    outfile.close()
    for i in range(len(fam)):
        ps = np.array(picks_)[np.array(fam[i])]
        inds = fam[i]
        m = masters[i]
        for j in range(len(inds)):
            outfile = open(output_loc, 'a')
            outfile.write("%s\t" % ps[j])
            outfile.write("%s\t" % inds[j])
            outfile.write("%s\t" % i)
            outfile.write("%s\t" % masters[i])
            outfile.write("%s\t" % matrix_save[m][inds[j]])
            outfile.write("%s\n" % shifts_save[m][inds[j]])
            outfile.close()

    return()
```

C.3 $K_{1,2}$ values

This function is again applicable to a sample trace which is an ObsPy Trace object. In this instance, to capture a suitable 'pre-event' window, I recommend and always have used a longer trace that begins 15s before the earthquake first arrival P-pick time and spans to 45s after the pick. The pick time from the start of the trace is required as a parameter (in seconds).

```
import numpy as np
```

```
def kslope(sample, pickpt):
    y=sample.data
    # Define 5 seconds before the pick to determine the pre-pick avg noise
    pre_onset_avg = np.mean(abs(y[0:int(pickpt*100.)]))
    # Find the peak
    peak_loc = np.argmax(y)
    peak_val = np.amax(y)
    # Create a new list that we can search from the peak onwards
    search_y = abs(y[peak_loc:])
    mavgs = []
    temps = []
    sw=200 # search window =sw, window for calculating averages in samples, not sec
    interval = int(0.5*sw)
    for i in range(0, len(search_y)-sw, sw):
        temp = np.mean(search_y[i:i+interval])
        if temp < 1.5*pre_onset_avg:
            mavgs.append(i+peak_loc+interval)
            temps.append(temp)
        else:
            pass


    def k_func(t, y, A):
        k=(1./t)*np.log(y/A)
        return(k)
    # Quality control step to ensure that y2>y1
    if peak_val>pre_onset_avg:
        k1 = k_func(((peak_loc/100.)-pickpt), peak_val, pre_onset_avg)
```

```
        y1 = pre_onset_avg
        y2 = peak_val
        x1 = pickpt
        x2 = (peak_loc/100.) - pickpt
    else:
        k1 = -999.99
        y1 = -999.99
        y2 = -999.99
        x1 = -999.99
        x2 = -999.99


    if len(mavgs)==0:
        k2 = -999.99
        y3 = -999.99
        x3 = -999.99
    elif temps[0]>peak_val:
        k2 = -999.99
        y3 = -999.99
        x3 = -999.99
    else:
        k2 = k_func(mavgs[0]/100., temps[0], peak_val)
        y3 = temps[0]
        x3 = mavgs[0]/100.



    return(k1, k2, x1, y1, x2, y2, x3, y3)
```

C.4 Generating synthetic waveforms

This is a small sample of a function to generate synthetic waveforms. For further detail refer to the flowchart in figure 3.13.

```
from scipy.signal import periodogram
import numpy as np

def synth(fileloc, figloc):
synthtraces = []

# 1) Generate synthetic - single peak with decay
fs = 100.0
f1 = 2.0
sample_len = 30
t = np.arange(fs*sample_len)
y = np.array([np.sin(2*np.pi*f1 * (i/fs))*np.exp(-(i*0.002))*600 for i in t])
f_, pxx_ = periodogram(y, fs=fs)
trace = y
t = np.arange(0, 30, 0.01)
title = 'Synthetic single peak'
spectrafig(t, trace, title, figloc)
synth1 = np.vstack((t, trace))
synthtraces.append(synth1)
```

```
# 2) Generate synthetic - harmonic peaks with decay
fs = 100.0
f1 = 1.5
f2 = 3.0
f3 = 4.5
sample_len = 30 # in seconds
t = np.arange(fs*sample_len)
y1 = [np.sin(2*np.pi*f1 * (i/fs))*np.exp(-(i*0.002))*600 for i in t]
y2 = [np.sin(2*np.pi*f2 * (i/fs))*0.7*np.exp(-(i*0.002))*600 for i in t]
y3 = [np.sin(2*np.pi*f3 * (i/fs))*0.4*np.exp(-(i*0.002))*600 for i in t]
y = np.array(y1)+np.array(y2)+np.array(y3)
f_, pxx_ = periodogram(y, fs=fs)
trace = y
title = 'Synthetic harmonic'
t = np.arange(0, 30, 0.01)
spectrafig(t, trace, title, figloc)
synth2 = np.vstack((t, trace))
synthtraces.append(synth2)


# 3) Generate synthetic - noisy narrow peak
t = np.arange(0, 30, 0.01)
title = 'Synthetic narrow peak LP'
trace = []
with open(str(fileloc)+'narrow_update2.txt') as f:
    for line in f:
        values = line.split()
        temp = complex(values[0])
```

```
        val = (temp.real)*300000
        trace.append(val)
spectrafig(t, trace, title, figloc)
synth3 = np.vstack((t, trace))
synthtraces.append(synth3)

# 4) Generate synthetic - noisy broad peak
title = 'Synthetic broad peak LP'
trace = []
with open(str(fileloc)+'broad_update2.txt') as f:
    for line in f:
        values = line.split()
        temp = complex(values[0])
        val = (temp.real)*300000
        trace.append(val)
spectrafig(t, trace, title, figloc)
synth4 = np.vstack((t, trace))
synthtraces.append(synth4)

# 5) Generate synthetic - VT
t = np.arange(0, 30, 0.01)
title = 'Synthetic VT'
trace = []
with open(str(fileloc)+'vt.txt') as f:
    for line in f:
        values = line.split()
        temp = complex(values[0])
```

```
        val = (temp.real)*100000
        trace.append(val)
spectrafig(t, trace, title, figloc)
synth5 = np.vstack((t, trace))
synthtraces.append(synth5)

return(synthtraces)
```

C.5 Generating synthetic waveforms

This is a piece of Python code which generates an interactive matplotlib window and allows the user to manually pick P- arrivals. This was pieced together with a lot of assistance from examples on stack overflow.

```
from obspy.core import read, Trace
from obspy.signal.trigger import recursive_sta_lta, trigger_onset
from obspy import UTCDateTime
import matplotlib.pyplot as plt
import numpy as np
import datetime as dt
from matplotlib.dates import date2num, num2date
from dateutil import parser
import os

#Set up data file path locations
path_data = './Data/'
path_picks = './Picks/manpicks_'
```

```
samples = './Samples/manpicks_'


#Import data and set up stats
file_select = 'EC.RETU..SHZ.D.2014.121'
os.mkdir(samples+file_select)
str1 = read(path_data+file_select)
str1.merge(fill_value='interpolate')
#start_time = str1[0].stats['starttime']
start_time = UTCDateTime(2014, 5, 1, 0, 0, 0) # manually input
end_time = str1[0].stats['endtime']
tr1 = str1[0]
df = tr1.stats.sampling_rate
n_points = tr1.stats.npts

#Define an empty matrix - to fill and use later
cat = np.zeros((2, 2))

#'Slice' the stream so it definitely starts at the start and end time
str1 = str1.slice(starttime=start_time, endtime=end_time)

#At this point, can make a copy of the data and filter as necessary
str1_filt = str1.copy()
str1_filt.filter('bandpass', freqmin=1.0, freqmax=40.0, corners=2, zerophase=True)
tr1 = str1_filt[0]
df = tr1.stats.sampling_rate

#From this, start to build an event catalogue
```

```
t0 = tr1.stats.starttime

print("t0: ", t0)

trace_len = 120.0 #How much of the trace do you want to look at, at once?

overlap = 15.0 #Overlap on screen between one trace and the next


###############

#YIELD FUNCTION

###############


#This determines the number of windows that the user will see for a given trace


def time_selection():

duration = n_points/df #length of trace

windows = int(np.floor(duration/(trace_len-overlap))) #floor finds lowest int

for n in range(1, windows):

yield n


############################

#DEFINE A KEY PRESS FUNCTION

############################

def onclick(event):

#global cat

if event.button == 1 and event.inaxes!=None: #If button 1 is pressed inside plot window

try:

global cat

pick_number = cat[:,0].max() + 1

t1 = t0 + dt.timedelta(seconds=event.xdata+n*(trace_len-overlap))
```

```
t2 = parser.parse(str(t1))
test_t=date2num(t2)
cat = np.vstack((cat, [pick_number, test_t]))
fig.clf() #Clear existing figure
waveplot(str1_filt, n, on_off, cat)

slice_st = t1 - dt.timedelta(seconds=5.0)
slice_et = t1 + dt.timedelta(seconds=25.0)
temp_slice = str1_filt.slice(starttime=UTCDateTime(slice_st),
    endtime=UTCDateTime(slice_et))
rename = str(slice_st)
rename2 = rename[11:13] # This will need to be tweaked depending on file name
rename3 = rename[14:16]
rename4 = rename[17:19]
rename5 = rename[20:]
print("Pick made at: ", rename2, ":", rename3, ":", rename4)
temp_slice.write('./Samples/'+rename2+'-'+rename3+'-'+rename4+'-'+rename5,
    format='MSEED')
fig.canvas.draw()

except StopIteration:
plt.gcf().canvas.mpl_disconnect(cid_dict['cid'])
del cid_dict['cid']

elif event.button == 3 and event.inaxes!=None:
try:
cat = cat[:-1,:]
```

```
fig.clf()
waveplot(str1_filt, n, on_off, cat)
fig.canvas.draw()

except StopIteration:
plt.gcf().canvas.mpl_disconnect(cid_dict['cid'])
del cid_dict['cid']

#########################
#DEFINE A TYPING FUNCTION
#########################
def ontype(event):
if event.key == 'z':
try:
global n
n = timegen.__next__()
fig.clf()
waveplot(str1_filt, n, on_off, cat)
fig.canvas.draw()

except StopIteration:
plt.gcf().canvas.mpl_disconnect(cid_dict['cid'])
del cid_dict['cid']

##############################
#DEFINE WAVE PLOTTING FUNCTION
##############################
```

```
def waveplot(str1_filt, n, on_off, cat):
t0 = str1_filt[0].stats.starttime
st = t0 + n*(trace_len-overlap)
et = st + trace_len

wave1 = str1_filt.slice(starttime=st, endtime=et)
on_off1 = on_off[np.logical_and(on_off[:,0]/df>=n*(trace_len-overlap), /
on_off[:,0]/df<=n*(trace_len-overlap)+trace_len),0]
st_mark = date2num(st.datetime)
et_mark = date2num(et.datetime)
cat_test = np.logical_and((cat[:,1]>st_mark), (cat[:,1]<=et_mark))
cat1 = cat[cat_test, 1]

npts = wave1[0].stats.npts
ax1 = fig.add_subplot(211)
t=np.arange(0, npts/df, 1/df)

ax1.plot(t, wave1[0].data - np.mean(wave1[0].data), 'b', linewidth=0.5)
ax1.axhline(0, color='k', linestyle=':')
fig.suptitle(wave1[0].stats.starttime)
ax1.set_xlabel('Time [s]')
ax1.set_ylim(-800,800)
ax1.set_xlim(0, 120)
ax1.grid(b=True)

ax2 = fig.add_subplot(212)
```

```
wave1.spectrogram(log=True, axes=ax2)
ax2.set_xlim(0, 120)
for i in range(len(on_off1)):
ax1.axvline(on_off1[i]/df - n*(trace_len-overlap), c='r', ls='--')
ax2.axvline(on_off1[i]/df - n*(trace_len-overlap), c='r', ls='--')
for i in range(len(cat1)):
ax1.axvline((cat1[i]-date2num(parser.parse(str(st))))*60*60*24, c='r')
ax2.axvline((cat1[i]-date2num(parser.parse(str(st))))*60*60*24, c='r')

#####################################
#CALLING FUNCTIONS AND GENERATING PLOT
#####################################

timegen = time_selection()
cid_dict = {} #empty dictionary for connection ID numbers

fig=plt.figure(figsize=(18,12))

#This is what connects the button pressing to the figure itself
#In each case, ontype and onclick require one input - event
cid_dict['cid'] = plt.gcf().canvas.mpl_connect('button_press_event',onclick)
cid_dict['cid'] = plt.gcf().canvas.mpl_connect('key_press_event',ontype)



#Set up some initial values to run
global n
n = 0
```

```
st = starttime=t0+n*(trace_len-overlap)


#Put everything through the waveplot() function and show
waveplot(str1_filt, n, on_off, cat)
plt.show()


np.savetxt((path_picks + file_select +'_cat.txt'), cat, delimiter='\t')
```

References

Aiken, C., & Peng, Z. (2014). Dynamic triggering of microearthquakes in three geothermal/volcanic regions of California. *Journal of Geophysical Research: Solid Earth*, *119*(9), 6992–7009. https://doi.org/10.1002/2014JB011218

Aki, K., Fehler, M., & Das, S. (1977). Source mechanism of volcanic tremor: fluid-driven crack models and their application to the 1963 Kilauea eruption. *Journal of Volcanology and Geothermal Research*, *2*(3), 259–287. https://doi.org/10.1016/0377-0273(77)90003-8

Akin, M., & Kiymik, M. K. (2000). Application of periodogram and AR spectral analysis to EEG signals. *Journal of Medical Systems*, *24*(4), 247–256.

Allen, R. V. (1978). Automatic earthquake recognition and timing from single traces. *Bulletin of the Seismological Society of America*, *68*(5), 1521–1532.

Allstadt, K., & Malone, S. D. (2014). Swarms of repeating stick-slip icequakes triggered by snow loading at Mount Rainier volcano. *Journal of Geophysical Research: Earth Surface*, *119*(5), 1180–1203. https://doi.org/10.1002/2014JF003086

Almendros, J., Abella, R., Mora, M. M., & Lesage, P. (2014). Array analysis of the seismic wavefield of long-period events and volcanic tremor at Arenal volcano, Costa Rica. *Journal of Geophysical Research: Solid Earth*, *119*(7), 5536–5559. https://doi.org/10.1002/2013JB010628

Alparone, S., Andronico, D., Lodato, L., & Sgroi, T. (2003). Relationship between tremor and volcanic activity during the Southeast Crater eruption on Mount Etna in early 2000. *Journal of Geophysical Research: Solid Earth*, *108*(B5). https://doi.org/10.1029/2002jb001866

Alvarado, A., Audin, L., Nocquet, J.-M., Jaillard, E., Mothes, P., Jarrìn, P., Segovia, M., Rolandone, F., & Cisneros, D. (2016). Partitioning of oblique convergence in the Northern Andes subduction zone: Migration history and the present-day boundary of the North Andean Sliver in Ecuador. *Tectonics*, *35*(5), 1048–1065. https://doi.org/https://doi.org/10.1002/2016TC004117

Anderson, J. F., Johnson, J. B., Steele, A. L., Ruiz, M. C., & Brand, B. D. (2018). Diverse Eruptive Activity Revealed by Acoustic and Electromagnetic Observations of the 14

July 2013 Intense Vulcanian Eruption of Tungurahua Volcano, Ecuador. *Geophysical Research Letters*, *45*(7), 2976–2985. https://doi.org/10.1002/2017GL076419

Anzieta, J. C., Ortiz, H. D., Arias, G. L., & Ruiz, M. C. (2019). Finding Possible Precursors for the 2015 Cotopaxi Volcano Eruption Using Unsupervised Machine Learning Techniques. *International Journal of Geophysics*. https://doi.org/10.1155/2019/6526898

Arámbula-Mendoza, R., Valdés-González, C., Varley, N., Reyes-Pimentel, T. A., & Juárez-García, B. (2016). Tremor and its duration-amplitude distribution at Popocatépetl volcano, Mexico. *Geophysical Research Letters*, *43*(17), 8994–9001. https://doi.org/10.1002/2016GL070227

Arcila, M., & Arcila, M. (1996). Geophysical monitoring of the Purace volcano, Colombia. *Annals of Geophysics*, *39*(2). https://doi.org/10.4401/ag-3970

Arellano, S. R., Hall, M., Samaniego, P., Le Pennec, J. L., Ruiz, A., Molina, I., & Yepes, H. (2008). Degassing patterns of Tungurahua volcano (Ecuador) during the 1999-2006 eruptive period, inferred from remote spectroscopic measurements of SO2 emissions. *Journal of Volcanology and Geothermal Research*, *176*(1), 151–162. https://doi.org/10.1016/j.jvolgeores.2008.07.007

Attivissimo, F., Savino, M., & Trotta, A. (2000). A study on nonlinear averagings to perform the characterization of power spectral density estimation algorithms. *IEEE Transactions on Instrumentation and Measurement*, *49*(5), 1036–1042.

Avouris, D. M., Carn, S. A., & Waite, G. P. (2017). Triggering of volcanic degassing by large earthquakes. *Geology*, *45*(8), 715–718. https://doi.org/10.1130/G39074.1

Bablon, M., Quidelleur, X., Samaniego, P., Le Pennec, J.-L., Lahitte, P., Liorzou, C., Bustillos, J. E., & Hidalgo, S. (2018). Eruptive chronology of tungurahua volcano (ecuador) revisited based on new k-ar ages and geomorphological reconstructions. *Journal of Volcanology and Geothermal Research*, *357*, 378–398.

Baillard, C., Crawford, W. C., Ballu, V., Hibert, C., & Mangeney, A. (2014). An automatic kurtosis-based P-and S-phase picker designed for local seismic networks. *Bulletin of the Seismological Society of America*, *104*(1), 394–409. https://doi.org/10.1785/0120120347

Bain, A. A., Calder, E. S., Cortés, J. A., Cortés, G. P., & Loughlin, S. C. (2019). Textural and geochemical constraints on andesitic plug emplacement prior to the 2004–2010 vulcanian explosions at Galeras volcano, Colombia. *Bulletin of Volcanology*, *81*(1), 1–25. https://doi.org/10.1007/s00445-018-1260-y

Bain, A. A., Kendrick, J. E., Lamur, A., Lavallée, Y., Calder, E. S., Cortés, J. A., Cortés, G. P., Gómez Martinez, D., & Torres, R. A. (2021). Micro-Textural Controls on Magma Rheology and Vulcanian Explosion Cyclicity. *Frontiers in Earth Science*, *0*, 703. https://doi.org/10.3389/FEART.2020.611320

Bame, D., & Fehler, M. (1986). Observations of long period earthquakes accompanying hydraulic fracturing. *Geophysical Research Letters*, *13*(2), 149–152. https://doi.org/10.1029/GL013i002p00149

Basantes-Serrano, R., Rabatel, A., Francou, B., Vincent, C., Maisincho, L., Cáceres, B., Galarraga, R., & Alvarez, D. (2016). Slight mass loss revealed by reanalyzing glacier mass-balance observations on Glaciar Antisana 15α (inner tropics) during the 1995-2012 period. *Journal of Glaciology*, *62*(231), 124–136. https://doi.org/10.1017/jog.2016.17

Battaglia, J., Hidalgo, S., Douchain, J. M., Pacheco, D. A., Cordova, J., Alvarado, A. P., & Parra, R. (2017). Swarms of small volcano-tectonic events preceding paroxysmal explosions of Tungurahua volcano (Ecuador). *AGUFM*, *2017*, S13B–0668.

Baxter, P. J., & Horwell, C. J. (2015). Impacts of Eruptions on Human Health, In *The encyclopedia of volcanoes*. https://doi.org/10.1016/b978-0-12-385938-9.00060-2

Bean, C. J., De Barros, L., & Lokmer, I. (2014). Long-period seismicity in the shallow volcanic edifice formed from slow-rupture earthquakes. *Nature Geoscience*, *7*(1), 71. https://doi.org/10.1038/ngeo2027

Béjar-Pizarro, M., Gómez, J. A., Staller, A., Luna, M. P., Pérez-López, R., Monserrat, O., Chunga, K., Lima, A., Galve, J. P., Díaz, J. J., Mateos, R. M., & Herrera, G. (2018). InSAR-based mapping to support decision-making after an earthquake. *Remote Sensing*, *10*(6), 899. https://doi.org/10.3390/rs10060899

Bell, A. F., Hernandez, S., Gaunt, H. E., Mothes, P., Ruiz, M., Sierra, D., & Aguaiza, S. X. (2017). The rise and fall of periodic 'drumbeat' seismicity at Tungurahua volcano, Ecuador. *Earth and Planetary Science Letters*, *475*, 58–70. https://doi.org/10.1016/j.epsl.2017.07.030

Bell, A. F., Hernandez, S., McCloskey, J., Ruiz, M., LaFemina, P. C., Bean, C. J., & Möllhoff, M. (2021a). *Dynamic earthquake triggering response tracks evolving unrest at Sierra Negra volcano, Galápagos Islands*.

Bell, A. F., La Femina, P. C., Ruiz, M., Amelung, F., Bagnardi, M., Bean, C. J., Bernard, B., Ebinger, C., Gleeson, M., Grannell, J., Hernandez, S., Higgins, M., Liorzou, C., Lundgren, P., Meier, N. J., Möllhoff, M., Oliva, S.-J., Ruiz, A. G., & Stock, M. J. (2021b). Caldera resurgence during the 2018 eruption of Sierra Negra volcano, Galápagos Islands. *Nature Communications 2021 12:1*, *12*(1), 1–9. https://doi.org/10.1038/s41467-021-21596-4

Bell, A. F., Naylor, M., Hernandez, S., Main, I. G., Gaunt, H. E., Mothes, P., & Ruiz, M. (2018). Volcanic eruption forecasts from accelerating rates of drumbeat long-period earthquakes. *Geophysical Research Letters*, *45*(3), 1339–1348. https://doi.org/10.1002/2017GL076429

Benson, P. M., Vinciguerra, S., Meredith, P. G., & Young, R. P. (2008). Laboratory simulation of volcano seismicity. *Science*, *322*(5899), 249–252. https://doi.org/10.1126/science.1161927

Berger, J., & Sax, R. L. (1981). Seismic Detectors: The State-of-the-Art. *Systems Science and Software*.

Bernard, B., & Samaniego, P. (2017). Escenarios eruptivos en el Volcán Cayambe y construcción de un árbol de eventos. *Sometido a: Jornadas de Ciencias de la Tierra VIII. Escuela Politécnica Nacional, Quito*.

Bernard, B., Battaglia, J., Proaño, A., Hidalgo, S., Vásconez, F., Hernandez, S., & Ruiz, M. (2016). Relationship between volcanic ash fallouts and seismic tremor: quantitative assessment of the 2015 eruptive period at Cotopaxi volcano, Ecuador. *Bulletin of Volcanology*, *78*(11). https://doi.org/10.1007/s00445-016-1077-5

Biggs, J., & Pritchard, M. E. (2017). Global volcano monitoring: What does it mean when volcanoes deform? *Elements*, *13*(1), 17–22. https://doi.org/10.2113/gselements.13.1.17

Bisina, K. V., & Azeez, M. A. (2017). Optimized estimation of power spectral density, In *Proceedings of the 2017 international conference on intelligent computing and control systems*, Institute of Electrical; Electronics Engineers Inc. https://doi.org/10.1109/ICCONS.2017.8250588

Bondár, I., & Storchak, D. (2011). Improved location procedures at the International Seismological Centre. *Geophysical Journal International*, *186*(3), 1220–1244. https://doi.org/10.1111/J.1365-246X.2011.05107.X

Boué, A., Lesage, P., Cortés, G., Valette, B., & Reyes-Dávila, G. (2015). Real-time eruption forecasting using the material Failure Forecast Method with a Bayesian approach. *Journal of Geophysical Research: Solid Earth*, *120*(4), 2143–2161. https://doi.org/10.1002/2014JB011637

Brodsky, E. E. (2006). Long-range triggered earthquakes that continue after the wave train passes. *Geophysical Research Letters*, *33*(15), 15313. https://doi.org/10.1029/2006GL026605

Brodsky, E. E., & Elst, N. J. v. d. (2014). The Uses of Dynamic Earthquake Triggering. *Annual Review of Earth and Planetary Sciences*, *42*, 317–339. https://doi.org/10.1146/ANNUREV-EARTH-060313-054648

Brodsky, E. E., Karakostas, V., & Kanamori, H. (2000). A new observation of dynamically triggered regional seismicity: Earthquakes in Greece following the August 1999 Izmit, Turkey earthquake. *Geophysical Research Letters*, *27*(17), 2741–2744. https://doi.org/10.1029/2000GL011534

Bustillos, J. A., Romero, J. E., Guevara, A. ; & Díaz-Alvarado, J. (2018). Tephra fallout from the long-lasting Tungurahua eruptive cycle (1999-2014): Variations through eruptive style transition and deposition processes. *Andean Geology*, *45*(1). https://doi.org/10.5027/andgeoV45n1-3036

Butcher, S., Bell, A. F., Hernandez, S., Calder, E., Ruiz, M., & Mothes, P. (2020). Drumbeat LP "Aftershocks" to a Failed Explosive Eruption at Tungurahua Volcano, Ecuador. *Geophysical Research Letters*, *47*(16). https://doi.org/10.1029/2020GL088301

Butcher, S., Bell, A. F., Hernandez, S., & Ruiz, M. (2021). Evolution of Seismicity During a Stalled Episode of Reawakening at Cayambe Volcano, Ecuador. *Frontiers in Earth Science*, *9*, 1. https://doi.org/10.3389/feart.2021.680865

Buurman, H., West, M. E., & Thompson, G. (2013). The seismicity of the 2009 Redoubt eruption. *Journal of Volcanology and Geothermal Research*, *259*, 16–30. https://doi.org/10.1016/j.jvolgeores.2012.04.024

Cameron, K. A., & Pringle, P. T. (1987). A detailed chronology of the most recent major eruptive period at Mount Hood, Oregon. *Geological Society of America Bulletin*, *99*(6), 845–851. https://doi.org/10.1130/0016-7606(1987)99<845:ADCOTM>2.0.CO;2

Cannata, A., Spedalieri, G., Behncke, B., Cannavò, F., Di Grazia, G., Gambino, S., Gresta, S., Gurrieri, S., Liuzzo, M., & Palano, M. (2015). Pressurization and depressurization phases inside the plumbing system of Mount Etna volcano: Evidence from a multiparametric approach. *Journal of Geophysical Research: Solid Earth*, *120*(9), 5965–5982. https://doi.org/10.1002/2015JB012227

Carrasco-Núñez, G., Vallance, J. W., & Rose, W. I. (1993). A voluminous avalanche-induced lahar from Citlaltépetl volcano, Mexico: Implications for hazard assessment. *Journal of Volcanology and Geothermal Research*, *59*(1-2), 35–46. https://doi.org/10.1016/0377-0273(93)90076-4

Cassidy, M., Cole, P. D., Hicks, K. E., Varley, N. R., Peters, N., & Lerner, A. H. (2015). Rapid and slow: Varying magma ascent rates as a mechanism for Vulcanian explosions. *Earth and Planetary Science Letters*, *420*, 73–84. https://doi.org/10.1016/J.EPSL.2015.03.025

Cassidy, M., Manga, M., Cashman, K., & Bachmann, O. (2018). Controls on explosive-effusive volcanic eruption styles. *Nature Communications*, *9*(1). https://doi.org/10.1038/s41467-018-05293-3

Caudron, C., Syahbana, D. K., Lecocq, T., Van Hinsberg, V., McCausland, W., Triantafyllou, A., Camelbeeck, T., Bernard, A., & Surono. (2015). Kawah Ijen volcanic activity: a review. *Bulletin of Volcanology*, *77*(3), 16. https://doi.org/10.1007/s00445-014-0885-8

Cayol, V., & Cornet, F. H. (1998). Effects of topography on the interpretation of the deformation field of prominent volcanoes—application to etna. *Geophysical Research Letters*, *25*(11), 1979–1982.

Ceballos, J. L., Euscátegui, C., Ramírez, J., Cañon, M., Huggel, C., Haeberli, W., & Machguth, H. (2006). Fast shrinkage of tropical glaciers in Colombia, In *Annals of glaciology*, Cambridge University Press. https://doi.org/10.3189/172756406781812429

Chamberlain, C. J., Townend, J., & Gerstenberger, M. C. (2020). RT-EQcorrscan: Near-real-time matched-filtering for rapid development of dense earthquake catalogs. *Seismological Research Letters*, *91*(6), 3574–3584. https://doi.org/10.1785/0220200171

Chouet, B. (1981). Ground motion in the near field of a fluid-driven crack and its interpretation in the study of shallow volcanic tremor. *Journal of Geophysical Research: Solid Earth*, *86*(B7), 5985–6016. https://doi.org/10.1029/JB086iB07p05985

Chouet, B. (1992). A Seismic Model for the Source of Long-Period Events and Harmonic Tremor, In *Volcanic seismology*. Springer, Berlin, Heidelberg. https://doi.org/10.1007/978-3-642-77008-1{_}11

Chouet, B. A. (1988). Resonance of a fluid-driven crack: radiation properties and implications for the source of long-period events and harmonic tremor. *Journal of Geophysical Research*, *93*(B5), 4375–4400. https://doi.org/10.1029/JB093iB05p04375

Chouet, B. A. (1996). Long-period volcano seismicity: Its source and use in eruption forecasting. *Nature*, *380*(6572), 309–316. https://doi.org/10.1038/380309a0

Chouet, B. A., & Dawson, P. (2011). Shallow conduit system at Kilauea Volcano, Hawaii, revealed by seismic signals associated with degassing bursts. *Journal of Geophysical Research: Solid Earth*, *116*(12). https://doi.org/10.1029/2011JB008677

Chouet, B. A., Dawson, P. B., James, M. R., & Lane, S. J. (2010). Seismic source mechanism of degassing bursts at Kilauea Volcano, Hawaii: Results from waveform inversion in the 10-50 s band. *Journal of Geophysical Research: Solid Earth*, *115*(9). https://doi.org/10.1029/2009JB006661

Chouet, B. A., Dawson, P., & Martini, M. (2008). Shallow-conduit dynamics at Stromboli Volcano, Italy, imaged from waveform inversions. *Geological Society Special Publication*, *307*, 57–84. https://doi.org/10.1144/SP307.5

Chouet, B. A., Dawson, P., Ohminato, T., Martini, M., Saccorotti, G., Giudicepietro, F., De Luca, G., Milana, G., & Scarpa, R. (2003). Source mechanisms of explosions at Stromboli Volcano, Italy, determined from moment-tensor inversions of very-long-period data. *Journal of Geophysical Research: Solid Earth*, *108*(B1), 7–1. https://doi.org/10.1029/2002jb001919

Chouet, B. A., & Matoza, R. S. (2013). A multi-decadal view of seismic methods for detecting precursors of magma movement and eruption. *Journal of Volcanology and Geothermal Research*, *252*, 108–175. https://doi.org/10.1016/j.jvolgeores.2012.11.013

Chouet, B. A., Page, R. A., Stephens, C. D., Lahr, J. C., & Power, J. A. (1994). Precursory swarms of long-period events at Redoubt Volcano (1989-1990), Alaska: Their origin and use as a forecasting tool. *Journal of Volcanology and Geothermal Research*, *62*(1-4), 95–135. https://doi.org/10.1016/0377-0273(94)90030-2

Clarke, A. B., Stephens, S., Teasdale, R., Sparks, R. S., & Diller, K. (2007). Petrologic constraints on the decompression history of magma prior to Vulcanian explosions at the Soufrière Hills volcano, Montserrat. *Journal of Volcanology and Geothermal Research*, *161*(4), 261–274. https://doi.org/10.1016/J.JVOLGEORES.2006.11.007

Clarke, A. B., Esposti Ongaro, T., & Belousov, A. (2015). Vulcanian Eruptions, In *The encyclopedia of volcanoes*. Elsevier. https://doi.org/10.1016/b978-0-12-385938-9.00028-6

Cogley, G., Kienholz, C., Miles, E., Sharp, M., & Wyatt, F. (2015). GLIMS Glacier Database. Boulder, CO. National Snow and Ice Data Center.

Coltorti, M., & Ollier, C. D. (2000). Geomorphic and tectonic evolution of the Ecuadorian Andes. *Geomorphology*, *32*(1-2), 1–19. https://doi.org/10.1016/S0169-555X(99)00036-7

Coulon, C. A., Hsieh, P. A., White, R., Lowenstern, J. B., & Ingebritsen, S. E. (2017). Causes of distal volcano-tectonic seismicity inferred from hydrothermal modeling. *Journal of Volcanology and Geothermal Research*, *345*, 98–108. https://doi.org/10.1016/j.jvolgeores.2017.07.011

Cusano, P., Petrosino, S., & Saccorotti, G. (2008). Hydrothermal origin for sustained Long-Period (LP) activity at Campi Flegrei Volcanic Complex, Italy. *Journal of Volcanology and Geothermal Research*, *177*(4), 1035–1044. https://doi.org/10.1016/j.jvolgeores.2008.07.019

D'Auria, L., Barrancos, J., Padilla, G. D., Pérez, N. M., Hernández, P. A., Melián, G., Padrón, E., Asensio-Ramos, M., & García-Hernández, R. (2019). The 2016 Tenerife (Canary Islands) Long-Period Seismic Swarm. *Journal of Geophysical Research: Solid Earth*, *124*(8), 2019JB017871. https://doi.org/10.1029/2019JB017871

Dawson, P. B., Benítez, M. C., Chouet, B. A., Wilson, D., & Okubo, P. G. (2010). Monitoring very-long-period seismicity at Kilauea Volcano, Hawaii. *Geophysical Research Letters*, *37*(18). https://doi.org/10.1029/2010GL044418

Decker, R. W. (1973). State-of-the-art in volcano forecasting. *Bulletin Volcanologique*, *37*(3), 372–393. https://doi.org/10.1007/BF02597635

Del Bello, E., Lane, S. J., James, M. R., Llewellin, E. W., Taddeucci, J., Scarlato, P., & Capponi, A. (2015). Viscous plugging can enhance and modulate explosivity of strombolian eruptions. *Earth and Planetary Science Letters*, *423*, 210–218. https://doi.org/10.1016/J.EPSL.2015.04.034

Del Pezzo, E., Bianco, F., & Borgna, I. (2013). Magnitude scale for LP events: A quantification scheme for volcanic quakes. *Geophysical Journal International*, *194*(2), 911–919. https://doi.org/10.1093/gji/ggt126

Detienne, M., Delmelle, P., Guevara, A., Samaniego, P., Opfergelt, S., & Mothes, P. A. (2017). Contrasting origin of two clay-rich debris flows at Cayambe Volcanic Complex, Ecuador. *Bulletin of Volcanology*, *79*(4), 27. https://doi.org/10.1007/s00445-017-1111-2

Diaz-Moreno, A., Roca, A., Lamur, A., Munkli, B. H., Ilanko, T., Pering, T. D., Pineda, A., & De Angelis, S. (2020). Characterization of Acoustic Infrasound Signals at Volcán de Fuego, Guatemala: A Baseline for Volcano Monitoring. *Frontiers in Earth Science*, *0*, 469. https://doi.org/10.3389/FEART.2020.549774

Diller, K., Clarke, A. B., Voight, B., & Neri, A. (2006). Mechanisms of conduit plug formation: Implications for vulcanian explosions. *Geophysical Research Letters*, *33*(20), 20302. https://doi.org/10.1029/2006GL027391

Dixon, J. E., Stolper, E. M., & Holloway, J. R. (1995). An experimental study of water and carbon dioxide solubilities in mid-ocean ridge basaltic liquids. Part I: calibration and solubility models. *Journal of Petrology*, *36*(6), 1607–1631. https://doi.org/10.1093/oxfordjournals.petrology.a037267

Druitt, T. H., Young, S. R., Baptie, B., Bonadonna, C., Calder, E. S., Clarke, A. B., Cole, P. D., Harford, C. L., Herd, R. A., Luckett, R., Ryan, G., Voight, B., & Voight, B. (2000). Episodes of cyclic Vulcanian explosive activity with fountain collapse at Soufrière Hills Volcano, Montserrat. *Geological Society of London*, *21*, 281–306.

Dziewonski, A. M., Chou, T.-A., & Woodhouse, J. H. (1981). Determination of earthquake source parameters from waveform data for studies of global and regional seismicity. *Journal of Geophysical Research: Solid Earth*, *86*(B4), 2825–2852. https://doi.org/10.1029/JB086iB04p02825

Eads, D. (2008). hcluster: Hierarchical clustering for scipy.

Edmonds, M. (2008). New geochemical insights into volcanic degassing. *Philosophical Transactions of the Royal Society A: Mathematical, Physical and Engineering Sciences*, *366*(1885), 4559–4579. https://doi.org/10.1098/rsta.2008.0185

Edmonds, M., & Woods, A. W. (2018). Exsolved volatiles in magma reservoirs. *Journal of Volcanology and Geothermal Research*, *368*, 13–30. https://doi.org/10.1016/J.JVOLGEORES.2018.10.018

Eguez, A., Alvarado, A., Yepes, H., Machette, M. N., Costa, C., Dart, R. L., & Bradley, L. A. (2003). Database and map of Quaternary faults and folds of Ecuador and its offshore regions. *US Geological Survey Open-File Report*, *3*, 289.

Eibl, E. P., Lokmer, I., Bean, C. J., Akerlie, E., & Vogfjörd, K. S. (2015). Helicopter vs. volcanic tremor: Characteristic features of seismic harmonic tremor on volcanoes. *Journal of Volcanology and Geothermal Research*, *304*, 108–117. https://doi.org/10.1016/j.jvolgeores.2015.08.002

Ekström, G., Nettles, M., & Dziewoński, A. M. (2012). The global CMT project 2004-2010: Centroid-moment tensors for 13,017 earthquakes. *Physics of the Earth and Planetary Interiors*, *200-201*, 1–9. https://doi.org/10.1016/j.pepi.2012.04.002

El Comercio. (2016). Cada 200 años el volcán Cayambe presenta actividad eruptiva [Accessed: 02-02-2021].

Elmore, W. C., & Heald, M. A. (1985). *Physics of Waves*. Courier Corporation.

Elst, N. J. v. d., & Brodsky, E. E. (2010). Connecting near-field and far-field earthquake triggering to dynamic strain. *Journal of Geophysical Research: Solid Earth*, *115*(B7), 7311. https://doi.org/10.1029/2009JB006681

Endo, E. T., & Murray, T. (1991). Real-time Seismic Amplitude Measurement (RSAM): a volcano monitoring and prediction tool. *Bulletin of Volcanology*, *53*(7), 533–545. https://doi.org/10.1007/BF00298154

Evans, J. R., & Allen, S. S. (1983). A Teleseism-Specific Detection Algorithm for Single Short-Period Traces. *Bulletin of the Seismological Society of America*, *73*(4), 1173–1186. https://doi.org/10.1785/BSSA0730041173

Fazio, M., Alparone, S., Benson, P. M., Cannata, A., & Vinciguerra, S. (2019). Genesis and mechanisms controlling tornillo seismo-volcanic events in volcanic areas. *Scientific reports*, *9*(1), 1–11. https://doi.org/10.1038/s41598-019-43842-y

Fee, D., Garcés, M., Patrick, M., Chouet, B., Dawson, P., & Swanson, D. (2010a). Infrasonic harmonic tremor and degassing bursts from Halema'uma'u Crater, Kilauea Volcano, Hawaii. *Journal of Geophysical Research: Solid Earth*, *115*(11), 11316. https://doi.org/10.1029/2010JB007642

Fee, D., Garces, M., & Steffke, A. (2010b). Infrasound from Tungurahua Volcano 2006-2008: Strombolian to Plinian eruptive activity. *Journal of Volcanology and Geothermal Research*, *193*(1-2), 67–81. https://doi.org/10.1016/j.jvolgeores.2010.03.006

Feng, L., Pazzi, V., Intrieri, E., Gracchi, T., & Gigli, G. (2019). Rockfall seismic features analysis based on in situ tests: Frequency, amplitude, and duration. *Journal of Mountain Science*, *16*(5), 955–970.

Ferrari, L., & Tibaldi, A. (1992). Recent and active tectonics of the north-eastern Ecuadorian Andes. *Journal of Geodynamics*, *15*(1-2), 39–58. https://doi.org/10.1016/0264-3707(92)90005-D

Fischer, T. P., Morrissey, M. M., Marta Lucía Calvache, V., Diego Gòmez, M., Roberto Torres, C., Stix, J., & Williams, S. N. (1994). Correlations between SO 2 flux and long-period seismicity at Galeras volcano. *Nature 1994 368:6467*, *368*(6467), 135–137. https://doi.org/10.1038/368135a0

Fournier, R. O. (2007). Hydrothermal systems and volcano geochemistry, In *Volcano deformation*. Springer Berlin Heidelberg. https://doi.org/10.1007/978-3-540-49302-0-10

Frank, W. B., Shapiro, N. M., & Gusev, A. A. (2018). Progressive reactivation of the volcanic plumbing system beneath Tolbachik volcano (Kamchatka, Russia) revealed by long-period seismicity. *Earth and Planetary Science Letters*, *493*, 47–56. https://doi.org/10.1016/j.epsl.2018.04.018

Fremont, M. J., & Malone, S. D. (1987). High precision relative locations of earthquakes at Mount St. Helens, Washington (USA). *Journal of Geophysical Research*, *92*(B10). https://doi.org/10.1029/jb092ib10p10223

Friedlander, B., Porat, B., & Porat, B. (1984). The Modified Yule–Walker Method of ARMA Spectral Estimation. *IEEE Transactions on Aerospace and Electronic Systems*, *AES-20*(2), 158–173. https://doi.org/10.1109/TAES.1984.310437

Gaunt, H. E., Burgisser, A., Mothes, P. A., Browning, J., Meredith, P. G., Criollo, E., & Bernard, B. (2020). Triggering of the powerful 14 July 2013 Vulcanian explosion at Tungurahua Volcano, Ecuador. *Journal of Volcanology and Geothermal Research*, *392*, 106762. https://doi.org/10.1016/j.jvolgeores.2019.106762

Gibbons, S. J., Bøttger Sørensen, M., Harris, D. B., & Ringdal, F. (2007). The detection and location of low magnitude earthquakes in northern Norway using multi-channel waveform correlation at regional distances. *Physics of the Earth and Planetary Interiors*, *160*(3-5), 285–309. https://doi.org/10.1016/j.pepi.2006.11.008

Gibbons, S. J., & Ringdal, F. (2006). The detection of low magnitude seismic events using array-based waveform correlation. *Geophysical Journal International*, *165*(1), 149–166. https://doi.org/10.1111/j.1365-246X.2006.02865.x

Gil Cruz, F., & Chouet, B. A. (1997). Long-period events, the most characteristic seismicity accompanying the emplacement and extrusion of a lava dome in Galeras Volcano, Colombia, in 1991. *Journal of Volcanology and Geothermal Research*, *77*(1-4), 121–158. https://doi.org/10.1016/S0377-0273(96)00091-1

Global Volcanism Program. (2013a). Atitlan (342060) (v4.10.1 (2). Smithsonian Institution. https://doi.org/https://doi.org/10.5479/si.GVP.VOTW4-2013

Global Volcanism Program. (2013b). Cayambe (352006) (v. 4.9.3 (). Smithsonian Institution. https://doi.org/https://doi.org/10.5479/si.GVP.VOTW4-2013

Global Volcanism Program. (2013c). Galeras (351080) (v4.10.1 (2). Smithsonian Institution. https://doi.org/https://doi.org/10.5479/si.GVP.VOTW4-2013

Global Volcanism Program. (2013d). Hood (322010) (v 4.10.1 (). Smithsonian Institution. https://doi.org/https://doi.org/10.5479/si.GVP.VOTW4-2013

Global Volcanism Program. (2013e). Volcanoes of the World, v. 4.8.5 Venzke, E (ed.)

Global Volcanism Program. (2018). Report on Tungurahua (Ecuador) (E. Venzke, Ed.). *Bulletin of the Global Volcanism Network*, *43*(2). https://doi.org/10.5479/si.GVP.BGVN201802-352080

Gomberg, J., Reasenberg, P. A., Bodin, P., & Harris, R. A. (2001). Earthquake triggering by seismic waves following the Landers and Hector Mine earthquakes. *Nature 2001 411:6836*, *411*(6836), 462–466. https://doi.org/10.1038/35078053

Gomberg, J., & Bodin, P. (1994). Triggering of the Ms=5.4 Little Skull Mountain, Nevada, Earthquake with Dynamic Strains. *Bulletin of the Seismological Society of America*, *84*(3), 844–853.

Gomberg, J., & Johnson, P. (2005). Dynamic triggering of earthquakes. *Nature 2005 437:7060*, *437*(7060), 830–830. https://doi.org/10.1038/437830a

Gottschämmer, E., Rohnacher, A., Carter, W., Nüsse, A., Drach, K., De Angelis, S., Lavallée, Y., Kendrick, J. E., Roca, A., Castellanos, P., Chigna, G., & Rietbrock, A. (2021). Volcanic emission and seismic tremor at Santiaguito, Guatemala: New insights from long-term seismic, infrasound and thermal measurements in 2018–2020. *Journal of Volcanology and Geothermal Research*, *411*, 107154. https://doi.org/10.1016/J.JVOLGEORES.2020.107154

Green, D. N., Neuberg, J., & Cayol, V. (2006). Shear stress along the conduit wall as a plausible source of tilt at Soufrière Hills volcano, Montserrat. *Geophysical Research Letters*, *33*(10). https://doi.org/10.1029/2006GL025890

Green, D. N., & Neuberg, J. W. (2006). Waveform classification of volcanic low-frequency earthquake swarms and its implication at Soufrière Hills Volcano, Montserrat. *Journal of Volcanology and Geothermal Research*, *153*(1-2), 51–63. https://doi.org/10.1016/j.jvolgeores.2005.08.003

Guillier, B., & Chatelain, J. L. (2006). Evidence for a seismic activity mainly constituted of hybrid events at Cayambe volcano, Ecuador. Interpretation in a iced-domes volcano context. *Comptes Rendus - Geoscience*, *338*(8), 499–506. https://doi.org/10.1016/j.crte.2006.03.004

Guillier, B., Samaniego, P., Ruiz, M., & Chatelain, J.-L. (1999). Steady long-period activity at Cayambe volcano, Ecuador: location, spectral analysis and consequences. *Fourth ISAG, Goettingen (Germany)*, 303–306.

Haapala, J., Escobar Wolf, R., Vallance, J., Rose, W., Griswold, J., Schilling, S., Ewert, J., & Mota, M. (2005). Volcanic Hazards at Atitlán Volcano, Guatemala. *US Geological Survey, Open-File Report*, *1043*.

Hale, A. J. (2007). Magma flow instabilities in a volcanic conduit: Implications for long-period seismicity. *Physics of the Earth and Planetary Interiors*, *163*(1-4), 163–178. https://doi.org/10.1016/J.PEPI.2007.05.001

Hall, M. L., Robin, C., Beate, B., Mothes, P., & Monzier, M. (1999). Tungurahua Volcano, Ecuador: Structure, eruptive history and hazards. *Journal of Volcanology and Geothermal Research*, *91*(1-2), 1–21. https://doi.org/10.1016/S0377-0273(99)00047-5

Hall, M. L., Steele, A. L., Bernard, B., Mothes, P. A., Vallejo, S. X., Douillet, G. A., Ramón, P. A., Aguaiza, S. X., & Ruiz, M. C. (2015). Sequential plug formation, disintegration by Vulcanian explosions, and the generation of granular Pyroclastic Density Currents at Tungurahua volcano (2013-2014), Ecuador. *Journal of Volcanology and Geothermal Research*, *306*, 90–103. https://doi.org/10.1016/j.jvolgeores.2015.09.009

Hammer, C., & Neuberg, J. W. (2009). On the dynamical behaviour of low-frequency earthquake swarms prior to a dome collapse of Soufrière Hill volcano, Montserrat. *Geophysical Research Letters*, *36*(6), L06305. https://doi.org/10.1029/2008GL036837

He, P., Hetland, E. A., Wang, Q., Ding, K., Wen, Y., & Zou, R. (2017). Coseismic slip in the 2016 Mw 7.8 Ecuador earthquake imaged from sentinel-1A radar interferometry. *Seismological Research Letters*, *88*(2), 277–286. https://doi.org/10.1785/0220160151

Heidarzadeh, M., Murotani, S., Satake, K., Takagawa, T., & Saito, T. (2017). Fault size and depth extent of the Ecuador earthquake (Mw7.8) of 16 April 2016 from teleseismic and tsunami data. *Geophysical Research Letters*, *44*(5), 2211–2219. https://doi.org/10.1002/2017GL072545

Hellweg, M. (2000). Physical models for the source of Lascar's harmonic tremor. *Journal of Volcanology and Geothermal Research*, *101*(1-2), 183–198. https://doi.org/10.1016/S0377-0273(00)00163-3

Hickey, J., Lloyd, R., Biggs, J., Arnold, D., Mothes, P., & Muller, C. (2020). Rapid localized flank inflation and implications for potential slope instability at Tungurahua volcano, Ecuador. *Earth and Planetary Science Letters*, *534*, 116104. https://doi.org/10.1016/j.epsl.2020.116104

Hidalgo, S., Battaglia, J., Arellano, S., Steele, A., Bernard, B., Bourquin, J., Galle, B., Arrais, S., & Vásconez, F. (2015). SO2 degassing at Tungurahua volcano (Ecuador) between 2007 and 2013: Transition from continuous to episodic activity. *Journal of Volcanology*

and Geothermal Research, *298*, 1–14. https://doi.org/10.1016/j.jvolgeores.2015.03.022

Hill, D. P., & Prejean, S. G. (2015). Dynamic Triggering, In *Treatise on geophysics: Second edition*. Elsevier Inc. https://doi.org/10.1016/B978-0-444-53802-4.00078-6

Hill, D. P., Reasenberg, P. A., Michael, A., Arabaz, W. J., Beroza, G., Brumbaugh, D., Brune, J. N., Castro, R., Davis, S., DePolo, D., Ellsworth, W. L., Gomberg, J., Harmsen, S., House, L., Jackson, S. M., Johnston, M. J., Jones, L., Keller, R., Malone, S., ... Zollweg, J. (1993). Seismicity remotely triggered by the magnitude 7.3 landers, California, earthquake. *Science*, *260*(5114), 1617–1623. https://doi.org/10.1126/science.260.5114.1617

Hill, D. P. (2008). Dynamic Stresses, Coulomb Failure, and Remote TriggeringDynamic Stresses, Coulomb Failure, and Remote Triggering. *Bulletin of the Seismological Society of America*, *98*(1), 66–92. https://doi.org/10.1785/0120070049

Hill, D. P., Dawson, P., Johnston, M. J. S., Pitt, A. M., Biasi, G., & Smith, K. (2002a). Very-long-period volcanic earthquakes beneath Mammoth Mountain, California. *Geophysical Research Letters*, *29*(10), 8–1. https://doi.org/10.1029/2002GL014833

Hill, D. P., Pollitz, F., & Newhall, C. (2002b). Earthquake-volcano interactions. *Physics Today*, *55*(11), 41–47. https://doi.org/10.1063/1.1535006

Hoblitt, R., Walder, J., Driedger, C., Scotf, K., Pringle, P., & Vallance, J. (1998). Volcano Hazards from Mount Rainier, Washington, Revised 1998. US Department of the Interior, US Geological Survey.

Holschneider, M., Narteau, C., Shebalin, P., Peng, Z., & Schorlemmer, D. (2012). Bayesian analysis of the modified Omori law. *Journal of Geophysical Research: Solid Earth*, *117*(B6). https://doi.org/10.1029/2011JB009054

Hori, S., Fukao, Y., Kumazawa, M., Furumoto, M., & Yamamoto, A. (1989). A new method of spectral analysis and its application to the Earth's free oscillations: the 'Sompi' method. *Journal of Geophysical Research*, *94*(B6), 7535–7553. https://doi.org/10.1029/JB094iB06p07535

Hotovec, A. J., Prejean, S. G., Vidale, J. E., & Gomberg, J. (2013). Strongly gliding harmonic tremor during the 2009 eruption of Redoubt Volcano. *Journal of Volcanology and Geothermal Research*, *259*, 89–99. https://doi.org/10.1016/j.jvolgeores.2012.01.001

Hotovec-Ellis, A. J., Shelly, D. R., Hill, D. P., Pitt, A. M., Dawson, P. B., & Chouet, B. A. (2018). Deep fluid pathways beneath Mammoth Mountain, California, illuminated by migrating earthquake swarms. *Science Advances*, *4*(8), eaat5258. https://doi.org/10.1126/sciadv.aat5258

Huggel, C., Ceballos, J. L., Pulgarín, B., Ramírez, J., & Thouret, J. C. (2007). Review and reassessment of hazards owing to volcano-glacier interactions in Colombia, In *Annals of glaciology*, Cambridge University Press. https://doi.org/10.3189/172756407782282408

IGEPN. (2015). Informe del estado del Volcán Tungurahua [https://www.igepn.edu.ec/tungurahua-informes/tung-diarios/tung-d-2015?limit=20&limitstart=20, Accessed: 11-11-2019].

IGEPN. (2016a). Informe del estado del Volcán Tungurahua [https://www.igepn.edu.ec/tungurahua-informes/tung-diarios/tung-d-2016?sort=created_on&direction=asc&limit=20&limitstart=40, Accessed: 24-01-2020].

IGEPN. (2016b). Informe Especial Nº 5- Volcán Cayambe: Actualización de la actividad [https://www.igepn.edu.ec/cayambe-informes/cay-especiales/cay-e-2016, Accessed: 12-11-2020].

Ignatieva, A., Bell, A. F., & Worton, B. J. (2018). Point process models for quasi-periodic volcanic earthquakes. *arXiv preprint arXiv:1803.07688*.

Instituto Nacional de Sismologia Vulcanologia Meteorologia e Hidrologia (INSIVUMEH). (2021). Estaciones Sismologicas [https://insivumeh.gob.gt/uncatergorized/estaciones-sismologicas/ Accessed: 02-07-2021].

International Seismological Centre (ISC). (2021). International Seismograph Station Registry (IR). https://doi.org/https://doi.org/10.31905/EL3FQQ40

Iverson, R. M. (2008). Dynamics of seismogenic volcanic extrusion resisted by a solid surface plug, Mount St. Helens 2004–2005. *A Volcano Rekindled: The Renewed Eruption of Mount St. Helens, 2004–2006*, *1750*, 425–460. https://doi.org/10.3133/pp175021

James, M. R., Lane, S. J., & Chouet, B. A. (2006). Gas slug ascent through changes in conduit diameter: Laboratory insights into a volcano-seismic source process in low-viscosity magmas. *Journal of Geophysical Research: Solid Earth*, *111*(B5), n/a–n/a. https://doi.org/10.1029/2005JB003718

Johnson, J. B., & Lees, J. M. (2000). Plugs and chugs - seismic and acoustic observations of degassing explosions at Karymsky, Russia and Sangay, Ecuador. *Journal of Volcanology and Geothermal Research*, *101*(1-2), 67–82. https://doi.org/10.1016/S0377-0273(00)00164-5

Johnson, J. B., Ruiz, M. C., Ortiz, H. D., Watson, L. M., Viracucha, G., Ramon, P., & Almeida, M. (2018). Infrasound Tornillos Produced by Volcán Cotopaxi's Deep Crater. *Geophysical Research Letters*, *45*(11), 5436–5444. https://doi.org/10.1029/2018GL077766

Johnson, J. B., & Ripepe, M. (2011). Volcano infrasound: A review. Elsevier. https://doi.org/10.1016/j.jvolgeores.2011.06.006

Jones, J., & Malone, S. D. (2005). Mount Hood Earthquake Activity: Volcanic or Tectonic Origins? *Bulletin of the Seismological Society of America*, *95*(3), 818–832. https://doi.org/10.1785/0120040019

Jónsdóttir, K., Roberts, R., Pohjola, V., Lund, B., Shomali, Z. H., Tryggvason, A., & Böðvarsson, R. (2009). Glacial long period seismic events at Katla volcano, Iceland. *Geophysical Research Letters*, *36*(11), L11402. https://doi.org/10.1029/2009GL038234

Jónsdóttir, K., Tryggvason, A., Roberts, R., Lund, B., Soosalu, H., & Böðvarsson, R. (2007). Habits of a glacier-covered volcano: Seismicity patterns and velocity structure of Katla volcano, Iceland, In *Annals of glaciology*, Cambridge University Press. https://doi.org/10.3189/172756407782282499

Julian, B. R. (1994). Volcanic tremor: nonlinear excitation by fluid flow. *Journal of Geophysical Research*, *99*(B6). https://doi.org/10.1029/93jb03129

Kanamori, H. (1977). The energy release in great earthquakes. *Journal of Geophysical Research*, *82*(20), 2981–2987. https://doi.org/10.1029/JB082I020P02981

Kárník, V., Kondorskaya, N. V., Riznitchenko, J. V., Savarensky, E. F., Soloviev, S. L., Shebalin, N. V., Vanek, J., & Zátopek, A. (1962). Standardization of the earthquake magnitude scale. *Studia Geophysica et Geodaetica*, *6*(1), 41–48. https://doi.org/10.1007/BF02590040

Kawakatsu, H., & Cadena, G. P. (1991). Focal Mechanisms of the March 6, 1987 Ecuador Earthquakes. CMT Inversion with a First Motion Constraint. *Journal of Physics of the Earth*, *39*(4), 589–597. https://doi.org/10.4294/jpe1952.39.589

Kayal, J. R. (2008). *Earthquake magnitude, intensity, energy, power law relations and source mechanism* (tech. rep.). Geological Survey of India.

Kendrick, J. E., Lavallée, Y., Hirose, T., Di Toro, G., Hornby, A. J., De Angelis, S., & Dingwell, D. B. (2014). Volcanic drumbeat seismicity caused by stick-slip motion and magmatic frictional melting. *Nature Geoscience*, *7*(6), 438–442. https://doi.org/10.1038/ngeo2146

Kendrick, J. E., Lavallée, Y., Varley, N. R., Wadsworth, F. B., Lamb, O. D., & Vasseur, J. (2016). Blowing Off Steam: Tuffisite Formation As a Regulator for Lava Dome Eruptions. *Frontiers in Earth Science*, *0*, 41. https://doi.org/10.3389/FEART.2016.00041

Kern, C., Deutschmann, T., Werner, C., Sutton, A. J., Elias, T., & Kelly, P. J. (2012). Improving the accuracy of SO2 column densities and emission rates obtained from upward-looking UV-spectroscopic measurements of volcanic plumes by taking real-

istic radiative transfer into account. *Journal of Geophysical Research: Atmospheres*, *117*(D20), 20302. https://doi.org/10.1029/2012JD017936

Kim, K., Lees, J. M., & Ruiz, M. C. (2014). Source mechanism of Vulcanian eruption at Tungurahua Volcano, Ecuador, derived from seismic moment tensor inversions. *Journal of Geophysical Research: Solid Earth*, *119*(2), 1145–1164. https://doi.org/10.1002/2013JB010590

Koleszar, A. M., Kent, A. J., Wallace, P. J., & Scott, W. E. (2012). Controls on long-term low explosivity at andesitic arc volcanoes: Insights from Mount Hood, Oregon. *Journal of Volcanology and Geothermal Research*, *219-220*, 1–14. https://doi.org/10.1016/J.JVOLGEORES.2012.01.003

Koulakov, I., & Vargas, C. A. (2018). Evolution of the Magma Conduit Beneath the Galeras Volcano Inferred From Repeated Seismic Tomography. *Geophysical Research Letters*, *45*(15), 7514–7522. https://doi.org/10.1029/2018GL078850

Krischer, L., Megies, T., Barsch, R., Beyreuther, M., Lecocq, T., Caudron, C., & Wassermann, J. (2015). ObsPy: A bridge for seismology into the scientific Python ecosystem. *Computational Science and Discovery*, *8*(1). https://doi.org/10.1088/1749-4699/8/1/014003

Kumagai, H., & Chouet, B. A. (1999). The complex frequencies of long-period seismic events as probes of fluid composition beneath volcanoes. *Geophysical Journal International*, *138*(2). https://doi.org/10.1046/j.1365-246X.1999.00911.x

Kumagai, H., & Chouet, B. A. (2000). Acoustic properties of a crack containing magmatic or hydrothermal fluids. *Journal of Geophysical Research: Solid Earth*, *105*(B11), 25493–25512. https://doi.org/10.1029/2000JB900273

Kumagai, H., Chouet, B. A., & Dawson, P. B. (2005). Source process of a long-period event at Kilauea volcano, Hawaii. *Geophysical Journal International*, *161*(1), 243–254. https://doi.org/10.1111/j.1365-246X.2005.02502.x

Kumagai, H., Placios, P., Ruiz, M., Yepes, H., & Kozono, T. (2011). Ascending seismic source during an explosive eruption at Tungurahua volcano, Ecuador. *Geophysical Research Letters*, *38*(1), n/a–n/a. https://doi.org/10.1029/2010GL045944

Kumagai, H., Yepes, H., Vaca, M., Caceres, V., Naga, T., Yokoe, K., Imai, T., Miyakawa, K., Yamashina, T., Arrais, S., Vasconez, F., Pinajota, E., Cisneros, C., Ramos, C., Paredes, M., Gomezjurado, L., Garcia-Aristizabal, A., Molina, I., Ramon, P., … Inoue, H. (2007). Enhancing volcano-monitoring capabilities in Ecuador. *Eos, Transactions American Geophysical Union*, *88*(23), 245–246. https://doi.org/10.1029/2007EO230001

Kumazawa, M., Imanishi, Y., Fukao, Y., Furumoto, M., & Yamamoto, A. (1990). A theory of spectral analysis based on the characteristic property of a linear dynamic system.

Geophysical Journal International, *101*(3), 613–630. https://doi.org/10.1111/j.1365-246X.1990.tb05574.x

Lamb, O., Lees, J., Marin, L. F., Lazo, J., Rivera, A., Shore, M., & Lee, S. (2020). Investigating potential icequakes at Llaima volcano, Chile. *Volcanica*, *3*(1), 29–42. https://doi.org/10.30909/vol.03.01.2942

Lamur, A., Kendrick, J., Wadsworth, F., & Lavallée, Y. (2019). Fracture healing and strength recovery in magmatic liquids. *Geology*, *47*(3), 195–198. https://doi.org/10.1130/G45512.1

Latter, J. H. (1981). Volcanic earthquakes, and their relationship to eruptions at Ruapehu and Ngauruhoe volcanoes. *Journal of Volcanology and Geothermal Research*, *9*(4), 293–309. https://doi.org/10.1016/0377-0273(81)90041-X

Le Pennec, J. L., Jaya, D., Samaniego, P., Ramón, P., Moreno Yánez, S., Egred, J., & van der Plicht, J. (2008). The AD 1300-1700 eruptive periods at Tungurahua volcano, Ecuador, revealed by historical narratives, stratigraphy and radiocarbon dating. *Journal of Volcanology and Geothermal Research*, *176*(1), 70–81. https://doi.org/10.1016/j.jvolgeores.2008.05.019

Le Pennec, J. L., Ruiz, G. A., Ramón, P., Palacios, E., Mothes, P., & Yepes, H. (2012). Impact of tephra falls on Andean communities: The influences of eruption size and weather conditions during the 1999–2001 activity of Tungurahua volcano, Ecuador. *Journal of Volcanology and Geothermal Research*, *217-218*, 91–103. https://doi.org/10.1016/J.JVOLGEORES.2011.06.011

Lees, J. M., Johnson, J. B., Ruiz, M., Troncoso, L., & Welsh, M. (2008). Reventador Volcano 2005: Eruptive activity inferred from seismo-acoustic observation. *Journal of Volcanology and Geothermal Research*, *176*(1), 179–190. https://doi.org/10.1016/j.jvolgeores.2007.10.006

Lehr, J., Eckel, F., Thorwart, M., & Rabbel, W. (2019). Low-Frequency Seismicity at Villarrica Volcano: Source Location and Seismic Velocities. *Journal of Geophysical Research: Solid Earth*, *124*(11), 11505–11530. https://doi.org/10.1029/2018JB017023

Lemarchand, N., & Grasso, J. R. (2007). Interactions between earthquakes and volcano activity. *Geophysical Research Letters*, *34*(24). https://doi.org/10.1029/2007GL031438

Lengliné, O., Duputel, Z., & Ferrazzini, V. (2016). Uncovering the hidden signature of a magmatic recharge at Piton de la Fournaise volcano using small earthquakes. *Geophysical Research Letters*, *43*(9), 4255–4262. https://doi.org/10.1002/2016GL068383

Lesage, P. (2008). Automatic estimation of optimal autoregressive filters for the analysis of volcanic seismic activity. *Natural Hazards and Earth System Sciences*, *8*(2), 369–376. https://doi.org/10.5194/nhess-8-369-2008

Lesage, P. (2007). SEISMO_VOLCANALYSIS: Signal analysis tools for seismo-volcanic events. User Manual.

Lesage, P. (2009). Interactive Matlab software for the analysis of seismic volcanic signals. *Computers and Geosciences*, *35*(10), 2137–2144. https://doi.org/10.1016/j.cageo.2009.01.010

Lin, C. H. (2017). Dynamic triggering of volcano drumbeat-like seismicity at the Tatun volcano group in Taiwan. *Geophysical Journal International*, *210*(1), 354–359. https://doi.org/10.1093/gji/ggx172

Lipovsky, B. P., & Dunham, E. M. (2015). Vibrational modes of hydraulic fractures: Inference of fracture geometry from resonant frequencies and attenuation. *Journal of Geophysical Research: Solid Earth*, *120*(2), 1080–1107. https://doi.org/10.1002/2014JB011286

Lokmer, I., Saccorotti, G., Di Lieto, B., & Bean, C. J. (2008). Temporal evolution of long-period seismicity at Etna Volcano, Italy, and its relationships with the 2004-2005 eruption. *Earth and Planetary Science Letters*, *266*(1-2), 205–220. https://doi.org/10.1016/j.epsl.2007.11.017

Loughlin, S. C., Sparks, R. S. J., Sparks, S., Brown, S. K., Jenkins, S. F., & Vye-Brown, C. (2015). Global volcanic hazards and risk. *Cambridge University Press*.

Luna, B. Q. (2007). *Assessment and modelling of two lahars caused by "Hurricane Stan" at Atitlan, Guatemala, October 2005* (Doctoral dissertation). University of Oslo.

Lyons, J. J., Waite, G. P., Rose, W. I., & Chigna, G. (2010). Patterns in open vent, strombolian behavior at Fuego volcano, Guatemala, 2005-2007. *Bulletin of Volcanology*, *72*(1), 1–15. https://doi.org/10.1007/s00445-009-0305-7

Main, I. G. (1999). Applicability of time-to-failure analysis to accelerated strain before earthquakes and volcanic eruptions. *Geophysical Journal International*, *139*(3), F1–F6. https://doi.org/10.1046/j.1365-246x.1999.00004.x

Major, J., Scott, W., Driedger, C., & Dzurisin, D. (2005). Mount St. Helens Erupts Again; Activity from September 2004 through March 2005. *U.S. Geological Survey Fact Sheet*, *3036*, 4.

Manciati, C., Villacís, M., Taupin, J.-D., Cadier, E., Galárraga-Sánchez, R., & Cáceres, B. (2014). Empirical mass balance modelling of South American tropical glaciers: case study of Antisana volcano, Ecuador. *Hydrological Sciences Journal*, *59*(8), 1519–1535. https://doi.org/10.1080/02626667.2014.888490

Manga, M., & Brodsky, E. (2006). Seismic triggering of eruptions in the far field: Volcanoes and geysers. *Annu. Rev. Earth Planet. Sci*, *34*, 263–291. https://doi.org/10.1146/annurev.earth.34.031405.125125

Manley, G. F., Pyle, D. M., Mather, T. A., Rodgers, M., Clifton, D. A., Stokell, B. G., Thompson, G., Londoño, J. M., & Roman, D. C. (2020). Understanding the timing of eruption end using a machine learning approach to classification of seismic time series. *Journal of Volcanology and Geothermal Research*, *401*, 106917.

Marple, S. L., Carey, W. M., Bendat, J. S., & Piersol, A. G. (1989). Digital Spectral Analysis with Applications Engineering Applications of Correlation and Spectral Analysis, by. *Citation: The Journal of the Acoustical Society of America*, *86*, 2043. https://doi.org/10.1121/1.398548

Marsden, L. H., Neuberg, J. W., Thomas, M. E., Mothes, P. A., & Ruiz, M. C. (2019). Combining Magma Flow and Deformation Modeling to Explain Observed Changes in Tilt. *Frontiers in Earth Science*, *7*. https://doi.org/10.3389/feart.2019.00219

Matoza, R. S., Fee, D., & López, T. M. (2014). Acoustic characterization of explosion complexity at Sakurajima, Karymsky, and Tungurahua volcanoes. *Seismological Research Letters*, *85*(6), 1187–1199. https://doi.org/10.1785/0220140110

Matoza, R. S., Shearer, P. M., Lin, G., Wolfe, C. J., & Okubo, P. G. (2013). Systematic relocation of seismicity on Hawaii Island from 1992 to 2009 using waveform cross correlation and cluster analysis. *Journal of Geophysical Research: Solid Earth*, *118*(5), 2275–2288. https://doi.org/10.1002/JGRB.50189

McCausland, W. A., Gunawan, H., White, R. A., Indrastuti, N., Patria, C., Suparman, Y., Putra, A., Triastuty, H., & Hendrasto, M. (2019). Using a process-based model of pre-eruptive seismic patterns to forecast evolving eruptive styles at Sinabung Volcano, Indonesia. *Journal of Volcanology and Geothermal Research*, *382*, 253–266. https://doi.org/10.1016/j.jvolgeores.2017.04.004

McGonigle, A. J. S., & Oppenheimer, C. (2003). Optical sensing of volcanic gas and aerosol emissions. *Geological Society London, Special Publications*, *213*(1), 149–168. https://doi.org/10.1144/GSL.SP.2003.213.01.09

McNutt, S. R. (1986). Observations and analysis of B-type earthquakes, explosions, and volcanic tremor at Pavlof Volcano, Alaska. *Bulletin of the Seismological Society of America*, *76*(1), 153–175. https://doi.org/10.1785/BSSA0760010153

McNutt, S. R. (2002). Volcano seismology and monitoring for eruptions. *International Geophysics Series*, *81*, 383–406.

McNutt, S. R., & Roman, D. C. (2015). Volcanic Seismicity, In *The encyclopedia of volcanoes*. Elsevier. https://doi.org/10.1016/b978-0-12-385938-9.00059-6

Métaxian, J.-P. (2003). Seismicity related to the glacier of Cotopaxi Volcano, Ecuador. *Geophysical Research Letters*, *30*(9), 1483. https://doi.org/10.1029/2002GL016773

Minakami, T., Ishikawa, T., & Yagi, K. (1951). The 1944 Eruption of Volcano Usu in Hokkaido, Japan: History and mechanism of formation of the new dome "Syowa-Sinzan". *Bulletin Volcanologique*, *11*(1), 45–157. https://doi.org/10.1007/BF02596029

Molina, I., Kumagai, H., García-Aristizábal, A., Nakano, M., & Mothes, P. (2008). Source process of very-long-period events accompanying long-period signals at Cotopaxi Volcano, Ecuador. *Journal of Volcanology and Geothermal Research*, *176*(1), 119–133. https://doi.org/10.1016/j.jvolgeores.2007.07.019

Molina, I., Kumagai, H., Le Pennec, J. L., & Hall, M. (2005). Three-dimensional P-wave velocity structure of Tungurahua Volcano, Ecuador. *Journal of Volcanology and Geothermal Research*, *147*(1-2), 144–156. https://doi.org/10.1016/j.jvolgeores.2005.03.011

Molina, I., Kumagai, H., & Yepes, H. (2004). Resonances of a volcanic conduit triggered by repetitive injections of an ash-laden gas. *Geophysical Research Letters*, *31*(3). https://doi.org/10.1029/2003GL018934

Moran, S. C. (2004). Seismic monitoring at Cascade volcanic centers, 2004: Status and recommendations. *US Department of the Interior, US Geological Survey*.

Moran, S. C., Malone, S. D., Qamar, A. I., Thelen, W. A., Wright, A. K., & Caplan-Auerbach, J. (2008). *A Volcano Rekindled: The Renewed Eruption of Mount St Seismicity Associated with Renewed Dome Building at Mount St. Helens, 2004-2005* (tech. rep.).

Mothes, P. A., Yepes, H. A., Hall, M. L., Ramón, P. A., Steele, A. L., & Ruiz, M. C. (2015). The scientific-community interface over the fifteen-year eruptive episode of Tungurahua Volcano, Ecuador. *Journal of Applied Volcanology*, *4*(1). https://doi.org/10.1186/s13617-015-0025-y

Mousavi, S. M., Zhu, W., Sheng, Y., & Beroza, G. C. (2019). CRED: A Deep Residual Network of Convolutional and Recurrent Units for Earthquake Signal Detection. *Scientific Reports*, *9*(1), 1–14. https://doi.org/10.1038/s41598-019-45748-1

Muller, C., Biggs, J., Ebmeier, S. K., Mothes, P., Palacios, P. B., Jarrín, P., Edmonds, M., & Ruiz, M. (2018). Temporal evolution of the magmatic system at Tungurahua Volcano, Ecuador, detected by geodetic observations. *Journal of Volcanology and Geothermal Research*, *368*, 63–72. https://doi.org/10.1016/j.jvolgeores.2018.11.004

Narváez, L., Cepeda, H., & Stix, J. (1997). Tornillo-type seismic signals at Galeras volcano, Colombia, 1992–1993. *Journal of Volcanology and Geothermal Research*, *77*(1-4), 159–171. https://doi.org/10.1016/S0377-0273(96)00092-3

Neuberg, J. W. (2000). Characteristics and causes of shallow seismicity in andesite volcanoes. *Philosophical Transactions of the Royal Society A: Mathematical, Physical and Engineering Sciences*, *358*(1770), 1533–1546. https://doi.org/10.1098/rsta.2000.0602

Neuberg, J. W., Collinson, A. S., Mothes, P. A., C. Ruiz, M., & Aguaiza, S. X. (2018). Understanding cyclic seismicity and ground deformation patterns at volcanoes: Intriguing lessons from Tungurahua volcano, Ecuador. *Earth and Planetary Science Letters*, *482*, 193–200. https://doi.org/10.1016/j.epsl.2017.10.050

Neuberg, J. W., Luckett, R., Baptie, B., & Olsen, K. (2000). Models of tremor and low-frequency earthquake swarms on Montserrat. *Journal of Volcanology and Geothermal Research*, *101*(1-2), 83–104. https://doi.org/10.1016/S0377-0273(00)00169-4

Neuberg, J. W., Tuffen, H., Collier, L., Green, D. N., Powell, T., & Dingwell, D. (2006). The trigger mechanism of low-frequency earthquakes on Montserrat. *Journal of Volcanology and Geothermal Research*, *153*(1-2 SPEC. ISS.), 37–50. https://doi.org/10.1016/j.jvolgeores.2005.08.008

Nishimura, T., & Hamaguchi, H. (1993). Scaling law of volcanic explosion earthquake. *Geophysical Research Letters*, *20*(22), 2479–2482. https://doi.org/10.1029/93GL02793

Nocquet, J. M., Jarrin, P., Vallée, M., Mothes, P. A., Grandin, R., Rolandone, F., Delouis, B., Yepes, H., Font, Y., Fuentes, D., Régnier, M., Laurendeau, A., Cisneros, D., Hernandez, S., Sladen, A., Singaucho, J. C., Mora, H., Gomez, J., Montes, L., & Charvis, P. (2017). Supercycle at the Ecuadorian subduction zone revealed after the 2016 Pedernales earthquake. *Nature Geoscience*, *10*(2), 145–149. https://doi.org/10.1038/ngeo2864

Omori, F. (1911). The Usu-san eruption and earthquake and elevation phenomena. *Bulletin of the Imperial Earthquake Investigation Committee*, *5*, 1–38.

Pallister, J. S., Cashman, K. V., Hagstrum, J. T., Beeler, N. M., Moran, S. C., & Denlinger, R. P. (2013). Faulting within the Mount St. Helens conduit and implications for volcanic earthquakes. *GSA Bulletin*, *125*(3-4), 359–376. https://doi.org/10.1130/B30716.1

Parisio, F., Vinciguerra, S., Kolditz, O., & Nagel, T. (2019). The brittle-ductile transition in active volcanoes. *Scientific Reports*, *9*(1), 1–10. https://doi.org/10.1038/s41598-018-36505-x

Park, I., Jolly, A., Kim, K. Y., & Kennedy, B. (2019). Temporal variations of repeating low frequency volcanic earthquakes at Ngauruhoe Volcano, New Zealand. *Journal of Volcanology and Geothermal Research*, *373*, 108–119. https://doi.org/10.1016/j.jvolgeores.2019.01.024

Park, I., Jolly, A., Lokmer, I., & Kennedy, B. (2020). Classification of long-term very long period (VLP) volcanic earthquakes at Whakaari/White Island volcano, New Zealand. *Earth, Planets and Space*, *72*(1), 92. https://doi.org/10.1186/s40623-020-01224-z

Peng, Z., Hill, D. P., Shelly, D. R., & Aiken, C. (2010). Remotely triggered microearthquakes and tremor in central California following the 2010 Mw 8.8 Chile earthquake. *Geophysical Research Letters*, *37*(24), 24312. https://doi.org/10.1029/2010GL045462

Peng, Z., Wu, C., & Aiken, C. (2011). Delayed triggering of microearthquakes by multiple surface waves circling the Earth. *Geophysical Research Letters*, *38*(4). https://doi.org/10.1029/2010GL046373

Petersen, T. (2007). Swarms of repeating long-period earthquakes at Shishaldin Volcano, Alaska, 2001-2004. *Journal of Volcanology and Geothermal Research*, *166*(3-4), 177–192. https://doi.org/10.1016/j.jvolgeores.2007.07.014

Phillipson, G., Sobradelo, R., & Gottsmann, J. (2013). Global volcanic unrest in the 21st century: An analysis of the first decade. *Journal of Volcanology and Geothermal Research*, *264*, 183–196. https://doi.org/10.1016/j.jvolgeores.2013.08.004

Poland, M. P., & Anderson, K. R. (2020). Partly Cloudy With a Chance of Lava Flows: Forecasting Volcanic Eruptions in the Twenty-First Century. *Journal of Geophysical Research: Solid Earth*, *125*(1). https://doi.org/10.1029/2018JB016974

Power, J. A., & Lalla, D. J. (2010). Seismic Observations of Augustine Volcano, 1970-2007. Chapter 1 in The 2006 eruption of Augustine Volcano, Alaska. *US Geological Survey*. https://doi.org/10.3133/pp17691

Power, J. A., Lahr, J. C., Page, R. A., Chouet, B. A., Stephens, C. D., Harlow, D. H., Murray, T. L., & Davies, J. N. (1994). Seismic evolution of the 1989-1990 eruption sequence of Redoubt Volcano, Alaska. *Journal of Volcanology and Geothermal Research*, *62*(1-4), 69–94. https://doi.org/10.1016/0377-0273(94)90029-9

Preece, K., Gertisser, R., Barclay, J., Charbonnier, S. J., Komorowski, J.-C., & Herd, R. A. (2016). Transitions between explosive and effusive phases during the cataclysmic 2010 eruption of Merapi volcano, Java, Indonesia. *Bulletin of Volcanology 2016 78:8*, *78*(8), 1–16. https://doi.org/10.1007/S00445-016-1046-Z

Prejean, S. G., Hill, D. P., Brodsky, E. E., Hough, S. E., Johnston, M. J., Malone, S. D., Oppenheimer, D. H., Pitt, A. M., & Richards-Dinger, K. B. (2004). Remotely triggered seismicity on the United States west coast following the Mw 7.9 Denali fault earthquake. *Bulletin of the Seismological Society of America*, *94*(6 SUPPL. B), 348–359. https://doi.org/10.1785/0120040610

Prejean, S. G., & Hill, D. P. (2018). The influence of tectonic environment on dynamic earthquake triggering: A review and case study on Alaskan volcanoes. *Tectonophysics*, *745*, 293–304. https://doi.org/10.1016/j.tecto.2018.08.007

Richardson, J. P., Waite, G. P., & Palma, J. L. (2014). Varying seismic-acoustic properties of the fluctuating lava lake at Villarrica volcano, Chile. *Journal of Geophysical Research: Solid Earth*, *119*(7), 5560–5573. https://doi.org/10.1002/2014JB011002

Roman, D. C. (2017). Automated detection and characterization of harmonic tremor in continuous seismic data. *Geophysical Research Letters*, *44*(12), 6065–6073. https://doi.org/10.1002/2017GL073715

Roman, D. C., & Cashman, K. V. (2018). Top–Down Precursory Volcanic Seismicity: Implications for 'Stealth' Magma Ascent and Long-Term Eruption Forecasting. *Frontiers in Earth Science*, *6*, 124. https://doi.org/10.3389/feart.2018.00124

Ross, Z. E., Trugman, D. T., Hauksson, E., & Shearer, P. M. (2019). Searching for hidden earthquakes in Southern California. *Science*, *364*(6442), 767–771. https://doi.org/10.1126/science.aaw6888

Rossing, T. D., & Fletcher, N. H. (2004). *Principles of vibrations and sound*. ASA.

Ruiz, M. C., Lees, J. M., & Johnson, J. B. (2006). Source constraints of Tungurahua volcano explosion events. *Bulletin of Volcanology*, *68*(5), 480–490. https://doi.org/10.1007/s00445-005-0023-8

Saccorotti, G., Chouet, B., & Dawson, P. (2001). Wavefield properties of a shallow long-period event and tremor at Kilauea Volcano, Hawaii. *Journal of Volcanology and Geothermal Research*, *109*(1-3), 163–189. https://doi.org/10.1016/S0377-0273(00)00310-3

Salvage, R. O., & Neuberg, J. W. (2016). Using a cross correlation technique to refine the accuracy of the Failure Forecast Method: Application to Soufrière Hills volcano, Montserrat. *Journal of Volcanology and Geothermal Research*, *324*, 118–133. https://doi.org/10.1016/j.jvolgeores.2016.05.011

Salvatier, J., Wiecki, T. V., & Fonnesbeck, C. (2016). Probabilistic programming in Python using PyMC3. *PeerJ Computer Science*, *2*, e55. https://doi.org/10.7717/peerj-cs.55

Samaniego, P., Monzier, M., Robin, C., & Hall, M. L. (1998). Late Holocene eruptive activity at Nevado Cayambe Volcano, Ecuador. *Bulletin of Volcanology*, *59*(7), 451–459. https://doi.org/10.1007/s004450050203

Samaniego, P., Martin, H., Monzier, M., Robin, C., Fornari, M., Eissen, J. P., & Cotten, J. (2005). Temporal evolution of magmatism in the Northern Volcanic Zone of the Andes: The geology and petrology of cayambe volcanic complex (Ecuador). *Journal of Petrology*, *46*(11), 2225–2252. https://doi.org/10.1093/petrology/egi053

Sanderson, R. W., Johnson, J. B., & Lees, J. M. (2010). Ultra-long period seismic signals and cyclic deflation coincident with eruptions at Santiaguito volcano, Guatemala. *Journal of Volcanology and Geothermal Research*. https://doi.org/10.1016/j.jvolgeores.2010.08.007

Saragiotis, C. D., Hadjileontiadis, L. J., Rekanos, I. T., & Panas, S. M. (2004). Automatic P phase picking using maximum kurtosis and κc-statistics criteria. *IEEE Geoscience and Remote Sensing Letters*, *1*(3), 147–151. https://doi.org/10.1109/LGRS.2004.828915

Schuster, R. L., Nieto, A. S., O'Rourke, T. D., Crespo, E., & Plaza-Nieto, G. (1996). Mass wasting triggered by the 5 March 1987 Ecuador earthquakes. *Engineering Geology*, *42*(1), 1–23. https://doi.org/10.1016/0013-7952(95)00024-0

Sennert, S. K. (2016). Report on Cayambe (Ecuador). Weekly Volcanic Activity Report, 14 December-20 December 2016.

Sgattoni, G., Gudmundsson, Ó., Einarsson, P., Lucchi, F., Li, K. L., Sadeghisorkhani, H., Roberts, R., & Tryggvason, A. (2017). The 2011 unrest at Katla volcano: Characterization and interpretation of the tremor sources. *Journal of Volcanology and Geothermal Research*, *338*, 63–78. https://doi.org/10.1016/j.jvolgeores.2017.03.028

Shelly, D. R., Beroza, G. C., & Ide, S. (2007). Non-volcanic tremor and low-frequency earthquake swarms. *Nature*, *446*(7133), 305–307. https://doi.org/10.1038/nature05666

Shelly, D. R., Moran, S. C., & Thelen, W. A. (2013). Evidence for fluid-triggered slip in the 2009 Mount Rainier, Washington earthquake swarm. *Geophysical Research Letters*, *40*(8), 1506–1512. https://doi.org/10.1002/grl.50354

Shensa, M. J. (1977). The deflection detector - its theory and evaluation on short-period seismic data. *Texas Instruments Inc Dallas Equipment Group*.

Sherburn, S., Scott, B. J., Nishi, Y., & Sugihara, M. (1998). Seismicity at White Island volcano, New Zealand: A revised classification and inferences about source mechanism. *Journal of Volcanology and Geothermal Research*, *83*(3-4), 287–312. https://doi.org/10.1016/S0377-0273(98)00022-5

Sigmundsson, F., Pinel, V., Lund, B., Albino, F., Pagli, C., Geirsson, H., & Sturkell, E. (2010). Climate effects on volcanism: influence on magmatic systems of loading and unloading from ice mass variations, with examples from Iceland. *Philosophical Transactions of the Royal Society A: Mathematical, Physical and Engineering Sciences*, *368*(1919), 2519–2534. https://doi.org/10.1098/rsta.2010.0042

Sipkin, S. A., & Needham, R. E. (1989). Moment-tensor solutions estimated using optimal filter theory: global seismicity, 1984–1987. *Physics of the earth and planetary interiors*, *57*(3-4), 233–259. https://doi.org/10.1016/0031-9201(93)90001-P

Sparks, R. S. (2003). Forecasting volcanic eruptions. *Earth and Planetary Science Letters*, *210*(1-2), 1–15. https://doi.org/10.1016/S0012-821X(03)00124-9

Sparks, R. S., Biggs, J., & Neuberg, J. W. (2012). Monitoring volcanoes. American Association for the Advancement of Science. https://doi.org/10.1126/science.1219485

Sparks, S. R. J., Sigurdsson, H., & Wilson, L. (1977). Magma mixing: a mechanism for triggering acid explosive eruptions. *Nature*, *267*(5609), 315–318. https://doi.org/10.1038/267315a0

Steffke, A. M., Fee, D., Garces, M., & Harris, A. (2010). Eruption chronologies, plume heights and eruption styles at Tungurahua Volcano: Integrating remote sensing techniques and infrasound. *Journal of Volcanology and Geothermal Research*, *193*(3-4), 143–160. https://doi.org/10.1016/j.jvolgeores.2010.03.004

Stix, J., Torres C., R., Narváez M., L., Cortés J., G. P., Raigosa A., J., Gómez M., D., & Castonguay, R. (1997). A model of vulcanian eruptions at Galeras volcano, Colombia. *Journal of Volcanology and Geothermal Research*, *77*(1-4), 285–303. https://doi.org/10.1016/S0377-0273(96)00100-X

Stoica, P., & Moses, R. L. (2005). Spectral analysis of signals. Pearson Prentice Hall Upper Saddle River, NJ.

Swindell, W. H., & Snell, N. S. (1977). Station processor automatic signal detection system, phase i: Final report, station processor software development. *Texas Instruments Incorporated, Dallas, Texas*.

Thelen, W., Malone, S., & West, M. (2011). Multiplets: Their behavior and utility at dacitic and andesitic volcanic centers. *Journal of Geophysical Research: Solid Earth*, *116*(8). https://doi.org/10.1029/2010JB007924

Thompson, L. G., Mosley-Thompson, E., Davis, M. E., & Brecher, H. H. (2011). Tropical glaciers, recorders and indicators of climate change, are disappearing globally. *Annals of Glaciology*, *52*(59), 23–34. https://doi.org/10.3189/172756411799096231

Tibaldi, A., Ferrari, L., & Pasquarè, G. (1995). Landslides triggered by earthquakes and their relations with faults and mountain slope geometry: an example from Ecuador. *Geomorphology*, *11*(3), 215–226. https://doi.org/10.1016/0169-555X(94)00060-5

Tierz, P., Loughlin, S. C., & Calder, E. S. (2019). VOLCANS: an objective, structured and reproducible method for identifying sets of analogue volcanoes. *Bulletin of Volcanology 2019 81:12*, *81*(12), 1–22. https://doi.org/10.1007/S00445-019-1336-3

Traphagan, J., & Lees, J. (2020). Modeling source parameters of quasi-periodic tremor. *Volcanica*, *3*(2), 251–262. https://doi.org/10.30909/VOL.03.02.251262

Tuffen, H. (2010). How will melting of ice affect volcanic hazards in the twenty-first century? *Philosophical Transactions of the Royal Society A: Mathematical, Physical and Engineering Sciences*, *368*(1919), 2535–2558. https://doi.org/10.1098/rsta.2010.0063

Tuffen, H., Dingwell, D. B., & Pinkerton, H. (2003). Repeated fracture and healing of silicic magma generate flow banding and earthquakes? *Geology*, *31*(12), 1089–1092. https://doi.org/10.1130/G19777.1

Uchide, T., Horikawa, H., Nakai, M., Matsushita, R., Shigematsu, N., Ando, R., & Imanishi, K. (2016). The 2016 Kumamoto–Oita earthquake sequence: aftershock seismicity gap and dynamic triggering in volcanic areas. *Earth, Planets and Space 2016 68:1*, *68*(1), 1–10. https://doi.org/10.1186/S40623-016-0556-4

Unglert, K., & Jellinek, A. M. (2017). Feasibility study of spectral pattern recognition reveals distinct classes of volcanic tremor. *Journal of Volcanology and Geothermal Research*, *336*, 219–244. https://doi.org/10.1016/j.jvolgeores.2017.03.006

USGS. (2021). Earthquake Catalog Search [https://earthquake.usgs.gov/earthquakes/search/, Accessed: 20-01-2021].

Utsu, T., Ogata, Y., S, R., & Matsu'ura. (1995). The Centenary of the Omori Formula for a Decay Law of Aftershock Activity. *Journal of Physics of the Earth*, *43*(1), 1–33. https://doi.org/10.4294/jpe1952.43.1

Vanderkulk, W., Rosen, F., & Lorenz, S. (1965). Large aperture seismic array signal processing study. *IBM Final Report, ARPA Contract Number SD-296*.

Varley, N. R., Arámbula-Mendoza, R., Reyes-Dávila, G., Stevenson, J., & Harwood, R. (2010a). Long-period seismicity during magma movement at Volcán de Colima. *Bulletin of Volcanology*, *72*(9), 1093–1107. https://doi.org/10.1007/s00445-010-0390-7

Varley, N., Arámbula-Mendoza, R., Reyes-Dávila, G., Sanderson, R., & Stevenson, J. (2010b). Generation of vulcanian activity and long-period seismicity at Volcán de Colima, Mexico. *Journal of Volcanology and Geothermal Research*, *198*(1-2), 45–56. https://doi.org/10.1016/j.jvolgeores.2010.08.009

Varnam, M., Burton, M., Esse, B., Kazahaya, R., Salerno, G., Caltabiano, T., & Ibarra, M. (2020). Quantifying Light Dilution in Ultraviolet Spectroscopic Measurements of Volcanic SO2 Using Dual-Band Modeling. *Frontiers in Earth Science*, *8*, 468. https://doi.org/10.3389/feart.2020.528753

Veloza, G., Styron, R., & Taylor, M. (2012). Open-source archive of active faults for northwest South America. *GSA Today*, *22*(10). https://doi.org/10.1130/GSAT-G156A.1

Voight, B. (1988). A method for prediction of volcanic eruptions. *Nature*, *332*(6160), 125. https://doi.org/10.1038/332125a0

Wadge, G. (2004). Measuring the Rate of Lava Effusion by InSAR, In *Fringe 2003 workshop esa sp-550*.

Waite, G. P., Chouet, B. A., & Dawson, P. B. (2008). Eruption dynamics at Mount St. Helens imaged from broadband seismic waveforms: Interaction of the shallow magmatic and hydrothermal systems. *Journal of Geophysical Research: Solid Earth*, *113*(2). https://doi.org/10.1029/2007JB005259

Walter, T. R., & Amelung, F. (2007). Volcanic eruptions following M9 megathrust earthquakes: Implications for the Sumatra-Andaman volcanoes. *Geology*, *35*(6), 539–542. https://doi.org/10.1130/G23429A.1

Walter, T. R., Wang, R., Zimmer, M., Grosser, H., Lühr, B., & Ratdomopurbo, A. (2007). Volcanic activity influenced by tectonic earthquakes: Static and dynamic stress triggering at Mt. Merapi. *Geophysical Research Letters*, *34*(5). https://doi.org/10.1130/G23429A.1

Westfall, P. H. (2014). Kurtosis as Peakedness, 1905–2014. R.I.P. *American Statistician*, *68*(3), 191–195. https://doi.org/10.1080/00031305.2014.917055

White, R. A., & McCausland, W. A. (2019). A process-based model of pre-eruption seismicity patterns and its use for eruption forecasting at dormant stratovolcanoes. *Journal of Volcanology and Geothermal Research*, *382*, 267–297. https://doi.org/10.1016/j.jvolgeores.2019.03.004

White, R. A., Miller, A. D., Lynch, L., & Power, J. (1998). Observations of hybrid seismic events at Soufriere Hills Volcano, Montserrat: July 1995 to September 1996. *Geophysical Research Letters*, *25*(19), 3657–3660. https://doi.org/10.1029/98GL02427

White, R., & McCausland, W. (2016). Volcano-tectonic earthquakes: A new tool for estimating intrusive volumes and forecasting eruptions. *Journal of Volcanology and Geothermal Research*, *309*, 139–155. https://doi.org/10.1016/j.jvolgeores.2015.10.020

Wiemer, S., & Katsumata, K. (1999). Spatial variability of seismicity parameters in aftershock zones. *Journal of Geophysical Research: Solid Earth*, *104*(B6), 13135–13151. https://doi.org/10.1029/1999JB900032

Withers, M., Aster, R., Young, C., Beiriger, J., Harris, M., Moore, S., & Trujillo, J. (1998). A comparison of select trigger algorithms for automated global seismic phase and event detection. *Bulletin of the Seismological Society of America*, *88*(1), 95–106.

Wollherr, S., Gabriel, A.-A., & Mai, P. M. (2019). Landers 1992 "Reloaded": Integrative Dynamic Earthquake Rupture Modeling. *Journal of Geophysical Research: Solid Earth*, *124*(7), 6666–6702. https://doi.org/10.1029/2018JB016355

Woods, J., Donaldson, C., White, R. S., Caudron, C., Brandsdóttir, B., Hudson, T. S., & Ágústsdóttir, T. (2018). Long-period seismicity reveals magma pathways above a laterally propagating dyke during the 2014–15 Bárðarbunga rifting event, Iceland. *Earth and Planetary Science Letters*, *490*, 216–229. https://doi.org/10.1016/j.epsl.2018.03.020

Worni, R., Huggel, C., Stoffel, M., & Pulgarín, B. (2012). Challenges of modeling current very large lahars at Nevado del Huila Volcano, Colombia. *Bulletin of Volcanology*, *74*(2), 309–324. https://doi.org/10.1007/s00445-011-0522-8

Yepes, H., Audin, L., Alvarado, A., Beauval, C., Aguilar, J., Font, Y., & Cotton, F. (2016). A new view for the geodynamics of Ecuador: Implication in seismogenic source definition and seismic hazard assessment. *Tectonics*, *35*(5), 1249–1279. https://doi.org/10.1002/2015TC003941

Yoshimoto, M., Kumagai, H., Acero, W., Ponce, G., Vásconez, F., Arrais, S., Ruiz, M., Alvarado, A., Pedraza García, P., Dionicio, V., Chamorro, O., Maeda, Y., & Nakano, M. (2017). Depth-dependent rupture mode along the Ecuador-Colombia subduction zone. *Geophysical Research Letters*, *44*(5), 2203–2210. https://doi.org/10.1002/2016GL071929

Yukutake, Y., Honda, R., Harada, M., Doke, R., Saito, T., Ueno, T., Sakai, S., & Morita, Y. (2017). Analyzing the continuous volcanic tremors detected during the 2015 phreatic eruption of the Hakone volcano. *Earth, Planets and Space*, *69*(1). https://doi.org/10.1186/s40623-017-0751-y

Zobin, V. (2012). *Introduction to volcanic seismology* (2nd ed.). Elsevier. https://doi.org/https://doi.org/10.1016/C2011-0-06141-0

Zobin, V. M., Battaglia, J., Melson, W., & Sudo, Y. (2019). Two-stage modeling of Strombolian-type eruptions and quantification of the model parameters: Insight from the seismic and acoustic signals. *Physics of the Earth and Planetary Interiors*, *297*, 106318. https://doi.org/10.1016/j.pepi.2019.106318

Zobin, V. M., Peral, J. J., Nava, F., & Bretón, M. (2015). Vulcanian explosions in the process of building-destruction of the lava dome of andesitic volcano: Insight from the seismic signals recorded at Volcán de Colima, México. *Physics of the Earth and Planetary Interiors*, *244*, 1–10. https://doi.org/10.1016/j.pepi.2015.05.001